

INORGANIC AND POLYMERIC MICROSIEVES

STRATEGIES TO REDUCE FOULING

DISSERTATION

to obtain
the doctor's degree at the University of Twente,
on the authority of the rector magnificus,
prof. dr. W.H.M. Zijm,
on account of the decision of the graduation committee,
to be publicly defended
on Friday 9th December 2005 at 15.00

by

Míriam Gironès I Nogué

born on 4th January 1977
in Girona (Catalonia), Spain

This dissertation has been approved by:

Promotor: Prof. dr. -ing. M. Wessling

Assistant-promotor: Dr. ir. R.G.H. Lammertink

"Live as if you were to die tomorrow. Learn as if you were to live forever"

Mahatma Gandhi (1869 - 1948)

To my parents, Joan and Carme

This work was financially supported by the Dutch Ministries of Education, Culture, Science, Economics and Environmental Affairs. Research was carried out within the framework of the EET Program, Project nr. EETK20033.

Inorganic and Polymeric Microsieves
Strategies to reduce Fouling

PhD Thesis, University of Twente, The Netherlands

ISBN: 90-365-2289-7

© Míriam Gironès, Enschede , 2005

No part of this work may be reproduced by print, photocopy, or any other means without permission of the author

Cover design by Marcel Boerrigter and Míriam Gironès

Printed by PrintPartners Ipskamp, Enschede

Contents

Chapter 1	1
Introduction	
1.1 Microfiltration: basic concepts	2
1.2 State-of-the-art of high flux Microfiltration	3
1.3 Flux decline in Microfiltration: bottlenecks and strategies to reduce fouling	5
1.4 Current MF applications in Food and Dairy industry	9
1.5 Scope of this thesis	11
1.6 References	13
Chapter 2	15
Characterization and surface modification of silicon nitride	
2.1 Introduction	16
2.2 Materials and methods	18
2.2.1 Materials	18
2.2.2 Hydrophilization/cleaning of silicon nitride surfaces	18
2.2.3 Self-assembled monolayer (SAM) formation	18
2.2.4 Dip and spin coating	18
2.2.5 Characterization techniques	19
2.3 Results and discussion	20
2.3.1 Surface properties of unmodified silicon nitride dices	20
2.3.2 RF oxygen plasma treatment of silicon nitride	21
2.3.3 Hydrophobic silanization of silicon nitride	23
2.3.4 Physical adsorption: polymer dip and spin coating	24
2.4 Conclusions	30
2.5 Acknowledgements	30
2.6 References	30
Chapter 3	33
The role of wetting on the water flux performance of Si_xN_y microsieves	
3.1 Introduction	34
3.2 Fabrication and structure of silicon nitride microsieves	35

3.3	Materials and methods	39
3.3.1	Materials	39
3.3.2	Wetting and flux measurements	39
3.3.3	Microsieve inspection	41
3.4	Results and discussion	41
3.4.1	Clean water flux measurement with unmodified microsieves	41
3.4.2	Specific wetting procedure for different microsieve surfaces	43
3.4.3	Effect of water purity on flux performance	44
3.4.4	Effect of wetting procedure and air on hydrophobized microsieves	48
3.5	Conclusions	51
3.6	References	51
 Chapter 4		53
Fouling studies of silicon nitride microsieves with model solutions		
4.1	Introduction	54
4.2	Materials and methods	56
4.2.1	Materials	56
4.2.2	Crossflow filtration	56
4.2.3	Scanning Electron (SEM) and Optical Microscopy	57
4.2.4	Zeta-potential and particle size of BSA solutions (DLS)	57
4.2.5	Analysis	58
4.3	Results and discussion	58
4.3.1	Fouling studies with model proteins	58
a.	Effect of pH and viscosity	58
b.	Effect of concentration and pressure	63
c.	Influence of equipment: pressurized vessel versus gear pump	65
d.	Aggregate removal: pre-filtration	66
4.3.2	Fouling behavior prediction by pore blocking	68
4.3.3	Fouling studies with latex solutions	70
4.4	Conclusions	73
4.5	Acknowledgements	73
4.6	References	74

Chapter 5	77
Strategies to reduce protein fouling with Si_xN_y microsieves	
I. Backpulsing and air sparging	
5.1 Introduction	78
5.2 Materials and methods	80
5.2.1 Materials	80
5.2.2 Crossflow filtration of proteins with backpulsing and air sparging	81
5.2.3 Optical Microscopy	82
5.3 Results and discussion	83
5.3.1 Effect of water forward and backflushing	83
5.3.2 Effect of in-line permeate backpulsing with Si _x N _y microsieves	84
a. Optimization of pulse power and frequency	86
b. Effect of permeate backpulsing as a function of BSA solution concentration	89
5.3.3 Effect of discontinuous and continuous air sparging on BSA permeability	90
5.3.4 Effect of continuous air sparging on lysozyme permeability	96
5.4 Conclusions	97
5.5 Acknowledgements	98
5.6 References	98
Chapter 6	101
Strategies to reduce protein fouling with Si_xN_y microsieves	
II. Surface modification with PEG polymers	
6.1 Introduction	102
6.2 Materials and methods	104
6.2.1 Materials	104
6.2.2 Synthesis of Poly (PEGMA-r-TMSMA) random copolymer	104
6.2.3 Poly (PEGMA-r-TMSMA) SAM formation and protein adhesion studies on oxide-based surfaces	105
a. Protein patterning with a microfluidic device and confocal fluorescence microscopy	105
b. Static protein adsorption (thickness determination by ellipsometry)	106

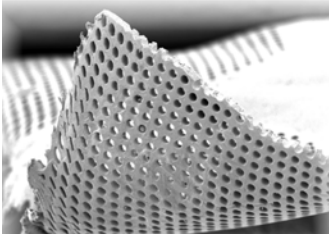
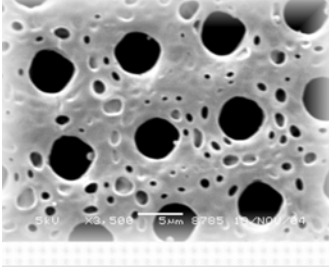
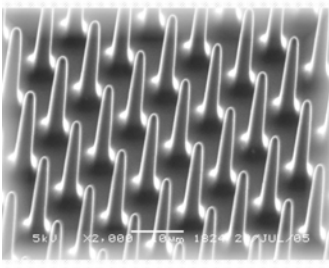
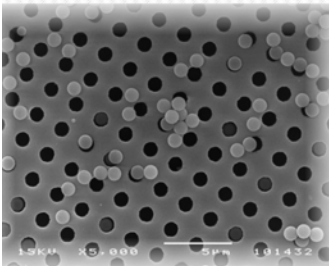
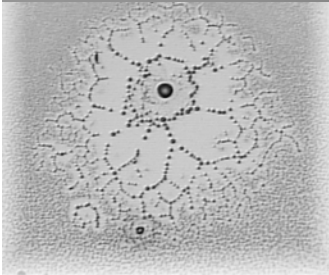
6.2.4	Crossflow filtration of BSA and skimmed milk	106
6.2.5	Optical microscopy	107
6.3	Results and discussion	107
6.3.1	Construction of protein-repellant surfaces (Poly(PEGMA-r-TMSMA))	107
a.	Characterization of covalently grafted Poly (PEGMA-r-TMSMA)	107
b.	Evaluation of the non-fouling properties	110
6.3.2	Effect of in-line permeate backpulsing with Poly (PEGMA-r-TMSMA) coated microsieves	113
6.3.3	Effect of in-line air sparging and permeate backpulsing with Poly (PEGMA-r-TMSMA) coated microsieves	115
6.3.4	Application: Skimmed milk filtration with unmodified and PEG-coated silicon nitride microsieves	116
6.4	Conclusions	120
6.5	Acknowledgements	121
6.6	References	121
Chapter 7		123
Fabrication and characterization of polymeric microsieves		
7.1	Introduction	124
7.2	Phase Separation Micromolding	126
7.3	Materials and methods	127
7.3.1	Materials	127
7.3.2	Microsieve fabrication by Phase Separation Micromolding	128
7.3.3	Mold design: support shape and pillar dimensions	130
7.3.4	Material densification by thermal treatment	131
7.3.5	Microsieve characterization	131
7.4	Results and discussion	132
7.4.1	Fabrication of PES microsieves by PS _μ M	132
a.	VIPS: Vapor bath residence time and temperature	132
b.	LIPS: Water bath coagulation time	134
c.	Influence of co-solvent or volatile additive	134
d.	Mold design: influence of the support structure	135
e.	Optimized PES microsieves	136
7.4.2	Fabrication of PES/PVP and PES-PEO microsieves	137

a. PES-PVP	137
b. PES-PEO	140
c. Comparison of the materials and microsieves produced by PS _μ M	141
7.4.3 Microsieve pore downscaling: pillar design and thermal reduction of PES and PES-PEO microsieves	143
a. Tuning of perforation diameter as a function of pillar dimensions	143
b. Tuning of perforation diameter by thermal treatment	146
7.5 Conclusions	150
7.6 Acknowledgements	151
7.7 References	151
Chapter 8	153
Microfiltration with polymeric microsieves	
8.1 Introduction	154
8.2 Materials and methods	156
8.2.1 Materials	156
8.2.2 Crossflow microfiltration of BSA, milk and beer	157
8.2.3 SEM and Optical Microscopy	158
8.2.4 Analysis	158
8.3 Results and discussion	158
8.3.1 Fouling studies with a model protein (BSA)	158
a. PES unmodified microsieves (5 μm)	158
b. Thermally-treated PES microsieves (2 μm)	160
c. Fouling reduction strategies	161
8.3.2 Comparison of polymeric microsieves and commercial membranes	169
8.3.3 Skimmed milk filtration	172
8.3.4 Microfiltration of white Belgian beer	175
8.4 Conclusions	177
8.5 Acknowledgements	178
8.6 References	179

Chapter 9	181
Conclusions and Outlook	
9.1 Introduction	182
9.2 Conclusions	182
9.3 Relevant aspects for future applications	186
9.3.1 Si _x N _y microsieves	186
9.3.2 Polymeric microsieves	188
9.4 Acknowledgements	191
9.5 References	191
Summary	193
Samenvatting	195
Resum	197
Acknowledgements	199
Curriculum vitae and publications	203

Chapter 1

Introduction



1.1 Microfiltration: basic concepts

Microfiltration is the oldest process in membrane technology. The first commercial membranes were available in the 1920s, mainly used for bacteriological analysis of water [1]. Throughout the years, successful applications in microfiltration (MF) have grown rapidly in different fields such as biotechnology, automobile, water treatment, electronics and food industry. In pressure-driven MF some of the target solutes or particles to be retained include mainly bacteria, viruses and yeast cells, but also synthetic latex particles or colloidal silica. The approximate size of such components ranges from 0.05 to 10 μm , and they can be filtered at pressures ≤ 2 bar [2]. Microfiltration is an expanding business; MF membranes and membrane units are estimated to represent 40% of the current sales in the whole membrane business, while market research results indicate that the average annual growth of MF is about 10% [3].

Microfiltration is applied in two different operation modes: dead-end and crossflow. Both use a pressure drop across the membrane as driving force for permeation. The simplest design is the dead-end operation mode, where the feed flow is perpendicular to the membrane. The retained particles build up in time on the membrane, forming a cake layer, which increases the resistance to filtration and causes the permeate flux to decline [2, 4].

In 1907 Bechhold found that in the filtration of suspensions a flow parallel to the filter increased the filtrate flow [3]. Later on, this operation mode was called crossflow (or tangential flow) and has been used in the past decades as a successful alternative to dead-end. The advantage of crossflow versus dead end is the control of concentration polarization and cake layer build-up [4], resulting in increased permeation rates during longer periods of time. The shear exerted by the feed solution flowing parallel to the membrane surface can sweep the deposited particles towards the retentate side so that the cake layer remains relatively thin (see Figure 1a). In dead-end filtration, the cake grows constantly and gives a more steep flux decline.

In the case of crossflow microfiltration a cake layer will be built up gradually. After some time a steady state is reached because the transport of particles to the cake layer is in equilibrium with the back transport of particles into the feed stream. As shown in Figure 1b, a steady or quasi-steady flux is achieved once the cake layer has reached its steady-state thickness. In real applications long-term flux decline is sometimes observed even after there is no more cake growth, as a result of membrane compaction or fouling. Nevertheless, for stationary industrial applications, crossflow operation is preferred because the membrane suffers less fouling in time.

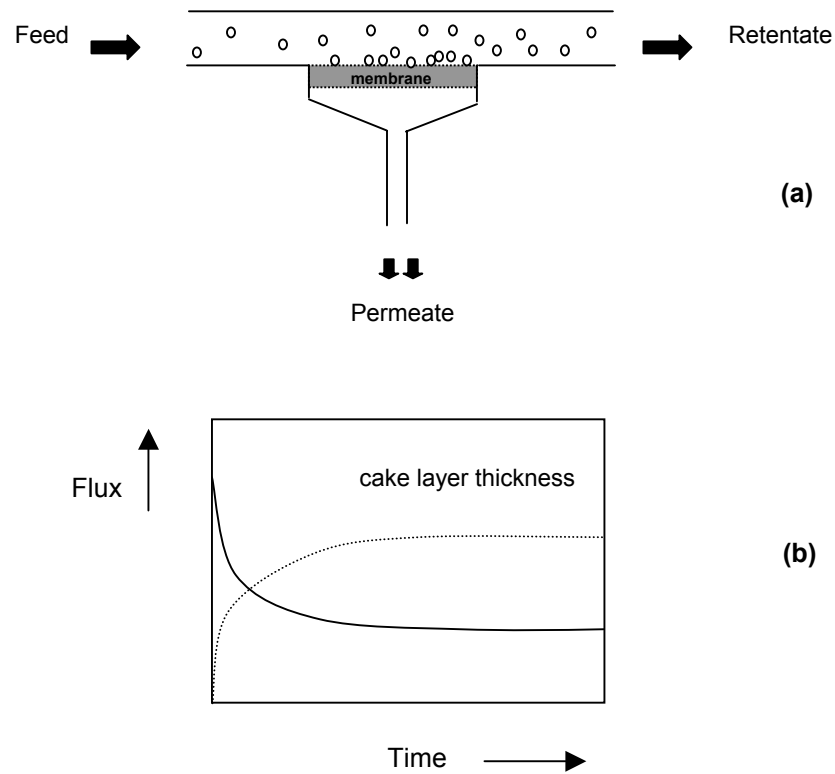


Figure 1. Principle of crossflow filtration (a) and flux characteristics of an operation in crossflow mode (b).

1.2 State-of-the-art of high flux Microfiltration

Two types of membranes are distinguished in microfiltration: screen filters and depth filters [1]. Screen filters have straight-through pores and their separation principle is based on the sieving mechanism. All particles with sizes bigger than the pore diameter are retained, whereas particles smaller than the pore size can pass with relative ease through the pores. Screen filters can be made either by track etching or by lithographic techniques. On the other hand, depth filters have a random, tortuous porous structure and retain particles by adsorption within the bulk of the filter. Schematics of both membrane morphologies are depicted in Figure 2.

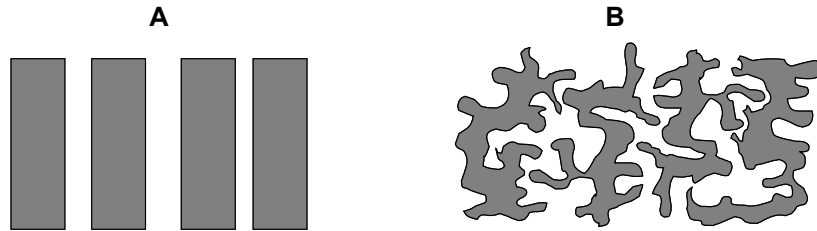


Figure 2. Schematic representation of a cross-section of a screen-filter (A) and a depth-filter (B).

Great effort is nowadays being deployed in developing new membrane materials and designs to replace conventional polymeric and ceramic membranes used in traditional MF applications. Since such applications are well understood, today's main goal is to increase production and membrane effectiveness. The bottleneck for traditional MF membranes is normally the relationship between permeability and selectivity, which is usually compromised.

Microsieve membranes are very thin flat-sheet devices that contain pores with the same size and shape all along their surface. They can be made of inorganic materials such as silicon nitride or polymers like polysulfone (Psf), polyethersulfone (PES), polyimide (PI) and polyvinylidene fluoride (PVDF), among others. Silicon nitride microsieves are fabricated by lithographic techniques used in the semiconductor industry [5-7], whereas polymeric microsieves are fabricated by Phase Separation Micromolding (PS μ M) [8]. Currently, silicon nitride microsieves are implemented in applications like the separation of blood cells or bacteria and the clarification of beer.

One of the advantages of microsieves, regardless of their inorganic or polymeric nature, is that the fabrication process allows enough flexibility to control the porosity and the pore size and shape (perfectly round or slits). Pore sizes are available from 10 μm to 0.5 μm . They also have high porosity and permeabilities, and very thin selective layers compared to commercial depth-filters (microsieve pore size/membrane thickness=1). The main advantage of the thin selective layer is that the resistance to mass transfer can be reduced. Moreover, for screen filters like microsieves, internal fouling can be suppressed. However, the fact that screen filters have straight-through pores is a double-edged sword. The degree of membrane pore interconnectivity and the size and permeability of foulant deposits can greatly affect the filtration flux. In the case of fouling by pore blocking, lower membrane performance can be observed with membranes with straight-through pores. If the foulant clogs the pores no further

permeation takes place, contrary to what would happen to membranes with interconnected pores.

Ho and Zydney [9] recently performed studies on membranes with both interconnected and straight-through pores, finding that the rate of flux decline for membranes with interconnected pores is much smaller than that for membranes with tortuosity equal to 1. In more interconnected structures the fluid is able to flow under and around blockages. The degree of radial flow underneath foulant blockages is a function not only of the ratio of the radial and axial permeabilities of the membrane but also of the ratio of the radius of the blockage and the membrane thickness [10].

For this reason, some membrane manufacturers have recently focused their attention to the development of polymeric depth-filters that have a good permeability/selectivity correlation and can withstand fouling. Membrana (Germany) recently developed a new MF PES membrane, DuraPES®, which aims to compete with other well-known commercial membranes. DuraPES® membranes are presented as strongly asymmetric membranes with an 'internal' porous layer with pore sizes much smaller than on both surfaces. A comparison between DuraPES® and various commercial membranes (Osmonics Micron, AMC Accupore, Pall Supor, Sartorius Sartopore, Millipore Express and Millipore Durapore) with similar pore size and porosity was recently presented by Ulbricht and co-workers [11]. They concluded that DuraPES® presented the narrowest pore size distribution, largest water permeability, highest volume porosity and lowest flux decline with 2 g/l Bovine Serum Albumin (BSA) at pH=5 and 4 bar. These findings open a new horizon for these depth filters in microfiltration applications, which can very well compete with other novel membranes like microsieves.

1.3 Flux decline in Microfiltration: bottlenecks and strategies to reduce fouling

The main problem in microfiltration, where very high permeation fluxes and complicated feeds containing a broad particle size distribution are present, is concentration polarization and subsequent fouling. In the case of high-flux microfiltration membranes, especially microsieves, fouling is a very sensitive issue. Because of their large porosity and permeability, more severe and rapid fouling than in other systems takes place.

Concentration polarization is the build-up of rejected solutes at the liquid boundary layer near the membrane. If there is a certain degree of mixing, diffusion and inertial lift of the rejected

components can result in a backtransport to the bulk. Convection of particles towards the module exit due to the crossflow will then limit their accumulation on the membrane. If the transport of the rejected components back to the bulk solution is not fast enough, deposition of material on or in the membrane occurs. This process is known as *fouling*.

Particle deposition is a process that is governed mainly by the hydrodynamic forces acting on the particle near the membrane surface [12]. The important forces on the particle include the viscous drag force performed by the flowing fluid, the hydrodynamic lift force arising from the inertial interactions between particle and solid boundary and diffusional forces due to Brownian motion. The dominant force for small particles is Brownian motion, which is responsible for the equilibrium state in macrosolute-membrane interactions. As the particle size increases, the importance of Brownian diffusion decreases since it becomes too slow. Deposition of bigger particles will occur when the forces towards the membrane surface are greater than the repulsive interactions between particles, inertial lift forces and shear-induced diffusion.

The analysis of the flux decline due to particle deposition is of special importance since it can provide some insight to the phenomena that take place during microfiltration. Depending on the solute and the process conditions, different blocking mechanisms that explain the flux decline during membrane filtration have been developed [13-15]:

- Complete blocking (pore blocking)
- Standard blocking (pore narrowing)
- Intermediate blocking (long term deposition)
- Cake formation (gel/cake layer)

These mechanisms are schematically shown in Figure 3. Pore blocking (a) is caused by rejected particles bigger than the membrane pores. This mechanism assumes that each particle arriving at the membrane contributes in the complete inactivation of one or more pores, causing a dramatic flux decline. Pore narrowing (c) is mostly caused by smaller components that can adhere to the internal pore wall, accumulate or bridge and finally clog the pore. Intermediate blocking (b) is the stage preceding cake layer formation (d). A cake layer is formed when each particle arriving to the surface accumulates on each other, thus completely blocking the membrane surface. The flux decline due to particles can be governed by one mechanism but it can also be a combination of more than one. Although these mechanisms are developed for the filtration of proteins, they are also valid for different types of solutes.

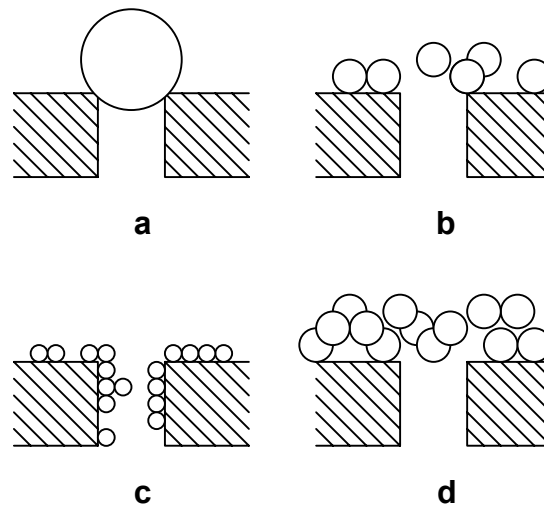


Figure 3. Schematic view of particle deposition mechanisms: complete blocking (a), intermediate blocking (b), standard blocking or pore narrowing (c) and cake formation (d).

Particle deposition is often a reversible type of fouling, which can be prevented or reduced by a variety of methods. For instance, coagulants can be added to the feed so that the particles aggregate and can subsequently be swept off the membrane. Process parameters like crossflow velocity or shear can also be increased. Shear flow is a major strategy to control mass transfer near the membrane wall. Some of the techniques shown to be effective for surface shear enhancement include [16, 17]:

- turbulence promoters
- pulsatile flow and vortex generation
- two-phase flow (gas bubbling)
- corrugated membrane surfaces
- forward flushing/ pulsing

Turbulence can be promoted by using baffles, like helical relief geometries [18]. Broussous *et al.* reported that helical stamps used inside a tubular ceramic membrane resulted in a 6-fold increase of the permeate flux compared to using smooth surfaces [19]. Dean vortices, which are centrifugal instabilities produced in curved channels when the critical Dean number is exceeded, have also been a mean to improve the flux of dairy whey and Baker's yeast [20], as well as *E. Coli.* and mammalian cells in hollow fiber modules [21].

The injection of **air bubbles** or **gas sparging** is a resource to enhance mass transfer. The secondary flows and bubbles promote mixing and reduce the thickness of the concentration polarization layer. When the bubble diameter exceeds the channel diameter (from the module, in flat sheets, or from the hollow fibers) slugs are formed, which can displace the boundary layer and cause the local pressure to fluctuate. Another flow regime commonly observed is bubble flow, which occurs when the gas bubbles are significantly smaller than the fiber or channel size [17]. Air sparging in combination with hollow-fiber or flat-sheet UF membranes is very useful to enhance the flux of dextrans and proteins [22] enzymes or microparticles [23], or more specifically, to fractionate protein mixtures [24]. In microfiltration, the main uses are related to enhance yeast filtration [25, 26]. Other applications include air sparging in membrane bed reactors for wastewater treatment [27] and nanofiltration [28, 29]. The enhancement of permeate flux by gas bubbling is clearly demonstrated in all these studies.

Flow instabilities can also be induced by pulses, with approaches like **backflushing**, **forward flushing** or **backpulsing**. These strategies are generally considered as cleaning methods because they remove deposited matter from the surface. Backflushing and backpulsing are based on temporary permeate flow reversal, while crossflushing is the stoppage of permeate flow while crossflow is maintained. The main difference between a backpulse and a backflush is the force and time used to lift accumulated deposits off the membrane. Generally, in backflushing flow reversal occurs for a few seconds once every several minutes, while backpulsing occurs at a higher frequency and the pulses are applied for a short time (< 1s) [30, 31]. The efficiency of both techniques depends strongly on the frequency, pulse duration, pressure, etc. Levesley and coworkers [32] used high frequency backflushing (1s pulse at 1 Hz frequency) for the microfiltration of yeast homogenate suspensions using a ceramic tubular membrane. Backflushing resulted in a 5.4 times increased solute flux compared to the non-backflushing situation. Davis and coworkers [31] used high-frequency short backpulses (0.1-1 s) to increase the permeate flux of washed bacterial suspensions and bacterial fermentation broths. Washed bacterial suspensions were easier to backpulse, in comparison to bacterial fermentation broths, due to lower concentration of suspended components. Davis *et al.* reported higher flux of proteins from bacterial cell debris by applying high-frequency backpulsing [33]. Beolchini and coworkers also emphasized the importance of backpulsing with skimmed bovine milk filtration using ceramic tubular membranes with a pore diameter around 1.4 μm [34]. Backpulsing was required in order to reduce membrane fouling and achieve milk permeation.

For adherent foulants and irreversible fouling other approaches than the ones discussed above are generally used. Irreversible fouling is triggered by hydrophobic interactions, hydrogen bonding, van der Waals attractions and other effects. Some of the methods to eliminate this kind of fouling are based on modifying the membrane surface by moieties that repel certain components or change the surface charge of the material. Physically coating the surface with water-soluble polymers or surfactants for a temporary effect, or grafting monomers by UV or electron beam irradiation are also frequently reported techniques.

1.4 Current MF applications in Food and Dairy Industry

Membrane processes have been key tools in food processing for a long period of time. Most of these processes aim to transform raw products from agriculture to safe consumer products. Membrane processes give the food industry three main advantages: food safety, competitiveness and environmental friendliness [35].

Microfiltration plays an important role in clarification of fruit juices and rough beer, as well as in bacterial removal and globular fat fractionation in milk.

In the field of **fruit juices**, membrane filtration allows the separation of pulp from the serum of citric juices like orange, lemon, grapefruit, etc., exotic (pineapple, kiwi) and pulpy (peach, pear, apricot) fruits. Juice concentrates with excellent organoleptic properties after dilution are also produced. Microfiltration and RO can produce clarified concentrates from turbid juices or pulps or stable pulp concentrates, with a high sugar content. These stable clarified pulp concentrates are difficult to produce with other techniques and are widely used as starting materials for the production of beverages and other food products.

The **brewing industry** is one of the most conservative in terms of using traditional processes to maintain the quality and taste of the product. However, this sector is gradually changing, implementing new techniques to improve the process. Currently, industrial microfiltration applications concern the clarification of rough beer to eliminate yeast and colloids responsible for haze and sterile filtration of clarified beer. The separation of such solid particles is very important for obtaining a clear bright beer. For more than a century, this process has been done by conventional dead-end filtration with diatomaceous earth (Kieselguhr), but a great potential exists today for microfiltration to be implemented here. Heineken is currently running an industrial plant with a MF unit for rough beer clarification, with a capacity of 10,000 l/h [35]. To keep a high membrane performance regular backflushes and specific cleaning procedures (enzymatic, oxidative and alkaline) are applied.

Microfiltration in **wine industry** delivers outstanding results when it comes to producing microbiologically stable and clear wines. It is normally performed with polysulfone or ceramic membranes and periodical backflushing, giving high yeast and bacteria reduction. Most importantly, with this operation most of the characteristics of wine (turbidity, color, filterability index, colloids content and dissolved gas) remain unaltered by microfiltration.

Milk is one of the most challenging feeds in food industry. Crossflow microfiltration of **dairy products** is a very interesting subject in this investigation. Our research originates from a larger project (D-Force), which intends to fractionate the components of milk with membranes, especially microsieves, so that a better product quality is obtained. This novel process would eliminate high-temperature treatments like pasteurization or sterilization. The ideal process scheme, together with the milk components that would be obtained, is shown in Figure 4. The basic concept behind the D-Force project is the fractionation of milk components using a stack of microsieves with different pore sizes, so that the various desired molecules are obtained and used, for instance, to enrich certain products and increase their nutritional value.

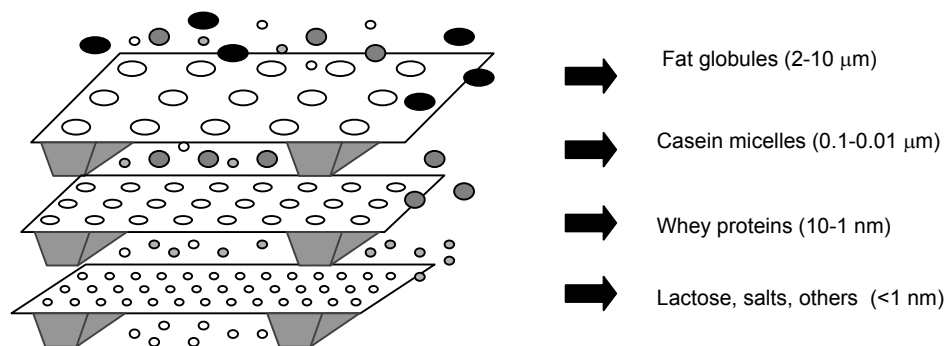


Figure 4. Schematic representation of the ideal milk fractionation process with a stack of microsieve membranes.

Nowadays, milk fractionation and crossflow microfiltration are mainly targeted to three applications [36]:

- bacteria removal
- defatting or globular fat fractionation
- micellar casein concentration for cheese production

Heat treatment and bactofugation (reduction of bacteria and spores by centrifugation) are the most common methods to lower the bacterial content of milk and milk products [35]. Bacteria in milk have sizes from 0.4 to 2 μm ; different systems have been tested to retain such components, being ceramic membranes the most popular. In a review of Saboya and Maubois [37], a bacterial decimal reduction of 3.5 was reported with Sterilox membranes (pore sizes around 1.4 μm). Recently, Beolchini and coworkers have reported similar results (bacterial reduction between 2 and 3) for ovine and bovine skimmed milk [38], using Membralox membranes with pore sizes around 1.4 μm and backpulsing. Kromkamp and Van Rijn [39] reported that a decimal reduction of 6.6 could be achieved with SMUF (Simulated Milk Ultra Filtrate) and 0.5 μm silicon nitride microsieves.

Milk fat globules have a size distribution ranging from 0.1 to 15 μm [40]. The globules between 1 and 8 μm contain 90% or more of the total volume of milk fat. Traditionally fat has been separated by centrifugation, although this method does not yield a 100% recovery and can damage the properties of the globules.

Another well-known application of microfiltration in dairy food processing is the concentration of casein micelles for cheese production or for enriching other products. If skimmed milk is microfiltrated through alumina or zirconia ceramic membranes with pore sizes about 0.1-0.2 μm , for instance, a permeate with a composition similar to sweet whey is obtained. The retentate is an enriched solution of native and micellar calcium phosphocaseinate, which is purified by diafiltration and then vacuum evaporated and spray-dried [35, 37]. Micellar casein enriched milk is used to improve the cheesemaking process because it coagulates faster and produces firmer curds.

Up to now we have just given a glimpse on the possibilities and application of microfiltration membranes in food industry. Currently, new developments are being introduced in fields where traditional processes were used. Therefore, it is only a matter of time and research efforts for new technologies to be implemented in such fields.

1.5 Scope of this thesis

This thesis deals with a novel generation of high-flux screen filters: microsieve membranes, and their potential use as microfiltration membranes in the food industry. Not much literature is yet available concerning their filtration performance, which could be very interesting and promising for future industrial applications. For this purpose, a great part of this research is dedicated to study the performance of microsieves, especially with model protein solutions like BSA.

The first microsieves were made of silicon nitride, an inorganic material used in semiconductors, biosensors, cantilevers, etc. Since little is known about the application of silicon nitride as membrane material, **Chapter 2** is fully dedicated to the study and characterization of its surface properties. A summary on several surface modification methods and materials is also given.

Chapter 3 introduces the concept of silicon nitride microsieves. Furthermore, it deals with the wetting properties of silicon nitride microsieves and their influence on the water flux. Different microsieves modified with the most promising coatings studied in Chapter 2 are tested.

In **Chapter 4** fouling with different model protein solutions is investigated. Most of the work is presented for BSA, a 'soft' globular protein thoroughly studied by many researchers. The fouling behavior of BSA with 1.2 μm pore diameter silicon nitride microsieves is presented, as a function of several parameters like pH, concentration, pressure, equipment used, etc. The mechanism behind flux decline is also studied with the classical pore blocking theory. For comparison, a glimpse on other protein (lysozyme) and particle (synthetic latex particles) solutions is presented.

Chapters 5 and 6 describe some strategies to retard/suppress flux decline and enhance permeation. In **Chapter 5** strategies like forward and backflushing, together with backpulsing and air sparging are presented. In **Chapter 6** an intrinsic-membrane approach is discussed, which involves the synthesis and application of an antifouling polymer coating: poly (TMSMA-r-PEGMA). The combination of an antifouling coating, with backpulsing and air sparging is also studied here. The chapter concludes with a real application like skimmed milk filtration, making use of all the knowledge gained in the previous chapters.

Recently, also microfabricated polymeric membranes with a very well-defined structure and thin selective layer were realized. Polymeric microsieves represent an alternative to the expensive inorganic microsieves in many aspects, not only in terms of fabrication or economy but also in terms of performance and fouling. Therefore, all the details of their fabrication and structural optimization are presented in **Chapter 7**. Here, an investigation of different fabrication materials and factors that affect the microsieve structure is performed. The pore size optimization is investigated by mold design or by thermal treatment of the polymer used.

To finalize the experimental chapters, a broad study of the performance of PES microsieves is described in **Chapter 8**. Fouling studies with BSA, milk and beer are performed, together with

the application of the best strategies investigated in the previous chapters. A short comparison in terms of backpulsing efficiency of 2 μm PES microsieves with commercial track-etched membranes and depth-filters is also described here.

To conclude this thesis an outlook is given in **Chapter 9**, where a summary of the most significative conclusions is offered. Moreover, some additional results, personal views and recommendations are given for further research.

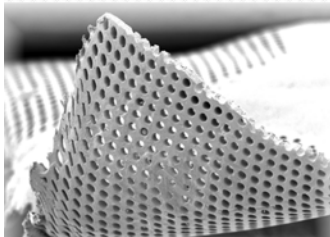
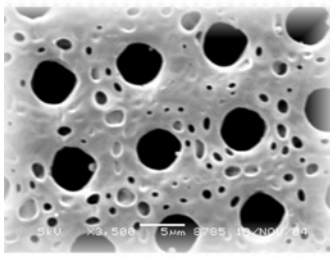
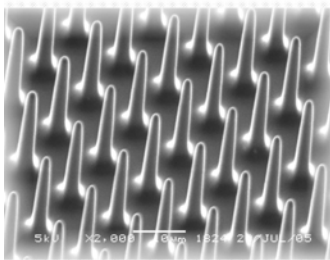
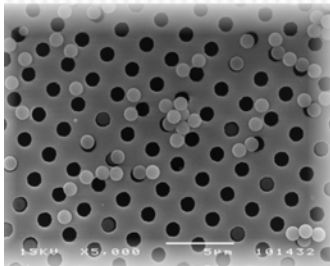
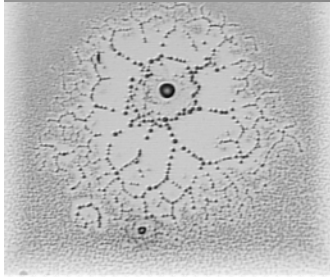
1.6 References

- [1] I.H. Huisman, Microfiltration; In: I. D Wilson, Encyclopedia of Separation Science, Academic Press, San Diego, 2000.
- [2] M.H.V. Mulder, Basic Principles of Membrane Technology, Kluwer Academic Publishers, Dordrecht, 1996.
- [3] S. Ripperger, J. Altmann, Crossflow microfiltration – state of the art, Sep. Purif. Technol. 26 (1997) 19.
- [4] R.W. Baker, Membrane Technology and Applications, John Wiley & Sons, Chichester, 2004.
- [5] C.J.M. Van Rijn, WO9513860, 'Membrane filter as well as a method of manufacturing the same', 1995.
- [6] S. Kuiper, Development and applications of microsieves, PhD Thesis, University of Twente, The Netherlands, 2000.
- [7] C.J.M. van Rijn, W. Nijdam, S. Kuiper, G.J. Veldhuis, H.A.G.M. van Wolferen, M.C. Elwenspoek, Microsieves made with laser interference lithography for micro-filtration applications. J. Micromech. Microeng. 9 (1999) 170.
- [8] L. Vogelaar, Phase Separation micromolding, PhD Thesis, University of Twente, The Netherlands, 2005.
- [9] C.C Ho, A.L. Zydney, A combined pore blockage and cake filtration model for protein fouling during microfiltration, J. Colloid Interf. Sci. 232 (2000) 389.
- [10] C.C Ho, A.L. Zydney, Theoretical analysis of the effect of membrane morphology on fouling during microfiltration, Sep. Sci. Technol. 34 (1999) 2461.
- [11] M. Ulbricht, Presented at the NAMS meeting, Providence, 2005.
- [12] L.J. Zeman, A.L. Zydney, Microfiltration and ultrafiltration: principles and applications, Marcel Dekker, New York, 1996.
- [13] J. Hermia, Constant pressure blocking filtration laws – Application to power-law non-newtonian fluids, Trans. IChemE 60 (1982) 183.
- [14] W.R. Bowen, J.I. Calvo, A. Hernández, Steps of membrane blocking in flux decline during protein microfiltration, J. Membr. Sci. 101 (1995) 153.
- [15] M. Wessling, Two-dimensional stochastic modelling of membrane fouling, Sep. Purif. Technol. 24 (2001) 375.
- [16] N. Al-Bastaki, A. Abbas, Use of fluid instabilities to enhance membrane performance: a review, Desalination 136 (2001) 255.
- [17] Z. F. Cui, S. Chang, A.G. Fane, The use of gas bubbles to enhance membrane processes, J. Membr. Sci. 221 (2003) 1.
- [18] L. Broussous, P. Schmitz, E. Prouzet, L. Becque, A. Larbot, New ceramic membranes designed for crossflow filtration enhancement, Sep. Purif. Technol. 25 (2001) 333.

- [19] L. Broussous, J.C. Ruiz, A. Larbot and L. Cot, Stamped ceramic porous tubes for tangential filtration, *Sep. Purif. Technol.* 14 (1998) 53.
- [20] H. B. Winzeler, G. Belfort, Enhanced performance for pressure-driven membrane processes: The argument for fluid instabilities, *J. Membr. Sci.* 80 (1993) 35.
- [21] S. Luque, H. Maluubhotla, G. Gehlert, R. Kuriyel, S. Dzengeleski, S. Pearl, G. Belfort, A new coiled hollow-fiber module design for enhanced microfiltration performance in biotechnology, *Biotechnol. Bioeng.* 65 (1999) 247.
- [22] S. R. Bellara, Z. F. Cui, D. S. Pepper, Gas sparging to enhance permeate flux in ultrafiltration using hollow fibre membranes, *J. Membr. Sci.* 121 (1996) 175.
- [23] S. Laborie, C. Cabassud, L. Durand-Bourlier, J. M. Laine, Fouling control by air sparging inside hollow fibre membranes-effects on energy consumption, *Desalination* 118 (1998) 189.
- [24] Q.Y. Li, R. Ghosh, S.R. Bellara, Z.F. Cui, Z.F. D.S. Pepper, Enhancement of ultrafiltration by gas sparging with flat sheet membrane modules, *Sep. Purif. Technol.* 14 (1998) 79.
- [25] H. W. Sur, Z. Cui, Experimental study on the enhancement of yeast microfiltration with gas sparging, *J. Chem. Technol. Biotechnol.* 76 (2001) 477.
- [26] M. Mercier, C. Fonade, C. Lafforgue-Delorme, Yeast suspension filtration: enhancement using an upward gas/liquid slug flow-Application to continuous alcoholic fermentation with cell recycle, *Biotechnol. Bioeng.* 58 (1998) 47.
- [27] I. Chang, I. Judd, Air sparging of a submerged MBR for municipal wastewater treatment, *Process Biochemistry* 37 (2002) 915.
- [28] D. Ducom, C. Cabassud, Air sparging for flux enhancement in nanofiltration membranes: application to O/W stabilised and non-stabilised emulsions, *J. Membr. Sci.* 204 (2002) 221.
- [29] D. Ducom, C. Cabassud, Possible effects of air sparging for nanofiltration of salted solutions, *Desalination* 156 (2003) 267.
- [30] R. Sondhi, R. Bhave, Role of backpulsing in fouling minimization in crossflow filtration with ceramic membranes, *J. Membr. Sci.* 186 (2001) 41.
- [31] V. Kuberkar, R. Davis, Flux enhancement for membrane filtration of bacterial suspensions using high frequency backpulsing, *Biotechnol. Bioeng.* 60 (1998) 77.
- [32] J.A. Levesley, M. Hoare, The effect of high frequency backflushing on the microfiltration of yeast homogenate suspensions for the recovery of soluble proteins, *J. Membr. Sci.* 158 (1999) 9.
- [33] C. S. Parnham, R. H. Davis, Protein recovery from bacterial cell debris using crossflow microfiltration with backpulsing, *J. Membr. Sci.* 118 (1996) 259.
- [34] F. Beolchini, F. Veglio, D. Barba, Microfiltration of bovine and ovine milk for the reduction of microbial content in a tubular membrane: a preliminary investigation, *Desalination* 161 (2004) 251.
- [35] G. Daufin, J. P. Escudier, H. Carrere, S. Berot, L. Fillaudeau, M. Decloux, Recent and emerging applications of membrane processes in the food and dairy industry, *Trans. IChemE* 79 (2001) 89.
- [36] G. Brans, C.G.P.H. Schroën, R.G.M. van der Sman, R.M. Boom, Membrane fractionation of milk, *J. Membr. Sci.* 243 (2004) 263.
- [37] L.V. Saboya, J-L. Maubois, Current developments of microfiltration technology in the dairy industry, *Lait* 80 (2000) 541.
- [38] F. Beolchini, S. Cimini, L. Mosca, F. Veglio, D. Barba, Microfiltration of Bovine and ovine milk for the reduction of microbial content: effect on some operating conditions on permeate flux and microbial reduction, *Sep. Sci. Technol.* 40 (2005) 757.
- [39] C.J.M. van Rijn, J. Kromkamp, Method for filtering milk, WO Patent 0209527 (2001).
- [40] H. Goudédranche, J. Fauquant, J-L. Maubois, Fractionation of globular milk fat by membrane microfiltration, *Lait* 80 (2000) 93.

Chapter 2

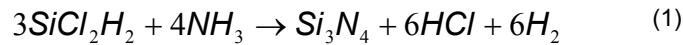
Characterization and surface modification of silicon nitride



2.1 Introduction

Microfabricated inorganic membranes such as microsieves have excellent sieving properties. Their thin selective layer is made of silicon nitride and they possess a high surface porosity and patterned pore structure combined with mechanical strength. Silicon nitride is used to manufacture microfabricated membranes like microsieves but it is also commonly used for microcircuit and microsensor fabrication due to its optimal chemical, electrical, optical, and mechanical properties [1]. An overview of such properties is shown in Table 1.

Stoichiometric silicon nitride (Si_3N_4) can be deposited by either plasma-enhanced chemical-vapor deposition (PECVD) or low-pressure chemical vapor deposition (LPCVD), the latter being the technique used to deposit the silicon nitride for microsieves. The gases used in LPCVD processes are usually SiH_2Cl_2 or SiH_4 , as a Silicon source, and NH_3 as nitrogen source, using different compositions of the gas mixture [2]. The deposition reaction is such as:



LPCVD is normally performed between 700 and 760°C, while lower temperatures (around 400°C) are used in PECVD processes [3]. Silicon nitride films deposited by chemical vapor deposition (CVD) are widely used in microelectronics and optoelectronics. Such films can be used as passivation layers [4], gate dielectrics of thin film transistors [5, 6], as a mask layer for selective silicon oxidation [7], insulator and as masks for local oxidation and selective doping [8]. For microsieve production, silicon-rich or low-stress silicon nitride (Si_xN_y) is used. By increasing the silicon content in the silicon nitride film, the tensile film stress reduces [2, 9]. Thick films can be deposited and patterned with a lower risk of fracture, but also the HF etching rate is much lower, being easier for those films to resist release etches in the membrane manufacturing process [1].

Generally, silicon nitride oxidizes much slower than silicon (30 times slower) and has high fracture toughness, hardness (its Young's modulus is close to alumina and is, for instance, 3 times higher than titanium and 3 times lower than diamond), wear resistance, and electrical resistivity. Since its melting point is around 1900°C, it has excellent thermal properties; it can be used until around 800°C [10]. Its chemical stability, though, is limited in certain ways. Silicon nitride is inert in acidic environment and in most known organic solvents. Although it is not inert in strongly basic environments (specially if it is deposited on silicon and pinholes are present), it is more stable than silicon in such media.

Table 1. Properties of silicon nitride [1, 11]

Property	Value
Molecular Weight	140.8 g/mol
Dielectric Constant	6-7
Refractive index	2.01
Density	2.9-3.2 g/cm ³
Melting point	~1900°C
Young's Modulus	270 GPa
Modulus of Rupture	414-580 MPa
Thermal Conductivity	16-33 W/m/K
Thermal diffusivity	0.32 cm ² /s

In the compilation of Bergström *et al.* [12] it is shown that measurements performed on silicon nitride powders present great scattering in the results. Isoelectric points (IEP) between pH=3 and pH=9 were reported, suggesting that the IEP depends very much on the solution media and the extent of oxidation of the surface. Evidence of oxidation of silicon nitride surfaces in atmospheric environment has been reported by various authors [10, 13-17], mainly confirmed by X-Ray Photoelectron Spectroscopy (XPS) measurements. Moreover, Rahaman *et al.* [13] reported that silicon nitride often presents an oxide layer on the surface with a variable thickness that can reach several nanometers.

The sensitivity of silicon nitride surfaces to chemical compositional changes is not very advantageous for membrane-related applications. The change of surface composition can cause loss in performance and adsorption of undesired components as well as a low reproducibility of the separation. If well-defined surfaces with constant quality are obtained, it is more likely that optimal membrane performance and separation are achieved.

For this purpose, well-known surface modification strategies to produce either hydrophilic (for low protein adhesion purposes) or hydrophobic surfaces (for organic applications) can be used. Among them, the most used are polymer grafting, Self Assembled Monolayer (SAMs) chemisorption with protein/bacterial repellent moieties and/or silanated fluorocompounds, and plasma treatment [18-24]. Such treatments will deliver tailored surfaces that can be used in protein separations or solvent purification, for instance.

In this chapter an overview of some of the surface properties of Si_xN_y is given. Besides, several pathways to modify silicon nitride surfaces are described and characterized, including plasma treatment, surface grafting and polymer adsorption.

2.2 Materials and methods

2.2.1 Materials

Silicon-rich silicon nitride (Si_xN_y) dices provided by Aquamarijn B.V. ($1 \times 1 \text{ cm}^2$), Si_xN_y microsieves and silicon wafers were used as substrates for modification.

Ultrapure water ($18.2 \text{ M}\Omega\text{cm}$) for the contact angle measurements was obtained with a Millipore purification unit (MilliQ plus). All the other reagents were of analytical grade and were used without any pre-treatment.

2.2.2 Hydrophilization/Cleaning of silicon nitride surfaces

Si_xN_y dices and microsieves were oxygen plasma treated using a Plasma Fab 508 (Electrotech) reactor. The pressure was 0.33 mbar; process time 10–15 minutes; 50% oxygen flux and 500 W of RF power. After plasma treatment, samples were immediately used for the characterization tests and silanization experiments. Alternatively, dices were cleaned with 'piranha solution' ($\text{H}_2\text{SO}_4/\text{H}_2\text{O}_2$ 3:1 v/v) for an hour and rinsed thoroughly with ultrapure water.

2.2.3 Self-assembled monolayer (SAM) formation

Water-stable hydrophobic SAMs based on a perfluorinated octyltrichlorosilane, FOTS (Fluka, >97%), were formed on silicon nitride dices either in liquid phase or by Chemical Vapor Deposition [25]. For the SAM formation in liquid phase, plasma-treated silicon nitride dices were immersed in a 2.5 mM solution of silane in a mixture of dried n-hexadecane and chloroform (4/1 v/v) for one hour at room temperature. Afterwards the dices were thoroughly washed with isopropanol, water and dried under nitrogen. The last step consisted of curing in a nitrogen oven at 100°C for one hour. For the vapor-deposited FOTS, Si_xN_y dices were plasma treated and exposed to FOTS vapor for 4.5 h at 120°C in a nitrogen atmosphere.

2.2.4 Dip and Spin coating

Dip coating was performed with two types of polymers: Pluronics (PEO-PPO-PEO) and a PEG-PEI (Poly(ethyleneglycol)-polyethyleneimine) complex. 0.1% Pluronic solutions of F108 (ICI, Mw= 14600 g/mol) and F127 (Sigma, Mw= 12600 g/mol) were prepared in ultrapure

water. Then a dip coating was applied during 10-15 min to the silicon nitride dices, followed by rinsing with ultra pure water and nitrogen drying.

PEG-PEI was synthesized according to the method described by van Alstine *et al.* [26]. Plasma treated dices were immersed in a 1% PEG-PEI solution in carbonate buffer for one hour at 50°C. Afterwards the substrates were rinsed in ultrapure water to remove the excess of polymer and nitrogen-dried.

Polymer solutions with concentrations from 1 to 0.3 wt% were spin coated on oxygen plasma treated silicon nitride dices and microsieves at 4000 rpm. The spin-coated samples were dried in a nitrogen oven at 150°C for several hours and stored at the same temperature in a vacuum oven. PES 6020 (Polyethersulfone) from Amoco Udel, PEO-PBT (Poly(ethyleneoxide)-poly(butylene terephthalate)) block-copolymer (Isotis), PES/PVP blends 4:1 (Polyethersulfone/polyvinylpyrrolidone) and a PES-PEO block copolymer with 8 wt% PEO (Gambro) were used as polymers for spin coating. All polymers were dissolved in NMP (N-methyl-2-pyrrolidone) except for PEO-PBT, which was dissolved in CHCl₃ (chloroform).

2.2.5 Characterization techniques

Contact Angle Measurements

Static water contact angles were measured using a Goniometer (Dataphysics Contact Angle System). The sessile drop method was used to determine the static contact angle, θ , of water on silicon nitride dices before and after modification. The results are averages over 3 measurements on each sample.

X-ray Photoelectron Spectroscopy (XPS)

XPS (PHI Quantum 2000 Scanning ESCA Microprobe) was used to study the chemical composition of the unmodified and modified wafer dices. The XPS system was equipped with an Al K α X-Ray radiation source ($h\nu=1878.5$ eV), providing a 100 μ m diameter X-ray beam. The total number of elements present was determined from 0 to 1000 eV survey scans, while the C (1s), N (1s), O (1s) and Si (2p) atomic percentages were acquired from detailed scans at a take-off angle of 45° and 2×10^{-8} torr working pressure.

Ellipsometry

The oxide thickness on silicon dices was determined with a VASE (VB-400) spectroscopic ellipsometer (Woollam) at an angle of incidence of 75°. The measurements were performed by Dr. Herbert Wormeester at the Applied Optics Group of the University of Twente.

Scanning Electron Microscopy (SEM)

The morphology of coated microsieve membranes by spin coating was visualized by Scanning Electron Microscopy (SEM, Microscope JEOL JSM-5600LV, at 5 kV). The samples were sputtered with a thin gold film (30 nm).

2.3 Results and discussion

2.3.1 Surface properties of unmodified silicon nitride wafers

In this section the surface characteristics of unmodified Si_xN_y dices are presented. Table 2 shows an overview of the average percentages of the elements on unmodified silicon nitride samples. The dices were treated with different cleaning methods and the elements on the surface were determined by XPS. The concentrations of carbon, nitrogen, oxygen and silicon are given, as well as the O/Si and O/N ratios, for direct comparison between surfaces.

For unmodified silicon nitride dices, the results shown in Table 2 indicate that the surface mainly consisted of N, O and Si. The elevated oxygen concentration (around 21%) indicates the presence of a native oxide layer. Previous studies have already shown that oxygen is often present on metal, ceramic and alloy surfaces as a native oxide [10, 27-29]. The tendency of silicon nitride to oxidation has been studied as well [13, 30]. Comparable element concentrations and ratios have been reported in literature by several authors on nanosized powders and LPCVD silicon nitride [31-34].

Table 2. O/Si, O/N ratios and atomic percentages of elements present on unmodified and cleaned silicon nitride dices with: acetone, isopropanol (IPA), H_2SO_4 95-98%, HNO_3 65% and a mixture of sulphuric acid and peroxide ('piranha').

Sample	XPS Atomic Percentage				Atomic Ratio		
	C	N	O	Si	O/Si	O/N	C/O
<i>Untreated Si_xN_y</i>	5.79	37.20	21.41	35.59	0.59	0.55	0.27
<i>acetone- Si_xN_y</i>	16.15	34.26	18.2	31.39	0.58	0.53	0.89
<i>IPA-Si_xN_y</i>	6.93	37.9	21.32	33.85	0.63	0.56	0.32
<i>H_2SO_4-Si_xN_y</i>	3.59	39.5	21.85	35.06	0.62	0.55	0.16
<i>HNO_3-Si_xN_y</i>	3.03	40.23	21.29	35.45	0.6	0.53	0.14
<i>Piranha-Si_xN_y</i>	3.65	39.47	21.81	35.06	0.63	0.57	0.17

In silicon technology, sample ageing in air is considered as oxidation and/or adsorption of contaminants on the surface. As a result of contamination, increased carbon percentages and increasing water contact angles are measured [35]. From the XPS results in Table 2, clear evidence of hydrocarbon contamination was observed when silicon nitride dices were rinsed with acetone, since the carbon content increased significantly compared to the other samples (also the C/O ratio). The same effect but in a lower extent was also observed with isopropanol. In both cases, contamination is left on the surface after rinsing with the organic solvent. These findings clearly indicate that rinsing with an organic solvent is not a suitable method to clean silicon nitride wafers.

The acid-cleaned and 'piranha'-cleaned samples demonstrate that there is not much difference between the composition of such surfaces compared to untreated ones (O/Si and O/N ratios are almost identical).

Evidence of ageing can also be obtained from the contact angles of untreated silicon nitride wafers. The unmodified dices presented great scattering, with contact angle values ranging from 30 to 70°. These results, together with the XPS data, indicate the variability in surface contamination of unmodified silicon nitride.

2.3.2 RF Oxygen plasma treatment of silicon nitride

Oxygen plasma was applied on the surfaces to homogenize and hydrophilize them by oxidation. For the plasma treated wafers, the XPS results (see Table 3) show that the major elements present in the first 10 nm (the take-off angle is 45°, which is translated in an analysis depth of around 10 nm) are oxygen (66%) and silicon (26%). These percentages and the increased O/N and O/Si ratios strongly indicate that the silicon nitride surface is oxidized, as reported by other authors in previous studies [36]. Moreover, the Si/N ratios change extremely after oxidation (from almost 1 to 7), which confirms that little nitrogen is present and that the outer layer is similar to SiO₂.

Table 3. O/Si, O/N ratios and atomic percentages of elements present on unmodified and oxidized/oxygen plasma treated (O₂-Si_xN_y) silicon nitride wafers.

Sample	XPS Atomic Percentage				Atomic Ratio		
	C	N	O	Si	O/Si	Si/N	O/N
Si _x N _y	5.8±0.5	37.2±0.5	21.4±0.5	35.6±0.5	0.6	≈ 1	0.5
O ₂ -Si _x N _y	3.4±0.6	3.6±1.1	65.8±0.8	25.9±1.6	2.6	7	15.6

The oxide layer thickness on silicon nitride was estimated by XPS at about 5-10 nm. Since the oxide layer on silicon nitride could not be determined by ellipsometry, the measurements were made on silicon dices. The ellipsometric measurements on oxidized silicon agreed with the XPS results, resulting in a thickness of approx. 6.2 nm. After such a plasma treatment wafers became fully wettable ($\theta \approx 0^\circ$).

With these results we can confirm that oxygen plasma is a very effective method to hydrophilize silicon-based surfaces. However, oxidized samples can adsorb contaminants present in the storage media and change their surface properties. Therefore it is very important to control the storage media of plasma treated wafers. Ageing or contamination of oxygen plasma treated samples in different atmospheres was examined by monitoring contact angles in time (see Figure 1).

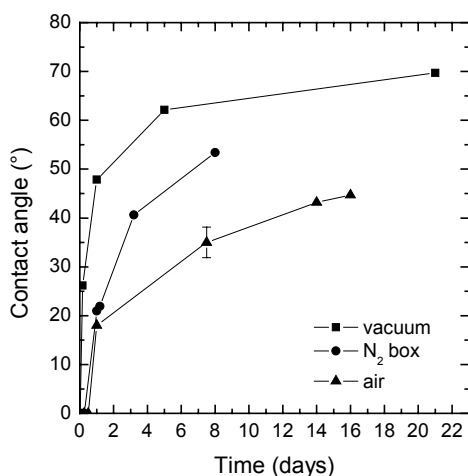


Figure 1. Contact angles as a function of storage time, for plasma treated samples stored in air, vacuum and nitrogen.

In the case of samples stored under vacuum, the surface hydrophobicity increased very rapidly with increasing storage time (from 0 to 50° in 24 h, and reaching values close to 70° after 20 days) probably due to adsorption of oil residues from the vacuum oven and the pump. Samples stored in a nitrogen-rich environment (N₂-box) also suffered ageing translated in contact angle increase, although in a less significant extent compared to vacuum stored surfaces. Nitrogen was provided through a main line from a large reservoir and, therefore, was of low purity. Contaminants present in the piping may have also adsorbed on the

surfaces during storage time. The samples stored in air were kept in petri dishes, without further treatment.

Contact angles of freshly plasma-treated dices had values below 20° during the first two days after treatment, which indicated their high hydrophilicity. Such contact angle values increased in time due to sample ageing and, after two weeks, values around 40° were found. XPS data obtained for plasma treated samples after two weeks confirm that samples remained oxidized. The oxygen percentage remained very high (around 60%) and only the carbon percentage experienced an increase from 4% to 8.4%. The influence in surface contamination expressed by contact angles is significant because the adsorption of hydrocarbon molecules renders the surface more hydrophobic.

From these results we can point out that, after any plasma oxidation and before any other treatment, samples should be used within a couple of hours and stored preferably in air.

2.3.3 Hydrophobic silanization of silicon nitride

Once having successfully hydrophilized silicon nitride, attention was also paid to hydrophobization strategies. Hydrophobization would be useful for applications involving anti-stiction coatings, solvent purifications, water-in-oil membrane emulsifications, distillation or pervaporation, for instance.

A quite straight-forward method for hydrophobization is silanization with alkylchlorosilanes, by forming self-assembled monolayers [22, 37]. The reaction of the alkylchlorosilane with the surface silanol groups results in a Si-O-Si covalent bond [38]. In our case, oxidized silicon nitride was hydrophobized by a silanization step with 1H, 1H, 2H, 2H-perfluorooctyltrichlorosilane (FOTS). Two types of surfaces with different hydrophobicity were obtained depending on the coating procedure: FOTS coating in solution or vapor deposition. Silicon nitride dices with FOTS SAM's that were produced in solution exhibited contact angle values of approximately 105°. More hydrophobic surfaces, with water contact angles of 112°, were obtained for dices with a monolayer formed by FOTS vapor deposition. Similar results were obtained by Maboudian *et al.* [37] with a slightly different compound, FDTS (perfluorodecyltrichlorosilane). The thermal and chemical stability of such layers was studied by Geerken *et al.* [39], who concluded that FOTS layers were stable in water, under acidic and alkaline conditions in a range from pH=2 to 11.5 at 80°C up to more than 200 hours.

Both types of FOTS-modified dices were also stable in our storage conditions (air, room temperature) for several months and in water at room temperature.

2.3.4 Physical adsorption: polymer dip and spin coating

In the previous sections, strategies to render silicon nitride surfaces hydrophilic or hydrophobic have been presented. However, we also investigated other ways to modify silicon nitride making use of polymers. A summary of the outcome of our investigation with the different methods and polymers is shown in Table 4 at the end of this chapter.

Pluronic (PEO-PPO-PEO) block copolymers

Polymers containing Polyethyleneglycol, PEG (also called Polyethyleneoxide, PEO), in their basic structure are expected to be good candidates as coatings to increase hydrophilicity and prevent/reduce protein adhesion [40-42]. An example of such polymers are Pluronic block copolymers, which can consist of ethylene oxide (EO) and propylene oxide (PO) monomers arranged in three blocks: the central one (PO), which is more hydrophobic, and the end EO hydrophilic tails. The most likely mechanism of adsorption of these surfactants on hydrophobic surfaces is mainly through the PPO block [43]. For hydrophilic surfaces, at low polymer equilibrium concentrations both PEO and PPO segments lie flat on the surface, while at higher concentrations there is competition between the different blocks. Due to such competition, the most hydrophilic blocks are forced to be exposed to the solution forming so-called brushes [44, 45]. Since some authors [46-48] reported that Pluronic brushes are easy to apply and low protein binding was observed on surfaces that were treated with such coatings, we applied the same treatment to silicon nitride dices.

The scattering of contact angles on dices that were not oxidized prior to coating indicated the poor reproducibility and homogeneity of the coating method. Plasma treated samples coated with F108 and F127 exhibited very low contact angles, very similar to the values obtained with plasma treated dices. We observed that, when taken out of the Pluronic solution, they were fully wetted by the polymer. However, when rinsing with water, wettability changed substantially because the thin liquid layer on the surface was fastly removed. Since the mechanism of Pluronic adhesion is physical adsorption, it seems quite probable that polymer adhesion is so weak on the smooth silicon nitride dices that the chains can be easily desorbed when the samples are rinsed in water. Other works report similar observations on silica surfaces [44], where only a very thin layer of Pluronics was detected. The reason for the low adsorption is again the equilibrium of adsorption-desorption of the polymeric 'brushes'.

PEG-PEI polyelectrolyte layers

Adding polyelectrolyte layers by ionic bonding is an alternative method to attach charged polymers that can be functionalized with PEG segments [49]. PEG segments can render surfaces hydrophilic and are able to repel proteins [41, 50]. The synthesized polymer with

polyethylene imine and methoxy poly(ethylene glycol) was successfully attached to oxidized silicon nitride, forming a layer of approximately 5 nm detected by XPS. The XPS data confirmed the presence of the polymer on silicon nitride, since the carbon percentage increased from 3% (plasma treated dices) to 20%, and the nitrogen percentage from 4% to almost 8%. Advanced element analysis of C and N confirmed the presence of the C peaks belonging to C-N (PEI), C-O (PEG) and a very small peak that seemed to correspond to C=O. For nitrogen three N peaks were detected (one from the nitride, PEI and N-O, probably from the oxidized substrate). The coated dices were hydrophilic ($\theta=30^\circ$), however, the stability of the layer was very limited. Contact angles increased in time when stored in air, water and acid media. In 0.1 M NaOH, the coating and even silicon nitride etched away after 15 days of storage.

Polymer spin coating

Deposition of polymers on surfaces can also be achieved by spin coating a polymer solution on a substrate. In our case, PES, PES-PEO and PEO-PBT copolymers and a blend of PES/PVP were used. A pre-treatment with oxygen plasma was always required for coating experiments in order to enhance wetting of the substrate.

Contact angles for these samples were also measured. Experimental data show that the contact angles for PES coated surfaces are around 80° . For the copolymer PES-PEO slightly lower angles were measured, although there was a large scattering of the data. By using a PES/PVP blend and increasing the PVP ratio, lower contact angles were obtained ($50-60^\circ$). The PEO-PBT copolymer also exhibited angles around 50° .

PES-based polymers are not hydrophilic in nature due to their aromatic moieties in the backbone. However it is possible to modify a polymer surface and render it more hydrophilic. Park *et al.* [51] reported a method to hydrophilize Polysulfone membranes and render them hydrophilic and more protein resistant than the unmodified material. In their research, oxygen plasma was used to introduce hydroxyl, carbonyl and carboxyl groups on the surface. The modified membranes performed much better in terms of water and gelatine permeability. Although the material and membrane morphology used by Park were different than our films, we had several indications that the method would also be applicable for dense films of polyethersulfone.

Several films of PES were prepared and placed in the oxygen plasma reactor at different RF power and times. The water contact angle was measured just before, just after and after a few days of treatment. Also SEM pictures were taken to determine if the treatment damaged the surface (too aggressive plasma could etch the polymer surface). The most optimal treatment was obtained by treating a PES sample at 500 W during 1 minute; with this treatment no

surface damage was observed and temporary hydrophilization was successful. Figure 2 shows the contact angle of a PES film after plasma treatment stored in air during two months. An increase of the contact angles was observed in time, however, after 60 days the final contact angle was still 20° lower than the one for the unmodified PES.

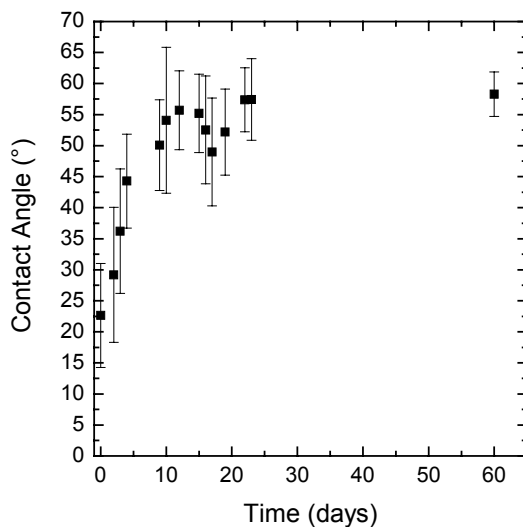


Figure 2. Contact angles as a function of storage time, for a plasma- treated PES film stored in air.

Hydrophilicity can be one of the requirements for the desired coating, however, stability is also a very important parameter that must be taken into account. Therefore, we measured the contact angles of the coated layers in different media (water, acidic solution at pH=2 and basic solution at pH=13) at room temperature for several days. The results showed that all polymers used in the spin coating experiments were stable in aqueous solutions, except PEO-PBT. This polymer swelled and detached from the silicon nitride surface. All polymers (PES, PES-PEO, PES/PVP) were stable under acidic conditions, and relatively stable under caustic conditions. After the stability measurements no delamination from the surface was observed, only a decrease in the contact angle values of the surfaces immersed in the alkaline solutions, due to oxidation and dissolution of the polymers.

Because the coatings obtained with the previous polymers were the most promising from the three tested in terms of stability, we investigated their feasibility on microsieves. One of the drawbacks of coating porous media by spin coating is pore blockage. When the viscosity of the polymer solution is relatively high the polymer cannot coat the pores homogeneously and blockage will occur. In our case the coating parameters were optimized. The most optimal

results were obtained using 0.3 wt% polymer concentration, 4000 rpm as spinning velocity and 60 s as spinning time.

To illustrate the effect of pore blocking, Figure 3 shows SEM images of coated microsieves with solutions with different polymer concentrations.

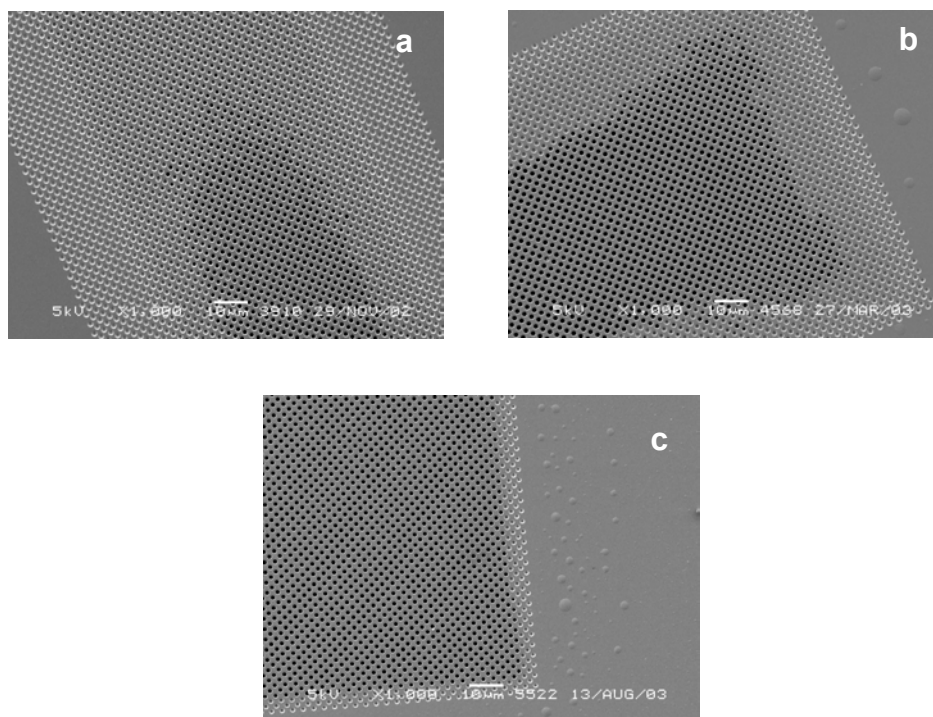


Figure 3. SEM images of microsieve pore grids coated with 10% (a), 1% (b) and 0.3 % (c) PES 6020 solutions. The light gray areas indicate pores blocked by a polymer layer; when more diluted polymer solutions are used less pore blockage is observed. The white horizontal bar indicates 10 μm .

Here it is clearly seen that lower polymer concentration results in less pore blockage. The structures obtained with 0.3 wt% polymer could possibly fulfill our expectations, however, the effective membrane area is reduced at the edge of the porous grid.

These polymers were, moreover, stable in aqueous conditions when coated on microsieves. Preliminary filtrations were performed and, after microscope inspection, the polymer was still present. Therefore no delamination took place.

The thickness of the coated polymer is however still an issue to be optimized, since it is approximately few hundreds of nm. Ideally, a very thin coating (polymer monolayer, few nm thick) would be more desirable in order to avoid pore blocking or narrowing.

A summary of all the materials and outcomes of the coatings used in this chapter is presented in Table 4. Here the material description, together with the contact angle, thickness (when measured) and additional comments about stability are presented.

Table 4. Summary of the properties of all coatings investigated in this chapter (chemical formula or structure created on silicon nitride, type of material used, contact angles, thickness determined by ellipsometry or XPS and additional information such as stability and homogeneity).

Coating	Chemical Formula ----- Structure on Si _x N _y	Type	θ (°)	d _{exp} (nm)	Comments
OXIDE		-	≈ 0	5-10	Very homogeneous but temporary hydrophilizing method. Stable in air only for a day (adsorption of contaminants).
FOTS	$(CF_3)(CF_2)_2(CH_2)_2-SiCl_3$	Fluka >97%	105 (liq) 112 (vap)	1.7	Very homogeneous, hydrophobic coating. Stable in water, acids and alkali solutions until pH=11.5 and 80°C.
Pluronics		F 108 F 127	≈ 30 (Si _x N _y) ≈ 15 (O ₂ -Si _x N _y) ≈ 35 (Si _x N _y) ≈ 15 (O ₂ -Si _x N _y)	-	Low homogeneity and adhesion. Detachable in water. Low reproducibility on unmodified Si _x N _y . Contact angles depend on substrate. Low homogeneity and adhesion. Detachable in water. Low reproducibility on unmodified Si _x N _y . Contact angles depend on substrate.
PEG-PEI		MeO- PEG 5000	30	5-10	Polymer detectable by XPS (detection of ≠ C, N bonds). Ionic bonding between oxidized Si _x N _y and polyimine, very unstable.
PES		6020	80	100 nm	Increased adhesion on oxidized Si _x N _y . Thermally and chemically stable coating. Can be temporary hydrophilized.
PES-PEO		RTN 6622/1	60-75		Increased adhesion on oxidized Si _x N _y . Stable in water and acids, relatively stable in alkalis.
PEO-PBT		60% PEO 40% PBT	50		Increased adhesion on oxidized Si _x N _y . Film detaches from Si _x N _y in water, due to swelling and water adsorption PEO.
PES/PVP		6020/ PVP K90	50-60		Increased adhesion on oxidized Si _x N _y . Stable in water and acids, relatively stable in alkalis. Tuneable hydrophilicity.

2.4 Conclusions

It is possible to modify a silicon nitride surface changing its physical and chemical properties by the strategies presented in this chapter. To create very hydrophilic surfaces oxygen plasma is a very suitable method, since a very homogeneous oxide layer between 5-10 nm can be grown on silicon-based materials. Hydrophilicity, however, can only be maintained for a limited time (ex. 2 days) because contaminants present in the atmosphere can adsorb on the oxide and change the surface properties drastically. To obtain very hydrophobic surfaces ($\theta > 100^\circ$) silanization with perfluorinated chlorosilanes provides a good option.

Polymeric coatings applied by physical adsorption give not such positive results in terms of stability and homogeneity. Both Pluronic coatings and PEG-PEI adducts are not even stable in aqueous solutions since they desorb upon rinsing.

Spin coating is a versatile method because it enables the use of a great range of polymers. Nevertheless, the biggest limitation of the method lies on the application on porous materials. Permanent hydrophilicity and thickness control to avoid pore blocking are issues that can be a great drawback if such coatings have to be applied on microfabricated devices like microsieves. The study of the microsieve performance as a function of hydrophilicity is the goal of the next chapter.

2.5 Acknowledgements

The author would like to acknowledge Dr. Herbert Wormeester, from the Applied Optics Group (University of Twente) for performing the ellipsometric measurements. Dr. Bernd Krause, from Gambio GmbH (Germany) is acknowledged for kindly providing the PES-PEO block copolymer; Wietze Nijdam (Aquamarijn B.V.) is acknowledged for providing the silicon nitride dices.

2.6 References

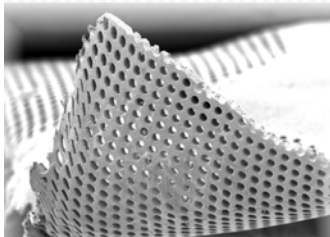
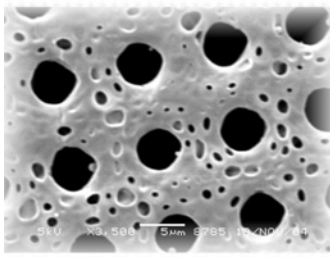
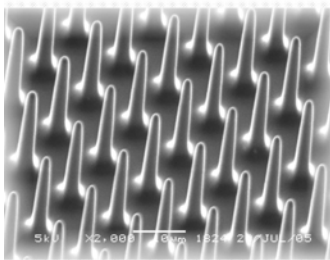
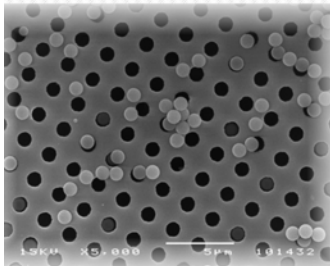
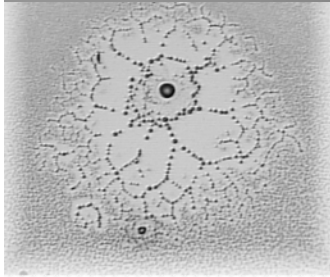
- [1] M. Madou, Fundamentals of Microfabrication, CRC Press, New York, 1997.
- [2] P.J. French, P.M. Sarro, R. Mallée, E.J.M Fakkeldij, R.F. Wolfenbittel, Optimization of a low-stress silicon nitride process for surface-micromachining applications, Sens. Actuators A 58 (1997) 149.
- [3] L.S. Zamboni, R.D. Mansano, R. Furlan, Silicon nitride deposited by inductively coupled plasma using silane and nitrogen, Vacuum 65 (2002) 213.
- [4] A.J. Lowe, M.J. Powell, S.R. Elliot, The electronic properties of plasma-deposited films of hydrogenated amorphous SiN_x (0 < x < 1.2), J. Appl. Phys. 59 (1986) 1251.
- [5] J.C. Barbour, H.J. Stein, O.A. Popov, M. Yonder, C.A. Outten, Silicon nitride formation from a silane-nitrogen electron cyclotron resonance plasma, J. Vac. Sci. Technol. A 9 (1991) 480.

- [6] Y. Kuo, PECVD silicon nitride as a gate dielectric for amorphous silicon thin film transistor process and device performance, *J. Electrochem. Soc.* 142 (1995) 186.
- [7] M. Krüger, R. Arens-Fischer, M. Thönissen, H. Münder, M. G. Berger, H. Lüth, S. Hilbrich and W. Theiss, Formation of porous silicon on patterned substrates, *Thin Solid Films* 276 (1996) 257.
- [8] V.I. Belyi, *Silicon nitride in electronics*, Elsevier Science, Amsterdam, 1988.
- [9] P. Pan, W. Berry, The composition and physical properties of LPCVD silicon nitride deposited with different $\text{NH}_3/\text{SiH}_2\text{Cl}_2$ gas ratios, *J. Electrochem. Soc.* 132 (1985) 3001.
- [10] M. Schwartz, *Handbook of structural ceramics*, McGraw-Hill, New York, 1992.
- [11] J.F. Shackelford, W. Alexander, *CRC Materials Science and Engineering Handbook*, CRC Press, Boca Raton, 2001.
- [12] R.J Pugh and L. Bergström, *Surface and colloid chemistry in advanced ceramics processing*, Marcel Dekker, New York, 1994.
- [13] M.N. Rahaman, Y.Boiteux, L.C.de Jonghe, Surface characterization of silicon nitride and silicon carbide powders, *Am. Ceram. Soc. Bull.* 65 (1986) 1171.
- [14] J. Szepvolgyi, I. Mohai, J. Gubicza, Atmospheric ageing of nanosized silicon nitride powders, *J. Mater. Chem.* 11 (2001) 859.
- [15] T. Mikolajick, R. Kuhnhold, R. Schnupp, H. Ryssel, The influence of surface oxidation on the pH-sensing properties of silicon nitride, *Sens. Actuators B* 58 (1999) 450.
- [16] D. Leonard, Y. Chevolot, O. Bucher, H. Sigrist, H. J. Mathieu, TOF-SIMS and XPS study of photoactivatable reagents designed for surface glycoengineering, *Surf. Interface Anal.* 26 (1998) 783.
- [17] B. Pignataro, G. Grasso, L. Renna, G. Marletta, Adhesion properties on nanometric scale of silicon oxide and silicon nitride surfaces modified by 1-octadecene, *Surf. Interface Anal.* 33 (2002) 54.
- [18] Y. Uyama, K. Kato, Y. Ikada, Surface modification of Polymers by grafting, *Adv. Polym. Sci.* 37 (1998) 1.
- [19] L. Yan, W.T.S. Huck, G. M. Whitesides, Self-assembled monolayers (SAMs) and synthesis of planar micro- and nanostructures, *J. Macromol. Sci.* 44 (2004) 176.
- [20] D. Everhart, Self-assembling monolayers: alkane thiols on gold, in K. Holmberg's *Handbook of Applied Surface and Colloid Chemistry*, Wiley, New York, 2001.
- [21] R.C. Chapman, E. Ostuni, M.N. Liang, G. Meluleni, E. Kim, L. Yan, G. Pier, H. S. Warren, G. M. Whitesides, Polymeric thin films that resist the adsorption of proteins and the adhesion of bacteria, *Langmuir* 17 (2001) 1225.
- [22] R. Maboudian, W.R. Ashurst, C. Carraro, Self-assembled monolayers as anti-stiction coatings for MEMS: characteristics and recent developments, *Sens. Actuators B* 82 (2000) 219.
- [23] M. Sugawara, *Plasma etching: fundamentals and applications*, Oxford Univeristy Press, New York, 1998.
- [24] N. Inagaki, *Plasma surface modification and plasma polymerization*, Technomic, Lancaster, 1996.
- [25] A. Hozumi, K. Ushiyama, H. Sugimura, O. Takai, Fluoroalkylsilane monolayers formed by chemical vapor surface modification on hydroxylated oxide surfaces, *Langmuir* 15 (1999) 7600.
- [26] H. Derand, A. Larsson, J. Van Alstine, *Microfluidic surfaces*, WO 01/47637, 2001.
- [27] L.T. Canham, M.R. Houlton, W.Y. Leong, C. Pickering, J.M. Keen, Atmospheric impregnation of porous silicon at room temperature, *J. Appl. Phys.* 70 (1991) 422.
- [28] F. Lukes, Oxidation of Si and GaAs in air at room temperature, *Surf. Sci.* 30 (1972) 91.
- [29] S.I. Raider, R. Flitsch, M.J. Palmer, Oxide growth on etched silicon in air at room temperature, *J. Electrochem. Soc.* 122 (1975) 413.
- [30] L.J. Bousse, S. Mostarshed, D. Hafeman, Combined measurement of surface potential and zeta potential at insulator/electrolyte interfaces, *Sens. Actuators B* 10 (1992) 67.
- [31] D. Leonard, Y. Chevolot, O. Bucher, H. Sigrist, H.J. Mathieu, TOF-SIMS and XPS study of photoactivatable reagents designed for surface glycoengineering, *Surf. Interface Anal.* 26 (1998) 783.

- [32] T. Mikolajick, R. Kuhnhold, R. Schnupp, H. Rysse, The influence of surface oxidation on the pH-sensing properties of silicon nitride, *Sens. Actuators B* 58 (1999) 450.
- [33] B. Pignataro, G. Grasso, L. Renna, G. Marletta, Adhesion properties on nanometric scale of silicon oxide and silicon nitride surfaces modified by 1-octadecene, *Surf. Interface Anal.* 33 (2002) 54.
- [34] J. Szepvolgyi, I. Mohai, J. Gubicza, Atmospheric ageing of nanosized silicon nitride powders, *J. Mater. Chem.* 11 (2001) 859.
- [35] S.T. Patton, K.C. Eapen, J.S. Zabinski, Effects of adsorbed water and sample aging in air on the $[\mu\text{J}]\text{N}$ level adhesion force between Si(100) and silicon nitride, *Tribol. Int.* 34 (2001) 481.
- [36] L.T. Yin, J.C. Chou, W.Y. Chung, T.P. Sun, S.K. Hsiung, Characteristics of silicon nitride after O_2 plasma surface treatment for pH-ISFET applications, *IEEE Transactions on Biomedical Engineering* 48 (2001) 340.
- [37] R. Maboudian, W.R. Ashurst, C. Carraro, Tribological challenges in micromechanical systems, *Tribol. Letters* 12 (2002) 95.
- [38] B.C. Bunker, R.W. Carpick, R.S. Assink, M.L. Thomas, M.G. Hankins, J.A. Voigt, D. Sipola, M.P. de Boer, G.L. Gulley, The impact of solution agglomeration on the deposition of self-assembled monolayers, *Langmuir* 16 (2000) 7742.
- [39] M.J. Geerken, T.S. van Zanten, R.G.H. Lammertink, Z. Borneman, W. Nijdam, C.J.M. van Rijn, M. Wessling, Chemical and thermal stability of alkylsilane based coatings for membrane emulsification, *Adv. Eng. Mater.* 6 (2004) 749.
- [40] B.E. Rabinow, Y.S. Ding, C. Qin, M.L. McHalsky, J.H. Schneider, K.A. Ashline, T.L. Shelbourn, R.M. Albrecht, Biomaterials with permanent hydrophilic surfaces and low protein adsorption properties, *J. Biomater. Sci. Pol Ed.* 6 (1994) 91.
- [41] J.M. Harris, *Poly (ethylene) glycol Chemistry-Biotechnical and Biomedical Applications*, Plenum Press, New York, 1995.
- [42] P. Kingshott and H.J. Griesser, Surfaces that resist bioadhesion, *Curr. Opin. Solid State Mater. Sci.* 4 (1999) 403.
- [43] J.A. Shar, T.M. Obey, T. Cosgrove, Adsorption studies of polyethers. Part 1: Adsorption onto hydrophobic surfaces, *Colloids Surf. A* 136 (1998) 21.
- [44] P. Alexandridis, T.A. Hatton, Poly(ethylene oxide)-poly(propylene oxide)-poly(ethylene oxide) block copolymer surfactants in aqueous solutions and at interfaces: thermodynamics, structure, dynamics and modelling, *Colloids Surf. A* 96 (1995) 1.
- [45] J.A. Shar, T.M. Obey, T. Cosgrove, Adsorption studies of polyethers. Part 2: Adsorption onto hydrophilic surfaces, *Colloids Surf. A* 150 (1999) 15.
- [46] C. L. Ng, H. K. Lee *et al.*, Prevention of protein adsorption on surfaces by polyethylene oxide-polypropylene oxide-polyethylene oxide triblock copolymers in capillary electrophoresis, *J. Chromatogr. A* 659 (1994) 427.
- [47] R.J. Green, M.C. Davies, C.J. Roberts, S.J.B. Tendler, A surface plasmon resonance study of albumin adsorption to PEO-PPO-PEO triblock copolymers, *J. Biomed. Mater. Res.* 42 (1998) 165.
- [48] S.M. O'Connor, A.P. De Anglis, S.H. Gehrke, G.S. Retzinger, Adsorption of plasma proteins on to poly(ethylene oxide)/poly(propylene oxide) triblock copolymer films: a focus on fibrinogen, *Biotechnol. Appl. Biochem.* 31 (2000) 185.
- [49] E. Kiss, C.G. Gölander, J.C. Eriksson, Surface grafting of polyethyleneoxide optimized by means of ESCA, *Progr. Colloid Polymer Sci.* 74 (1987) 113.
- [50] K. Holmberg, K. Bergström, C. Brink, E. Österberg, F. Tiberg, J.M. Harris, Effects on protein adsorption, bacterial adhesion and contact angle of grafting PEG chains to polystyrene, *J Adhes. Sci. Technol.* 7 (1993) 503.
- [51] K.S. Kim, K.H. Lee, K. Cho, C.E. Park, Surface modification of polysulfone ultrafiltration membrane by oxygen plasma treatment, *J. Membr. Sci.* 199 (2002) 135.

Chapter 3

The role of wetting on the
water flux performance of
 Si_xN_y microsieves



3.1 Introduction

Ideally, a microfiltration membrane should combine high porosity and a well-defined pore size, with a thin selective layer. However, as we mentioned in Chapter 1, conventional polymeric microfiltration membranes do not always fulfill these requirements and suffer from the trade-off between permeability and selectivity. Consequently, there is a great need for an alternative to the traditional membranes used in industry. Specialty high-flux membranes such as microsieves can be a new choice for several applications in the membrane field. They present a very well-controlled structure and pore size; their high porosity leads to very high fluxes and they can be operated at extremely low pressures, therefore providing an energy and economically friendly process.

Silicon nitride microsieves are produced by techniques well known in the semiconductor industry, including standard mask lithography or laser interference lithography [1, 2]. Although they present ideal structural properties, the material they are made of is not completely inert, as demonstrated in the previous chapter and recent work [3]. Silicon nitride surfaces are very sensitive to chemical compositional changes such as oxidation [3-5] or contaminant adsorption. That is why microsieve surfaces have to be tailored so that they can be applied in aqueous (milk defatting, water purification in cleanrooms, etc.) as well as non-aqueous (solvent purifications, water-in-oil emulsifications, etc.) applications. In chapter 2, a series of surface modification methods were studied to modify the surface properties of silicon nitride.

Wetting of such microfabricated architectures is a very important aspect in order to obtain the maximum membrane performance. An incorrect wetting procedure would have consequences for the final process, causing a loss in performance translated in flux decline and flux instabilities caused by air bubbles, for instance [6]. Wetting and control of surface properties is not only crucial in membrane technology but also in applications that use the ability of a liquid to either dewet or wet a surface. For instance, complex architectures such as Micro-Electro-Mechanical Systems (MEMS), microfluidic devices, biochips or miniaturized sensors can be fabricated by controlling wettability [8-10]. These devices are normally manufactured by surface patterning techniques such as soft lithography, self-assembly or pattern replication [11-13]. Wettability is also important in inkjet printing applications, for instance.

The main goal of this chapter is to study the influence of the surface properties on the microsieve performance in aqueous media, as well as the establishment of parameters that can disturb the flux or induce flux decline in aqueous systems. Unmodified, hydrophilized and hydrophobized microsieves will be used as model surfaces to study the influence of several parameters such as wetting procedure and feed composition on the membrane performance.

3.2 Fabrication and structure of Si_xN_y microsieves

Inorganic microsieve membranes are used for several microfiltration applications such as milk or beer filtration [14], since their development a decade ago [1, 2, 15-17]. As their name indicates, they can retain the desired components by sieving, with the aid of very well-defined pores. Some of their characteristics are: a very thin selective silicon nitride layer (approx. 1 μm), narrow pore size distribution, tunable pore size and shape and extremely high fluxes. All these properties make them revolutionary membranes in microfiltration due to their optimal size discrimination, low operational costs and low operating pressures.

The most common techniques to fabricate microsieves are standard mask lithography, used to produce membranes with pore sizes larger than 1 μm , and laser-interference lithography (for production of microsieves with pores smaller than 1 μm). The detailed process used by Fluxxion B.V. to fabricate the microsieves used in this thesis is depicted in Figure 1.

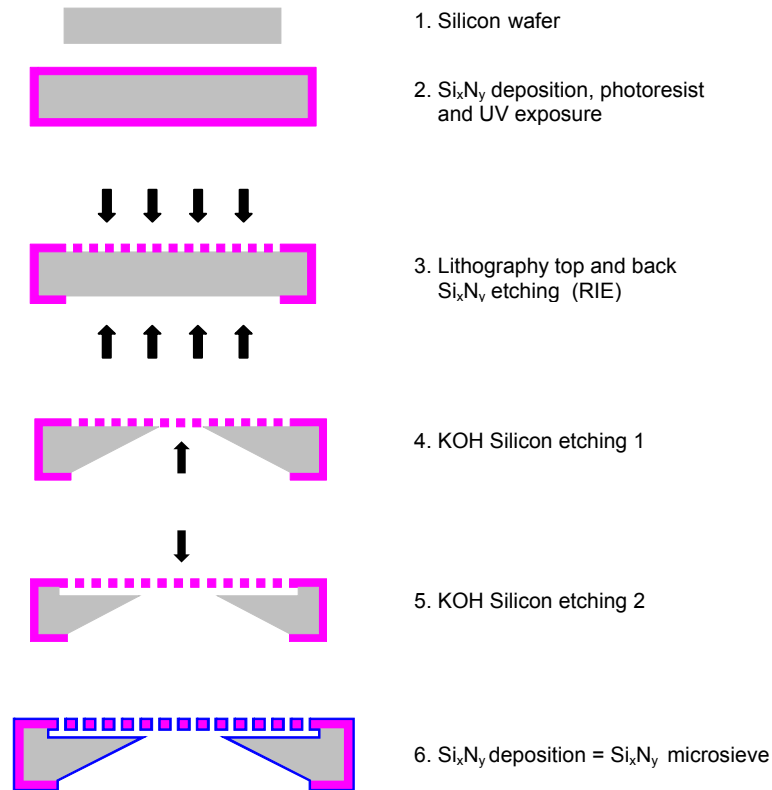


Figure 1. Fabrication process of a silicon nitride microsieve by standard mask lithography (Process scheme supplied by Fluxxion B.V).

In standard mask lithography a 1 μm low-stress silicon nitride is deposited on a standard silicon wafer by LPCVD. Then a photoresist layer is spin coated on top and exposed to UV light through a photomask. After development the pattern will then be transferred to the silicon nitride layer by means of RIE (Reactive Ion Etching) with a CHF_3/O_2 -plasma (step 3). To create the free open pores and the support bars underneath the sieve structure, the silicon wafer is then etched in KOH from the top and the bottom (steps 4 and 5) [1]. The final step (6) is the deposition of a silicon nitride layer. According to Kuiper et al. [17, 18], the previous method is not suitable to fabricate microsieves with pores smaller than 1 μm , due to the limitations of UV light. In this case, laser-interference lithography is recommended, since it can create regular patterns with feature sizes smaller than the wavelength of the light source [17]. The microsieves used in our research have an effective area of 1 cm^2 and 8 million pores. Each microsieve consists of 16 identical sieving beds that contain 10 pore grids (2000x115 μm), with approx. 51000 pores per grid. In Figure 2 a sieve bed (a), a pore grid (b), the pore morphology (c) and the membrane layer (d) of microsieves used in this work are displayed.

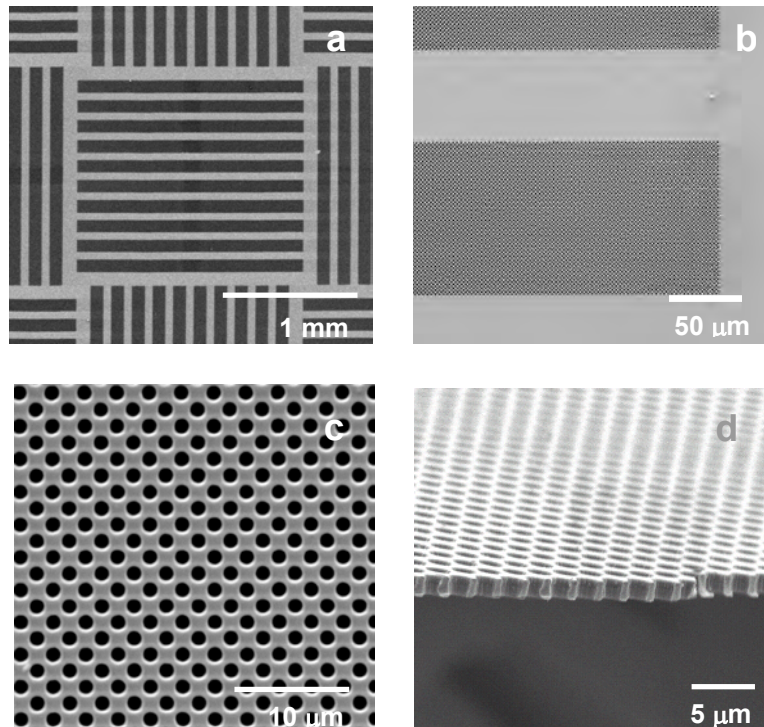


Figure 2. SEM images of a silicon nitride microsieve surface, (a) sieve bed, (b) pore grid, (c) close-up of pores, and (d) cross-section of the porous layer.

These microsieves have a pore size of 1.2 micrometers, a calculated porosity of 9 % and a pitch of 2.12 micrometers.

SEM images of the middle and edge of a grid are shown in Figure 3. Each grid (160 in total in every microsieve) has a 20-30 μm channel underneath, which is shown in Figure 3a (the top pore layer was deliberately taken off to display the channel). In a pore grid, only an area of approx. 200x115 μm (10% of the total pore population) is situated directly above the permeate outlet. The rest of the pores are situated above permeate channels that lead to the outlet.

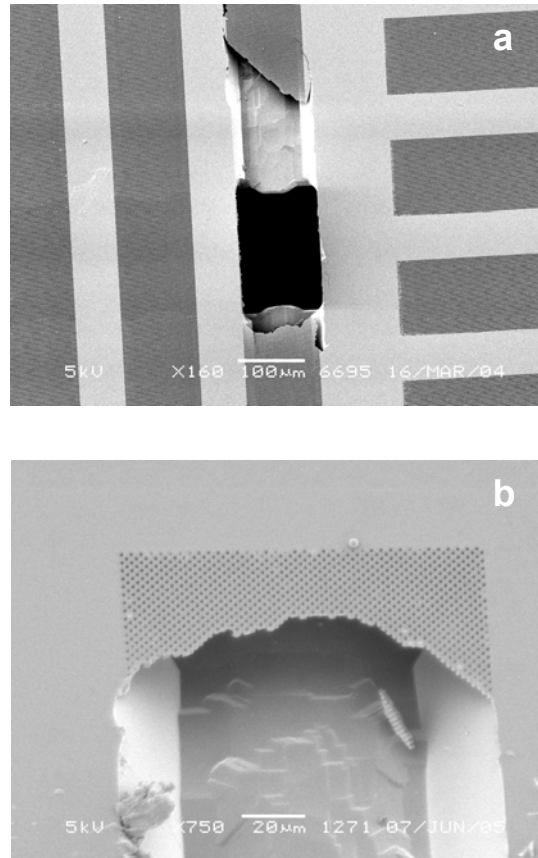
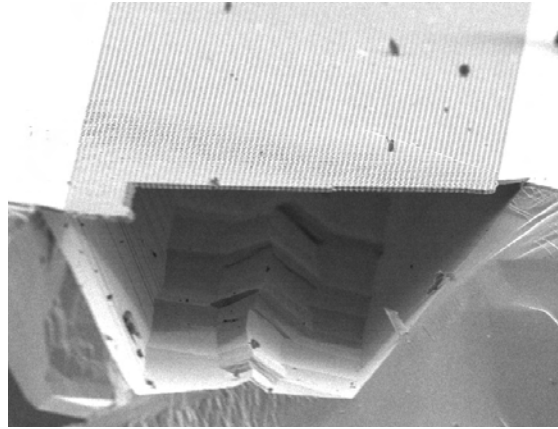
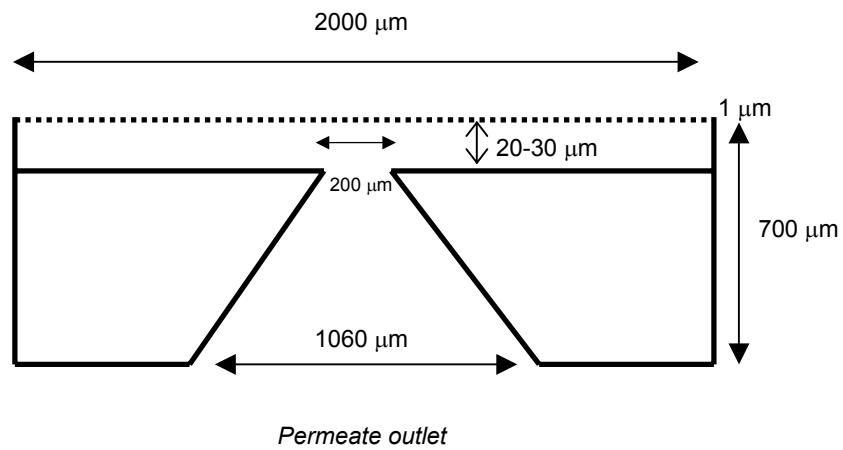


Figure 3. SEM images of a pore grid. In (a) the middle of a grid and permeate channel are shown, in (b) the edge of a grid is displayed. In both cases the pore layer has been removed to display the channel.

A cross-section of the microchannel is also displayed in Figure 4a. The lengthwise cross-section of one grid (Figure 4b) shows the channel beneath the top pore layer in detail. In a filtration, the fluid permeating the pores is collected and redirected to the middle of the grid (permeate outlet).



(a)



(b)

Figure 4. Cross-sectional SEM image of the edge of a pore grid (a) and schematic cross-section and dimensions of a grid or middle of sieving bed (b).

3.3 Materials and methods

3.3.1 Materials

Unmodified (silicon-rich silicon nitride, Si_xN_y), hydrophilized (oxygen plasma treated) and hydrophobized (FOTS coated) porous microsieve membranes, $1 \times 1 \text{ cm}^2$, were used for clean water flux measurements.

Ultrapure water ($18.2 \text{ M}\Omega\text{cm}$) for flux measurements was obtained with a Millipore purification unit (MilliQ plus). Isopropanol (IPA) and ethanol were used as wetting agents.

3.3.2 Wetting and Flux Measurements

The clean water permeability of microsieves was measured in the pressure range of 0.03-0.15 bar at $20 \pm 2^\circ\text{C}$ in crossflow mode.

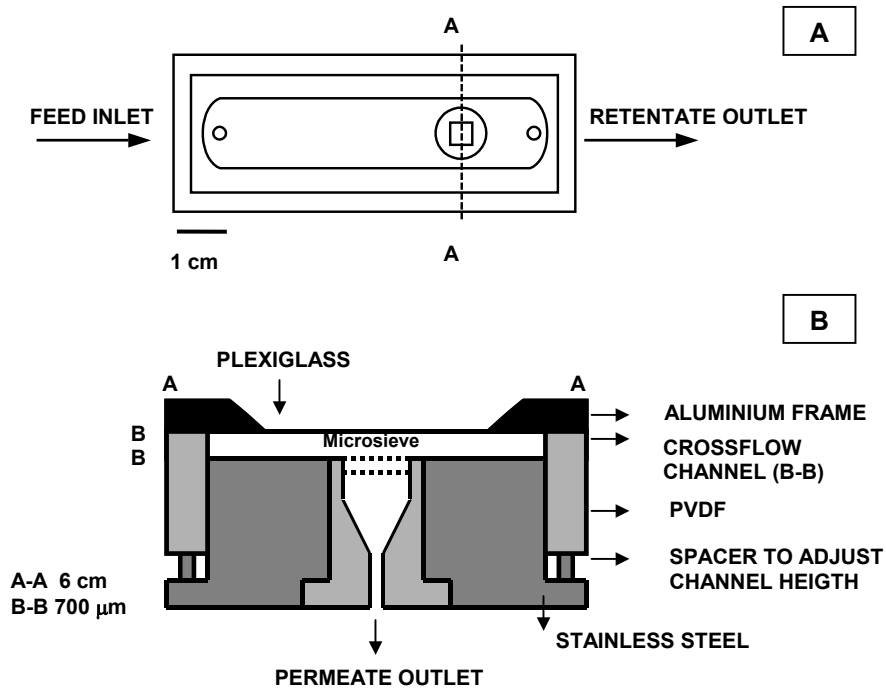


Figure 5. Schematic representation of the crossflow module used for the water flux measurements. Top view (a) and cross-section (b) of the permeation cell.

The permeation experiments were performed using a crossflow module with an effective membrane area of $1 \times 10^{-4} \text{ m}^2$ ($1 \times 1 \text{ cm}^2$ samples) and a crossflow channel height of $700 \text{ }\mu\text{m}$. A schematic representation of the module is shown in Figure 5.

Microsieves with different surface properties were used. Clean ultra pure MilliQ water was used as feed. The feed water was pre-treated with a degassing step for some experiments, while for other tests a gas flow was introduced in the feed, to saturate the water with air. In all tests, water was fed to the membrane module using a gear pump, as shown in Figure 6. A commercial Schleicher & Schuell $0.45 \text{ }\mu\text{m}$ Nylon pre-filter (FP 50/0.45 NL-QF20) was placed before the module to exclude any possible feed contamination.

To investigate the microsieve performance as a function of the wetting and system variables, water flux results can be expressed as relative permeability:

$$\text{Relative permeability (-)} = P_w / P_{w,\text{max}} \quad (1)$$

where P_w = water permeability at a given time, $P_{w,\text{max}}$ = maximum water permeability.

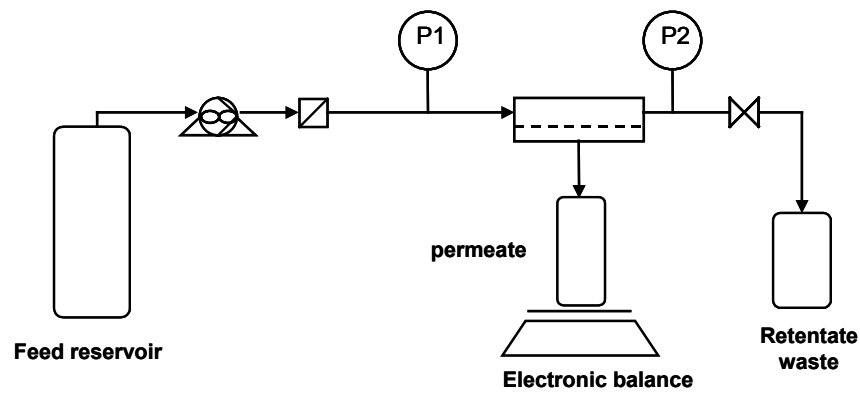


Figure 6. Schematic representation of the crossflow filtration set-up used for the water flux measurements.

Wetting the membrane depends on the properties of the liquid as well as the membrane material. The relationship between the minimum pressure Δp to be applied on the liquid to enter the pores of a membrane is given by the Laplace-Young equation [19-21]. Only if this breakthrough pressure is exceeded the liquid will penetrate the pore.

The pressure given by the Laplace-Young equation is:

$$\Delta p = \frac{-2\gamma_L \cos \theta}{r} \quad (2)$$

where γ_L is the surface tension of the liquid, θ is the contact angle of the liquid with the surface and r the membrane pore radius.

Equation 2 was used to estimate the bubble point of microsieves. Microsieve integrity was tested by visual control at the estimated pressures in low surface tension liquids, in order to detect possible defects. Microsieves were glued to a polysulfone holder and immersed in isopropanol ($\gamma=21.7 \times 10^{-3}$ N/m) or ethanol ($\gamma=22.8 \times 10^{-3}$ N/m). Pressure was applied from below the membrane; when bubbles were seen at lower pressures than the ones corresponding to the Laplace pressure determined by equation (2), the microsieve was discharged.

3.3.3 Microsieve inspection

Microsieve inspection before and after flux measurements was performed using a Zeiss optical microscope. For a more detailed inspection, microsieves were visualized by Scanning Electron Microscopy (SEM, Microscope JEOL JSM-5600LV, at 5 kV).

3.4 Results and discussion

3.4.1 Clean water flux measurement with unmodified microsieves

Equation 2 was used to estimate the bubble pressure of membranes with 1.2 μm pore diameter. For a pore radius of 0.6 μm , the pressure estimated for the gas to replace the liquid from the pores was 0.76 and 0.72 bar, for ethanol and isopropanol respectively ($\cos \theta=1$). Experimentally, bubble point pressures of 0.8 and 0.77 bar were measured, which indicates that this method is valid to determine the pore size of microsieves and eventually structural defects in the porous layer such as cracks or holes.

An average value of the water permeability was obtained for 1.2 μm microsieves, which was $3 \pm 0.5 \times 10^5$ l/m²hbar. In some cases, if lower permeabilities were obtained, it was due to microsieve imperfections in their structure.

Clean water fluxes for unmodified membranes were measured at an average crossflow velocity of 0.14 m/s (Area=1.75x10⁻⁵ m²). In these conditions, the Reynolds number was around 100 (laminar flow). The average fluid velocity in the pore is four times lower than the velocity at the pore entrance (0.14 and 0.04 m/s respectively).

The flow through a microsieve can be described by the Stokes flow, applicable at low Reynolds numbers. Van Rijn [1, 2] described the flow through thin wall like pores or cylindrical channels with length L and diameter d by the following equation:

$$J = \frac{n \cdot d_{pore}^3 \cdot \Delta p}{24 \cdot \mu \cdot A_m} \left[1 + \frac{16 \cdot L}{3\pi \cdot d_{pore}} \right]^{-1} [1 - f(\varepsilon)]^{-1} \quad (3)$$

where n is the number of pores, L and d_{pore} are the length and diameter of a pore, respectively, Δp is the applied pressure, μ is the solution viscosity, A_m represents the membrane area and ε is the porosity. The porosity function $f(\varepsilon)$ is defined as:

$$f(\varepsilon) = \sum_{i=1} a_i \varepsilon^{(2i+1)/2} \quad (4)$$

with $a_1= 0.894$, $a_2=0.111$ and $a_3=0.066$ [1]. For a silicon nitride microsieve with $L=1 \mu\text{m}$, $d_{pore}=1.2 \mu\text{m}$ and $\varepsilon= 0.09$, a permeability ($J/\Delta p$) of about $8.8 \times 10^5 \text{ l/m}^2\text{hbar}$ is obtained with this equation. The calculated permeability is almost three times higher than the measured water permeability. Just like Equation (3), the Hagen Poiseuille equation is not valid to describe the flow of a fluid through microsieve pore. Such equation assumes that the pore length is much higher than the pore radius, which is not the case for microsieves. Since the backstructure is not taken into account in neither of each equations, this could cause the overestimation of the permeability.

3.4.2 Specific wetting procedure for different microsieve surfaces

A specific wetting step is necessary before using any microsieves, which depends on the membrane surface properties. As discussed in Chapter 2, the modified surfaces present very different wettability characteristics (see Table 1).

Table 1. Contact angles of the surfaces used for the wetting experiments: unmodified (used as received), hydrophilized or oxidized by plasma and hydrophobized. For FOTS coated samples, two types of surface with different hydrophobicity were obtained depending on the coating procedure: hydrophobized-1 (coated in liquid FOTS) and hydrophobized- 2 (FOTS vapor deposition).

Surface used (Si_xN_y)	θ (°)
unmodified	50
oxygen plasma treated	≈ 0
Hydrophobized-1	105
Hydrophobized-2	112

All surfaces require different types of wetting: unmodified dices are best wettable with isopropanol (IPA), or IPA followed by a mixture of IPA/water 50/50; hydrophilized membranes are completely wettable with water, pure IPA and mixtures of water and isopropanol.

Hydrophobized microsieves are wettable if immersed in IPA for a prolonged time, e.g. 30 min or longer. Both types of hydrophobized sieves that had been initially immersed in water did not exhibit a measurable water flux during the same time frame and pressure compared to hydrophilized sieves (for a period of 10 minutes no flux could be measured).

According to equation 2, we can estimate the pressure needed to wet a pore with water ($\gamma_L=72.8 \times 10^{-3}$ N/m), in a FOTS-coated hydrophobic microsieve. For a pore radius of $0.6 \mu\text{m}$, minimum pressures of 0.62 and 0.89 bar are needed for complete water wetting, for surfaces with $\theta=105^\circ$ and 112° respectively. These calculations confirm the no-flux situation for water-immersed FOTS microsieves, since our working pressures were below 0.2 bar. The mechanisms behind phenomena such as pore activation or dewetting by air of hydrophobized microsieves will be discussed in detail in section 3.4.4.

A wetted or unwetted microsieve can also be visually identified. A partially wetted microsieve is presented in Figure 7a, where the lighter lines indicate dried pore grids and the darker zones fully wetted grids. The same microsieve, when fully wetted (darker colored), is shown in Figure 7b.

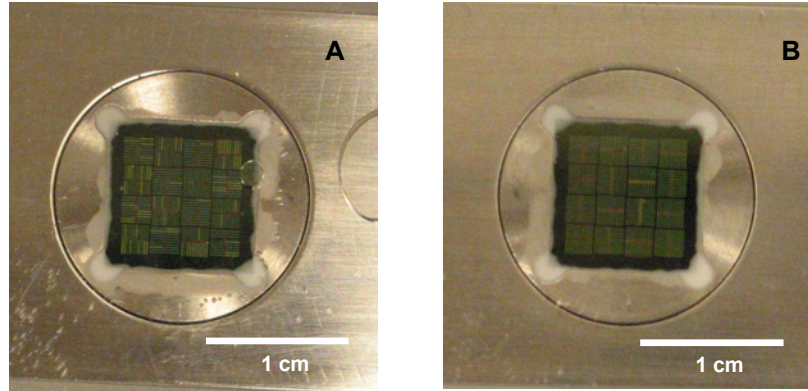


Figure 7. In-line optical images of the surface of a partially wetted (a) and a fully wetted (b) microsieve membrane.

3.4.3 Effect of water purity on flux performance

Due to the high product throughput, any undesired components in the system that can clog a pore will have a dramatic effect on the water flux. Even parameters extrinsically related to the membrane can play a crucial role. In a worst-case scenario the use of certain types of tubing and pump, for instance the combination of silicon tubing and a peristaltic pump, can diminish the water flux by 90% in 20 min, due to the fast deposition of contaminating material on the microsieve surface. An illustration of this effect is displayed in Figure 8.

After inspection under an optical microscope we could confirm that hydrophobic grease-like material covered the whole membrane surface. These results gave a clear indication that the use of a pre-filter would be necessary in order to study other parameters that can induce flux decline in clean water measurements

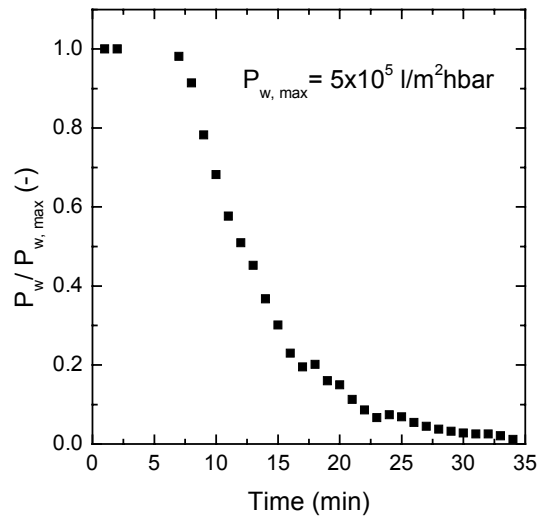


Figure 8. Fouling caused by the silicone tubing: Relative water permeability vs. time. Although the sieve used to illustrate this effect had slit-shaped pores ($0.8 \times 2.6 \mu\text{m}$) and higher porosity than the rest of the membranes used in this chapter, the same but slower effect was observed for the $1.2 \mu\text{m}$ round pores sieves.

Since surface wetting is crucial for achieving the maximum membrane performance in terms of flux, all membranes used were fully wetted with one or more appropriate wetting liquids. A pre-filter was placed in most of the occasions before the module to retain any contaminating particle and avoid phenomena such as in Figure 8.

At last, the composition of the feed water was also varied: for experiments where the influence of the pre-filter was studied, only untreated water was used; for tests where the influence on the air on the flux decline was the main target, either degassed or saturated water was used. In Table 2 an overview of the performed experiments is shown.

Table 2. Overview of the membrane surfaces used and the influence of the process parameters on the clean water flux stability. The microsieves tested are unmodified, hydrophilized and hydrophobized (Hydrophobized-Si_xN_y-1, with $\theta=105^\circ$, and Hydrophobized-Si_xN_y-2, with $\theta=112^\circ$). Three wetting procedures are used: a=IPA 100%+IPA/water 50/50, b=IPA 100% and c=water. The specifications for the water used in the filtrations stand for 1=untreated or directly taken from the MilliQ unit, 2=degassed and 3=saturated with air. P_{max}=maximum permeability, V_{1/2}=permeated volume at which flux has declined 50% and P_{loss} (%)=permeability loss, the subscript 1 indicates the initial permeability loss (first measuring point) and 2 the permeability loss caused by air after rewetting with isopropanol.

Code	Surface	Process parameters			Results		
		Wetting	Pre-filter	Water type	P _{max} [l/m ² hbar]	V _{1/2} [ml]	Remarks
A	Unmodified Si _x N _y	a	-	1	4.5x10 ⁵	1500	P _{loss} = 50%
B	Unmodified Si _x N _y	a	+	1	3.0x10 ⁵	-	stable and constant flux
C	Unmodified Si _x N _y	a	+	2	3.2x10 ⁵	-	stable and constant flux
D	Unmodified Si _x N _y	a	+	3	2.5x10 ⁵	-	stable and constant flux
E	Hydrophilized- Si _x N _y	b	+	1	4.6x10 ⁵	-	stable and constant flux
F	Hydrophilized- Si _x N _y	c	+	1	3.6x10 ⁵	-	stable and constant flux
G	Hydrophilized-Si _x N _y	c	+	2	2.5x10 ⁵	-	stable and constant flux
H	Hydrophilized-Si _x N _y	c	+	3	2.9x10 ⁵	-	stable and constant flux
I	Hydrophobized-Si _x N _y -1	b	-	3	2.0x10 ⁵	125	flux decline/fluctuations
J	Hydrophobized-Si _x N _y -1	b	+	3	0.6x10 ⁵	-	stable and constant flux
K	Hydrophobized-Si _x N _y -1	a	+	1	1.5x10 ⁵	-	(1.5 h wetted) stable flux
L	Hydrophobized-Si _x N _y -1	b	+	1	1.6x10 ⁵	-	(20' wetted) stable flux
M	Hydrophobized-Si _x N _y -2	b	+	1	3.6x10 ⁵	190	P _{loss} = 79% (air bubble)
N	Hydrophobized-Si _x N _y -2	b	+	1	3.6x10 ⁵	0	P _{loss1} =89%, P _{loss2} =54%
O	Hydrophobized-Si _x N _y -2	b	+	1	3.3x10 ⁵	0	P _{loss1} =51%, P _{loss2} =93%

The results are expressed in terms of maximum permeability (P_{max}) and permeated volume at which 50% or more of the permeability is lost ($V_{1/2}$); remarks are given in the cases where flux decline occurred.

As shown in Figure 9a, which illustrates the variation of permeability vs. permeated volume for experiments A and B, the use of a pre-filter was considered to be very important to exclude any contamination in the system because tests without pre-filter showed a great flux decrease in a short period of time caused by fouling (due to particles from the system). Further inspection of the membrane surface by SEM confirmed these results. If a pre-filter was used for hydrophilized membranes constant fluxes were measured, as seen in Figure 9b for test E. The same behavior was observed with fully wetted hydrophobized microsieves with contact angle around 105° .

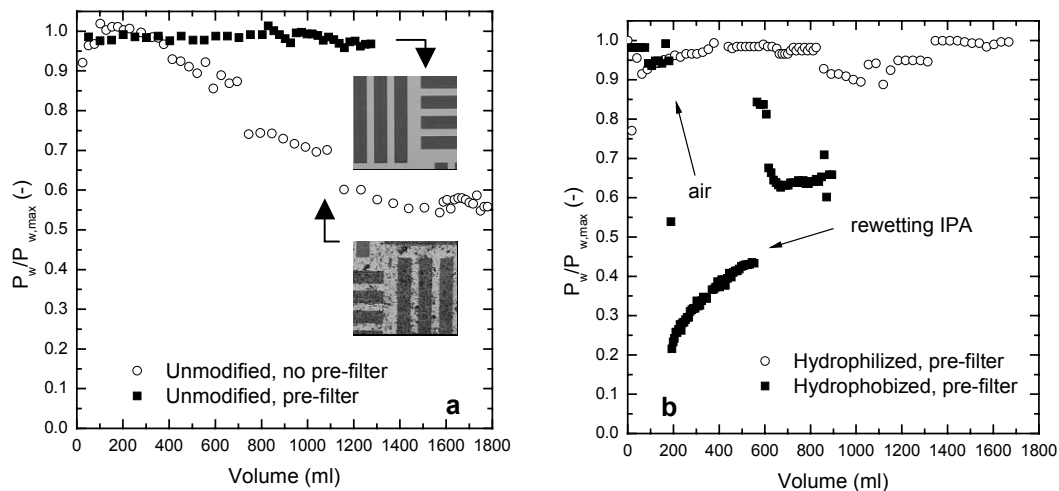


Figure 9. Relative clean water permeability vs. permeated volume of untreated water. (a) Effect of a pre-filter with unmodified microsieves and (b) permeability variation of a hydrophilized and hydrophobized ($\theta=112^\circ$) microsieve.

However, when highly hydrophobized surfaces ($\theta=112^\circ$) were tested, a different behavior was observed. Even if a proper wetting procedure with isopropanol was applied and the surface appeared to be wetted, in some cases no flux was measured at all. In other occasions like in test M, a stable and maximum water flux could be temporary obtained (see Figure 9b), until air from the system (air bubbles travelling along the module) strongly dewetted the membrane causing a dramatic permeability loss of 80%. Fluxes could be partially recovered if in-line wetting with isopropanol was applied, although this effect was not always successful.

Consecutive experiments with the same membrane (such as tests with codes M and N) were not reproducible because of dewetting of the permeate channels during the experiment.

No significant differences were observed between experiments performed with degassed or saturated water when a pre-filter was used and the surface was fully wetted. Flux measurements without pre-filter and saturated water as feed were unsuccessful to perform due to great pressure instabilities caused by big air bubbles and contaminating particles. Apart from the fact that the pre-filter influenced the amount of contamination present in the feed or in the system, it also varied the amount of air bubbles that flowed along the sieves in the case of saturated feed (large air bubbles collapsed on the polymeric pre-filter).

Bubble nucleation strongly depends on the concentration of dissolved gas in the system. We observed that, in the case of the most hydrophobic surfaces, nucleated air bubbles gave rise to severe flux decline. For the rest of the surfaces, air bubbles could nucleate and be retained inside the membrane module, which resulted in a temporary local pressure increase. In the case of fully wetted surfaces, this did not have major negative effects on the permeability, which remained constant and at its maximum value.

3.4.4 Effect of wetting procedure and air on hydrophobized microsieves

An extensive study was performed on the influence of the wetting procedure on the water flux of hydrophobized microsieves. Hydrophilized microsieves were not considered here, since complete wetting always occurred.

FOTS coatings produced in solution exhibited lower porosity due to the coating method, which probably caused some pore blocking. That resulted in lower water permeability values.

When hydrophobized microsieves with $\theta=105^\circ$ were partially wetted (by placing them only for a few minutes in IPA) the measured permeability experienced an increase as pressure increased. This clearly indicates that more pores are gradually being filled by water and more area is available for permeation (pore activation). When wetting is applied the pore activation mechanism may be as follows: if one part of the membrane is already filled with water and is in contact with both wetted and unwetted spots, water underneath the membrane will contact water above the pores, growing and collapsing together, gradually covering more surface.

In Figure 10 it can be seen how an increase of around 26% in relative water permeability takes place as water permeates through a hydrophobized microsieve for 30 min. In the experiment the pressure was increased in three steps (70, 87.25 and 122.5 mbar), and remained constant in each interval. The permeability increase can be attributed to pore activation. Rewetting of the same sieve with IPA for at least 1 hour led to three times higher flux and constant permeability around 0.61×10^5 l/m²hbar.

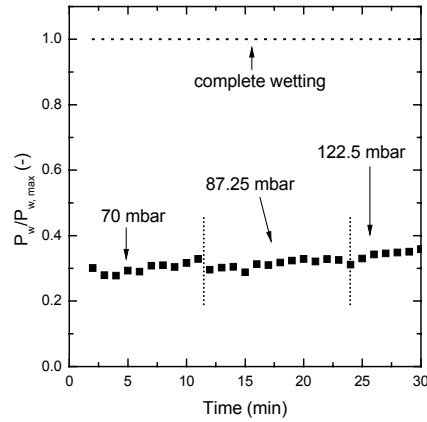


Figure 10. Relative clean water permeability for a hydrophobized microsieve, semi-wetted first (lower points) and completely wetted afterwards (upper line), achieving the maximum performance.

Figure 11 depicts the effect of partial wetting in detail. For a fully wetted hydrophobized membrane with maximum permeability of $1.75 \times 10^5 \text{ l/m}^2\text{hbar}$ the water flux remained constant beyond 1 hour. Afterwards, an off-line drying step was performed with a nitrogen flow, and a second wetting step was applied so that only partial wetting was achieved.

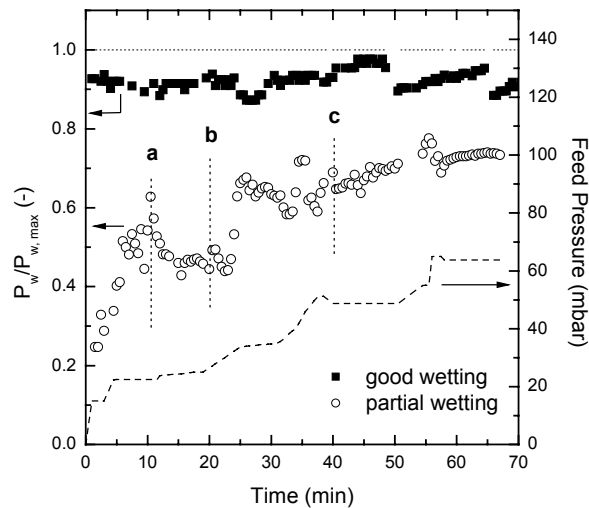


Figure 11. Relative clean water permeability of a fully wetted hydrophobized microsieve (■), and the same hydrophobized membrane after a partial wetting (○). For the partially wetted membrane, three phenomena are indicated: (a) bubble accumulation and flux decline, (b) bubble release and flux+pressure increase and (c) filtration interruption: the microsieve is left in water for 30 min and the process is reinitiated at constant pressure. The feed pressure applied with the semi-wetted microsieve is also plotted (-).

As it can be observed, during the first ten minutes of filtration, permeability increased due to pore activation, although it was only about 60% of the maximum value. Then we observed that bubbles present in the system accumulated on the membrane surface (a), which caused flux decline even though pressure increased from 22.5 to 25 mbar.

During the period of time from (a) to (b), air bubbles from the system were accumulated on the membrane surface and partially inactivated the pores in the vicinity, causing flux instabilities. At $t=20$ min (b), numerous bubbles were removed from the system, the permeability recovered but, at the same time, a pressure increase from 26 to 34 mbar took place, causing an increase in permeability as more pores became active for permeation. In the period from (b) to (c), although pressure increased 17 mbar, the permeability did not increase significantly. After 40 min the filtration was interrupted (c) and the membrane remained in water for the following 30 minutes to determine if dewetting took place. When filtration was reinitiated, the same permeability value was obtained as before pausing, and permeability kept increasing until the end of the process (approx. 70% of the maximum flux) even though pressure was constant for a certain time. Maximum flux may have been achieved if the filtration had continued for longer time and pressure was further increased, enhancing pore activation.

Another clear indication of good wetting, independently of the nature of the surface is the linearity of flux vs. pressure (constant permeability). Completely wetted sieves presented a constant maximal permeability even if pressure was changed throughout the measurement. Semi-wetted membranes presented increasing permeability with increasing pressure (pore activation).

As we mentioned in section 3.4.2, highly hydrophobized membranes coated by FOTS vapor deposition ($\theta=112^\circ$), did present anomalous behavior in terms of wetting and clean water permeability measurements. Even when in-line rewetting was applied and the membrane seemed wetted, flux instabilities were observed, making it unfeasible to obtain a well-controlled measurement. Moreover, if air bubbles from the system traveled from the feed side to the retentate outlet, a subsequent flux decline followed, which indicated that dewetting took place. Flux recovery could be achieved to some extent if in-line rewetting was applied.

3.5 Conclusions

Wetting, pore activation and the suppression of contamination play a very important role to achieve a maximum water flux. In our investigation, pre-conditioning was necessary as each surface needed a specific wetting method to activate all pores. Fully wetted unmodified and hydrophilized microsieves exhibited stable fluxes, especially when the system was free of air bubbles.

If no pre-wetting occurred, hydrophobized membranes ($\theta=105^\circ$ and 112°) showed no flux at the same pressure as hydrophilized membranes. Hydrophobized microsieves with water contact angles closer to 90° presented maximum performance if a proper wetting procedure was applied.

The combination of air bubbles and poor wetting resulted in a loss in performance: flux decline and a permeability far below the maximum expected value were measured. If any of the described systems contained air nucleation spots, a degassing step or forward flushing were effective ways to minimize the air disturbance and achieve a stable flux. However, for the hydrophobized surfaces with $\theta=112^\circ$, a stable and maximum clean water permeability was difficult to achieve due to membrane dewetting during operation. The microsieve design, with microchannels underneath the pore grids, may play a very important role in dewetting. When air bubbles enter the membrane module and flow along the sieve, inactivation of some membrane area by dewetting can take place.

As a final summary, it should be noted that for maximum and stable performance of microsieve membranes in water flux measurements, it is crucial to start the process with an air-free and clean system, and a fully wetted surface, preferably of hydrophilic nature.

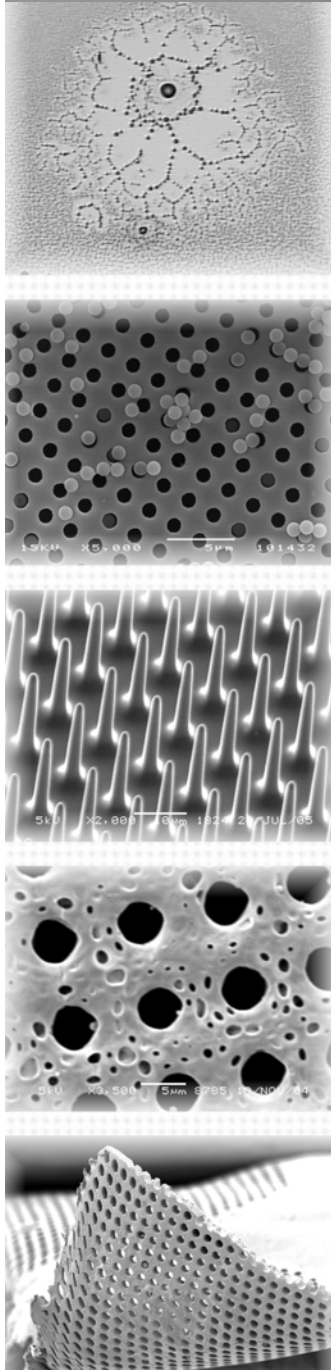
3.6 References

- [1] S. Kuiper, C.J.M. Van Rijn, W. Nijdam, M.C. Elwenspoek, Development and applications of very high flux microfiltration membranes, *J. Membr. Sci.* 150 (1998) 1.
- [2] C.J.M. Van Rijn, M.C. Elwenspoek, Microfiltration membrane sieve with silicon micromachining for industrial and biomedical applications, *IEEE Proceedings MEMS*, Amsterdam, 1995.
- [3] M. Gironès, Z. Borneman, R.G.H. Lammertink, M. Wessling, The role of wetting on the water flux performance of silicon nitride microsieves, *J. Membr. Sci.* 259 (2005) 55.
- [4] J. Szepvolgyi, I. Mohai, J. Gubicza, Atmospheric ageing of nanosized silicon nitride powders, *J. Mater. Chem.* 11 (2001) 859.
- [5] T. Mikolajick, R. Kuhnhold, R. Schnupp, H. Rysse, The influence of surface oxidation on the pH-sensing properties of silicon nitride, *Sens. Actuators B* 58 (1999) 450.

- [6] A.C. Simonsen, P.L. Hansen, B. Klosgen. Nanobubbles give evidence of incomplete wetting at a hydrophobic surface, *J. Colloid Interface Sci.* 273 (2004) 291.
- [7] M.C. García-Payo, M.A. Izquierdo-Gil, C. Fernández Pineda, Wetting study of hydrophobic membranes via liquid entry pressure measurements with aqueous alcohol solutions, *J. Colloid Interface Sci.* 230 (2000) 420.
- [8] G.M. Whitesides, P.E. Laibinis, Wet chemical approaches to the characterization of organic surfaces: self-assembled monolayers, wetting, and the physical-organic chemistry of the solid-liquid interface, *Langmuir* 6 (1990) 87.
- [9] A. Ulman, Wetting studies of molecularly engineered surfaces, *Thin Solid Films*, 273 (1996) 48.
- [10] Y. Xia, D. Qin, Y. Yin, Surface patterning and its application in wetting/dewetting studies, *Curr. Opin. Colloid Interface Sci.* 6 (2001) 54.
- [11] Y. Xia and G. Whitesides, Soft-lithography, *Angew. Chem. Int. Ed.* 37 (1998) 550.
- [12] M. Geissler, Y. Xia. Patterning: principles and some new developments, *Adv. Mater.* 16 (2004) 1249.
- [13] J.L. Wilbur, A. Kumar, H.A. Biebuyck, E. Kim, G.M. Whitesides, Microcontact printing of self-assembled monolayers: applications in microfabrication, *Nanotechnology* 7 (1996) 452.
- [14] S. Kuiper, C. van Rijn, W. Nijdam, O. Raspe, H. van Wolferen, G. Krijnen, M. Elwenspoek, Filtration of lager beer with microsieves: flux, permeate haze and in-line microscope observations, *J. Membr. Sci.* 196 (2002) 159.
- [15] C.J.M. van Rijn, 'Membrane filter as well as a method of manufacturing the same', WO9513860, 1995
- [16] C.J.M. van Rijn, W. Nijdam, S. Kuiper, G.J. Veldhuis, H.A.G.M. van Wolferen, M.C. Elwenspoek, Microsieves made with laser interference lithography for micro-filtration applications. *J. Micromech. Microeng.* 9 (1999) 170.
- [17] S. Kuiper, Development and applications of microsieves. PhD Thesis, University of Twente, The Netherlands, 2000.
- [18] S. Kuiper, M. de Boer, C.J.M. van Rijn, W. Nijdam & M.C Elwenspoek, Wet and dry etching techniques for the release of sub-micrometre perforated membranes, *J. Micromech. Microeng.* 10 (2000) 171.
- [19] M.H.V. Mulder, *Basic Principles of Membrane Technology*, Kluwer Academic Publishers, Amsterdam, 1996.
- [20] A.C.M. Franken, J.A.M. Nolten, M.H.V. Mulder, D. Bargeman, C.A. Smolders, Wetting criteria for the applicability of membrane distillation, *J. Membr. Sci.* 33 (1987) 315.
- [21] P.S. Kumar, J.A. Hogendoorn, P. Feron, G.F. Versteeg, New absorption liquids for the removal of CO₂ from dilute gas streams using membrane contactors, *Chem. Eng. Sci.* 57 (2002) 1639.

Chapter 4

Fouling studies of silicon nitride microsieves with model solutions



4.1 Introduction

In membrane-based applications where macromolecules such as proteins are involved, the loss of membrane performance by deposition/adsorption onto the surface is critical for the process sustainability. Today, protein fouling of microfiltration membranes is still an issue.

Throughout the years several studies [1-3] have proved that, even with pore sizes much larger than the protein size, fouling under dynamic condition occurs. Many factors can contribute to fouling, such as membrane surface properties, hydrodynamic conditions, solute concentration, etc.

The most pointed cause for the severe flux decline is aggregate formation [3-6]. This can be triggered by hydrophobic and/or electrostatic interactions or van der Waals forces [1, 7]. Changes in the media surrounding the protein, such as pH, ionic strength, heat, and the presence of an interface can affect the protein's conformational stability and result in aggregation/precipitation of the macromolecule. Subsequently, protein adsorption on or in the membrane can also occur. The extent of adsorption depends very much on protein-protein, protein-solvent and protein-membrane interactions [8].

One of the most studied model protein systems for understanding concentration polarization and fouling has been Bovine Serum Albumin (BSA). BSA is a 'soft' globular protein. 'Soft' proteins are macromolecules that are prone to undergo structural rearrangements when they adsorb to a surface [8]. It has a molecular weight of 67kDa and an isoelectric point (IEP, pH at which the net charge is zero) of 4.5-4.8. The primary structure of BSA is constituted by a single chain of about 580 amino acids, while its secondary structure mainly consists of α -helix fraction [8]. Initially, Bloomfield [10] postulated that BSA was an oblate ellipsoid with dimensions of 14x4x4 nm. However, X-ray crystallography data found by Charter and co-authors [11] indicated that BSA is composed by three domains forming a heart-shaped molecule. Bovine plasma contains about 35 g/l of BSA, which is responsible for blood pH regulation and the transport of metal-ions and phospholipids due to its high binding capacity [11]. BSA is also present in milk (0.4 g/l [12]) and, therefore, it is an interesting model compound for the study of dairy product separations.

Lysozyme is another protein often used in fouling studies. It is a small monomeric and globular 'hard' protein (undergoes limited conformational changes) and it has a molecular weight of approx. 14kDa, dimensions of 4.5x3x3 nm and an isoelectric point of 11. It can be found in egg white, and human tears or mucus. This enzyme is antibacterial due its potential to degrade the polysaccharides found in the cell walls of many bacteria.

As we mentioned already, concentration polarization and subsequent fouling are frequent phenomena in micro and ultrafiltration of proteins. In the case of BSA, experiments have shown that fluxes are higher when the pH of the solution is above the isoelectric point of the protein, when the ionic strength of the solution is low, and when the surface is hydrophilic [1]. Several authors have described the fouling mechanism of BSA in microfiltration. The proposed mechanism described by Kelly and Zydney [13] is initiated by the deposition and subsequent pore blockage of protein aggregates on the surface. These aggregates can serve as nucleation or attachment sites for further BSA deposition. At longer filtration times, the flux decline is usually governed by a cake filtration mechanism. The initial fouling due to pore blockage caused by aggregates has been corroborated by several authors, and extensively studied and modelled for BSA [14-16] and other protein systems [17].

Aggregation can be reduced by either pre-filtering or using modified proteins (ex. cysteinylated-BSA, without free thiol groups).

In certain applications, microsieves can overcome the role of other commercial membranes due to their enhanced selectivity/permeability features provided by their perfectly engineered surface [18-20]. In Chapter 3 we have presented some of the outstanding properties of microsieves, in terms of water permeability. Porous 1.2 μm microsieves present a large water flux. Unfortunately, large product throughputs normally involve severe fouling. In the case of microsieves, a study with such model proteins like BSA has not been reported in literature. Theoretically, the thin and smooth selective layer and perfectly-shaped straight pores (tortuosity=1) would be very advantageous to avoid internal fouling. Moreover, there's a growing interest in industry in using ceramic membranes for food processing because in such applications high productive membranes are normally used. In order to keep all equipment sterile, harsh chemical cleaning is needed (e.g. strong alkali media), but not all available commercial membranes, especially polymeric, can withstand such aggressive cleaning treatments. Microsieves do, and this, together with the potential to deliver high product volumes, makes them suitable to be implemented in this field.

In this chapter the first results concerning protein fouling with microsieves are obtained. To get more insight into the fouling mechanism of a model protein like BSA several process and solution parameters were varied (protein concentration, pH, pressure, etc.). As a complementation to BSA, a glimpse on the fouling behavior obtained with smaller globular proteins like Lysozyme (LYS) and model particles such as latex is presented.

The information gained with model solutions cannot be directly translated to more complex mixtures such as milk, fruit juices or beer but it can give a general idea of the fouling mechanism and provide solutions to reduce protein deposition.

4.2 Materials and methods

4.2.1 Materials

Silicon-rich silicon nitride (Si_xN_y) porous microsieve membranes ($1 \times 1 \text{ cm}^2$, pore size $1.2 \text{ }\mu\text{m}$) were kindly provided by OnStream MST (nowadays Fluxxion). The structural characteristics of the membranes used are described in detail in Chapter 3 (Section 3.2).

Ultrapure water ($18.2 \text{ M}\Omega\text{cm}$) for flux measurements was obtained with a Millipore purification unit (MilliQ plus). Bovine Serum Albumin (BSA) (Fraction V, Fluka) and chicken egg-white Lysozyme (LYS) (70.000 units/mg , Fluka) were used as model proteins. The feed solutions consisted of 0.1 and 1 g/l BSA, and 1 g/l LYS dissolved in filtered phosphate buffer 50 mM at $\text{pH}=6.8 \pm 0.1$. Solutions were freshly prepared and stored at 8°C for maximum 2 hours before use. Two aqueous latex solutions containing particles of approx. $0.6 \text{ }\mu\text{m}$ diameter were used for fouling tests. Results with 1 and $2 \text{ }\mu\text{m}$ particles are also presented in section 4.3.3. The $0.6 \text{ }\mu\text{m}$ solutions had concentrations of 4×10^7 and 0.4×10^7 particles/ml.

4.2.2 Crossflow filtration

The permeation experiments were performed in a cross-flow module with a channel height of $700 \text{ }\mu\text{m}$ and an effective membrane area of $1 \times 10^{-4} \text{ m}^2$ ($1 \times 1 \text{ cm}^2$ samples), which is described in Chapter 3.

The permeate weight was monitored in time; the permeability was calculated by dividing the flux by the operational pressure (average pressure between feed and retentate side). The clean water permeability was measured in the pressure range of $30\text{-}50 \text{ mbar}$ at $20 \pm 2^\circ\text{C}$ before any protein filtration; the measured clean water permeability (P_w) was approximately $2.5\text{-}3.0 \times 10^5 \text{ l/m}^2\text{hbar}$.

In the protein filtrations, the membranes were pre-treated with an alkaline solution, wetted with MilliQ water and subsequently placed in the module. After a stable clean water flux was obtained, the feed was exchanged by the protein solution (BSA, LYS) and the flux measured at an average pressure of $51 \pm 3 \text{ mbar}$, $10 \pm 2^\circ\text{C}$ and an average crossflow velocity of 0.165

m/s. Latex permeabilities were measured in dead-end mode at an average operational pressure of 65 mbar.

In all protein filtrations, the feed was pumped to the membrane module using a mzs-7223 microannular pump from HNP Mikrosysteme GmbH (Germany). The retentate was returned to the feed tank, which was kept under cooling and stirring throughout the duration of the experiment. In the tests where the influence of pre-filtering was studied, commercial 5 µm Polyester Nuclepore and 0.45 µm Schleicher & Schuell Nylon pre-filters (FP 50/0.45 NL-QF20) were placed in-line before the module and the feed pressure sensor. For the latex experiments and BSA filtrations where the influence of aggregation was studied a tank pressurized with nitrogen was used to feed the solutions to the module.

The microsieves were cleaned before and after use. The pre-treatment consisted in immersing the membranes in a 5 wt% alkaline solution (pH=12.2) at 50°C for 30-60 minutes, followed by a thorough rinsing with ultrapure water. After such treatment the membrane surface was fully wettable with water (contact angle < 20°).

Fouling curves will mostly be expressed as relative permeability versus time or permeated volume (V_p). Relative permeability is defined as

$$\text{Relative permeability (-)} = \frac{P_F}{P_w} \quad (1)$$

where P_F = permeability of the feed solution (BSA, LYS or latex), P_w = maximum water permeability (in some cases the term *fouling rate* will also be introduced, which is the absolute value of the slope of the relative permeability versus permeated volume plot. The higher the flux decline the higher the slope).

4.2.3 Scanning Electron (SEM) and Optical Microscopy

The morphology of the microsieve membranes was visualized by Scanning Electron Microscopy (SEM, Microscopes JEOL TSM 220A and JSM-5600LV, at 5 kV), after sputtering a gold layer (30 nm). Quick microsieve inspection before and after the flux measurements was performed with a Zeiss Axiovert 40 MAT optical microscope.

4.2.4 Zeta-potential and particle size of BSA solutions (Dynamic Light Scattering)

The average charge and particle size of BSA solutions were determined by Dynamic Light Scattering (DLS) (Malvern Zetasizer 2000). For the zeta-potentials, BSA solutions (1 g/l) were prepared in 50 mM acetate, phosphate and carbonate buffers to cover pH values ranging

from 3 to 11. Each solution was measured for 5 times at room temperature (25°C). The particle size of 10 g/l BSA solutions was measured before filtration at pH=7 and 4.5, but also at neutral pH during an experiment with pre-filtration (0.45 μm pre-filter).

4.2.5 Analysis

The concentration of BSA in the feed, permeate and after pre-filters was analyzed with a Cary 300 Scan UV-VIS spectrophotometer at $\lambda= 595$ nm, using the Bradford reagent (Sigma), when little permeate amounts (<1 ml) were obtained. When larger amounts were permeated, the feed and collected filtrate were analyzed directly at 280 nm. Solution viscosities were measured at different temperatures with a capillary viscometer (Normalab Analisis, France).

4.3 Results and discussion

4.3.1 Fouling studies with model proteins

a. Effect of pH and viscosity

It is well-known from literature that the properties of BSA solutions are greatly influenced by pH and ionic strength [1, 21-24]. These factors can cause a change in the protein conformation. The most unfavorable conformation is obtained at the IEP due to reduced electrostatic repulsions. Therefore the chances for aggregation/precipitation increase significantly [8]. To confirm these facts and determine the charge of BSA at different pH's the zeta-potential of different solutions was measured, from pH=3 to 11. Figure 1 shows a decrease of the zeta-potential with increasing pH, which is in very good agreement with literature data [25, 26].

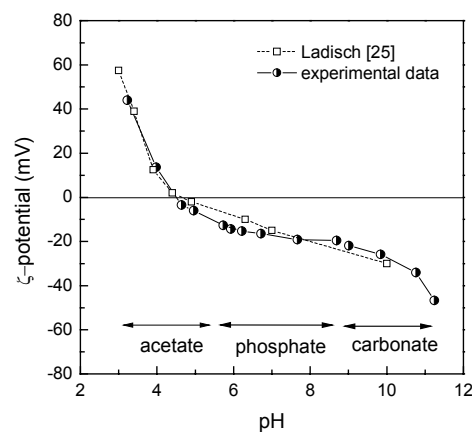


Figure 1. Zeta-potential of BSA solutions as a function of pH (from 3.2 to 11) determined by DLS.

The pH at which BSA has an average charge of zero (IEP) can be determined from the graph at pH=4.5. Above the IEP BSA is negatively charged and below the IEP the average charge of BSA is positive.

Fouling tests were made at the IEP (pH=4.6) and at pH 6.8, where the protein is negatively charged and more stable in terms of conformation. Figure 2 shows the relative permeability graphs versus permeated volume for these experiments.

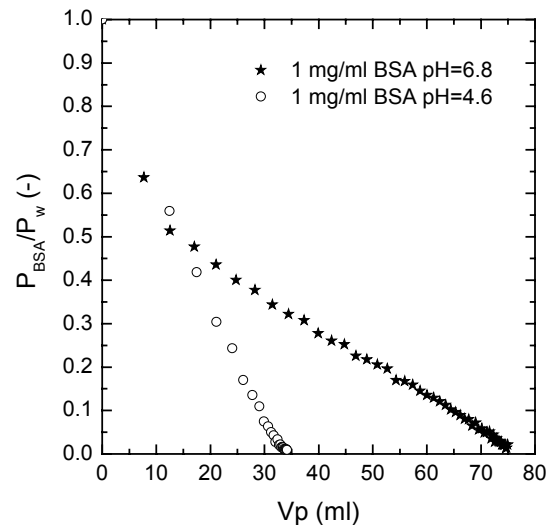


Figure 2. Relative permeability vs. permeated volume of 1 g/l BSA at different pH (4.6 and 6.8).

Rapid flux decline at both pH's is evident, with a more steep and severe decline (higher fouling rate) at pH=4.6, as already seen by other authors [1, 27-31]. The filtration time when permeability reached a zero value was only 12 minutes at pH 4.6. The highest fouling rate near the IEP is likely caused by BSA aggregation/precipitation and particle deposition due to reduced electrostatic repulsion. DLS results for fresh BSA solutions (10 g/l) at pH 4.5 and 7 confirm that, at the lowest pH, larger aggregates are present. The average size of BSA molecules at the IEP is around 12 nm. However, the detected peak has a broad shoulder until a particle size around 40 nm. At neutral pH, a sharper peak, with its maximum at 9.9 nm is detected, indicating that at this pH BSA molecules are smaller and mostly, in monomeric form [16].

At both pH's there is a strong initial flux decline (30-50% of P_w), caused by the increasing viscosity when exchanging water at room temperature with cooled BSA solution. A significant

increase of the viscosity with decreasing temperature was observed for BSA (Table 1). These findings agree with the observations of Monkos *et al.* [32]. In our case, while the viscosity of BSA at room temperature was almost equal to water (0.8 mPa.s), the viscosity at our experimental conditions (8°C) was 1.28 mPa.s (BSA viscosity is 1.61 times higher than water).

Although low temperature has not a beneficial effect for the initial flux we performed all filtrations at such temperature to avoid rapid protein denaturation during experimentation.

Table 1. Influence of the temperature on the viscosity of BSA solutions at pH 6.8.

Solution	T (°C)	η (mPa.s)	η_{BSA}/η_{H_2O}
MilliQ water	24.4	0.8	-
BSA pH=6.8 1 mg/ml	24.4	0.875±0.021	1.094
	10.2	0.98±0.071	1.225
	7.9	1.285±0.021	1.606

Apart from the initial flux reduction, a severe decline in permeability occurred in time at both pH's. However, only little protein retention was measured. At pH=7±0.1, for instance, a retention of approximately 6% was measured after 30 min, even though the measured flux was close to zero. If the surface of the microsieve was inspected after filtration, upon slightly flushing with water to eliminate the excess of protein, a deposited layer was observed. Figure 3a exhibits a view of some pore grids after a filtration at neutral pH. The light gray areas indicate deposited protein. In Figure 3b a higher magnification of a cross-section of two grids is displayed, again with deposited protein on the surface.

The decline observed when filtering BSA solutions can be caused by several mechanisms, including adsorption and aggregation leading to pore blocking [14-16]. Aggregates can form, bridge and narrow the pores until blocking them. Figure 3 gives an indication of this effect and the amount of protein that can be deposited on the surface.

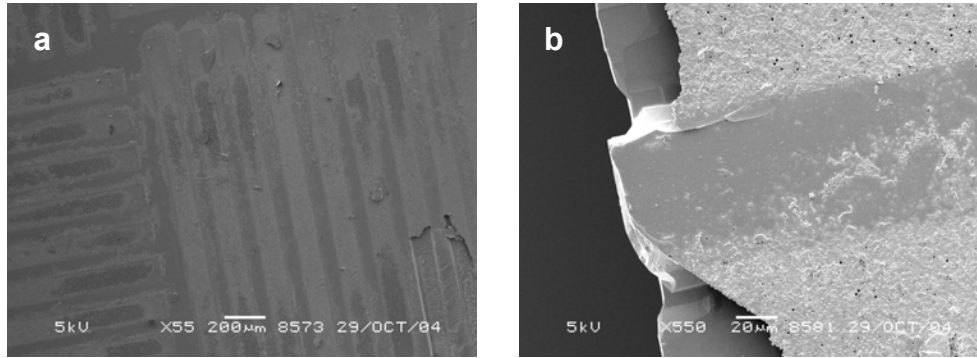


Figure 3. SEM pictures of (a) a top view of some pore grids with deposited BSA and (b) cross-section of two pore grids with a close-up of the deposits after a filtration at neutral pH.

As already mentioned, in the case of fouling by aggregation this effect would be stronger at pH's close to the IEP and at high ionic strengths, since the protein molecules are mainly uncharged and the conformation is changed. In our case, results shown in Figure 2 and experiments performed at higher ionic strength confirm these findings. If 0.2 M sodium chloride was added to the buffer at pH 4.6 and 6.7, a higher decrease in permeability took place than without salt. The differences in flux decline between both pHs became then very little. Addition of salt in the protein solution caused a reduction in the thickness of the electrical double layer. The protein charges were shielded by the salt ions (mainly at pH=7, at the IEP little net charge is observed) and electrostatic forces between protein molecules were greatly reduced, causing protein to aggregate in a greater extent [4, 8, 31].

From static BSA incubation experiments at pH=7.4 on untreated and oxygen plasma treated silicon dices, we determined by ellipsometric measurements that only a few nanometers (4 and 1.5 nm, respectively) of protein adsorbed on the untreated and hydrophilic silicon dices during five days. For a shorter period of time, Yin and co-authors [33] also found similar results to ours [34]. The fact that few static adsorption is measured on the membrane material indicates that there is little driving force for adsorption on such surfaces, which are comparable to unmodified and oxidized silicon nitride.

For comparison to BSA, a smaller and differently charged protein was used at neutral pH. Lysozyme (LYS) is a globular protein with a molecular weight of 14.6 kDa and IEP equal to 11. A much lower microsieve performance was observed when filtering LYS compared to BSA

at pH=7, as it can be observed in Figure 4. The main difference between the two solutions is the protein charge at neutral pH, which is negative and positive for BSA and LYS, respectively (solution viscosities for both proteins are quite similar).

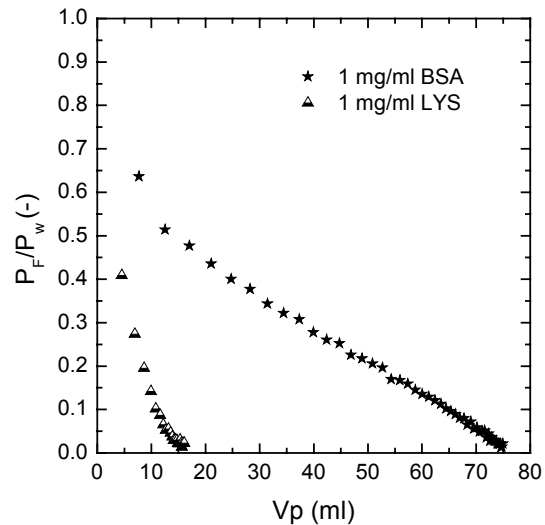


Figure 4. Relative permeability vs. permeated volume of 1 g/l BSA at pH 6.8 and 1g/l LYS at pH 7.

Studies of static adsorption of LYS at pH=7 reported higher adsorption below the IEP than above IEP, on negatively charged surfaces. Some investigations report higher adsorption for 1 g/l LYS on silica nanoparticles (negatively charged) at pH=7 than at pH=4, with adsorbed amounts at the silica/water interface of 2.1 and 3.5 mg/m², respectively [35-37]. Rezwan *et al.* [38] reported that positively charged LYS adsorbed in significantly higher amounts than BSA on negatively charged silica particles, due to increased electrostatic interactions between silica and LYS. According to these findings, more severe flux decline would be expected with LYS at neutral pH. This agrees very well with the results shown in Figure 4.

The loss in LYS permeability is much more severe than the permeability loss observed with BSA at its IEP, even with large pore sizes such as 1.2 μm. At neutral pH the severe decline might be caused by two phenomena: 1) aggregate deposition triggered by LYS precipitation and 2) electrostatic interactions between the protein and the microsieve surface. Unpublished results within the D-Force project framework indicate that the silicon nitride surfaces cleaned with the alkaline treatment reported in section 4.2.3 are negatively charged. At pH=6.8 positively charged LYS has, thus, more chance to adhere to the negative charged microsieves due to attractive electrostatic interactions. In the case of BSA such electrostatic interactions may be excluded, since BSA is mainly negatively charged at pH=7.

b. Effect of concentration and pressure

The influence of the BSA solution concentration on the membrane productivity was investigated. Two solutions of 0.1 and 1 g/l at $\text{pH}=6.9\pm 0.1$ were filtered through a $1.2\ \mu\text{m}$ microsieve at 53.5 ± 0.5 mbar. After a certain time, when either none or only 10% of the maximum permeability remained, the feed was exchanged by water. Before water was fed to the module, a very short rudimentary air forward flush (air pocket) was applied, dragging away all the protein solution out of the module.

For both concentrations, flux decline took place (see Figure 5), although at different rates. The results depicted in Figure 5 show differences in fouling rate (faster for the most concentrated solution) and productivity (the filtration with 0.1 g/l BSA resulted in a 2 times higher permeated volume).

Despite the fact that significant differences were observed between the decline caused by BSA solutions with different concentrations, only slight differences in the clean water flux permeability and recovery were observed after the water exchange. For all cases, without performing any chemical cleaning, the water permeability was recovered to 40-45% of its maximum and remained quite constant.

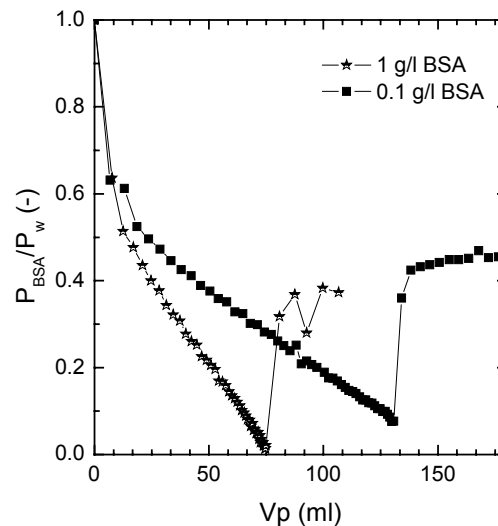


Figure 5. Relative permeability vs. permeated volume of BSA solutions at $\text{pH}=7$ with different concentrations (0.1 and 1g/l). After the relative permeability reached a value of zero or below 10% (for 0.1 g/l), the BSA solution was exchanged by water.

Fouling can be retarded if low working pressures are applied [1]. In our investigation, almost all protein experiments were performed at approx. 50 mbar, in order to keep constant

operational conditions and obtain a comparable set of data. However, the outcome of BSA filtrations at lower pressure was also taken into consideration. The flux decline at neutral pH but different operating pressures (17 and 53 mbar) is shown in Figures 6a and 6b.

For the same filtration time, lower flux loss (higher P_{BSA}/P_w) took place at lower pressures, because less protein volume permeated through the membrane. The membrane performance in terms of flux decline was thus, slightly higher at lower operating pressures: at 17 mbar 10% of the maximum flux remained after 20 minutes of filtration, while at 53 mbar the membrane did not permeate any longer. However, at lower pressures performance was lower in terms of productivity because less volume was collected in time.

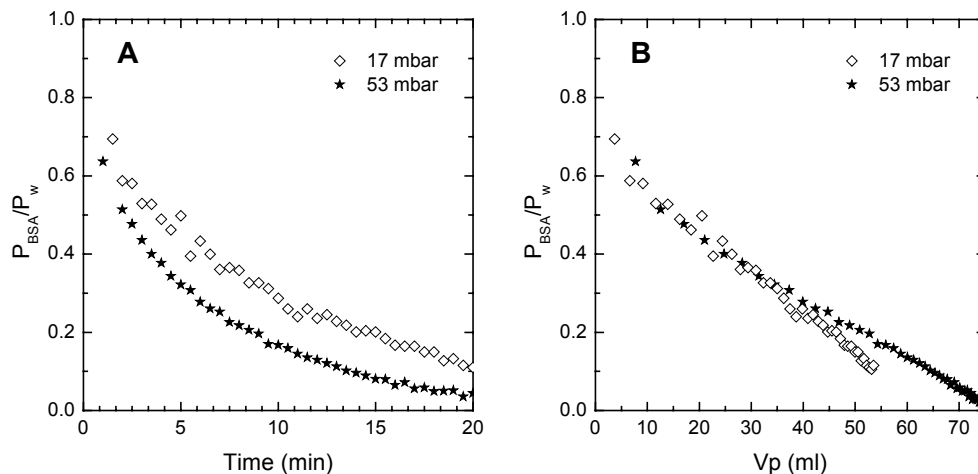


Figure 6. Relative permeability vs. time (a) and permeated volume (b) of a BSA solution at pH=7 as a function of pressure (17 and 53 mbar).

The differences observed at 17 and 53 mbar are not extremely large; if the filtration had been kept at 17 mbar (Figure 6b, white diamonds) until no permeation was observed, a V_p of about 60 ml could have been obtained (this being calculated by extrapolating the relative permeability at 17 mbar to zero volume). When the filtration was kept at a higher pressure (53 mbar), around 75 ml of BSA solution were collected as permeate. These little differences in performance indicate that BSA flux decline in our system does not strongly depend on pressure.

To summarize the influence of all the parameters discussed in this section, some of the results are presented in Table 2. Here the fouling rates (slope of the relative permeability

versus volume plot) are presented as a function of the variable tested. The most severe flux decline is observed with BSA at the IEP and LYS at neutral pH, probably due to aggregation and increased electrostatic interactions for LYS. Filtrations at low BSA concentration (0.1 g/l) present the lowest fouling rate, which also agrees well with results reported by other authors [4]. Similar fouling behavior is obtained with BSA at neutral pH independently of pressure (17 or 53 mbar).

Table 2. Influence of different variables on the protein fouling rate

Variable	Value	Conditions	Fouling rate ($\times 10^{-3}$ ml)
Pressure	17 mbar	1 g/l BSA	10.6
	53 mbar	pH=7	7.7
Concentration	0.1 g/l	pH=6.9 \pm 0.1	3.9
	1 g/l	53 \pm 1 mbar	7.7
pH	4.6	1g/l BSA	25.1
	6.8	50 \pm 2 mbar	7.7
Protein type	BSA	pH=6.9 \pm 0.1	7.7
	LYS	53 \pm 1 mbar	30

c. Influence of equipment: pressurized vessel versus gear pump

In our system a microannular gear pump was chosen because of the low wear of the gears, avoiding contaminant particles in the system. However, in this pump high shear rates were generated, possibly leading to protein denaturation. Therefore, a test with nitrogen pressure as the driving force for feeding the protein solution to the module was performed. In such case the proteins would experience less shear and less flux decline would be observed at the same conditions as in our standard filtration tests. The results of filtrations with the same procedure and conditions (BSA 1g/l, pH=6.8 and 4.6, pressure=50-60 mbar) are displayed in Figure 7.

The experiments performed using a gear pump to feed the protein resulted in a severe and rapid flux decline, delivering little amounts of permeated volume at both pHs (pH=4.6 and 6.8). If BSA was fed through a pressurized tank flux decline also occurred but at a much lower rate.

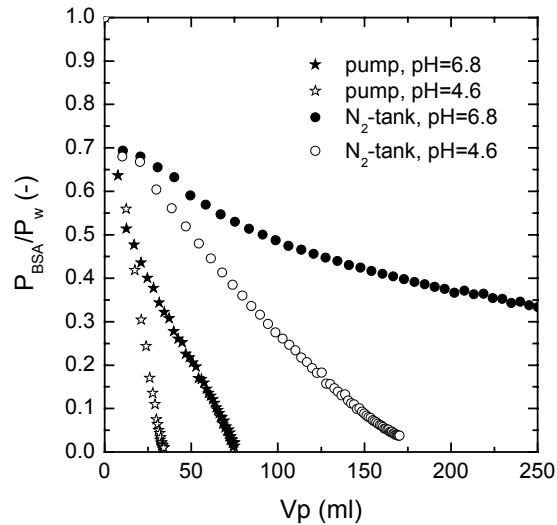


Figure 7. Relative permeability versus permeated volume of BSA solutions (1 g/l) at pH=6.8 and 4.6, using either a microannular pump or a nitrogen pressurized tank.

For both systems, when comparing the outcome at neutral pH and the IEP, a more steep flux loss occurred at the IEP of BSA. This might be triggered by protein conformational changes that result in aggregation (this will be further explored in the next section, d). In our case the most acute flux decline took place when by pumping the protein through a microannular gear pump at pH close to the IEP.

d. Aggregate removal: pre-filtration

Removal of large compounds such as aggregates by pre-filtration of the feed can help improving the permeate flux in MF and UF [1]. In order to demonstrate aggregation and pore blocking as the cause for the steep flux decline, we performed experiments with an in-line polymeric pre-filter. Figure 8 shows the influence of in-line pre-filtration of 1 g/l BSA solution at pH 6.7. When no pre-filter was used, the same effect was observed as in Figure 2. However, when a 5 μm polyester filter was used, fouling occurred in time but with a much lower rate, indicating that some of the aggregates were retained by the pre-filter.

By using the pre-filter with the smallest pore size (almost 1/3 of the membrane pores), initial flux decline also occurred (due to BSA viscosity and aggregate retention) but a stable and constant flux was subsequently measured, indicating that pore blocking did not take place.

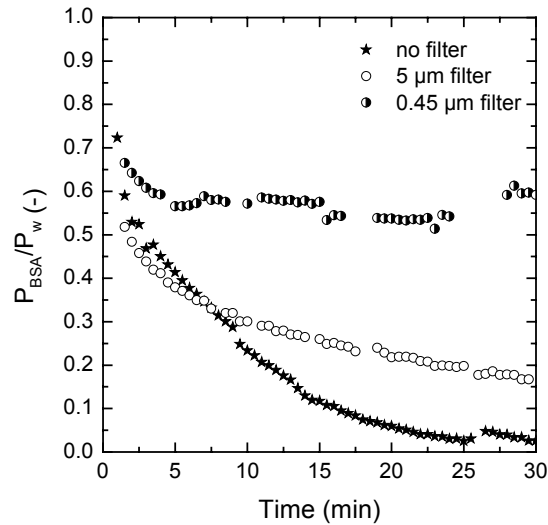


Figure 8. Relative permeability versus time of an unfiltered and two pre-filtered BSA solution experiments (5 and 0.45 μm pre-filter pore size) at $\text{pH}=6.7$.

The 5 μm pre-filter showed a very low retention (1.5%) for BSA after 40 minutes of filtration, while the 0.45 μm filter exhibited slightly higher retention of approximately 5% after the same period of time. Such retention is the result of the aggregate accumulation and adsorption on the polymeric pre-filter.

Aggregate deposition can be observed in the SEM images deployed in Figure 9. After 30 minutes of filtration using a 5 μm pre-filter (1g/l BSA solution at neutral pH) the membrane was directly freeze-dried (for approx. 30 h) and then inspected under the microscope.

In Figure 9a we can observe that some large BSA deposits (smaller than 5 μm) cause partial membrane blocking. In a close-up (Figure 9b), we can even notice the blockage of some pores in detail, either complete or partial. These images confirm what we already mentioned in the previous sections: the permeability loss in the filtration of BSA solutions is caused by aggregates that block the pores either completely or partially.

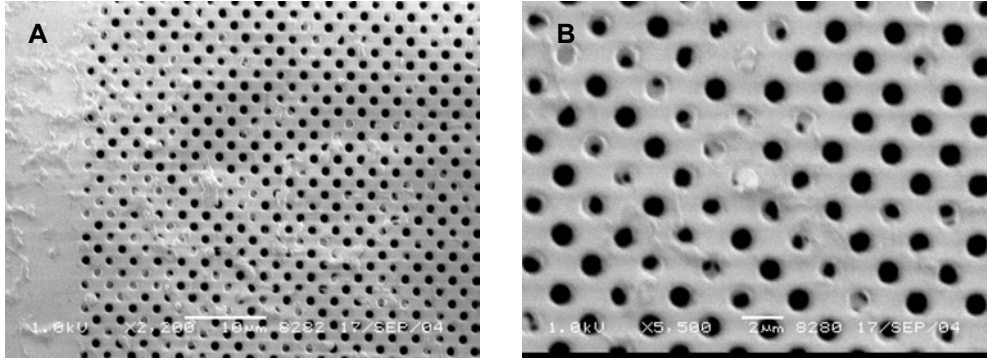


Figure 9. SEM images of a freeze-dried microsieve with deposited BSA, after pre-filtration (5 μm). Image A is taken at a magnification of 2500x and B at 5500x.

Dynamic light scattering results of the average particle size of BSA before and after one of the pre-filters also confirm that the largest BSA aggregates are retained. After 50 min of filtration, an average particle size of 11.8 nm is detected (small peak, from 2 to 20 nm) after the 0.45 μm filter. The average particle size before the pre-filter results in 2 peaks: a much more intense peak (7 times higher) with mean particle size equal to 11.2 nm and another less intense peak at 67 nm. These results confirm that larger aggregates are present before the filter.

4.3.2 Fouling behaviour prediction by pore blocking

From the previous sections, several findings indicate that pore blocking is the mechanism responsible for the severe BSA flux decline. Bowen *et al.* [15] described the consecutive stages of membrane blocking by interpreting their results on dead-end microfiltration of BSA solutions through track-etched membranes. They postulated that if the membrane possessed a narrow pore size distribution and if the pore size was smaller than the particle size, complete blocking would take place in the initial stage of filtration. For this mechanism a relationship between the first and second derivatives of the time (t) versus permeated volume (V) exists:

$$\frac{d^2t}{dV^2} = \alpha \left(\frac{dt}{dV} \right)^\beta \quad (2)$$

where α and β are the parameters of the blocking filtration laws for constant pressure. α is the product of the membrane surface blocked per unit of total permeated volume and the mean

initial velocity of the permeate. Bowen [15] derived values for β for different blocking models, being 2 the beta value for flux decline caused by pore blocking. Kilduff and coworkers [39] developed a model taking backtransport to the bulk caused by crossflow into account. They postulated that, if a single fouling mechanism dominates flux decline and if the effects of backtransport by crossflow are negligible, linear relationships between the characteristic coordinates (e.g. flux and volume, in the case of complete pore blocking) should be obtained. Our results clearly give linear relationships between such coordinates, indicating that backtransport to the bulk is not affecting the fouling mechanism.

Figure 10a shows the permeated volume as a function of time for a BSA filtration at pH 6.8 at 53 mbar. After some minutes of filtration, the permeation rate was greatly reduced and a plateau in the volume was reached. The first and second derivatives of time versus volume (dt/dV and d^2t/dV^2) were calculated, and a log-log plot of d^2t/dV^2 versus dt/dV (see Figure 10b) was obtained. The slope of this graph gives the value of β .

From Figure 10b the best fit for our experimental data gives a beta value (slope of logarithmic expression of formula (2)) of 2 ± 0.06 , which clearly confirms the behavior predicted by the classical pore blockage model.

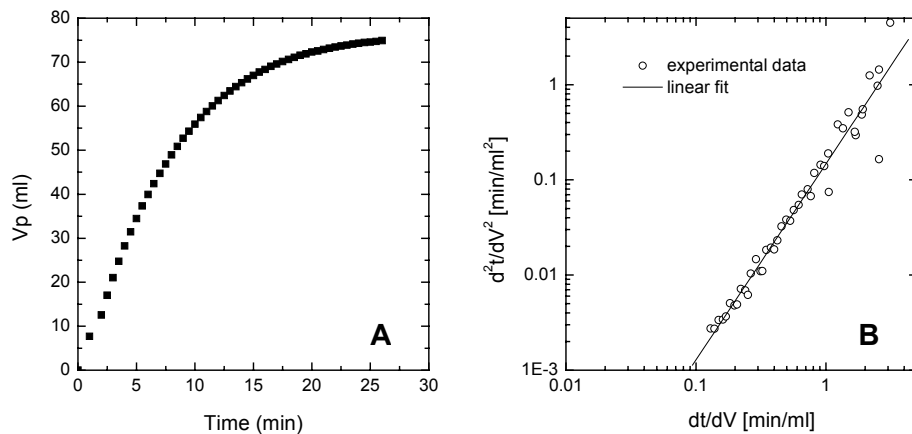


Figure 10. (A) Permeated volume versus time of 1 g/l BSA pH=6.8 and (B) d^2t/dV^2 versus dt/dV . The slope of the logarithmic plot of d^2t/dV^2 versus dt/dV gives the beta parameter in formula (2).

For the experiments performed at the isoelectric point the slope of the log-log plot was 1.6 ± 0.1 , indicating that, apart from pore blocking, adsorption is enhanced as well. In the case of lysozyme a beta value of 1.77 ± 0.3 was found, which can also indicate that a combination of pore blocking and adsorption are the reasons for flux decline.

These models [15-17] can predict the transition from pore blocking to classical cake filtration ($\beta=0$) by changes in the slope of the logarithmic plot of d^2t/dV^2 versus dt/dV . Our findings do not show any slope changes, thus complete pore blockage is assumed to be responsible for the BSA flux decline at neutral pH.

4.3.3 Fouling studies with latex solutions

As we mentioned in the introduction, protein fouling is a very relevant issue in micro and ultrafiltration. Therefore we have studied BSA filtrations as a function of several parameters in the previous sections. However, microsieves offer a great opportunity to study particle deposition (ex. Defatting steps, clarification, yeast separation, etc.) with model dispersions of hard round-shaped spheres such as latex. Latex filtrations with different sphere sizes can give information on how a pore is blocked and how the performance of a microsieve will be with feeds with different particle loads. When the pore and particle sizes are known, the mechanism for particle deposition (in dimers, trimers, etc) can also be determined.

Latex solutions with different concentration of particles with a diameter of $0.6 \mu\text{m}$ were tested. The goal was to determine the flux decline rate as a function of the particle concentration and study of the blockage by SEM analysis. For this purpose two solutions were used with the following concentrations: 4×10^7 and 0.4×10^7 particles/ml. The filtrations were performed in dead-end mode at constant pressure and the permeate volume was measured in time (see Figures 11a and 11b).

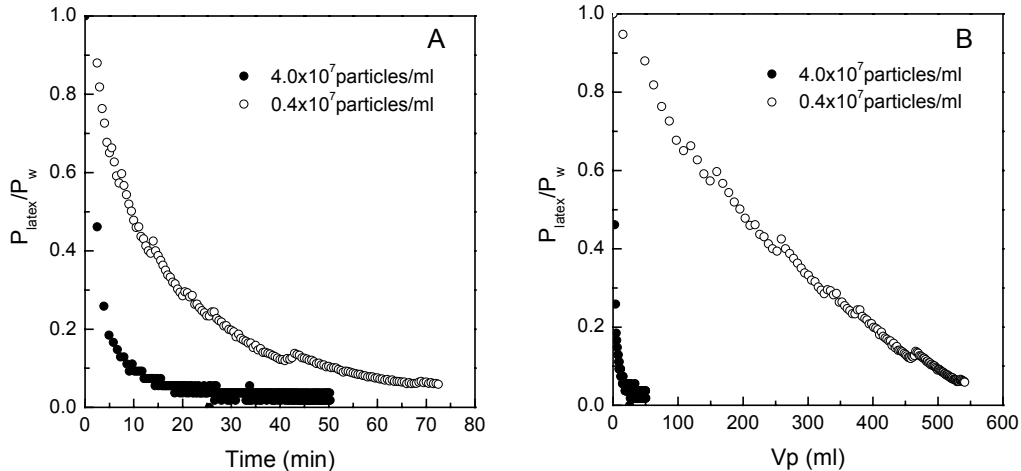


Figure 11. Dead-end latex flux decline of two latex solutions (4.0 and 0.4×10^7 particles/ml) as a function of time and permeated volume.

After filtration the microsieves were carefully flushed with water to remove the latex cake layer, while leaving only the first layer of particles on the surface.

The dead-end results show that severe flux decline occurs with the most concentrated solution, producing a permeated volume of only 50 ml. During filtration visual inspection of the membrane surface indicated that a latex cake layer built up very fast, obtaining a deposited white layer of latex particles just after some minutes. For the 10 times diluted feed, flux decline also occurred, though more gradually. In this case particle retention also took place because the cake layer could be visually detected. For this experiment, the slope (beta value) of the logarithmic plot of d^2t/dV^2 versus dt/dV was calculated as 1.6 ± 0.05 , indicating that the main fouling mechanism is more likely to be standard blocking or pore narrowing.

A post-filtration SEM analysis revealed how the blocking mechanism may have taken place. These results can be useful to predict the flux and fouling mechanism when spherical particles are used. From Figure 12A and B we can see that, in principle, two particles of $0.6 \mu\text{m}$ can block a pore. If they deposit exactly next to each other an open area is still available for water to flow through. When three particles deposit on a pore almost complete blockage takes place, although there is still some area available for water permeation.

For comparison to the $0.6 \mu\text{m}$ diameter spheres, we also examined how particles with diameter equal to and larger than the pore size would deposit. For the largest particles (1 and $2 \mu\text{m}$) the fouling mechanism was cake layer formation. Contrary to the tests with $0.6 \mu\text{m}$ latex, these experiments were performed in crossflow mode, using different particle concentrations (7×10^7 and 1×10^7 particles/ml for 1 and $2 \mu\text{m}$, respectively). In both cases a very rapid flux decline took place within a couple of minutes, until a steady state was reached resulting in a very low residual water flux. This is a characteristic effect observed with cake layers formed by hard particles. Since the cake formed by the latex spheres is not completely compact, water can still permeate through the voids between particles and residual fluxes can be measured.

With the largest spheres, lower concentrations should be used to gain more insight on the initial fouling mechanism. However, the SEM analysis after removing most of the cake can indicate how particles get located in/on the pores. Latex particles with diameters of 1 and $2 \mu\text{m}$ deposited on the microsieve surface and trapped inside the pores are shown in Figures 12 C and E, D and F, respectively. For particles with a diameter equal to the pore size only one particle is sufficient to be trapped inside a pore and block it completely. Larger particles cannot be trapped inside the pore but they are fully retained at the entrance of the pore. Due to their size, one particle can be deposited directly on the pore. These findings indicate that, when filtering particles of a certain size and shape, pore blocking is very likely to occur, which is the predominant mechanism for a variety of feeds (BSA, Lysozyme, latex).

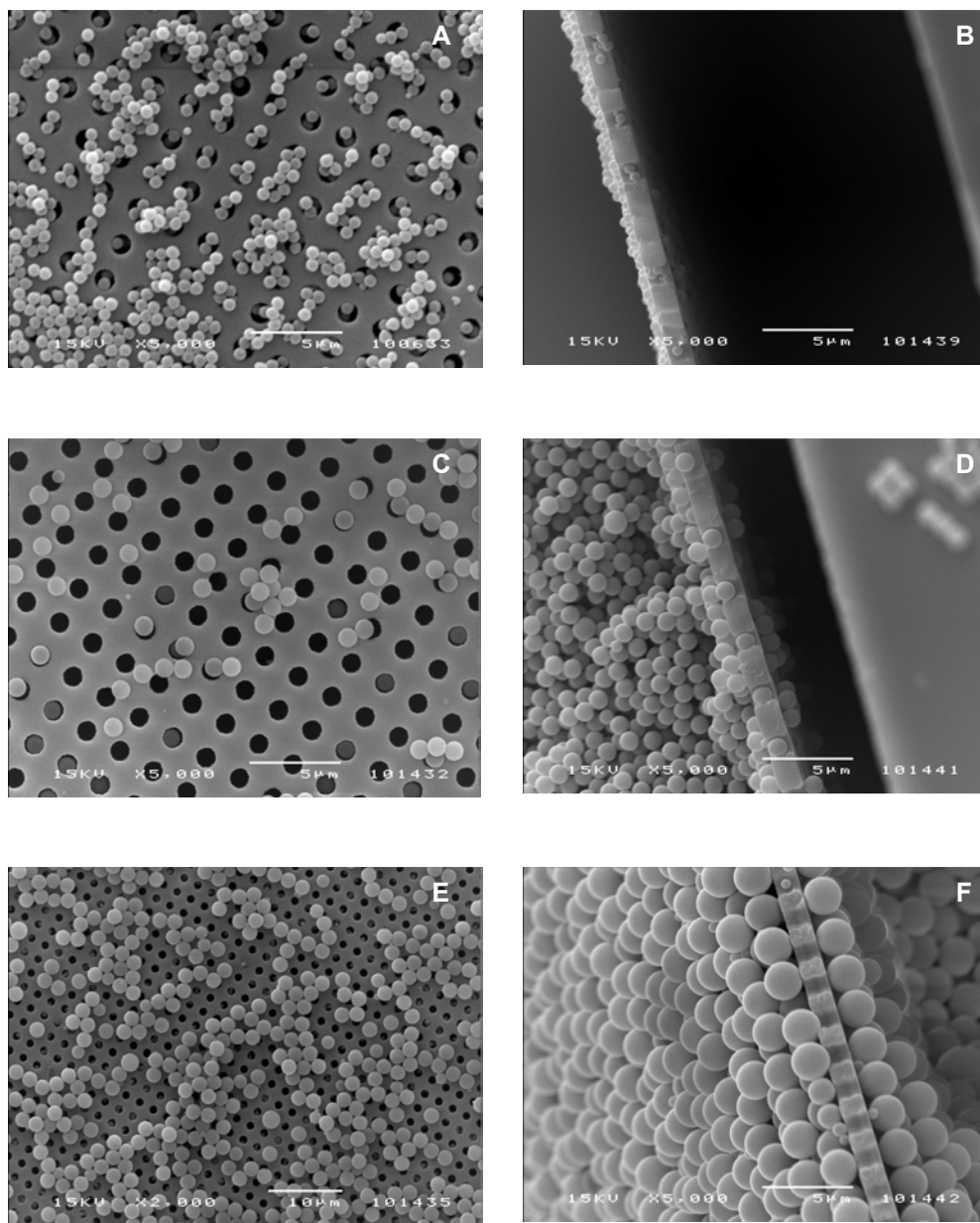


Figure 12. SEM images of microsieve top views with deposited latex particles with a diameter of 0.6 μm, (A) 1 μm (C) and 2 μm (E). Cross-sectional images indicating the level of pore blocking in detail are displayed in (B), (D), (F) for 0.6, 1 and 2 μm, respectively. All images are taken at 5000x magnification, except (e), which is taken at 2000x magnification.

4.4 Conclusions

In a crossflow BSA filtration with hydrophilic silicon nitride microsieves, fast and severe flux decline occurs even if the membrane pore size is much bigger than the single protein size. At neutral pH, even though the bare material does not present too much BSA adsorption and low retention values are measured, flux decline occurs, mainly caused by protein aggregation.

The fouling rate is higher at pH close to the isoelectric point, where a larger extent of aggregate deposition takes place. At higher ionic strength also an increased permeability loss takes place for the same reason, independently of the pH.

Apart from the effect of pH, the effect of other parameters like pressure, protein concentration, temperature and type of protein has been also considered. The most severe flux decline is observed with BSA at the IEP and LYS at neutral pH, probably due to protein precipitation (for BSA at the IEP) and increased attractive forces between the negatively charged microsieves and the positively charged LYS.

As mentioned previously, the main cause for permeability loss in filtrations of BSA solutions at neutral pH is aggregation. This is confirmed for BSA when constant and stable fluxes are measured when pre-filtering in-line. The equipment used for the crossflow filtrations has also a very important effect on aggregation. Using pumps that generate high shear rates, the protein structure can be altered and aggregation can occur. Aggregation can lead to pore blocking, which can be demonstrated using the classical pore blocking models. The data fittings show that, at neutral pH, pore blocking is the predominant mechanism responsible for flux decline. Alternatively, at the IEP adsorption may also take place.

A SEM study with latex particles of equal, half and twice the pore size indicates that pore blocking is likely to happen in microfabricated membranes with straight pores. However, depending on the foulant size and shape permeation of smaller molecules is still feasible, due to voids present in between the particles.

Since silicon nitride microsieves exhibit severe fouling in standard crossflow or dead-end filtrations, their performance decreases towards other commercial microfiltration membranes. In the next chapters, the integration of backpulsing, air sparging and other fouling reduction strategies will be discussed.

4.5 Acknowledgements

The author wishes to acknowledge Ronald Jansen, Frans Pronk and Lutgarde Lemmens from Fluxxion B.V. (Eindhoven) for kindly providing the silicon nitride microsieves. Lydia Bolhuis-Versteeg and Wika Wiratha are acknowledged for performing the DLS measurements.

4.6 References

- [1] A.D. Marshall, P.A. Munro, G. Trägårdh, The effect of protein fouling in microfiltration and ultrafiltration on permeate flux, protein retention and selectivity: a literature review, *Desalination* 91, (1993) 65.
- [2] G. Belfort, R.H. Davis and A.L. Zydney, The behavior of suspensions and macromolecular solutions in crossflow microfiltration, *J. Membr. Sci.* 96 (1994) 1.
- [3] S.T. Kelly, A.L. Zydney, Mechanisms for BSA fouling during microfiltration, *J. Membr. Sci.* 107 (1995) 115.
- [4] S.T. Kelly, W. Senyo Opong, A.L. Zydney, The influence of protein aggregates on the fouling of microfiltration membranes during stirred cell filtration, *J. Membr. Sci.* 80 (1993) 175.
- [5] C. Güell, R.H. Davis, Membrane fouling during microfiltration of protein mixtures, *J. Membr. Sci.* 119 (1996) 269.
- [6] C. Güell, P. Czekaj, R.H. Davis, Microfiltration of protein mixtures and the effects of yeast on membrane fouling, *J. Membr. Sci.* 155 (1999) 113.
- [7] L. J. Zeman, A. L. Zydney, *Microfiltration and ultrafiltration: principles and applications*, Marcel Dekker, New York, 1996.
- [8] M. Malmsten, Formation of adsorbed protein layers, *J. Colloid Interface Sci.* 207 (1998) 186.
- [9] E.L. Gelamo, C.H.T.P. Silva, H. Imasato, M. Tabak, Interaction of bovine (BSA) and human (HAS) serum albumins with ionic surfactants: spectroscopy and modeling, *Biochim. Biophys. Acta* 1594 (2002) 84.
- [10] V. Bloomfield, The structure of BSA at low pH, *Biochem. J.* 5 (1966) 684.
- [11] J.C. Charter, D.X. Ho, Structure of serum-albumin, *Adv. Protein Chem.* 45 (1994) 153.
- [12] J.L. Stein, K. Imhof, Milk and Dairy Products, In: *Ullmann's Encyclopedia of Industrial Chemistry*, Vol. A16, Elsevier, 1991.
- [13] S.T. Kelly, A.L. Zydney, Protein Fouling during microfiltration: comparative behavior of different model proteins, *Biotechnol. Bioeng.* 55 (1997) 91.
- [14] E.M. Tracey and R.H. Davis, Protein fouling of track-etched polycarbonate microfiltration membranes, *J. Colloid Interface Sci.* 167 (1994) 104.
- [15] W.R. Bowen, J.I. Calvo, A. Hernández, Steps of membrane blocking in flux decline during protein microfiltration, *J. Membr. Sci.* 101 (1995) 153.
- [16] C.C. Ho, A.L. Zydney, A Combined Pore Blockage and Cake Filtration Model for Protein Fouling during Microfiltration, *J. Colloid Interface Sci.* 232 (2000) 389.
- [17] L. Palacio, C.C. Ho, A. L. Zydney, Application of pore blockage-cake filtration model to protein fouling during microfiltration, *Biotechnol. Bioeng.* 79 (2002) 260.
- [18] S. Kuiper, C.J.M. Van Rijn, W. Nijdam, M.C. Elwenspoek, Development and applications of very high flux microfiltration membranes, *J. Membr. Sci.* 150 (1998) 1.
- [19] C.J.M. Van Rijn, M.C. Elwenspoek, Microfiltration membrane sieve with silicon micromachining for industrial and biomedical applications, *IEEE Proceedings MEMS*, Amsterdam, 1995.
- [20] M. Gironès, R.G.H. Lammertink, Z. Borneman, M. Wessling, The role of wetting on the water flux performance of microsieve membranes, *J. Membr. Sci.* 259 (2005) 55.
- [21] J.C. Bosma and J.A. Wesselingh, pH dependence of ion-exchange equilibrium of properties, *AIChE J.* 44 (1998) 2399.
- [22] S.P. Palecek and A.L. Zydney, Hydraulic permeability of protein deposits formed during microfiltration: effect of solution pH and ionic strength, *J. Membr. Sci.* 95 (1994) 71.
- [23] N.S. Pujar, A.L. Zydney, Electrostatic and kinetic interactions during protein transport through narrow pore membranes, *Ind. Eng. Chem. Res.* 33 (1994) 2473.
- [24] S.T. Kelly, A.L. Zydney, Protein Fouling during microfiltration: comparative behavior of different model proteins, *Biotechnol. Bioeng.* 55 (1997) 91.

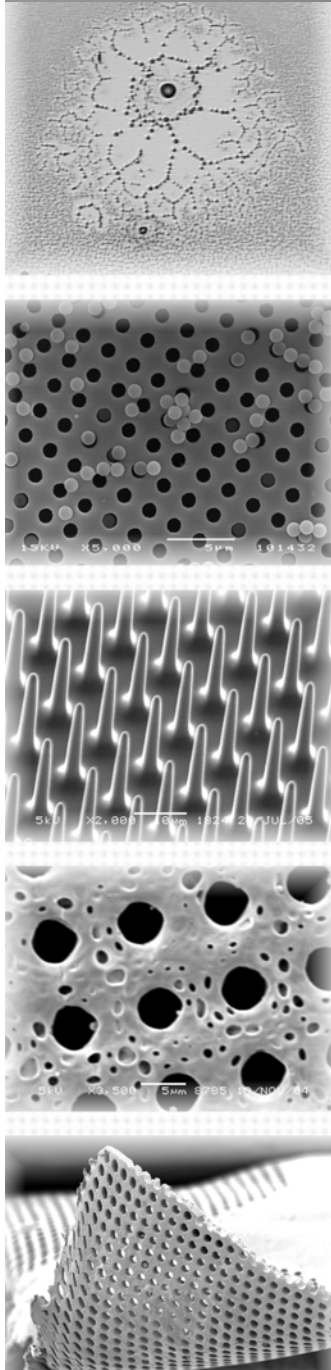
- [25] M.R. Ladisch, *Bioseparations Engineering: principles, practice and economics*, Wiley Interscience, New York (2001).
- [26] T. Coradin, A. Coupé, J. Livage, Interactions of bovine serum albumin and lysozyme with sodium silicate solutions, *Colloids Surf. B* 29 (2003) 189.
- [27] R. Chan, V. Chen, The effects of electrolyte concentration and pH on protein aggregation and deposition: critical flux and constant flux membrane filtration, *J. Membr. Sci.* 185 (2001) 177.
- [28] T.J. Su, J.R. Lu, Z.F. Cui, R.K. Thomas, Fouling of ceramic membranes by albumins under dynamic conditions, *J. Membr. Sci.* 173 (2000) 167.
- [29] K.L. Jones, C.R. O'Melia, Protein and humic acid adsorption onto hydrophilic membrane surfaces: effects of pH and ionic strength, *J. Membr. Sci.* 165 (2000) 31.
- [30] C. Velasco, M. Ouammou, J.I. Calvo, A. Hernandez, Protein fouling in microfiltration: deposition mechanism as a function of pressure for different pH, *J. Colloid Interface Sci.* 266 (2003) 148.
- [31] A. Persson, A.S. Jonsson, G. Zacchi, Transmission of BSA during crossflow microfiltration: influence of pH and salt concentration, *J. Membr. Sci.* 223 (2003) 11.
- [32] K. Monkos, Viscosity of bovine serum albumin aqueous solutions as a function of temperature and concentration, *Int. J. Biol. Macromol.* 18 (1996) 61.
- [33] P. Yin, G. Jin, Z. Tao, Competitive adsorption of collagen and bovine serum albumin-effect of the surface wettability, *Colloids Surf. B* 33 (2004) 259.
- [34] M. Gironès, Chapter 6 of this thesis.
- [35] P.M. Claesson, E. Bloomberg, J.C. Froberg, T. Nylander, T. Arnebrant, *Adv. Colloid Interface Sci.*, 57 (1995) 161.
- [36] T.J. Su, R.J. Green, Y. Wang, E.F. Murphy, J.R. Lu, Adsorption of Lysozyme onto the silicon oxide surface chemically grafted with a monolayer of pentadecyl-1-ol, *Langmuir* 16 (2000) 4999.
- [37] J.R. Lu, M. J. Swann, L.L. Peel, N. Freeman, Lysozyme adsorption studies at the silica/water interface using dual polarization interferometry, *Langmuir* 20 (2004) 1827.
- [38] K. Rezwan, L.P. Meier, L.J. Gauckler, Lysozyme and bovine serum albumin adsorption on uncoated silica and AIOOH-coated silica particles: the influence of positively and negatively charged oxide surface coatings, *Biomaterials* 26 (2005) 4351.
- [39] J.E. Kilduff, S. Mattaraj, J. Sensibaugh, J.P. Pieracci, Y. Yuan, G. Belfort, Modeling flux decline during nanofiltration of NOM with Poly(arylsulfone) membranes modified using UV-assisted graft polymerization, *Environ. Eng. Sci.* 19 (2002) 477.



Chapter 5

Strategies to reduce protein fouling with Si_xN_y microsieves

I. Backpulsing and air sparging



5.1 Introduction

Due to extreme concentration polarization (caused by the large fluxes), fouling of high-flux silicon nitride microsieves can be quite dramatic because membrane performance and product quality are lost in a very short period of time. As indicated in Chapter 4, small 'soft' proteins like BSA can aggregate resulting in severe fouling and pore blocking [1, 2]. Crossflow is often not sufficient to remove the adhered particles on the membranes surface or in the pores.

In this chapter process-related antifouling strategies will be discussed. One of the techniques frequently applied in industry is backpulsing. In crossflow filtration mode, backpulsing consists of reversing the transmembrane pressure/flow so that foulants are lifted off the membrane and transported by the retentate crossflow [3, 4]. The backpulses counteract concentration polarization above the membrane [3]; in between backpulses, cleaning is by the crossflow only. In this way, the overall filtration time between two cleaning cycles can be increased and higher permeation rates can be achieved. The principle of backpulsing is shown in Figure 1.

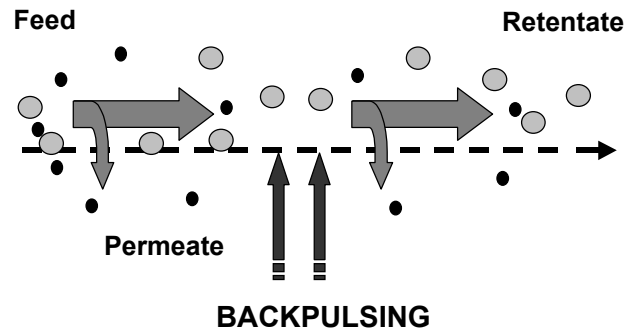


Figure 1. Principle of crossflow and backpulsing.

In literature, many authors distinguish between backpulsing and backflushing or backwashing. The fundamental difference between a backpulse and a backflush is the force and duration to lift accumulated matter off the membrane. Generally, in backflushing flow reversal occurs for a few seconds once every several minutes, while backpulsing occurs at a higher frequency and the pulses are applied for a short time (< 1s) [5, 6]. Both processes can use water, buffer or the permeate solution as liquids for flow reversal.

Different methods can be used to reverse the flow. Davis and coworkers have mostly used two solenoid valves coupled to the membrane module. One of the valves regulated the dosing of the backpulsing fluid, which is pressurized by nitrogen, and the other valve is directly

connected to the permeate outlet [4, 7]. Another possibility is the use of a piston that, by the application of a gas flow [5] or a magnetic force can move upwards and cause flow reversal through the membrane.

In microfiltration, backpulsing is a common technique used to retard fouling, either with ceramic or polymeric membranes, in hollow fiber or flat sheet configuration. Davis and coworkers proved reduced fouling during microfiltration with rapid backpulsing (short pulses at high frequencies) of yeast [8, 9], *Escherichia Coli* [4, 10] or bacterial lysates [7]. Other backpulsing applications involve the treatment of electroplating waste water with ceramic membranes [5], removal of clay in simulated drinking water [11] and, most recently, the purification of a polysaccharide conjugate vaccine with 0.1 μm Polysulfone membranes [12].

In this thesis several definitions of key-terms must be reformulated. In our case, in order to retard matter deposition on the membrane either a combination of forward flushing and single backflushing, or rapid backpulsing is applied. Forward flushing or crossflushing is the periodic stoppage of the permeate flow while maintaining crossflow across the membrane [13]. In this research *forward flushing* is performed by injecting water to the membrane module, with higher crossflow velocity than during filtration. Single *backflushing* is the sporadic injection of a large volume of water through the permeate outlet, during a longer time than 10 seconds. *Backpulsing* will be performed with much higher frequencies and lower pulse durations than the ones reported in literature for BSA and conventional polymeric membranes [13], by using the permeated liquid as backpulsing solution.

Another pathway to reduce fouling is to decrease concentration polarization by increasing the mass transfer coefficient at the membrane interface. This can be achieved in several ways: either operating at high crossflow velocities, using low flux membranes or increase turbulence locally [14]. To achieve the last, the use of turbulence promoters like spacers is very popular, as well as rotary module systems or air in RO and NF.

Another popular method is gas bubbling or air sparging, which consists of injecting gas bubbles into the liquid feed to generate a gas-liquid two-phase flow stream [15]. Air sparging allows flux enhancement in ultra and microfiltration of bacterial suspensions [16], dextran [17, 18], albumin [18], clay suspensions and natural surface waters [19], using different membrane geometries (tubular, hollow fibers and flat-sheets).

In the case of proteins, great benefits have been reported for enhancing the permeate flux by air sparging. Li and co-workers [20] investigated the effect of injecting air into the feed stream in a flat sheet module. Polysulfone and polyethersulfone membranes were used to filter four protein solutions, including Human Serum Albumin (HSA), Bovine Serum Albumin (BSA), Immunoglobulin (IgG) and Lysozyme (LYS). Gas sparging increased the permeate flux by 7-

50% and reduced the protein transmission due to reduced concentration polarization at the membrane surface caused by mixing or secondary flow. Gas sparging was also employed to fractionate protein mixtures, like HSA and IgG. Cui *et al.* [21] reported that almost complete separation of both proteins was achieved at relatively low air flow rates, with a 6-fold increased selectivity compared to fractionation without air. The increase in selectivity was caused by a reduction in HSA transmission triggered by a reduction of protein concentration at the membrane wall. In the same study, possible limitations of gas sparging in bioseparations were discussed. It was reported that protein damage mainly occurs in the foam and that the oxidizing effect from the oxygen in air is very low. Moreover, little enzymatic activity loss and protein structural change in the bulk liquid occurred when low gas sparging rates were used. Their results (performed at low air flow rates, < 50 ml/min) indicated that negligible damage to proteins was made, although fractionation was greatly enhanced.

In spite of the previous, gas sparging is not straight-forward for all systems. Its efficiency depends on the hydrodynamics near the membrane. Some of the factors that must be taken in account are: membrane orientation and type, module configuration and channel size, as well as flow direction (up or downwards in vertical tubes) and flow rate [15, 19].

As we mentioned at the beginning of this section, the main goal of this chapter is to study the effect of several fouling reduction strategies on the BSA flux using high-flux microfiltration microsieves. Strategies including forward or backflushing, backpulsing and air sparging will be considered to reduce the fouling rate and concentration polarization.

5.2 Materials and methods

5.2.1 Materials

Si_xN_y microsieves provided by OnStream (nowadays Fluxxion B.V.) (pore diameter 1.2 μm, 1x1 cm²) were used for the crossflow BSA filtrations. After a protein filtration and for reuse purposes, the membranes were cleaned in an alkali-based solution at pH=12 for at least 60 minutes, flushed with ultrapure water and dried under a nitrogen flow.

Ultrapure water (18.2 MΩcm) for flux measurements was obtained with a Millipore purification unit (MilliQ plus). A solution of 1 g/l of Bovine Serum Albumin (BSA) (Fraction V, Fluka) in filtered phosphate buffer 50 mM at pH=6.8 ± 0.1 was used as model protein for most tests. When the effect of the protein concentration was targeted, a 0.5 g/l BSA solution was also used. 1 g/l of Lysozyme (LYS) from Fluka at pH=7 in phosphate buffer was also used for the

air sparging experiments. The protein solutions were freshly prepared and stored at 8°C for maximum 2 hours before use.

A 0.45 µm Nylon pre-filter (FP 50/0.45 NL-QF20) was used in combination with backpulsing, in order to retain the largest protein aggregates. The pre-filter was placed after the pump and before the feed pressure sensor.

5.2.2 Crossflow filtration of proteins with backpulsing and air sparging

The clean water permeability of both unmodified and polymer coated microsieves was measured in the pressure range of 30-50 mbar at $20 \pm 2^\circ\text{C}$ before any protein filtration. The BSA permeability was measured at an average operating pressure of 50 mbar at $10 \pm 2^\circ\text{C}$, with an average crossflow velocity of 0.165 m/s, pumped through a microannular pump with retentate recirculation.

a. Permeate Backpulsing

An electromagnetic backpulsor (Aquamarijn Microfiltration B.V.) was used to periodically reverse the permeate flow. The backpulsor was directly connected to the permeate outlet of the crossflow module and to a computer, from where the settings were controlled. A detailed graphic showing the exact operational steps of the backpulsor is presented in Figure 2.

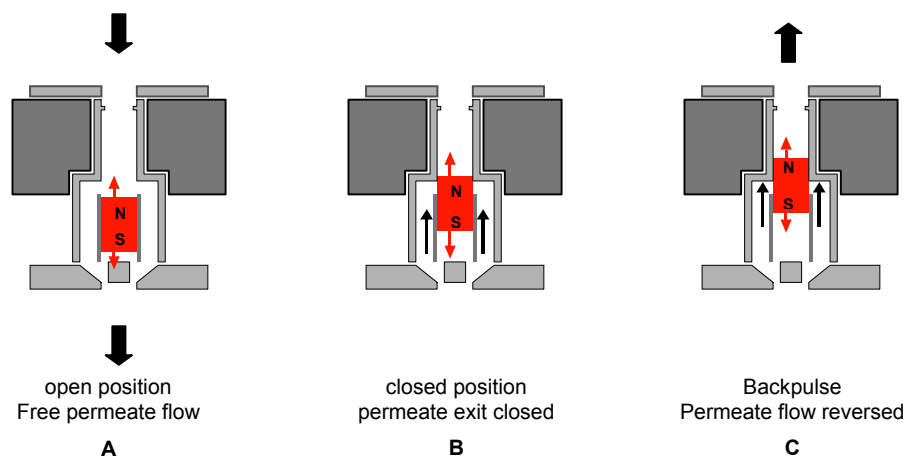


Figure 2. Operation principle of the magnetic backpulsor (block arrows indicate the flow direction). Before a pulse the piston is in its lowest position (A), so that permeate can flow freely to the permeate vessel. When a pulse is applied the piston moves upwards closing the outlet (B) and then continues to move forward pushing the permeate liquid to the feed channel (C).

When a filtration with backpulsing is performed, the piston is initially in a resting position at the bottom of the cylinder (A) and permeate can flow freely. When an electric current is applied through the coil of an electromagnet, the magnet piston is lifted in a cylindrical chamber of the unit. Here two steps occur: first the permeate outlet is closed (B) and then, as the piston reaches the highest position, permeate liquid is pushed back through the sieve (C). When no current is applied the piston returns to its initial position.

In our investigation variable backpulsing frequencies and power were used. In BSA filtrations frequencies were varied from 2 to 6.7 Hz, power (D) and pulse length (P) were kept constant at 64% and 20 ms, respectively. A schematic representation of the pulse profile of the electromagnetic backpulser is depicted in Figure 3.

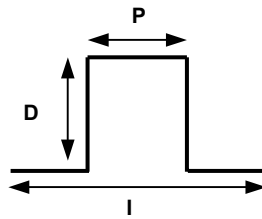


Figure 3. Pulse profile with variable interval time I ($I=1/\text{frequency}$), pulse length P and power D .

b. Feed air sparging

The application of discontinuous and continuous air sparging in BSA and LYS filtrations was also investigated in this research. An air flow was directly fed just before the feed pressure sensor and the module inlet. When applied discontinuously, the air was injected through a syringe at intermittent intervals, with a volume of approximately 0.5 ml. In the continuous air sparging experiments air from a compressed air reservoir was directly injected before the membrane module. The flow was regulated by a gas flow controller and it varied from 9.6 ml/min to 42 ml/min.

5.2.3 Optical Microscopy

Inspections of each microsieve before and after the flux measurements were performed with a Zeiss Axiovert 40 MAT optical microscope.

5.3 Results and discussion

In this chapter fouling curves will mostly be expressed as relative permeability of the protein solution ($P_{\text{BSA or LYS}} / P_w$) versus time or permeated volume (V_p). P_w is the clean water permeability of the microsieves used, approximately $2.5\text{--}3.0 \times 10^5 \text{ l/m}^2\text{hbar}$.

5.3.1 Effect of water forward and backflushing

Several strategies were taken in consideration in order to reduce the fouling rate. In the next section we will discuss the efficiency of water forward and backflushing at pH=6.8. Water forward flushing consisted of injecting a few ml of water in a discontinuous way through a syringe placed just before the entrance of the module, whereas backflushing consisted of injecting water off-line through the permeate outlet of the module.

As shown in Figure 4, a fairly constant average BSA permeability is obtained when in-line forward flushing is repeatedly applied.

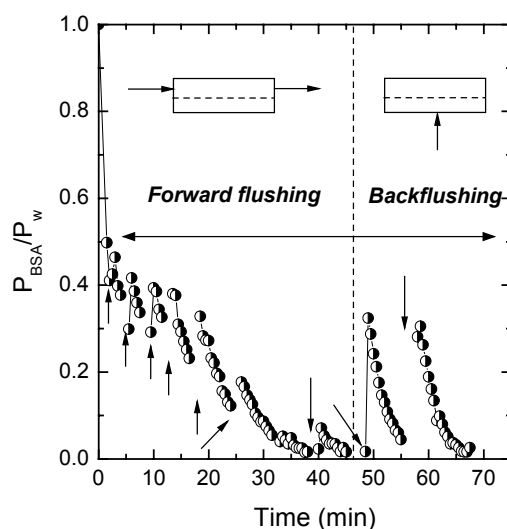


Figure 4. Effect of water forward flushing and backflushing on the flux recovery (arrows indicate when either one or the other was applied).

During the initial minutes of filtration, forward flushing was frequently applied and the BSA average permeability fairly stabilized. Each forward flush resulted in an increase of permeability about 15%. When water forward flushing was applied in less frequent intervals,

permeability was also recovered (15% increase) but remained much lower than when applied frequently.

Backflushing resulted in a more significant flux increase than forward flushing, independently of the frequency of application.

At $t=45$ min, when P_{BSA}/P_w was almost zero, the crossflow was stopped and backflushing was applied. The BSA filtration was then reinitiated and the flux was recovered until 32% of the maximum permeability. The filtration was prolonged and a successive backflushing provided a similar flux recovery. These findings indicate that water backflushing at low P_{BSA}/P_w is more efficient than forward flushing. Similar results were reported by Kuberkar *et al.* [13], who demonstrated that in BSA filtrations backflushing had a more significant effect than forward flushing, at least during the first few cleaning cycles. Belfort and co-workers also observed a more beneficial effect of water backflushing versus stirring to recover BSA flux in a dead-end filtration with polysulfone membranes [22].

However, since a flux recovery of 100% is not obtained even with backflushing, we may consider other factors playing a role such as the microsieve structure (see Figures 3 and 4 in Chapter 3). In a pore grid, which is approximately $2000 \times 115 \mu\text{m}$, only an area of approx. $200 \times 115 \mu\text{m}$ (5100 pores, 10% of the total pore population) is situated directly above the permeate outlet. The rest of the pores are situated above permeate channels that lead to the outlet. Brans *et al.* [23] performed computational fluid dynamics simulations using an adapted pore blocking model for latex dead-end filtrations with the same type of microsieves than the ones used in our research. They concluded that the support structure had a large effect on the flow resistance, and that the middle of a grid above the permeate channel had the highest permeation. That would explain why backflushing is not fully effective for the pores situated at the outer ends of the pore grid.

5.3.2 Effect of in-line permeate backpulsing with Si_3N_4 microsieves

Backpulsing is frequently used in industry to increase the efficiency of membrane filtration processes. The effect of continuous permeate backpulsing during the filtration of 1 g/l BSA solution ($\text{pH}=6.8$) with microsieves is demonstrated in Figure 5. Without backpulsing severe and rapid flux decline occurs (empty dots), as mentioned in the previous chapter.

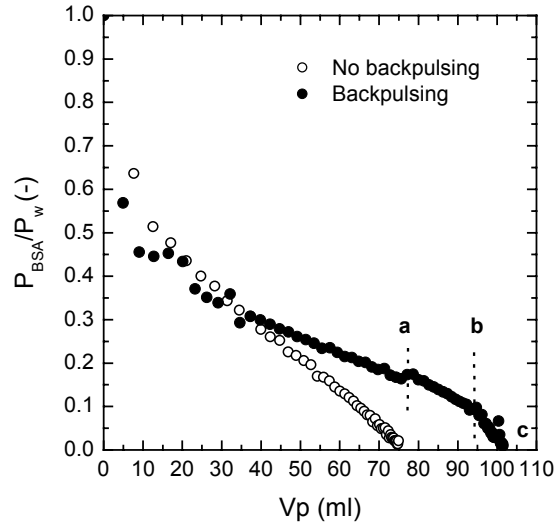


Figure 5. Influence of backpulsing on the permeation rate. In the test with backpulsing the frequency was increased from 6.7 (until (a)) to 3.3 Hz from (a) to (b); from (b) to (c) no backpulsing was applied.

When backpulsing is applied with a frequency of 6.7 Hz (full dots, until (a)), there is a slight reduction in the initial flux, compared to the non-backpulsing situation.

During a pulse, the pressure at the permeate side is elevated, causing a lower flux through the membrane. In our case, only the average pressure between feed and retentate (so-called operating pressure) is taken into account for the permeability calculation, and not the transmembrane pressure (TMP). Since the operating pressure is constant throughout the backpulsing period, the solute permeability is therefore lower. Moreover, backpulsing at high frequencies results in a lower average flux because less solute can permeate in between pulses.

Even though the initial permeability in the presence of pulsations is lower compared to pulse absence, fouling rate can be successfully reduced and more permeated volume is obtained.

In our case, a negative TMP was applied during each pulse, which caused a reversal of the permeate flow. The feed pressure (just before the membrane) and the permeate pressure (after the permeate outlet and before the backpulsing) were monitored in time during a filtration with water at 50 mbar, without (Figure 6a) and with pulses (6.7 Hz, 64 % power, Figure 6b).

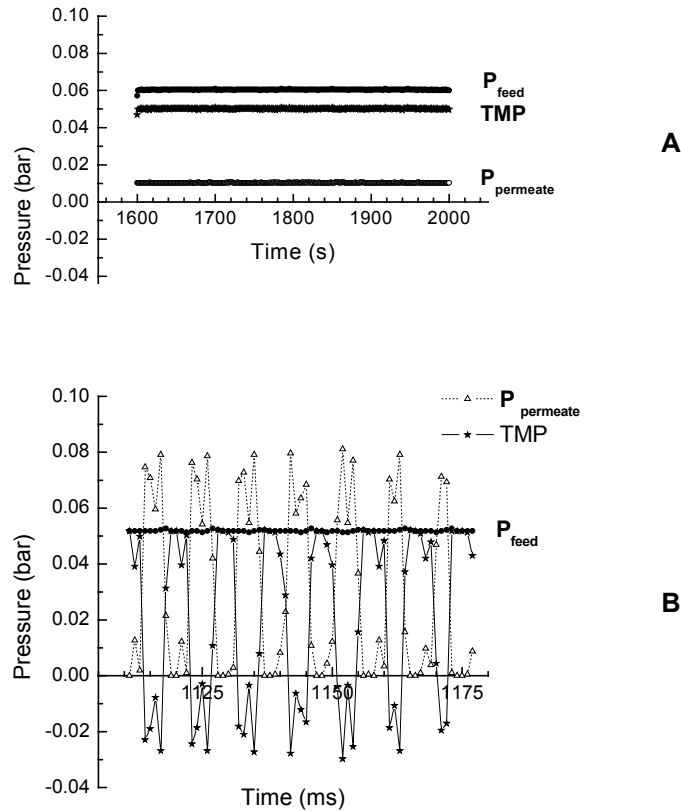


Figure 6. Pressure as a function of time using water as feed, without pulses (A) and with pulses (B) applied at 6.7 Hz, 64%, 20 ms.

As it is shown in Figure 6a, when no pulses were applied the transmembrane pressure ($P_{\text{feed}} - P_{\text{permeate}}$) was slightly lower than the feed pressure. As soon as pulses were applied (every 20 ms) a periodic increase of P_{permeate} above the feed pressure resulted in a negative TMP. In Figure 6b a detailed view of the pulse profile measured with water as feed during 75 ms is depicted. Backpulsing with silicon nitride microsieves is only partially effective to lift the deposited layer off the membrane because permeability still decreases in time. As we already mentioned in section 5.3.1, the great resistance to the flow offered by the backstructure may be the reason why the pulse is mitigated and the protein flux cannot be restored.

a. Optimization of pulse power and frequency

The operational backpulsing window in terms of pulse power and frequency was determined prior to the previously discussed experiments. First, the pressures obtained during 20 ms

water pulses at different power (from 45 to 80%) at 3.3 Hz were recorded and compared. Then, the power settings that resulted in higher efficiency or more negative TMP were selected and the backpulsing frequency was optimized for filtration of BSA solutions at neutral pH. The slopes of the permeability versus permeated volume were determined, which gave an indication of the fouling rate as a function of the frequency.

For the determination of the most optimal backpulsing power, water was used as a feed and pulses where applied at a frequency of 3.3 Hz at 20 mbar feed pressure. The feed and permeate pressures were registered for 45 and 64% power respectively. The outcome of this test is shown in Figure 7.

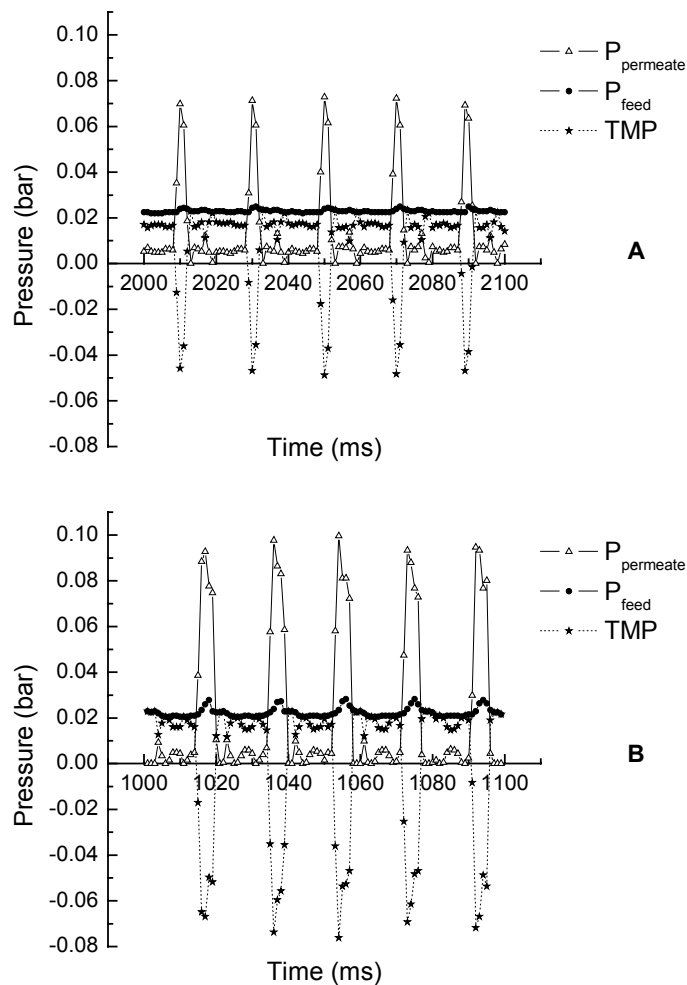


Figure 7. Pressure as a function of time in a backpulsing test with water at 20 mbar at 3.3 Hz and (A) 45%, and (B) 64% power.

In water, the main difference among pulses applied at different power is the peak value of the TMP. Higher absolute values of the TMP and, therefore, more effective pulses were obtained at 64% power. With water, a 42% increase of the pulse power (from 45 to 64%) at 3.3 Hz resulted in a 56% increase in negative TMP (from -50 to - 80 mbar). With these experimental conditions the pulse was also registered in the feed pressure (Figure 7b). Contrary to these results, no pulses were detected at the feed side when a BSA solution was filtered through a microsieve.

The influence of backpulsing frequency on flux decline was also studied. For the test where backpulsing was implemented (Figure 5, full dots), the frequency was reduced by a factor of two during filtration. The initial frequency was 6.7 Hz and was lowered to 3.3 Hz (a-b) until V=92 ml (b), then backpulsing was stopped, leading immediately to complete flux loss.

Table 1 displays the fouling rates (slope of relative permeability vs. permeated volume plot) of tests without backpulsing and with backpulsing at variable frequency (6.7, 5 and 3.3 Hz). From the results below we can clearly see that the fouling rate without backpulsing is almost double compared to experiments with backpulsing. Although the differences in slope for the various frequencies tested are not extremely large, we can see that the fouling rate is successfully reduced when backpulsing frequency is increased, even though the solute flux is lower.

Table 1. Effect of the backpulsing frequency on the fouling rate of BSA filtrations at pH=6.8. Fouling rate is expressed as a change in the relative permeability per permeated volume.

Variable	Frequency (Hz)	Fouling rate ($\times 10^{-3}$ ml)
<i>No backpulsing</i>	-	7.7 \pm 0.96
<i>Backpulsing</i>	3.3	4.84
	5	4.4
	6.7	4.07

Our observations point out that periodic backpulsing at low frequencies may not be effective to detach BSA from the microsieve surface. However, the trade-off of high-frequency backpulsing is the lower flux, as mentioned previously. These findings correspond very well to the predicted trends, which state that at low frequencies particle deposition in between pulses can occur, resulting in more flux decline. At high frequencies, though, a lower flux is obtained because the periods when permeate can be collected are much shorter [10, 24].

b. Effect of permeate backpulsing as a function of BSA solution concentration

In Chapter 4 experimental evidence indicated pore blocking as the cause flux decline during BSA filtration. Both the efficacy of the backpulse and the fouling rate will depend on the degree of aggregation of the solution, viscosity and protein-protein or protein-surface interactions. Theoretically, if less aggregation occurs permeation can be maintained for longer time. Moreover, if the deposited layer is not compact or the interactions between the aggregated protein clusters are weaker, it should be easier to remove them from the surface. At lower protein concentrations less aggregation should occur and therefore, a lower fouling rate should be observed. No differences in permeation or fouling rate were observed between experiments without backpulsing using 1 and 0.5 g/l BSA solutions. A distinct improvement was seen when backpulsing the most diluted BSA solution (see Figure 8).

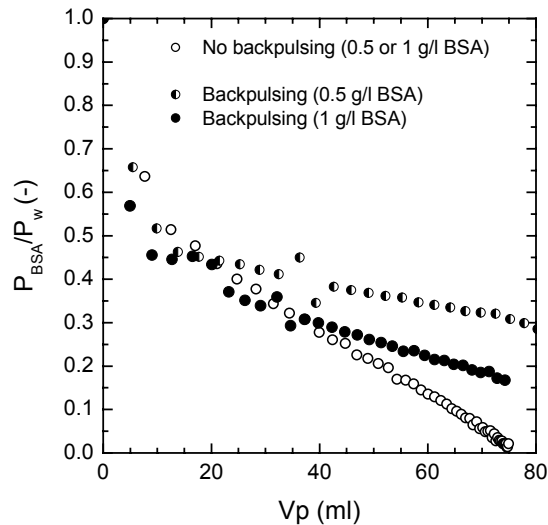


Figure 8. Influence of BSA concentration on the permeation rate. Backpulsing was performed at constant frequency (6.7 Hz), power (64%) and pulse length (20 ms). For comparison, the results for no backpulsing (independently of the two concentrations) are shown.

At a constant frequency of 6.7 Hz and 64% power, a higher permeation rate was measured for less concentrated (0.5 g/l) BSA feeds. With the least concentrated feed (0.5 g/l), fewer aggregate clusters are present per unit of permeated volume. Depending of the solution viscosity, for instance, different pulse efficiency might be obtained. That would result in a different membrane performance in terms of protein permeability.

5.3.3 Effect of discontinuous and continuous air sparging on BSA permeability

To assess the influence of air on the protein flux, two different approaches were taken into account. In the first place, air was dosed to the feed in a discontinuous way through a syringe (each dose containing approx. 0.5 ml air). In protein filtration, air bubbles affect the hydrodynamics in such a way that mass transfer and permeation are enhanced [20, 21]. Moreover, local changes of pressure and fluid hydrodynamic conditions can help to clear out the membrane surface from the deposited proteins. Contrary to backpulsing, the dosage of air pockets in a discontinuous manner resulted in an average stable BSA flux (1 mg/ml of BSA, pH=6.9), slightly lower than 20% of the maximum permeability (see Figure 9a). During the short periods when no air was applied the flux decreased with similar slopes (fouling rates) throughout the whole experiment.

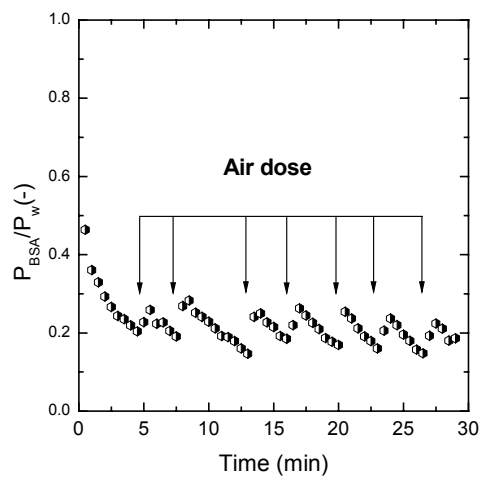


Figure 9. Discontinuous air sparging in filtration of a BSA solution. The arrows indicate the air dosages.

In fact, air can enhance mass transfer by reducing the polarization layer [15], and creates a combination of temporary increased pressure and local mixing. Air bubbles cause a perpendicular liquid flow away from the membrane able to remove part of the deposited aggregates from the surface. Figure 10 shows a computational fluid dynamics simulation (FEMLAB) of a fluid slug between two air bubbles on the membrane. The simulation data (crossflow of 0.165 m/s in a 700 micron high channel, laminar flow) illustrates a recirculating flow away from the surface, as seen in the down left corner. The fact that such transverse flow enhances mixing has been recently demonstrated by Günter and co-workers in PDMS microfabricated channels [25].

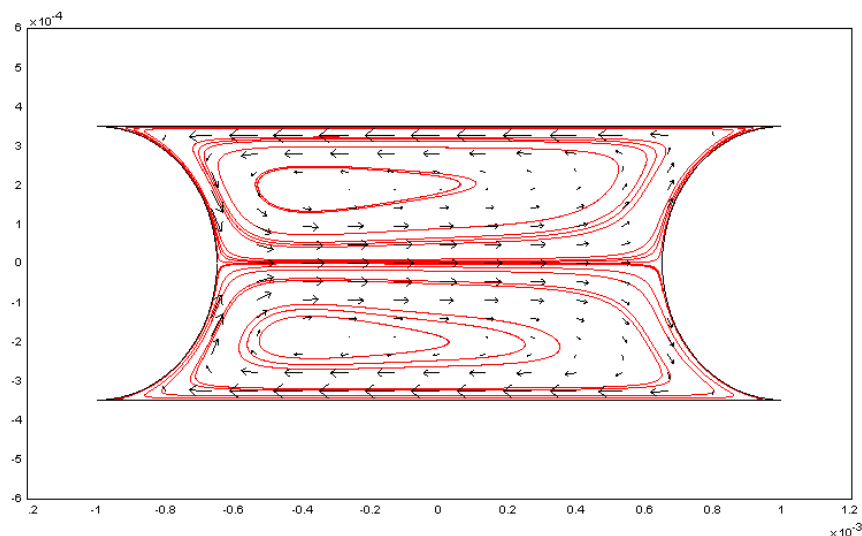


Figure 10. FEMLAB simulation of the fluid flow between two air bubbles, when passing over a membrane. The arrows indicate the liquid velocity and direction, and the continuous lines are the streamlines.

Contrary to our observations with water as a feed [26], air can be very beneficial to enhance permeation of a protein solution [20, 21]. BSA lowers the surface tension ($\gamma_{\text{BSA}}=54.5$ mN/m, $\gamma_{\text{H}_2\text{O}}=72.8$ mN/m, at 20°C) and improves the surface wetting. That is why no dewetting of the membrane takes place in BSA when air is present. If a continuous air flow is dispensed to the module even a more beneficial effect can be achieved. When air bubbles are injected to a channel, better mixing takes place and, moreover, the motion of air bubbles can drag particles away from the surface.

Air can have a negative effect on the protein flux if too large flows are applied. When too much air is dosed, permeation can be reduced due to a dilution of the liquid feed. In such case the flow transforms from bubbly flow (two-phase flow, with high air-liquid mixing) to a regime where the gas phase is predominant, with very little liquid regions. If less liquid regions are present less permeation can occur and, in the case of BSA, more foam can be formed. High gas sparging rates can induce foaming, activity loss and protein structural damage like tertiary structure change, fragmentation due to high shear and aggregation [21]. In our case foaming did not present a major problem.

Air was mixed with the feed BSA solution continuously and fed to the membrane module. The air-liquid slugs followed a straight trajectory throughout the whole module length, effectively traveling above the membrane and almost covering its whole surface (Figure 11).

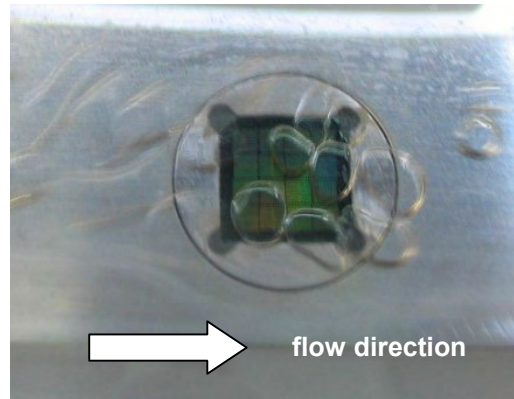


Figure 11. Continuous air sparging in BSA. The arrow indicates the direction of the liquid and air flow.

A preliminary experiment to study the optimal air flow is shown in Figure 12, using a BSA feed flow of 173 ml/min. Initially, air was introduced in the feed at 13 ml/min, and was increased stepwise until 42 ml/min every 5-8 minutes until $t=32$ min. At that point air flow was reduced first to 13 ml/min, and then to 10 ml/min.

At first, when air was initially dosed in the system (13 ml/min) a slight decline in relative permeability took place, since a few minutes were needed to stabilize pressure and flux after air dosage. Then, when the flow was increased to 18 ml/min, slightly lower permeability values were obtained, although they remained relatively constant. Increasing the flow to 30 ml/min decreased the absolute permeability a little more, until it reached a constant value ($\approx 20\%$). An increase of the flow to 42 ml/min led again to an initial loss in permeability, which stabilized and remained relatively constant during air dosage.

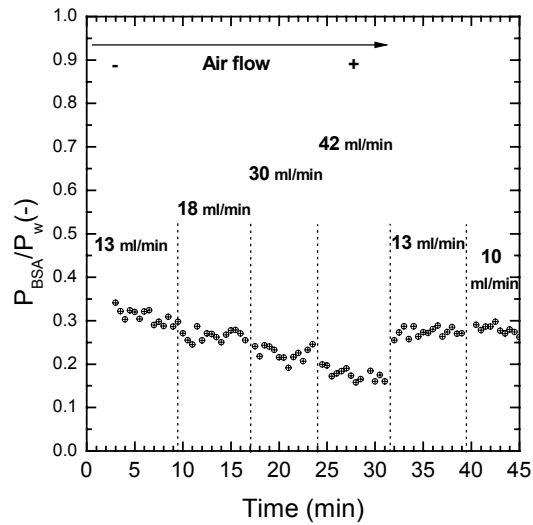


Figure 12. Effect of continuous and variable air sparging on the BSA flux at pH=6.8. Air flow rates varied from 10 to 42 ml/min.

Overall, a permeability loss of BSA was observed during the air dosage period with increasing air flow (from approx. 30% to 15%). However, a much larger permeated volume compared to a situation without air was obtained (twice as high). Alternatively, when the air flow was restored to a lower value (13 ml/min) at t=32 min, a constant and higher permeability was successfully obtained. Permeability reached similar values to the ones measured during the first minutes of filtration at 13 ml/min. Decreasing the flow to even lower values than 13 ml/min did not have any negative effect on the permeability, which remained constant in time.

The previous results are indicative of the importance of the magnitude of the air flow to obtain a constant protein flux. If the different regimes are taken individually and the relative permeability values noted, little permeability decrease takes place within the air dosage interval. Nevertheless, with increasing air flow a decrease in the relative permeability takes place.

Figure 13 exhibits the linear relationship between the protein permeability and air flow rate, together with the pressures measured throughout the experiment.

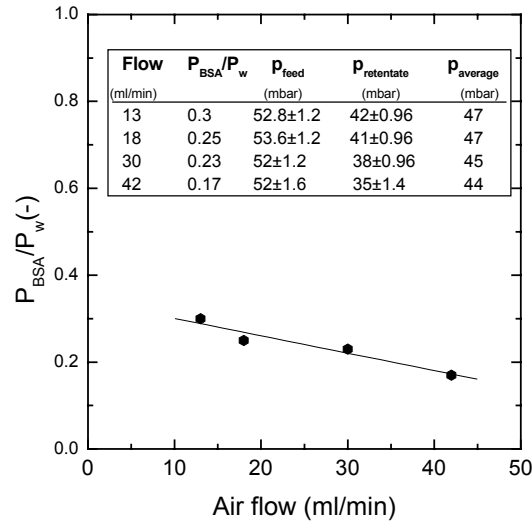


Figure 13. Relative BSA permeability versus air flow. The pressures registered at the feed and retentate varied systematically when air was added to the protein. On the table at the upper part of the graph a summary of the flows and permeabilities obtained, together with the feed and retentate pressures and the average pressure used to calculate the protein permeability: $p_{average} = (p_{feed} + p_{retentate})/2$ are given.

When air flowed through the module continuously and in a controlled manner, periodic changes in pressure occurred, which were registered by the sensors placed at the entrance and the retentate outlet of the module.

For air flows below 40 ml/min, feed and retentate pressures varied within a range of 2.4 mbar and 1.9 mbar, respectively. For the highest airflow, pressure fluctuated even more (3.2 and 2.8 mbar at the feed and the retentate side). These variations were taken into account for the permeability calculations. As the air flow increased the ratio between air and liquid volume (V_{air}/V_{BSA}) also increased linearly. That explains why a permeability decline is measured just when the air content is increased in the system. For these conditions BSA flow is around 173 ml/min, therefore, V_{air}/V_{BSA} increases from 7.7% to 24% with increasing air flow.

An overview of the outcome for the influence of air dosage at constant air flow (10 ml/min) is presented in Figure 14. When the filtration presented in Figure 12 was reinitiated at a lower air dosage, either no flux decline or flux loss was observed. When the air supply was suppressed (A) the protein flux declined very fast until the membrane was completely blocked.

As soon as air was introduced in the system a very successful recovery took place, reaching the same permeability as before suppressing the air.

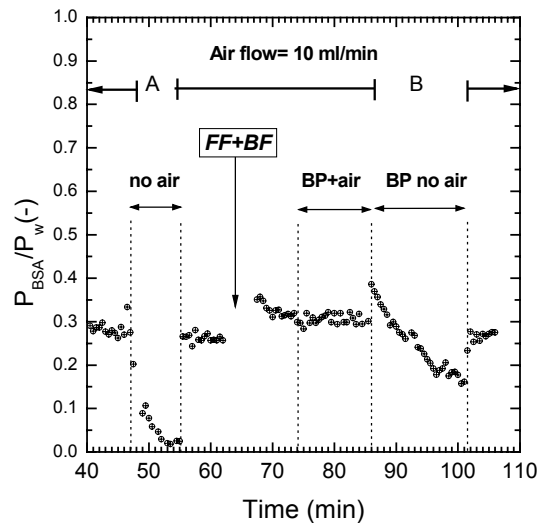


Figure 14. Continuous air sparging at constant air flow (10 ml/min) with a BSA solution at pH=6.8 (continuation of Figure 12). At the period (A) the air flow was suppressed, while at (B), apart from suppressing air, backpulsing was performed.

At t=65 min the module was forward and backflushed with water (FF+BF), and the filtration was reinitiated with air. Upon the flushing step, a slight recovery of the flux (from 27% to 32%) was measured.

Successively, backpulsing was initiated at 6.7 Hz, 64 % power and 20 ms pulse length, in combination with air sparging. As it occurred with only air, a constant and stable BSA flux was measured. Alternatively, if air was suppressed and the filtration operated only with backpulsing, flux decline was observed, less severe than in the case of no backpulsing. Stopping the pulses and reinitiating the air dosage resulted in constant flux/permeability at the initial air sparging value.

If the slopes from the relative permeability versus permeated volume of the regions without air (with and without backpulsing) are compared to the ones with air (Figure 14), an indication of the fouling rate and efficacy of the air sparging is obtained. For the regions where no air was dosed without and with backpulsing, slopes of -36×10^{-3} ml and -3×10^{-3} ml were measured,

respectively. The interval where a constant air flow was applied resulted in a slope close to zero, thus, constant permeability.

From the previous results we can conclude that the most enhanced situation is obtained by a BSA filtration with air sparging at low flow rates, followed by air sparging at higher rates. Backpulsing can enhance permeation but flux decline cannot be avoided.

5.3.4 Effect of continuous air sparging on the Lysozyme permeability

Air sparging as a method to reduce fouling delivered very successful results with BSA. It also resulted in very promising results when applied to other proteins like lysozyme (see Figure 15). Even though different air flows compared to BSA had to be applied for a successful effect, fluxes could be stabilized. Compared to BSA, a less ordered pattern of the air bubbles was observed when air sparging in lysozyme.

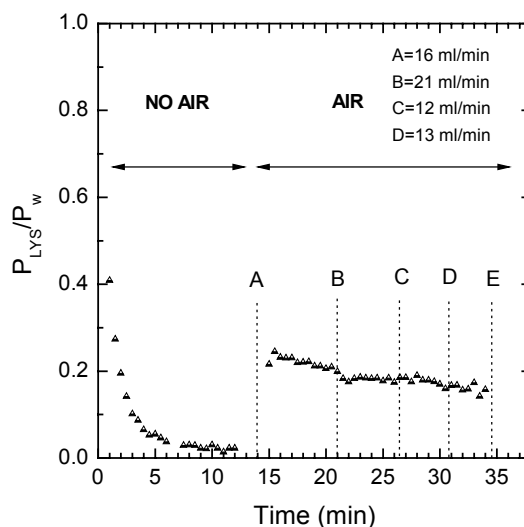


Figure 15. Relative LYS permeability versus time at neutral pH, without air sparging (until A) and with air sparging with variable air flows (from A to E).

A very rapid and severe permeability decline took place with 1 g/l LYS solution at pH=7 (LYS feed flow=173 ml/min). Permeability was immediately recovered from zero until 20% upon air sparging at 16 ml/min (A). During (A-B) the air flow was kept at 16 ml/min and a slight flux decline was observed, probably due to the lag-time for flow stabilization. Then the air flow was temporary increased to 21 ml/min (B-C) and successively decreased to 12-13 ml/min (C-D and D-E). In all those periods the overall permeability decreased slightly, however, air was still

able to remove LYS from the surface, even though less efficiently than with BSA. As mentioned in the previous chapter and reported by other authors [27], LYS adsorption on silicon-based surfaces at neutral pH also contributes to flux decline. In this sense, adhesion can reduce the efficiency of air sparging and lower permeabilities can be obtained.

5.4 Conclusions

In order to reduce fouling caused by globular proteins like BSA several strategies have been investigated in this chapter, such as forward and backflushing, permeate backpulsing and air sparging.

Backflushing resulted in a more significative flux recovery than forward flushing, independently of the frequency of application. Water backflushing was effective even at low P_{BSA}/P_w , resulting in approx. 30% flux recovery.

Permeate backpulsing consists in reversing the transmembrane pressure during a pulse. In this way the permeate flow is reversed, and returned to the feed side of the crossflow module. Backpulsing at high frequencies (6.7 Hz) was also an effective way to enhance the permeation rate, since the deposited aggregates could be removed from the membrane surface. The backpulsing power played an important role in the efficacy of the pulse: the higher the power the more negative the TMP. The first permeability values obtained when initiating backpulsing were lower than for the non-backpulsing situation. The permeated volume was successfully increased and the flux decrease retarded when backpulsing was applied.

Air sparging has a much more significant effect on the BSA flux recovery than backpulsing. By feeding relatively large air bubbles to the membrane module a bubbly flow forms, with periodic but short regimes of air and liquid. Due to the changed hydrodynamic conditions near the membrane surface, mixing is enhanced and concentration polarization is greatly reduced. In our observations, relatively low air flow rates (10-15 ml/min) with a liquid BSA flow of 180 ml/min, were the most optimal conditions to obtain a constant BSA permeability and large permeate volumes. Besides, air sparging was also suitable to recover fluxes in the case of other proteins, like Lysozyme. Constant protein fluxes with air sparging represent a breakthrough in microsieve filtration, whenever foaming does not represent a major problem.

In this work we have successfully applied strategies that allow higher permeation (like backpulsing) and stabilization of the BSA permeability (air sparging). Air sparging at low air flows has proved to be the most optimal technique to successfully suppress flux decline. The creation of a two-phase flow can enhance mass transfer, by creating a transverse flow that can remove the deposited aggregated layer.

5.5 Acknowledgements

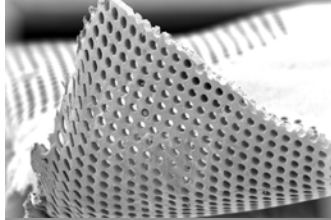
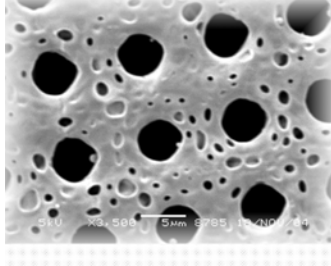
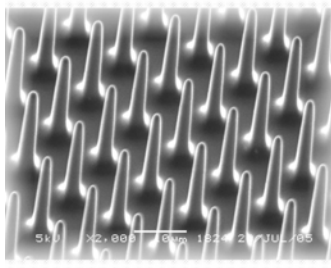
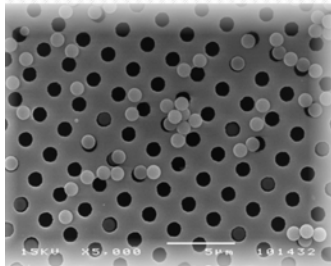
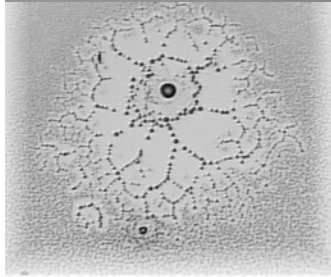
The author wishes to acknowledge Ronald Jansen, Frans Pronk and Lutgarde Lemmens from Fluxxion B.V. (Eindhoven) for kindly providing the silicon nitride microsieves. Maik Geerken is acknowledged for the assistance in the backpulsing profile tests and Rob Lammertink is acknowledged for performing the FEMLAB simulation.

5.6 References

- [1] S. T. Kelly, A. L. Zydney, Protein Fouling during microfiltration: comparative behavior of different model proteins, *Biotechnol. Bioeng.* 55 (1997) 91.
- [2] G. Belfort, R. H. Davis, A. L. Zydney, The behavior of suspensions and macromolecular solutions in crossflow microfiltration, *J. Membr. Sci.* 1 (1994) 95.
- [3] V. G. J. Rodgers, R. E. Sparks, Effect of transmembrane pressure pulsing on concentration polarization, *J. Membr. Sci.* 68 (1992) 149.
- [4] V. Kuberkar, P. Czekaj, R. Davis, Flux enhancement for membrane filtration of bacterial suspensions using high frequency backpulsing, *Biotechnol. Bioeng.* 60 (1998) 77.
- [5] R. Sondhi, R. Bhave, Role of backpulsing in fouling minimization in crossflow filtration with ceramic membranes, *J. Membr. Sci.* 186 (2001) 41.
- [6] R. Sondhi, Y. S. Lin, F. Alvarez, Crossflow filtration of chromium hydroxide suspension by ceramic membranes: fouling and its minimization by backpulsing, *J. Membr. Sci.* 174 (2000) 111.
- [7] C. S. Parnham, R. H. Davis, Protein recovery from bacterial cell debris using crossflow microfiltration with backpulsing, *J. Membr. Sci.* 118 (1996) 259.
- [8] W. D. Mores, R. H. Davis, Yeast foulant removal by backpulses in crossflow microfiltration, *J. Membr. Sci.* 208 (2002) 389.
- [9] W. D. Mores, R. H. Davis, Yeast-fouling effects in crossflow microfiltration with periodic reverse filtration, *Ind. Eng. Chem. Res.* 42 (2003) 130.
- [10] W. D. Mores, C. N. Bowman, R. H. Davis, Theoretical and experimental flux maximization by optimization of backpulsing, *J. Membr. Sci.* 165 (2000) 225.
- [11] W. F. Jones, R. L. Valentine, V. G. J. Rodgers, Removal of suspended clay from water using transmembrane pressure pulsed microfiltration, *J. Membr. Sci.* 157 (1999) 199.
- [12] E. Wen, L. D. Cinelli, D. Murray, R. J. Lander, S. L. Sagar, A. L. Lee, Purification of a polysaccharide conjugate vaccine using microfiltration membranes in backpulsing mode, *J. Membr. Sci.* 258 (2005) 23.

- [13] V. T. Kuberkar, R. H. Davis, Microfiltration of protein-cell mixtures with crossflushing or backflushing, *J. Membr. Sci.* 183 (2001) 1.
- [14] M. H. V. Mulder, *Basic Principles of Membrane Technology*, 2nd Edition, Kluwer Academic Publishers, Dordrecht, 1996.
- [15] Z. F. Cui, S. Chang, A. G. Fane, The use of gas bubbling to enhance membrane processes, *J. Membr. Sci.* 221 (2003) 1.
- [16] C. K. Lee, W. G. Chang, Y. H. Ju, Air slugs entrapped crossflow filtration of bacterial suspensions, *Biotechnol. Bioeng.* 41 (1993) 525.
- [17] Z. F. Cui, K. I. T. Wright, Gas-liquid two-phase cross-flow ultrafiltration using hollow fibre membranes, *J. Membr. Sci.* 90 (1994).
- [18] S. R. Bellara, Z. F. Cui, D. S. Pepper, Gas sparging to enhance permeate flux in ultrafiltration using hollow fibre membranes, *J. Membr. Sci.* 121 (1996) 175.
- [19] C. Cabassud, S. Laborie, L. Durand-Bourlier, J. M. Laine, Air sparging in ultrafiltration hollow fibers: relationship between flux enhancement, cake characteristics and hydrodynamic parameters, *J. Membr. Sci.* 181 (2001) 57.
- [20] Q. Y. Li, Z. F. Cui, D. S. Pepper, Enhancement of ultrafiltration by gas sparging with flat-sheet membrane modules, *Sep. Purif. Technol.* 14 (1998).
- [21] Q. Y. Li, Z. F. Cui, D. S. Pepper, Fractionation of HSA and IgG by gas sparged ultrafiltration, *J. Membr. Sci.* 136 (1997) 181.
- [22] A. Nabe, E. Staude, G. Belfort, Surface modification of polysulfone ultrafiltration membranes and fouling by BSA solutions, *J. Membr. Sci.* 133 (1997) 57.
- [23] G. Brans, J. Kromkamp, N. Pek, J. Gielen, J. Hek, C. J. M. v. Rijn, R. G. M. v. d. Sman, C. G. P. H. Schroën, R. M. Boom, Relation between flux behavior and microsieve design for latex particle filtration, in preparation.
- [24] S. Redkar, V. Kuberkar, R. H. Davis, Modeling of concentration polarization and depolarization with high-frequency backpulsing, *J. Membr. Sci.* 121 (1996) 229.
- [25] A. Günther, S.A. Khan, M. Thalmann, F. Trachsel, K.F. Jensen, Transport and reaction in microscale segmented gas-liquid flow, *Lab on a Chip* 4 (2004) 278.
- [26] M. Gironès, Z. Borneman, R. G. H. Lammertink, M. Wessling, The role of wetting on the water flux performance of microsieve membranes, *J. Membr. Sci.* 259 (2005) 55.
- [27] K. Rezwan, L.P. Meier, L.J. Gauckler, Lysozyme and bovine serum albumin adsorption on uncoated silica and AIOOH-coated silica particles: the influence of positively and negatively charged oxide surface coatings, *Biomaterials* 26 (2005) 4351.





Chapter 6

Strategies to reduce protein fouling with Si_xN_y microsieves

II. Surface modification with PEG polymers

6.1 Introduction

In the previous chapter, the benefits of air sparging for achieving constant protein solution permeability with silicon microsieves have been presented. Unfortunately, air sparging cannot be applied in most industrial applications due to foaming and risk of protein denaturation. For this reason, other antifouling strategies suitable to be applied in industry must be investigated. Backpulsing at high frequencies can enhance protein permeation with silicon nitride microsieves. Nonetheless, its effect is not sufficient to disturb the polarization layer and detach the deposited foulants completely. In a system with microsieves and Bovine Serum Albumin (BSA) aggregate deposition followed by pore blocking is the predominant mechanism for fouling [1]. In spite of this, a certain degree of adhesion of proteins to the surface may still occur.

In literature, the combination of surface modification and backpulsing are normally more effective in retarding or even suppressing fouling in microfiltration than the separated strategies [2, 3]. With certain coatings the deposited layers are not strongly attached and can be easily removed by the pulses. According to these findings, surface modification of silicon nitride microsieves with coatings that can prevent protein adhesion would be another approach to enhance flux and improve the filtration performance.

Traditionally, it has been widely postulated that hydrophilic membranes should be used in protein filtration so that less fouling occurs [4]. It is believed that proteins adsorb more onto non-hydrophilic surfaces due to attractive interactions between hydrophobic areas of a protein and hydrophobic surfaces. This is normally followed by conformational changes or protein unfolding, which results in the hydrophobic core of the macromolecule exposed to the surface. A gain in entropy caused by dehydration of both protein and surface is the driving force for adsorption [4, 5]. Even though there is quite a general acceptance about the driving forces for protein adsorption [6], the correlation between wettability and adsorption has been questioned in a great extent. Adsorption depends on a large number of variables and parameters such as charge (charged hydrophilic surfaces can also adsorb proteins of the opposite charge), pH and ionic strength, and not only on the hydrophilic/hydrophobic surface distinction measured by contact angles, for instance. Contact angles are frequently averaged properties over a larger area, while adsorption is a result of local interactions [5]. Furthermore, the surfaces that are most resistant to protein adsorption are often intermediate in hydrophilicity, for instance the ones containing oligo(ethyleneglycol) groups [7]. With this knowledge, complementary variables other than wettability should be taken into account to design an antifouling surface.

In order to evaluate the performance of several coatings, researchers normally perform static protein adsorption. The extrapolation of such data to filtration performance is often not straightforward. In protein filtration, other parameters besides surface properties must be considered (hydrodynamics, solution properties, membrane morphology, etc.). In fact, depending on the predominant fouling mechanism surface properties may play a minor role on the flux decline.

In medical or biological applications where protein or cell-resistant surfaces are requested, polyethylene glycol (PEG)-based compounds are frequently used as coating candidates [8, 9]. PEGs in aqueous solution are highly mobile molecules with large exclusion volume, and mainly free of charges [10]. The inertness of PEG-based surfaces is based on steric repulsion, since van der Waals contributions are low and electrostatic interactions negligible [11, 12]. Protein repellency increases with molecular weight, PEG surface coverage and chain length [11-13].

Self-assembled monolayers (SAMs) are a very useful tool to create surfaces with covalently attached PEG chains because compact and thin layers can be attached in one step. The most explored SAMs containing PEG moieties are oligo (ethyleneglycol) alkanethiolates on gold surfaces [7,14,15] and oligo (ethyleneglycol)-terminated silanes [16, 17]. Silanated-PEGs are widely used to modify oxide-based surfaces like silicon, glass or titania but they are also potentially suitable for silicon nitride microsieves. Recently, Jon and co-workers have reported a method to create non-fouling surfaces via multiple covalent bonds by ultrathin self-assembled monolayers [18]. The advantage of this method is that only a simple substrate functionalization with OH groups is required, and one-step PEG grafting can be achieved using a stable random copolymer.

The main goal of this research is to reduce flux decline of proteins. In this chapter the effect of an antifouling PEG-based coating on the flux of BSA solutions will be studied with silicon nitride microsieves. The combination of surface modification and several strategies such as forward or backflushing, backpulsing or air sparging will be taken in consideration for process optimization. With the results and observations from the model protein experiments, the most promising and optimal experimental conditions will be extrapolated to a real feed like skimmed milk. Sterilized milk is normally treated above 100°C to reduce the bacterial content, and it usually contains a maximum fat percentage of 0.5%.

Milk filtration with silicon nitride microsieves is the final aim of the research framework in which this investigation is found. Therefore, a glimpse on the fouling behavior of microsieves with milk is also described in this thesis.

6.2 Materials and methods

6.2.1 Materials

Silicon and silicon-rich silicon nitride (Si_xN_y) dices ($1 \times 1 \text{ cm}^2$ wafer samples), glass slides and Si_xN_y microsieves were used for the surface modification. The surface modified Si_xN_y microsieves (pore size $1.2 \text{ }\mu\text{m}$, $1 \times 1 \text{ cm}^2$) were used for BSA and milk crossflow filtrations. Ultrapure water ($18.2 \text{ M}\Omega\text{cm}$) for flux measurements was obtained from a Millipore purification unit MilliQ plus. 1 mg/ml of BSA (Fraction V, Fluka) dissolved in filtered phosphate buffer 50mM at $\text{pH}=6.8 \pm 0.1$ was used as model protein for most tests. The protein solutions were freshly prepared and stored at 8°C for maximum 2 hours before use.

In milk filtrations, commercially available sterilized skimmed milk (Euroshopper, $\text{pH}=7$) was used directly as feed without any pre-treatment.

6.2.2 Synthesis of Poly (PEGMA-r-TMSMA) random copolymer

The random block copolymer poly (TMSMA-r-PEGMA) was synthesized by free radical polymerization under anhydrous conditions (see Figure 1).

10 mmol (4.75 g , 1 eq.) of inhibitor-free poly (ethylene glycol) methyl ether methacrylate (PEGMA, Sigma) with average molecular weight 475 Da were added to 10 mmol (2.5 g , 1 eq.) of 3-(trimethoxysilyl)- propyl methacrylate (TMSMA, Sigma) in 14 ml tetrahydrofuran (THF), using 0.1 mmol (16.5 mg , 0.01 eq.) of 2, 2-Azobis-isobutyronitril (AIBN) as initiator. The reaction was kept in a flask under an argon flow at 70°C for 24 h . The excess of solvent was evaporated first at 40°C , and then in vacuum for 8 hours at room temperature. The product was obtained as a viscous liquid, and characterized by $^1\text{H NMR}$ (400 MHz , CDCl_3).

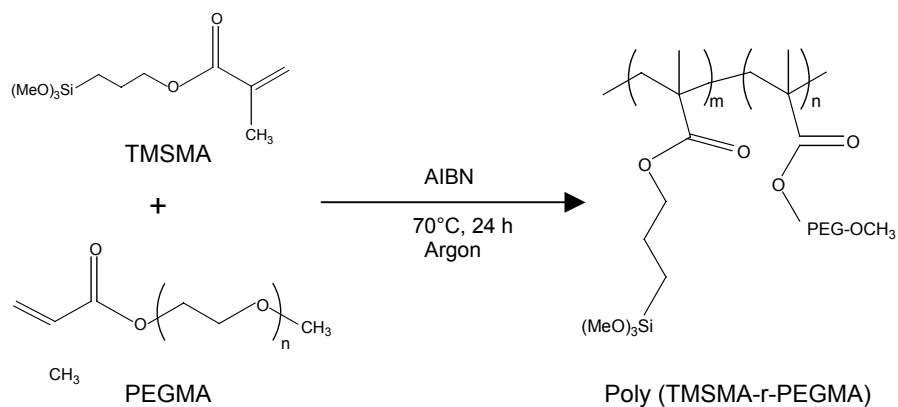


Figure 1. Poly (TMSMA -r-PEGMA) synthesis by free radical polymerization of TMSMA and PEGMA.

6.2.3 Poly (PEGMA-r-TMSMA) SAM formation and protein adhesion studies on oxide-based surfaces

Polymeric SAMs of the copolymer were covalently grafted on three types of surfaces: silicon, silicon nitride and glass. The coating procedure was as follows: first the substrates were oxidated by oxygen plasma at 500 W for 10 min. Then the samples were dipped into a 5 g/l poly (TMSMA-r-PEGMA) solution in methanol (pre-filtered through a commercial 0.45 μm filter) for 1 h at room temperature. Afterwards, a rinsing step in methanol and a curing step in a nitrogen oven at 120°C for 15 minutes were applied.

After grafting, the surfaces were characterized in terms of wettability (contact angles) and surface elemental composition (XPS) and protein adhesion. The grown oxide by oxygen plasma and polymer coating thickness were determined on silicon with a VASE (VB-400) spectroscopic ellipsometer (Woollam) at an angle of incidence of 75°.

a. Protein patterning with a microfluidic device and confocal fluorescence microscopy

Qualitative protein adsorption information was obtained by detecting the fluorescence intensity of labeled BSA on unmodified and polymer coated microscope glass slides. Glass was used as a substrate because silicon and silicon nitride surfaces give background fluorescence, which masks the labeled protein.

A PDMS stamp with microfluidic channels (see Figure 2) was fabricated by soft lithography [19].

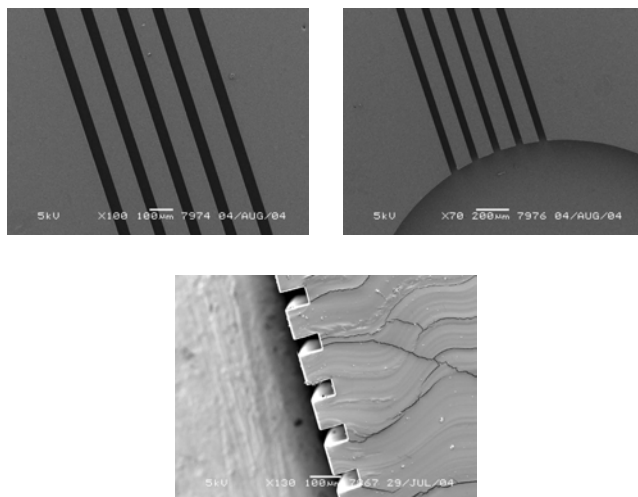


Figure 2. Scanning Electron Microscope pictures of the PDMS replica containing 5 microchannels communicated by an inlet and outlet reservoir.

PDMS (Sylgard 184, 1:10 mixture of the curing agent and the elastomer) was degassed for some minutes and poured on a silicon wafer containing a pattern with microfluidic channels. The stamp was formed by curing the PDMS on the silicon wafer at 70° for 2-3 h. When solidification was complete a PDMS replica was obtained by peeling the stamp from the wafer. The replica contained a structure with two circular reservoirs communicated by five identical channels of approximately 50 μm width and 80 μm depth. The PDMS stamp was used to define the microfluidic channels.

A 0.5 mg/ml FITC-BSA solution in saline phosphate buffer (PBS) at pH=7.4 was injected through the feed inlet. The protein solution was pumped through the channels for an hour. Afterwards, the channels were rinsed with a phosphate buffer solution (pH=7.4) and MilliQ water to remove the excess of non-adsorbed protein. The fluorescent pattern of the adsorbed FITC-BSA was detected by Laser Scanning Confocal Microscopy (Carl Zeiss LSM 510 microscope, equipped with an argon laser module from Carl Zeiss Inc., Thornwood, NY). Images were acquired at 488 nm (10% transmission) using 10x and 40x objectives.

b. Static protein adsorption. Thickness determination by ellipsometry

The adsorption of 1 mg/ml BSA at pH=7.4 at 20°C on unmodified, plasma oxidized and polymer coated silicon dices was measured in time by ellipsometry (VASE ellipsometer at 75°, λ=632.8 nm). The amount of adsorbed BSA, Γ_{BSA} (mg/cm²), was calculated from equation (1), according to the model developed by de Feijter [20]:

$$\Gamma_{BSA} = \frac{d_{BSA}(n_{BSA} - n_0)}{(dn/dC)} \quad (1)$$

where d_{BSA} is the thickness of the BSA layer (cm). n_{BSA} is the refractive index of BSA and is equal to 1.37 [20, 21], n_0 is the refractive index of the medium (air, $n_0=1$), and (dn/dC) is the protein refractive index increment, which is considered to be 0.187 cm³/g.

6.2.4 Crossflow filtration of BSA and skimmed milk with PEG-coated microsieves

The microsieves used in this chapter were pre-wetted with water. The clean water permeability of polymer coated microsieves was measured in the pressure range of 30-50 mbar at 20±2°C before the filtration of BSA and/or milk solution.

BSA permeability was measured at a transmembrane pressure of 50±3 mbar at 10±2°C and pH= 7±0.2, with an average crossflow velocity of 0.165 m/s (pumped in recirculation mode

through a microannular pump). The BSA flux decline without and with backpulsing was compared at the same experimental conditions. Backpulsing was performed at 6.7 Hz, 64 % power and 20 ms pulse length. Air sparging was also used to investigate its influence on the protein flux decline, and was applied at 13 ml/min, with the set-up described in Chapter 5. Skimmed milk filtration was performed between 18-38 bar at 7°C (pH=7), with both cleaned microsieves (submitted to an alkaline treatment at 50°C for 30-60 minutes, as described in Chapter 4) and PEG coated microsieves. Backpulsing and air sparging were also applied to the filtration to enhance permeation.

6.2.5 Optical Microscopy

Optical microscope images of the membrane surfaces were taken with a Zeiss Axiovert 40 MAT Optical Microscope.

6.3 Results and discussion

6.3.1 Construction of protein-repellant surfaces: covalent grafting of Poly(PEGMA-r-TMSMA) on oxide-based surfaces and microsieves

The random copolymer poly (PEGMA-r-TMSMA) was synthesized by free radical polymerization using the method described by Jon *et al.* [18]. The polymer was moisture-sensitive and was kept in a sealed container under an inert atmosphere. Otherwise, crosslinking of the chains could occur easily due to the methoxysilane end groups. The polymer was characterized by ^1H NMR, where the most characteristic peaks corresponded to $\delta=4.13$, ($\text{CO}_2\text{-CH}_2$) at PEGMA, and $\delta=3.92$, ($\text{CO}_2\text{-CH}_2$) at TMSMA. The molecular weight was then estimated by viscosity and compared by polystyrene standards in CHCl_3 . By this method a molecular weight of approximately 830 kDa was obtained. This is significantly higher than the values reported by Jon and co-authors [18], presumably due to some crosslinking of the polymer chains. After polymer characterization, the chains were covalently grafted to oxidized silicon, glass and silicon nitride. The anchoring part (TMSMA) can attach to the surface OH groups through Si-O covalent bonds, forming a dense packed layer with multiple PEGMA end groups, able to reduce non-specific adsorption (Figure 3).

a. Characterization of covalently grafted Poly (PEGMA-r-TMSMA)

Prior to coating, the thickness of the native oxide on silicon and the oxide grown by plasma were measured by ellipsometry, resulting in layers of about 2 and 6 nm, respectively. Upon

grafting, a Poly (PEGMA-r-TMSMA) film of ca. 2.3 nm was detected on silicon in dry state. Jon *et al.* [18] predicted the structure of the grafted film as shown in Figure 3. They also estimated that, if the PEG side chains were aligned vertically, a thickness similar to the one we report here would be obtained.

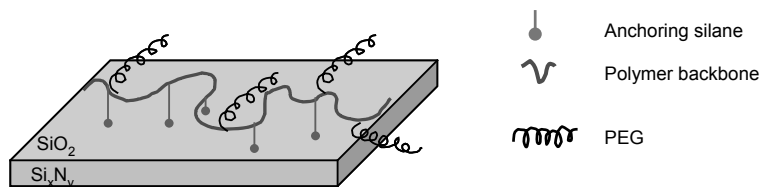


Figure 3. Predicted structure of the Poly (PEGMA-r-TMSMA) copolymer on oxidized surfaces (eg. oxidized silicon nitride) [18].

With the measured polymer thickness, d_p (cm) and the density of the crystalline PEG film (ρ_0), assumed to be 1.08 g/cm^3 , the surface concentration of the PEG film can be estimated with the following formula:

$$\Gamma_{\text{PEG}} = d_p \rho_0 \quad (\mu\text{g/cm}^2) \quad (2)$$

With a layer thickness of 2.3 nm, Equation 2 results in a polymer surface concentration Γ_{PEG} of $0.246 \mu\text{g/cm}^2$.

The monolayers were also characterized by XPS to determine the elemental composition of the polymer layer on silicon and silicon nitride (see Table 1).

Table 1. XPS elemental composition on unmodified silicon and silicon nitride, plasma treated silicon nitride and polymer coated silicon nitride and silicon.

Silicon Nitride	C 1s	N 1s	O 1s	Si 2p
Unmodified	7.88	37.54	22.52	33.86
O ₂ -plasma	3.99	4.22	66.24	25.55
<i>poly(PEGMA-r-TMSMA)</i>	27.30	2.3	52.32	18.08

Silicon	C 1s	O 1s	Si 2p
Unmodified	9.6	40.81	49.59
<i>poly(PEGMA-r-TMSMA)</i>	26.99	53.22	19.79

For silicon nitride samples, the oxygen content increases significantly after the oxidation by plasma, as expected and previously observed [22, 23]. After grafting with the polymer, the carbon content as well as the C/O ratios increased significantly on both substrates, indicating the presence of the polymer layer. Very similar element percentages and C/O ratios were measured for the grafted polymer on silicon and silicon nitride. Moreover, high-resolution carbon spectra confirmed the presence of the polymerization product on the surfaces (Figure 4).

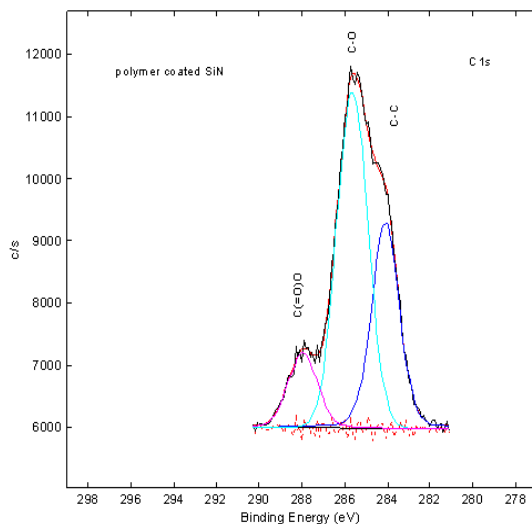


Figure 4. High-resolution carbon XPS spectrum on PEG-coated silicon nitride dices. The same results were obtained on silicon.

The carbon peak resulted in three clear peaks of carbons present in the product backbone, the most intense being C-O, followed by C-C, and C(=O)O as the least intense.

Subsequently, the wettability of the modified samples was monitored by static water contact angles using the sessile-drop method. Table 2 shows the water contact angle results on glass, silicon and silicon nitride.

Table 2. Water contact angles on uncleaned, oxidized and polymer coated glass, silicon and silicon nitride.

Substrate	Uncleaned	O₂-plasma	Poly(TMSMA-r-PEGMA)
Glass	20-45°	0°	51.5±3°
Silicon	29.6±0.24°	0°	
Silicon nitride	30.95±0.3°	0°	

Even though the uncleaned substrates had very different initial contact angles, after polymer grafting all samples have contact angle values around 50°. The contact angles of all coated substrates stored in air were constant for more than two months. Also constant contact angles were measured after the coated substrates were immersed in saline phosphate buffer pH=7.4 at 20°C, indicating that the layer did not detach from the surface. These findings agree very well with the stability results of Khademhosseini and co-workers [24] in aqueous solutions.

A different situation was observed when the substrates were exposed to an alkaline environment (pH=12 for 30 min at 50°C), which corresponds to the cleaning treatment of the silicon nitride microsieves after a protein filtration. After such treatment contact angles of around 20° were measured. The increased water wettability of the cleaned substrates suggests that the polymer detaches from the surface due to hydrolysis of the Si-O bond.

b. Evaluation of the non-fouling properties

Protein adsorption for poly (TMSMA-r-PEGMA) random copolymer coatings was studied qualitatively and quantitatively.

Qualitative information was obtained by studying the emitted fluorescence of a FITC-BSA pattern transferred on unmodified and polymer coated glass slides with a PDMS stamp. The glass slides were placed under a confocal microscope and the fluorescence was measured at 488 nm. The pictures taken after patterning clearly indicate the channels through which the protein flowed, by the fluorescence detected (see Figure 5).

On the unmodified glass slides a clear fluorescent pattern is detected (Figure 5 A). On the contrary, almost no fluorescence is detected on the coated slides (Figure 5 B). In the fluorescent profile from uncoated and coated slides (Figure 5 C) higher fluorescence intensity was detected for unmodified glass while almost no fluorescent intensity was detected on the coated samples, indicating that poly (PEGMA-r-TMSMA) strongly suppresses BSA adhesion.

For comparison, the fluorescence of hydrophobized slides ($\theta=105^\circ$) coated with a perfluorinated silane (FOTS) was measured. Figure 6 illustrates higher magnification (40x) pictures of two channels on unmodified (A), poly (PEGMA-r-TMSMA) coated (B) and FOTS coated glass slides (C). No detectable protein is present on the PEG coated samples, contrary to the other slides. As expected, BSA also adheres on the hydrophobic surfaces. From the profiles of the unmodified and FOTS glass, little differences in color intensity can be seen, therefore it is very difficult to determine in which case more adsorption takes place. Moreover, at this magnification a certain degree of fluorescence quenching might have occurred during the observation time, which can result in lower intensity.

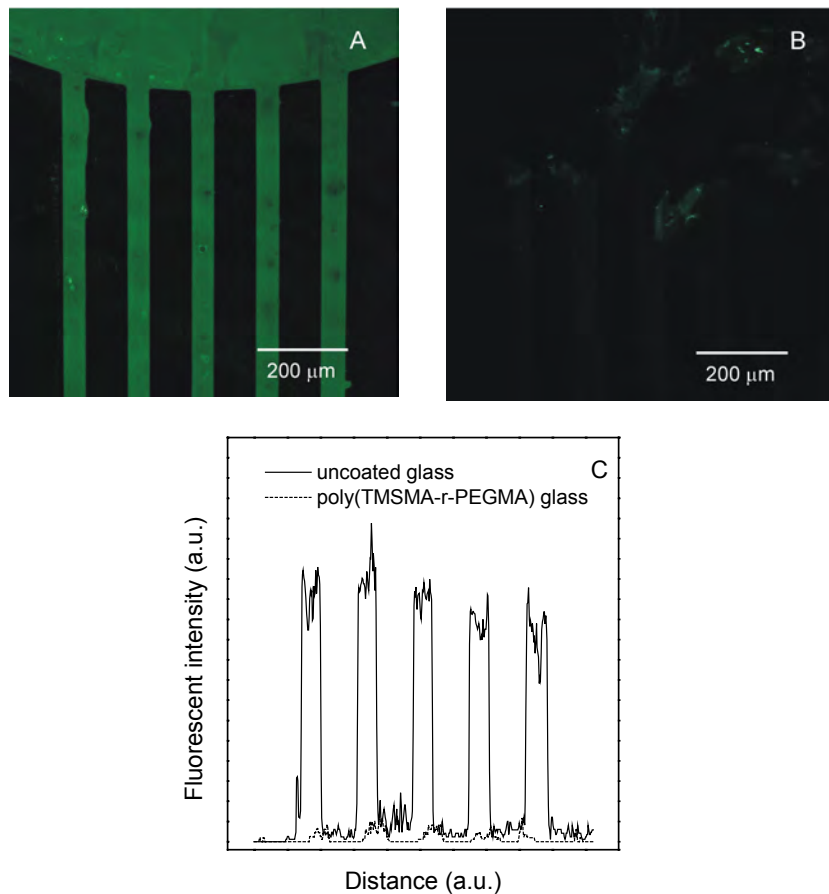


Figure 5. Confocal microscopy images (10x magnification) of patterned unmodified (A) and poly (TMSMA-r-PEGMA) (B) coated glass slides. The green pattern indicates the pathway of adsorbed FITC-BSA. Fluorescent intensity profile (C) of Figures (A) and (B).

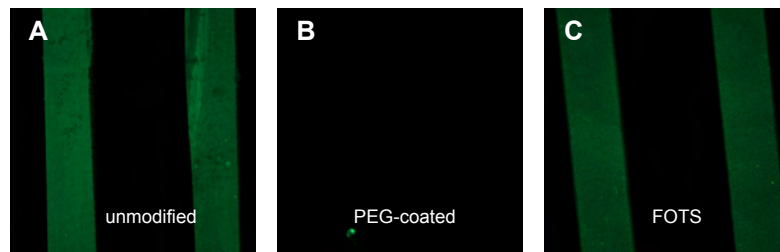


Figure 6. Confocal microscopy images (40x magnification) of patterned unmodified (A), poly (TMSMA-r-PEGMA) coated (B) and FOTS coated (C) glass slides. The green pattern indicates the pathway of adsorbed FITC-BSA.

Quantitative BSA adsorption results for unmodified, oxidized (by plasma treatment) and PEG coated silicon dices were obtained by ellipsometry. The BSA thicknesses and adsorbed concentrations are shown in Figure 7.

After 5 days no detectable amounts of protein adhered on the PEG coated samples. Meanwhile, BSA layers of 3.95 nm and 1.4 nm were measured on untreated and oxidized silicon dices, respectively. The measured Γ_{BSA} after 120 h of incubation represent approximately 1 and 1/2 a monolayer of protein on untreated and oxidized silicon, since one adsorbed monolayer of BSA is about 6-8.4 mg/m² [25]. Ying *et al.* reported similar results as the ones obtained in our study, for Γ_{BSA} on silicon after 2 h of incubation [26].

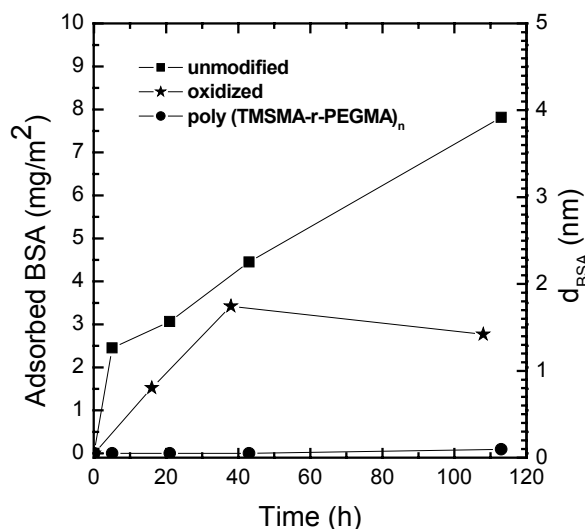


Figure 7. BSA thicknesses (d_{BSA}) and adsorbed BSA (Γ_{BSA}) measured by ellipsometry on unmodified, oxidized and PEG coated silicon dices.

In such a period of time, water contact angles increased from 30° to approximately 80° for the unmodified silicon dices, and from 0° to 40° for the oxidized surfaces. The increase in contact angles for unmodified and oxidized silicon also indicates that BSA is adsorbed on the surface. The contact angles of PEG coated samples remained constant during 5 days.

The outstanding antifouling properties presented by the PEG-copolymer coated samples are due to the steric hindrance caused by the large exclusion volume of the PEG molecules. This makes this material a great candidate for coating microsieves for reduced adsorption. Silicon nitride microsieves with pore diameter of 1.2 μm were coated by the

method described in section 6.2.3 and further filtrations were performed with BSA and skimmed milk.

6.3.2 Effect of in-line permeate backpulsing with Poly (PEGMA-r-TMSMA) coated microsieves

The coated microsieves used in this chapter present clean water permeabilities from 2 to 3×10^5 l/m²hbar. The scattering in permeabilities is caused by the coating method, which can sometimes result in accumulated polymer on the microsieve. The filtration of BSA at 50 mbar (pH=7.1) through a poly (PEGMA-r-TMSMA)-modified microsieve delivered exactly the same results as with an untreated or alkaline-cleaned membranes. Flux declined very rapidly during the first minutes of filtration, until it reached no permeation approximately 65 ml (see empty stars, Figure 8a).

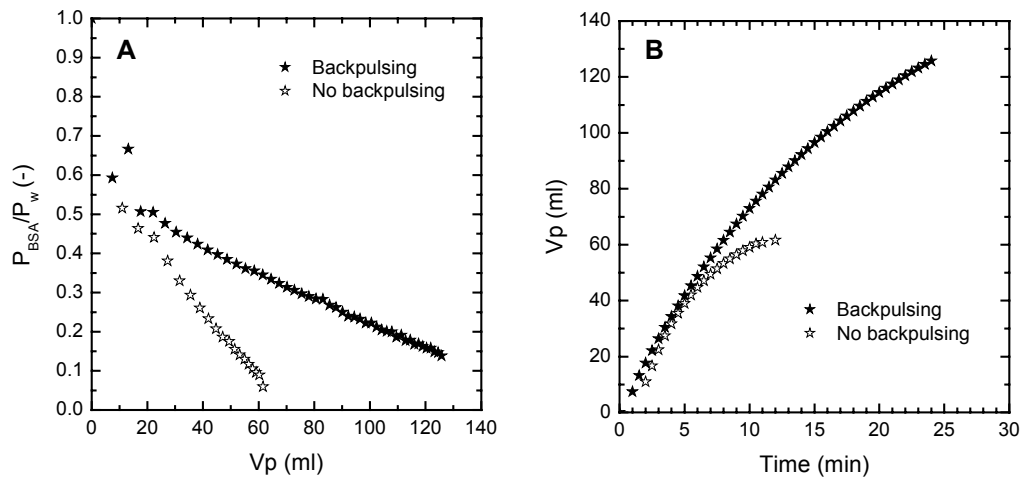


Figure 8. Relative BSA permeability versus permeated volume (A) and permeated volume versus time (B) of 1 g/l BSA at pH=7.1, without (empty stars) and with (full stars) backpulsing, for PEG coated microsieves.

Fouling without any pulsing or air sparging is independent of the surface chemistry because it is caused by particle (BSA aggregate) deposition. This phenomenon has been already observed for other authors for different feeds and coatings made of acrylic acid and poly (ethylene glycol) methyl ether methacrylate [2, 3].

A great improvement in permeation was obtained with backpulsing. If the permeated volume is extrapolated to zero relative permeability, a 2.5-fold increase of the permeated volume is

obtained, compared to the non-backpulsing test (see Figure 8a). In both cases the membrane productivity in time was very similar during the first minutes of filtration. However, while the permeated volume increased in time for the coated membranes, a plateau was reached in 15 min for the uncoated microsieves.

The reason for BSA flux decline is assumed to be pore blocking by aggregate deposition [27-29] therefore surface modification alone cannot suppress flux decline. With backpulsing, more beneficial results for BSA permeation were obtained with poly (PEGMA-r-TMSMA) coated microsieves, compared to untreated membranes. Even though flux declined throughout the experiment, higher permeated volumes and BSA permeabilities were obtained with PEG-coated microsieves. This indicates that, due to reduced interactions between the PEG-coated surface and BSA, backpulsing is more effective in removing deposited aggregates from the coated microsieve surfaces. Figure 9 depicts this situation in detail.

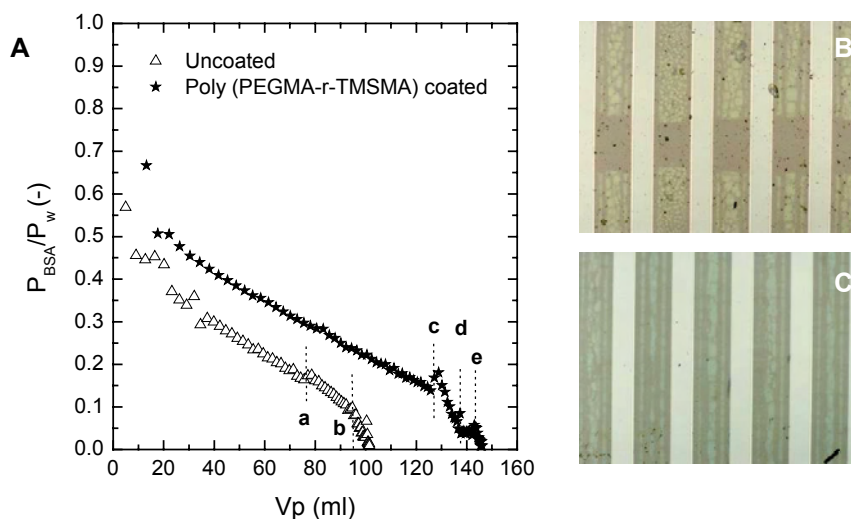


Figure 9. (A) Relative BSA permeability versus permeated volume for an uncoated and coated microsieve with backpulsing. For the uncoated membrane the backpulsing frequency was decreased from 6.7 Hz to 3.3 Hz (a), and backpulsing was stopped at (b). For the coated membrane backpulsing was kept at 6.7 Hz until (c). During the period (c-d) and from (e) no backpulsing was applied. In the region (d-e) backpulsing was reinitiated. Figures (B) and (C) represent optical microscope images (10x) of the microsieves used for the previous filtrations. After filtering, the microsieves were flushed with water to remove the excess of deposited protein.

Productivity (permeated volume) is significantly enhanced when backpulsing is applied with a PEG-coated microsieve, suggesting that the deposited protein layer is removed easily (Figure

9a). The results for the uncoated membrane were already presented in section 5.3.2 in Chapter 5.

The benefits of the PEG coating are also indicated in Figures 9b and c. After filtration the microsieves were removed from the module and washed with water to remove the adsorbed protein. Upon microscope inspection, the cleanest surfaces corresponded to the PEG-coated microsieves. On the contrary, some residues were detected on the uncoated surface.

In summary, although aggregate deposition and pore blocking are the mechanisms behind BSA flux decline independently of the microsieve surface, microsieves can still benefit from PEG based coatings. The backpulsing efficiency is increased with the coating because steric hindrance of the highly mobile PEG molecules reduces protein adsorption and the deposited layer is easier to remove.

6.3.3 Effect of in-line air sparging and permeate backpulsing with Poly (PEGMA-r-TMSMA) coated microsieves

Air sparging is a very effective method to increase productivity in the filtration of BSA solutions with uncoated microsieves [30]. The performance of air sparging in a BSA filtration (1 g/l, pH=7) using a PEG-coated microsieve is presented in Figure 10.

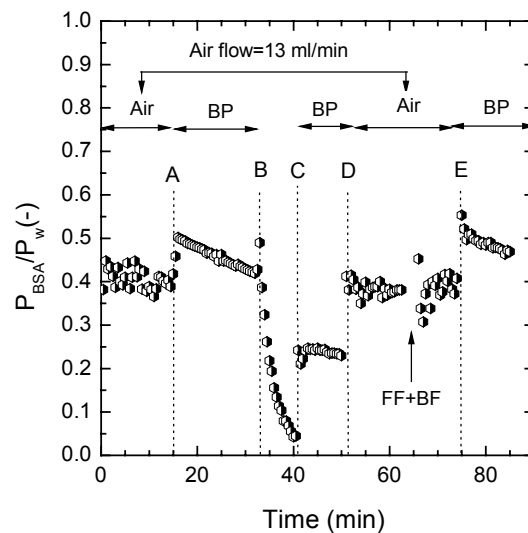


Figure 10. Relative BSA permeability versus time with a poly (PEGMA-r-TMSMA) coated microsieve. The abbreviation *BP* indicates backpulsing and *FF+BF* indicates forward and backflushing with water. Until (A) an air flow was applied; from (A-B) air was suppressed but backpulsing applied; from (B-C) neither air nor backpulsing were applied; during (C-D) only backpulsing was performed and during (D-E) only air; from (E) to the end of the test only backpulsing was valid.

Initially and until (A), the air flow was 13 ml/min (BSA flow = 170 ml/min). In such period permeability remained constant (42%). From A to B air sparging was stopped and backpulsing was initiated, at a frequency of 6.7 Hz. Backpulsing did not result in a constant permeability (approx. 10% decline in 15 min). Nevertheless, the fouling rate during this region was significantly lower compared to the region where no backpulsing or air was used (B-C). A remarkable increase in permeability occurred upon backpulsing reinitiation (C), due to aggregate removal. During (C-D) permeability remained fairly constant, and experienced a large increase when air sparging was performed at 13 ml/min (D). During the air sparging period (D-E) the highest and constant permeability was obtained (40%) because of enhanced mass transfer. These permeability values were not even increased by water forward and backflushing, indicating that the surface remained fairly free of deposits. The experiment finalized with backpulsing (from (E) to the end), where again a 10% decline in permeability was obtained. Approximately 500 ml of BSA solution were permeated throughout the course of the experiment.

Subsequently, the microsieve was rinsed with water and inspected under the optical microscope. No deposited matter was observed after rinsing (as previously shown in Figure 9c).

As concluded in Chapter 5 for unmodified microsieves, air sparging is an extremely helpful tool to increase BSA permeation. Air sparging in combination with PEG-coatings is more effective than backpulsing. BSA permeabilities can even be maintained constant at higher values with PEG-microsieves (10% higher than for unmodified microsieves) because the deposited layer is removed easier.

6.3.4 Application: Skimmed milk filtration with unmodified and PEG-coated silicon nitride microsieves

Commercial sterilized skimmed milk was used as feed. The filtration was operated with backpulsing, varying the frequency throughout the experiment from 6.7 to 2.5 Hz. Figures 11a and b show the results for an uncoated and a PEG-coated microsieve, respectively.

The differences between the two types of membrane are obvious: a constant permeability was obtained for the coated microsieves for all backpulsing frequencies and independently of the pressure used, whereas with the unmodified microsieves milk permeability decreased even with optimized backpulsing settings.

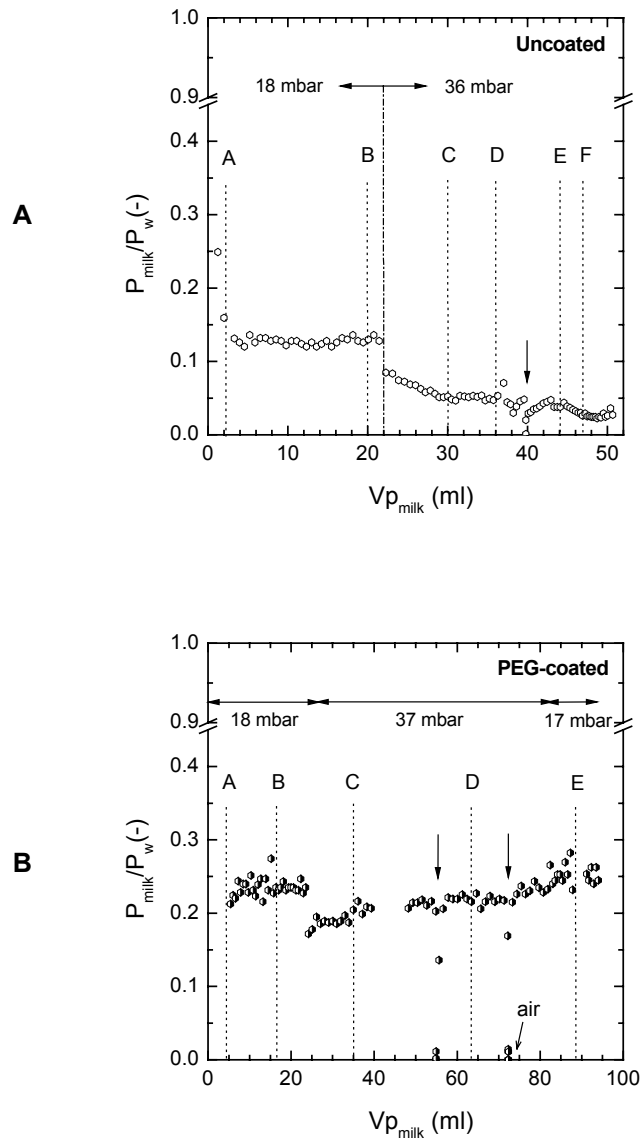


Figure 11. Relative milk permeability versus permeated volume with an unmodified microsieve (A) and a PEG-coated microsieve (B), with backpulsing. The arrows indicate the moment when backpulsing was stopped. The applied backpulsing frequencies in (A) are the following: (A-B)=3.3 Hz, (B-C)=2.5 Hz, (C-D)=3.3 Hz, (D-E)=6.7 Hz, (E-F)=3.3 Hz and (F)=6.7 Hz. For the coated microsieve (B) the applied backpulsing frequencies are: (A-B)=3.3 Hz, (B-C)=2.5 Hz, (C-D)=6.7 Hz, (D-E)=3.3 Hz, and from (E)=3.3 Hz. During (D-E) air sparging was temporary applied (13 ml/min).

With the uncoated microsieves (Figure 11a) a frequency to 3.3 Hz (A) resulted in a constant permeability (approx 13%). At (B) frequency was even decreased further, to 2.5 Hz. Permeability was then constant but, as pressure increased a factor 2, permeability suddenly decreased. The increase in pressure resulted in enhanced deposition, and backpulsing was not effective to remove the deposited layer under these conditions. When the frequency was increased to 3.3 Hz (C-D), a constant permeability was obtained. From (D) to (E) higher frequency (6.7 Hz) implied a slight permeability decline because of the resistance offered by the backpulser. Permeability dropped to zero when the backpulser was stopped (indicated by the arrow) but reinitiation of the pulses led to some permeability recovery. Alternatively decreasing pulse frequency to 3.3 Hz (E-F) and increasing it to 6.7 Hz (F) again did not increase permeability, which decreased finally to zero due to pulse inefficiency.

For a PEG-coated membrane, permeabilities are plotted for different backpulsing settings in Figure 11b. During (A-B) frequency was set at 3.3 Hz and the operating pressure at 18 mbar. Although fluctuations occurred, permeability remained constant for more than 10 min. A decrease of backpulsing frequency to 2.5 Hz (B-C) resulted in a constant permeability as well. However, when the pressure was increased to 37 mbar a similar effect as observed for the uncoated membranes occurred. Initially, a permeability drop (20% loss) took place but then, contrary to the situation without coating, it remained constant. As we mentioned above, the drop in permeability may be attributed to the lower efficiency of the backpulser: as more volume permeates through the membrane a higher amount of matter can be deposited. After some seconds, an equilibrium between deposited and pulsed matter occurs, resulting in a stable permeability. An increase in frequency (C) resulted in a constant permeability too. During (C-D), backpulsing was stopped for a short time (indicated by the arrow) and permeability decreased to zero immediately. Restarting the pulses resulted in a recovery of the permeability. In the period from (D-E) permeate was pulsed at 3.3 Hz and a relatively constant flux was obtained, until the pulses were stopped. Here permeability decreased again to zero very rapidly. At that point, air was dosed to the system at 13 ml/min but permeability did not increase, indicating that air sparging was not suitable to remove the milk deposits under these conditions. A permeability increase did occur when backpulsing was restarted at 3.3 Hz, efficiently removing the deposited cake layer.

Skimmed milk is a complex mixture constituted by 9-10% total solids, 0.1-0.2% fat, 3.2-3.4% proteins, 4.6-5.0% lactose and minerals like calcium, potassium and sodium [31]. Although identification of the components present in the permeate was not performed, a comparison between the feed and permeate absorbance was done by spectrometry. The absorbance of

both fractions was analyzed at 280 nm to study changes in the total protein concentration. At this wavelength no differences in absorbance were detected.

Retention of larger components could not be quantified with these measurements; for this purpose HPLC measurements or particle size distribution by light scattering techniques could be useful to determine fractionation. In our case Dynamic Light Scattering did not allow the identification of the particle size, due to limitations of the equipment used.

The main differences between the skimmed milk filtrations with unmodified and poly (PEGMA-r-TMSMA) modified microsieves were that higher, more stable and constant milk fluxes were observed with the coated membranes, independently of the backpulsing settings. As also observed with BSA, the PEG moieties reduce the adsorption of foulants to the surface, which results in a more successful effect of backpulsing. For the same time and backpulsing settings, a 2-fold enhancement of the permeated volume was obtained with the coated membranes. Eventually, the permeability of the unmodified microsieves decreased almost to zero, while the one for the coated membranes remained constant around 25%.

Furthermore, also clear differences could be seen between their clean water fluxes after milk filtration. In both cases very stable water permeabilities higher than milk were measured. However, the relative clean water permeability was 1.6 times higher for the coated sieves (it reached almost 80% of the maximum value). Subsequently, the surfaces were further rinsed with water and inspected under an optical microscope. As displayed in Figure 12, the surfaces of the coated microsieves were completely free of deposits, while some foulants were observed above the porous regions of the untreated membrane.

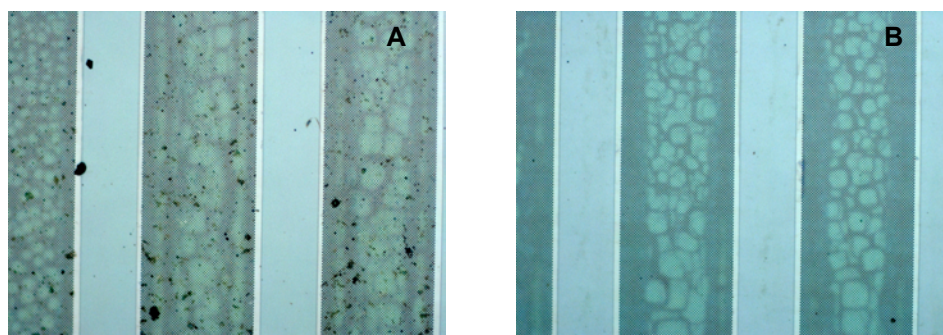


Figure 12. Optical microscope images (20x) of the microsieve surfaces used for the milk filtrations, after rinsing with water. Image (A) depicts the surface of the unmodified and (B) the surface of the PEG-coated membrane.

The results obtained during milk filtration, the recovery of the water flux (partially for the uncoated membranes and almost totally for the coated microsieves) and the images shown previously suggest that the deposited milk components were not strongly bound to the surface of the PEG-coated microsieve. The clean water flux was restored for 80% and the surface did not present many visible particles. For the uncoated membrane the situation was however distinct: interactions between the surface and milk components resulted in lower fluxes and particulate material was observed on the surfaces.

6.4 Conclusions

An additional approach has been considered in this chapter to reduce fouling with BSA solutions. The combination of membrane modification with the random copolymer poly (TMSMA-r-PEGMA) and methods like backpulsing and air sparging have been studied.

Silicon, silicon nitride and glass surfaces were successfully grafted with the copolymer, forming a layer of approx. 2.3 nm, which was stable in air, water or PBS buffer pH=7.4. However, the polymer did not withstand alkaline conditions (pH=12, 50°C, 60 min). Very low BSA adsorption was measured on the coated samples, compared to untreated or oxidized dices. Such protein adsorption results prove that adsorption is not only dependent on hydrophilicity, as it has been believed for a long period of time, but on other factors like steric repulsion. In spite of this, relatively hydrophilic surfaces are normally preferred, as discussed in Chapter 3, since a good surface wettability in water is a must for the filtrations.

Even though pore blocking was determined to be the main cause for BSA flux decline in the previous two chapters, adsorption or interactions between proteins and the surface can take place. When backpulsing, microsieves could benefit from the properties of poly (TMSMA-r-PEGMA) coatings. Compared to unmodified microsieves, higher protein productivity was achieved, indicating that aggregate removal was more effective because of reduced adhesion. This was also observed by microscope inspection of the membrane surfaces after only water rinsing: polymer coated microsieves were much cleaner than uncoated membranes.

Air sparging was also proven to be an extremely helpful tool to achieve constant permeation of BSA solutions. Compared to backpulsing, air sparging was significantly more powerful: by using an air flow of 13 ml/min permeation could remain constant at very high values (40% relative permeability). BSA permeabilities could even be maintained constant at higher values with PEG-microsieves because the deposited layer was removed easier.

For skimmed milk filtration, air sparging did not have any positive effect on flux recovery or enhanced permeation. In this case backpulsing proved to be more effective. The main differences between the skimmed milk filtrations with unmodified and poly (PEGMA-r-TMSMA) modified microsieves were that higher, more stable and constant milk fluxes were observed with the coated membranes, independently of the backpulsing settings. As already observed for BSA and corroborating the previous observations, the surfaces of the coated microsieves were completely free of deposits after water rinsing, which confirmed that the PEG moieties were able to suppress interactions with the deposited materials very successfully.

6.5 Acknowledgements

The author wishes to acknowledge Ronald Jansen, Frans Pronk and Lutgarde Lemmens from Fluxxion B.V. (Eindhoven) for kindly providing the silicon nitride microsieves. Lydia Bolhuis-Versteeg is acknowledged for the assistance in the polymer synthesis, Clemens Padberg for the molecular weight/density measurements and Dr. Herbert Wormeester from the Applied Optics Group (University of Twente) is acknowledged for performing the ellipsometric measurements.

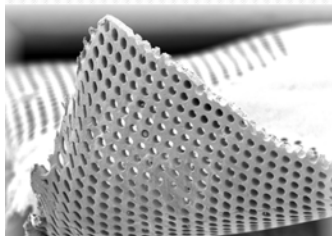
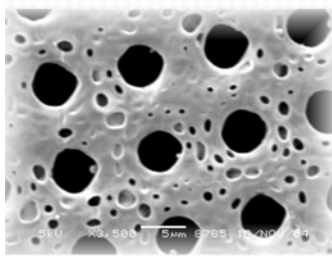
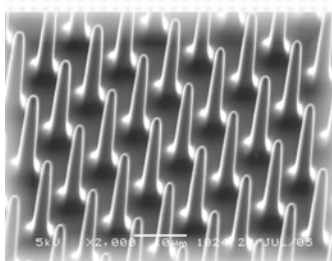
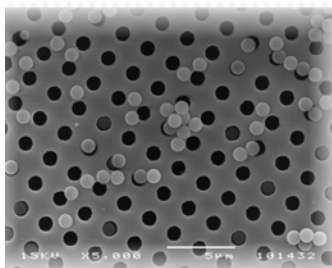
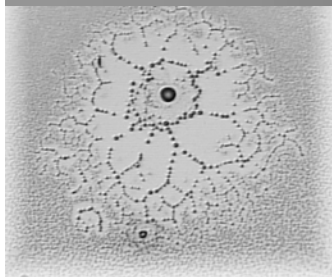
6.6 References

- [1] M. Gironès, Chapter 4 of this thesis.
- [2] H. Ma, C.N. Bowman, R.H. Davis, Membrane Fouling reduction by backpulsing and surface modification, *J. Membr. Sci.* 173 (2000) 191.
- [3] H. Ma, L.F. Hakim, C.N. Bowman, R.H. Davis, Factors affecting membrane fouling reduction by surface modification and backpulsing, *J. Membr. Sci.* 189 (2001) 255.
- [4] A.D. Marshall, P.A. Munro, G. Trägårdh, The effect of protein fouling in microfiltration and ultrafiltration on permeate flux, protein retention and selectivity: a literature review, *Desalination* 91 (1993) 65.
- [5] E. Ostuni, B.A. Grzybowski, M. Mrksich, C.S. Roberts, G.M. Whitesides, Adsorption of proteins to hydrophobic sites on mixed self-assembled monolayers, *Langmuir* 19 (2003) 1861.
- [6] W. Norde, Driving forces for protein adsorption at solid surfaces, in: M. Malmsten, *Biopolymers at interfaces*, Marcel Dekker, New York, 2003.
- [7] E. Ostuni, R.G. Chapman, R.E. Holmlin, S. Takayama, G.M. Whitesides, A survey of structure-property relationships of surfaces that resist the adsorption of proteins, *Langmuir* 17 (2001) 5606.
- [8] Van Alstine *et al.* Effect of chain density on inhibition of protein adsorption by poly(ethylene glycol) based coatings, *J. Colloid Interface Sci.* 202 (1998) 507.
- [9] Desai *et al.* Controlling nonspecific protein interactions in silicon biomicrosystems with nanostructured poly(ethylene glycol) films, *Langmuir* 18 (2002) 8728.

- [10] J.M. Harris, Poly(ethylene)glycol Chemistry-Biotechnical and Biomedical Applications, Plenum Press, New York, 1995.
- [11] C.G. Golander, J.N. Herron, K. Lim, P. Claesson, P. Stenius, J.D. Andrade, Properties of immobilized PEG films and the interaction with proteins: experiments and modeling, in Harris' Poly(ethylene)glycol Chemistry-Biotechnical and Biomedical Applications, Plenum Press, New York, 1995.
- [12] S.I. Jeon, L.H. Lee, J.D. Andrade, P.G.J. de Gennes, Protein-surface interactions in the presence of polyethylene oxide. I. Simplified theory, *J. Colloid Interface Sci.* 142 (1991) 149.
- [13] T. McPherson, A. Kidane, I. Szleifer, K. Park, Prevention of protein adsorption by tethered poly(ethylene oxide) layers: Experiments and single-chain mean-field analysis, *Langmuir* 14 (1998) 176.
- [14] K.L. Prime, G.M. Whitesides, Self-assembled organic monolayers: model systems for studying adsorption of proteins at surfaces, *Science* 252 (1991) 1164.
- [15] K.L. Prime, G.M. Whitesides, Adsorption of proteins onto surfaces containing end-attached (oligo)ethylene oxide: a model system using self-assembled monolayers, *J. Am. Chem. Soc.* 115 (1993) 10714.
- [16] S. Jo, K. Park, Surface Modification using silanated poly(ethylene glycols), *Biomaterials* 21 (2000) 605.
- [17] S. Lee, P. E. Laibinis, Protein-resistant coatings for glass and metal oxides surfaces derived from oligo(ethylene glycol)-terminated alkyltrichlorosilanes, *Biomaterials* 19 (1998) 1669
- [18] S. Jon, J. Seong, A. Khademhosseini, T.T. Tran, P.E. Laibinis, R. Langer, Construction of non-biofouling surfaces by polymeric self-assembled monolayers, *Langmuir* 19 (2003) 9989.
- [19] Y. Xia and G. Whitesides, Soft-lithography, *Angew. Chem. Int. Ed.* 37 (1998) 550.
- [20] J.A. de Feijter, J. Benjamins, F.A. Veer, Ellipsometry as a tool to study the adsorption behaviour of synthetic biopolymers at the air-water interface, *Biopolymers* 17 (1978) 1759.
- [21] H. Wormeester, E. S. Kooij, A. Mewe, S. Rekveld, B. Poelsema, Ellipsometric characterization of heterogeneous 2D layers, *Thin solid films* 455-456 (2004) 323.
- [22] M. Gironès, Chapter 2 of this thesis.
- [23] M. Gironès, Z. Borneman, R. G. H. Lammertink, M. Wessling, The role of wetting on the water flux performance of microsieve membranes, *J. Membr. Sci.* 259 (2005) 55.
- [24] A. Khademhosseini, S. Jon, K.Y. Suh, T.T. Tran, G. Eng, J. Yeh, J. Seong, R. Langer, Direct patterning of protein- and cell resistant polymeric monolayers and microstructures, *Adv. Mater.* 15 (2003) 1995.
- [25] G.A. Bornzini, I.F. Miller, The kinetics of protein adsorption on synthetics and modified natural surfaces, *J. Colloid Interface Sci.* 86 (1982) 539.
- [26] P. Ying, G. Jin, Z. Tao, Competitive adsorption of collagen and bovine serum albumin-effect of surface wettability, *Colloids Surf. B* 33 (2004) 259
- [27] S.T. Kelly, W. Senyo Opong, A. L. Zydney, The influence of protein aggregates on the fouling of microfiltration membranes during stirred cell filtration, *J. Membr. Sci.* 80 (1993) 175.
- [28] S. T. Kelly, A. L. Zydney, Mechanisms for BSA fouling during microfiltration, *J. Membr. Sci.* 107 (1995) 115.
- [29] M. Gironès, Chapter 4 of this thesis.
- [30] M. Gironès, Chapter 5 of this thesis.
- [31] A.D. Marshall, G. Daufin, Physico-chemical aspects of membrane fouling by dairy fluids, in: *Fouling and Cleaning in pressure driven membrane processes*, International Dairy Federation, Belgium, 1995.

Chapter 7

Fabrication and characterization of polymeric microsieves



7.1 Introduction

The potential of silicon nitride microsieves as microfiltration membranes has been thoroughly studied in the previous chapters. The fact that large product volumes can be achieved with such small membrane area can be very advantageous, however, large product throughput can often result in extreme fouling. Protein fouling can be reduced most effectively either using air sparging and/or applying surface modification procedures using PEG polymers [1]. Unfortunately, air sparging and surface modification with polymers like poly (TMSMA-r-PEGMA) cannot be used in applications that involve foodstuffs. Air can cause foaming and denaturation of some compounds, and only food-grade approved polymers can be applied as coatings. Until today, microsieves were fabricated out of silicon based materials. These limited material choices stems from their fabrication process, which relies on expensive cleanroom technology [2, 3]. An alternative for producing low cost microsieves could be offered by using polymers. The properties of polymeric microsieves can be tuned very easily depending on the material used, costs can be greatly reduced and the process simplified.

Phase Separation Micromolding (PS μ M) is a novel technique for polymeric microsieve fabrication. It allows the production of uniform, defect free microstructures and is suitable to process a wide range of materials [4-6]. PS μ M is based on the principle of polymer phase separation and, by casting a thin polymer film on a microstructured mold, microstructured polymer replicas can be obtained. In microsieve fabrication the mold contains pillars that perforate the polymer film. The mold design is critical for the final microsieve morphology: pillar shape, diameter, support dimensions, etc.

In fact, very few commercial polymeric membranes with specific and well-defined structural properties are available on the market. Track-etched membranes also possess straight-through pores, however, their porosity and pore distribution is sometimes compromised. Nowadays, research groups are also working on the fabrication of structures with well-defined pores. Goedel and co-workers have successfully prepared ultra-thin freestanding porous membranes by particle-assisted wetting [7, 8]. This technique involves the use of spherical colloidal particles of few hundreds of nm coated with a hydrophobic polymer. In water the particles form a very structured and densely-packed monolayer. If then a monomer is introduced to the system, it fills up the space between the particles and, upon crosslinking, a very strong layer is formed. A freestanding membrane containing pores with similar diameter to the colloids can be formed after dissolving the particles. Structures with very narrow pore size distribution and small pore diameters (50-100 nm) are obtained with this technique [9]. Other methods used to obtain well-patterned microporous structures include self-assembly of

rod-coil block-copolymers and templating with particles, emulsions, water droplets, etc. [10-14].

In this chapter the polymeric microsieve fabrication and the parameters that affect their properties will be explored. As a reference polymer, a well-known membrane material for MF and UF applications is used: polyethersulfone (PES) [15, 16]. PES is a suitable material for microsieve fabrication due to its high mechanical strength, resistance to acids and alkalis, and also thermal and chemical resistance [17]. The influence of fabrication parameters such as co-solvent, co-solvent evaporation rate, temperature and non-solvent immersion time are investigated. Furthermore, the influence of hydrophilic polymeric additives like Polyvinylpyrrolidone (PVP) on the membrane morphology and hydrophilicity is studied. Many authors have reported that PVP is a water-soluble pore-forming polymer that can suppress macrovoid formation and increase pore interconnectivity [18-20], but it can also affect the membrane hydrophilicity resulting in a permeability increase [21]. On the other hand, hydrophilized PES can be a potential candidate for applications where low protein adsorption is required [22].

Pore size tuning is also considered in the following sections. The perforation diameter of the microsieves obtained in this chapter can be modified via two approaches:

- (1) using pillars of various diameters (modified mold features)
- (2) applying a thermal treatment to the polymer so that shrinkage occurs.

Finally, other mold features such as support depth and shape will also be taken into consideration.

7.2 Phase Separation Micromolding

Phase Separation Micromolding (PS μ M) is a versatile microfabrication technique, capable to produce microstructures with a very broad range of polymers, including block copolymers, biodegradable and conductive polymers, without the need of using expensive cleanroom facilities [4]. PS μ M is based on polymer phase separation (the process is schematically depicted in Figure 1).

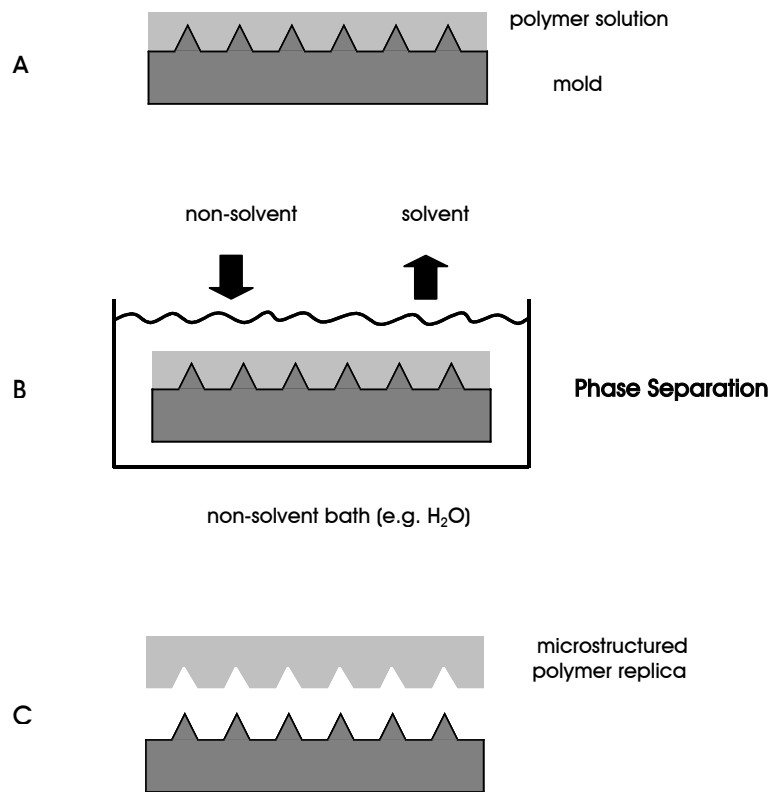


Figure 1. Schematic representation of liquid induced Phase Separation Micromolding.

A thin film of polymer solution is applied on a structured mold fabricated by standard photolithography (A). By immersing the solution in a non-solvent for the polymer, the non-solvent diffuses into the film while the solvent diffuses out. The solution will then phase separate into a polymer-lean and a polymer-rich phase, which solidifies and assimilates the shape of the mold (B). A microstructured polymer replica is then obtained and released from the mold (C).

In microsieve fabrication, phase separation occurs in two stages: vapor induced (VIPS) and liquid-induced phase separation (LIPS). During solidification, shrinkage of the polymer film on the mold takes place in two directions: lateral (in-plane) and thickness-wise. Thickness shrinkage takes place in a larger extent than lateral shrinkage, and it allows perforation of the film. A volatile co-solvent is usually added to boost shrinking during the first-stage of polymer solidification. After the solution is applied on the mold, the volatile additive evaporates causing a reduction in the polymer film thickness. The contraction of the film towards the mold structures (thickness shrinkage) will result in perforation and a completely open microstructure will be obtained. Lateral shrinkage allows loosening of the structured polymer from the mold and easy release of the replica.

7.3 Materials and methods

7.3.1 Materials

Commercially available PES Ultrason[®] E6020 (BASF), was used as base polymer for microsieve fabrication. N-methyl pyrrolidone (NMP) was selected as solvent, acetone and methyl-ethyl ketone (MEK) as co-solvent, and Span[®] 80 (Fluka) was added as additive for macrovoid suppression and reduction of the surface tension [4]. The standard composition of the casting solution was: 9.8 wt% PES, 49 wt% NMP, 39.2 wt% acetone and 2 wt% SPAN. After preparation, the solution was filtered through a 5 μm metal sieve.

PES-PEO block copolymer (Gambro), with 8 wt% PEO content, was also used to fabricate microsieves, using the same composition as with the PES reference solution.

Two types of PVP from Fluka were added into the reference PES polymer solution without SPAN: PVP K30, with molecular weight of 40kDa, and PVP K90, with molecular weight of ~360 kDa. The chemical formulas of the polymers used in this investigation are presented in Figure 2.

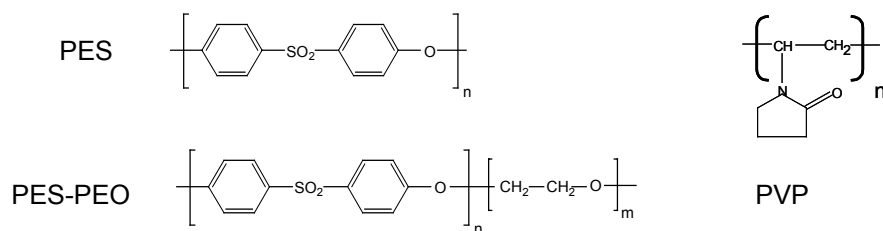


Figure 2. Chemical formulas of PES, PES-PEO and PVP.

Silicon molds with pillars, varying in length, width and shape were used for the microsieve fabrication. The molds were prepared by photolithographic techniques and silicon Deep Reactive Ion Etching. For standard microsieve fabrication, molds with straight pillars of approximately $5\ \mu\text{m}$ width and $20\ \mu\text{m}$ length were used. Each mold had a structured area of approximately $7\ \text{cm}^2$. The area was divided into 2500 fields, containing around 1800 pillars each. Microsieves fabricated with these molds would have a porosity of about 10%. Figure 3 depicts the structure of the standard molds. Between the pillar fields a deeper grid structure is present, providing a support structure in the polymeric replica.

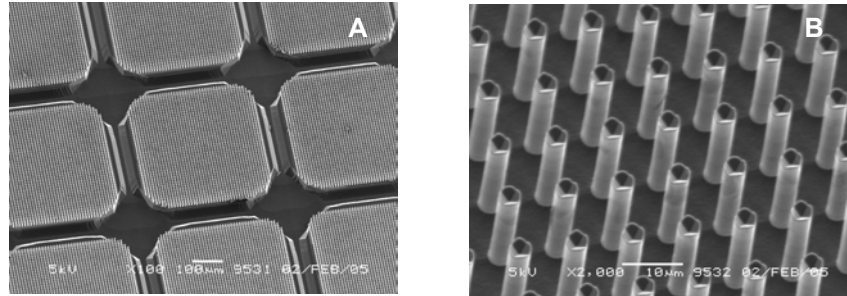


Figure 3. SEM images of a silicon mold containing pillars. (A): pillar fields and (B): higher magnification of the pillars used to perforate the polymer.

7.3.2 Microsieve fabrication by Phase Separation Micromolding

The polymer solution was poured onto the mold and spread along its surface with an adjustable casting knife. Figure 4 depicts the custom-made casting device used for microsieve fabrication.

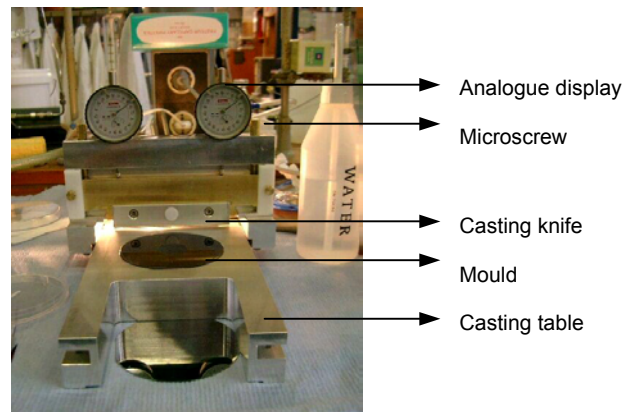


Figure 4. Photograph of the casting machine used to produce polymeric microsieves.

The height of the casting knife with respect to the mold was adjusted within 1 μm accuracy ($d_{\text{casting}}=27\text{-}35\ \mu\text{m}$, depending on mold), determining the microsieve thickness.

After casting, the mold was immediately placed in a *vapor bath* with a continuous N_2 flow saturated with water vapor at a certain temperature (VIPS). Due to the moisture and temperature in the bath, acetone rapidly evaporates out of the polymer film, allowing the total polymer thickness to decrease significantly. Simultaneously, water vapor mixes with the polymer solution in the initial phase separation and the film becomes turbid. The decrease in thickness and partial coagulation onto the mold result in the film perforation by the pillars (as shown in Figure 5).

After co-solvent evaporation and the first-stage of polymer coagulation, the mold was immersed in a non-solvent bath, *water bath*, at room temperature (LIPS). Further exchange of the remaining solvent by water was completed during the immersion time. The microsieves were peeled off the mold and dried in air. After casting, the mold was cleaned in NMP for 15 min and rinsed with acetone.

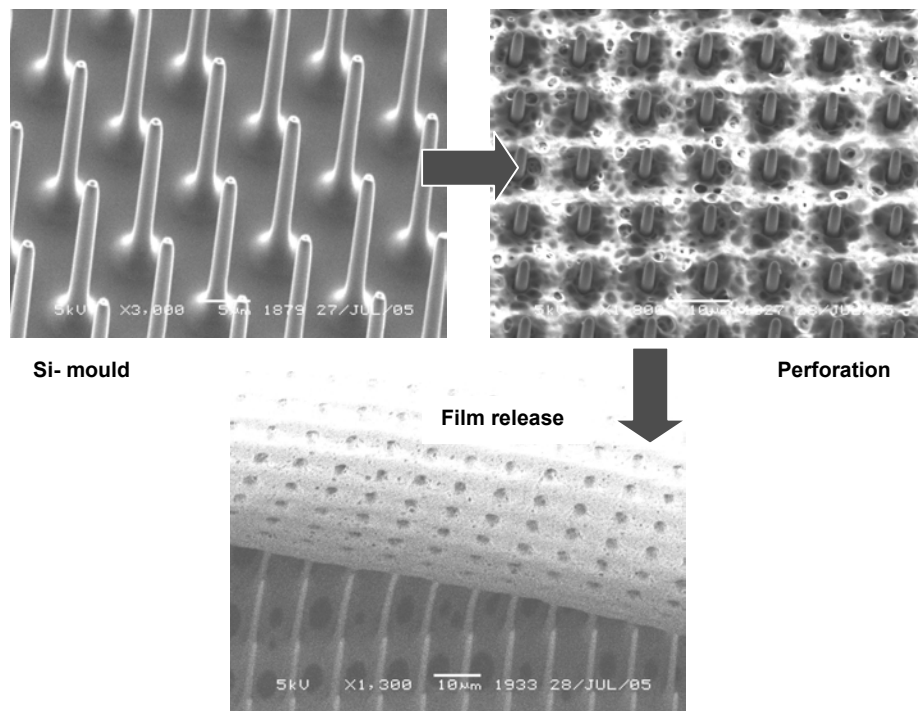


Figure 5. Perforation process with 1.5 μm wide pillars, followed by SEM. After casting the polymer solution, evaporation of acetone and polymer shrinkage allow perforation by the pillars. The film is released from the mold after complete solidification.

7.3.3 Mold design: support shape and pillar dimensions

The silicon molds presented in Figure 6 were used to investigate the influence of the support shape. Mold 1 has a diamond-shaped grid with inclined edges, while the support for mold 2 has a straight grid with vertical edges.

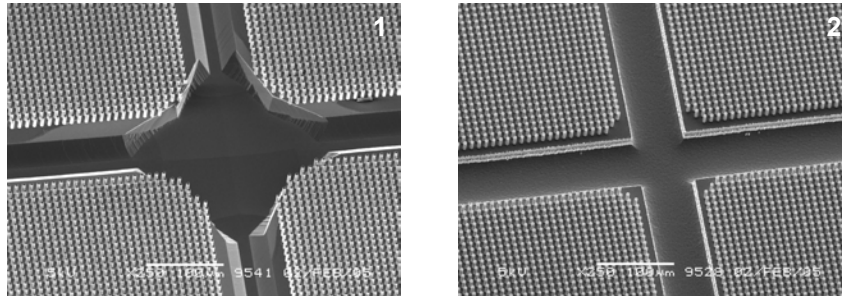


Figure 6. SEM images of molds 1 and 2 with a diamond-shaped and a square grid, respectively.

Three molds with different pillar dimensions were investigated in order to tune the microsieve pore or perforation diameter. The morphology of such molds is depicted in Figure 7.

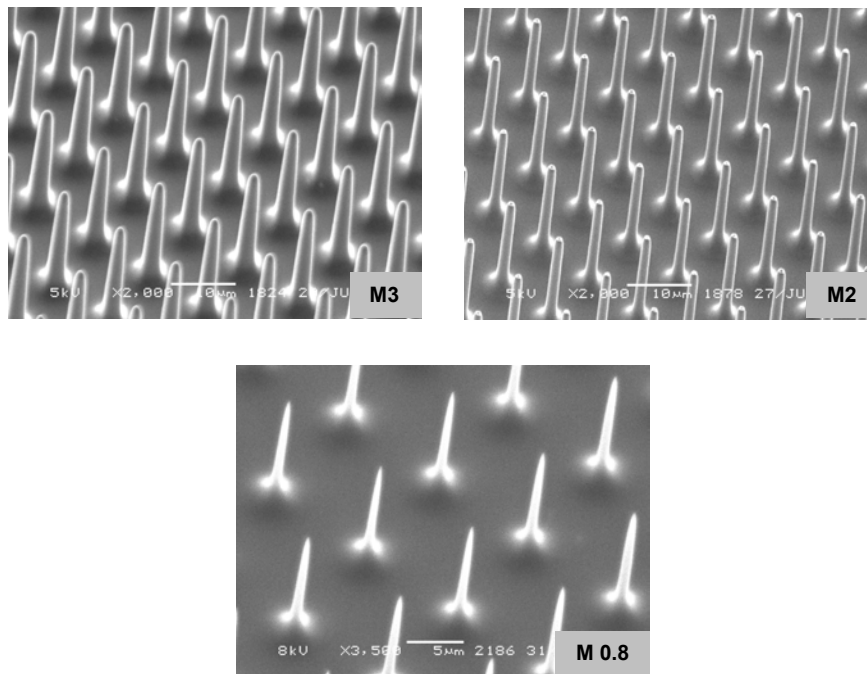


Figure 7. SEM images of silicon molds with average pillar base widths of 2.8 µm (M 3), 1.8 µm (M 2) and 0.8 µm (M 0.8).

The molds were fabricated at the Transducers Science and Technology Group. Two steps of lithography and etching were required for the pillar pattern and the grid. The pillar pattern was defined by optical lithography on (100) oriented silicon wafers using an EVG 620 mask aligner. After spin-coating with the adhesion promoter HMDS and a 1.7 μm thick positive resist layer, the wafer was exposed to 12 mW/cm^2 UV light. After exposure the resist layer was developed. The wafers were then etched by cryogenic DRIE (Deep Reactive Ion Etching) [23]. After standard HNO_3 cleaning to remove the photoresist, pillars with a diameter of 5 μm and a height of 20 μm were obtained. To decrease the diameter of the pillars, wafers were oxidized in a wet thermal oxidation furnace at 1150°C for different times. The oxide layer is removed afterwards by immersing the wafers for 90 s in buffered HF solution. In this way, by varying the oxidation times, the pillar dimensions can be decreased.

The pillar widths for each mold were: for *M3*, 2.3 μm at the middle and 2.8-3 μm at the base (Figure 7a); for *M2*, 1.5 μm at the middle and 1.8 μm at the base (Figure 7b) and for *M0.8*, 0.5 μm at the middle and 0.8 μm at the base (Figure 7c).

7.3.4 Material densification by thermal treatment

PES and PES-PEO microsieves were submitted to a thermal treatment above their glass transition temperature (T_g) in order to densify their structure and obtain smaller perforation dimensions. For this purpose a Carbolite TZF12/100 high temperature oven was used. The heat treatment was carried out under a nitrogen atmosphere (10 ml/min N_2 flow). The polymer microsieve was heated up to 150°C at a heating rate of 50°C/min. The temperature was kept at 150°C for 15 min and then raised to the desired treatment temperature at 5°C/min, and was kept constant for a controlled time. After the treatment the sample was rapidly quenched to room temperature.

The treatment temperature for PES varied from 240 to 260°C, for PES-PEO from 180 to 210°C, and for both the treatment time was varied from 15 to 60 min.

7.3.5 Microsieve characterization

Optical Microscopy and Scanning Electron Microscopy

The morphology of the molds and the microsieve membranes was visualized by Scanning Electron Microscopy (SEM, Microscope JSM-5600LV, at 5 kV). In some cases the membranes were sputtered with a thin gold layer (30 nm). Inspection after microsieve fabrication was always performed with a Zeiss Axiovert 40 MAT optical microscope.

Contact Angle Measurements

Static water contact angles were measured using a Goniometer (Dataphysics Contact Angle System). The sessile drop method was used to determine the static contact angle, θ , of water on unperforated films fabricated with the same procedure as the microsieves. The results were averages over 3 measurements on each sample.

Optical diffraction

Optical diffraction was used to determine the periodicity (d =diameter perforation+distance between two perforations) of the microsieves, in order to estimate the shrinking percentage after the thermal treatment. A microsieve was placed between a laser source (λ =645-665 nm) and a projection screen at a fixed distance (D =68 cm). The distance between the projected points on the screen (y) was measured, and the periodicity of the pattern (d) was calculated for an order (m):

$$d = \frac{(m\lambda D)}{y} \quad (1)$$

7.4 Results and Discussion

7.4.1 Fabrication of PES microsieves by PS μ M

The phase separation process described here consisted of two stages: *vapor-induced phase separation* (VIPS) followed by *liquid-induced phase separation* (LIPS). Some of the process variables in VIPS and LIPS are discussed below. For clarification, the term *microsieve pore* or *perforation* will define the pores created by pillar perforation, meanwhile the term *intrinsic pore* defines the pores from the polymer, originated by the phase inversion process.

a. VIPS: Vapor bath residence time and temperature (t_{vapor} , T_{vapor})

The residence time (t_{vapor}) of the film in the vapor bath was varied from 0 seconds to 4 min. The vapor bath temperature and the water bath immersion time were kept constant at 30°C and 3 minutes, respectively. Figure 8 shows that the perforation level increased with increasing coagulation time.

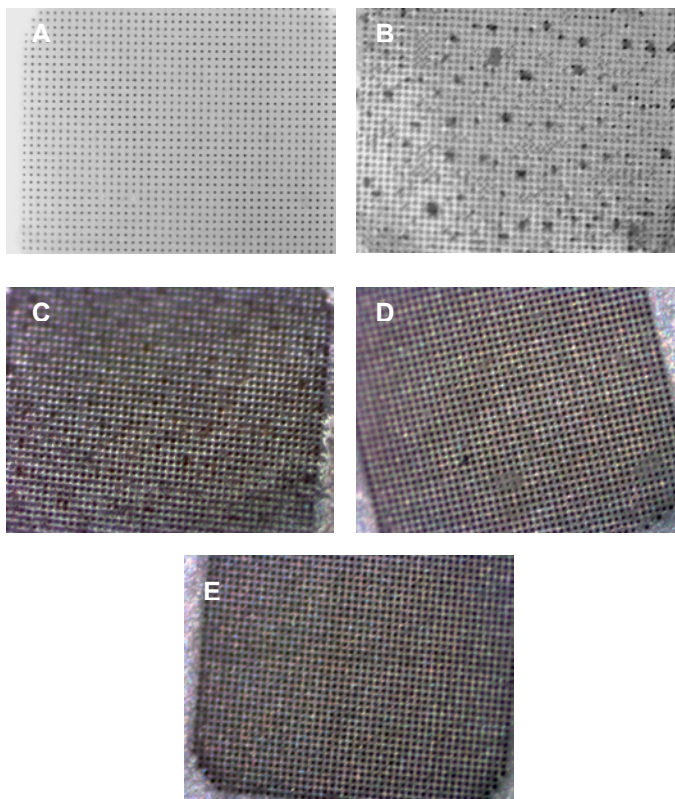


Figure 8. Optical microscope images (20x) of top surfaces of PES microsieves fabricated with different t_{vapor} (A= 0 s, B= 10 s, C=25 s, D=50 s, E=2, 4 min).

Figure 8a depicts a microsieve that was directly immersed in the water bath after casting. The film assimilated the shape of the mold on one side, but the pillars did not perforate the film (also confirmed by SEM). After $t_{\text{vapor}} = 10$ s (Figure 8b) a certain degree of perforation is observed in some areas only. Figures 8c and 8d show that the degree of perforation increases further with increasing t_{vapor} to 25 and 50 s.

Beyond vapor bath times of 1 min complete perforation occurs. The previous observations confirm that the perforation process is mostly initiated in the vapor bath, because sieves that were casted and immediately placed in the water bath exhibited no perforation. Furthermore, a film that was only exposed to the vapor bath but not to the water bath already displayed perforation.

The perforation process reached its maximum after 2 minutes, but to ensure maximum perforation, a standard $t_{\text{vapor}} = 3$ min was selected.

The influence of vapor bath temperature (T_{vapor}) on the perforation degree was studied, at 16, 35 and 40°C. t_{vapor} was kept at 3 min and the time of immersion in the water bath was kept at 3-5 min. No significant differences in the perforation level of the PES microsieves were detected by optical microscopy or SEM. Within the studied temperature range, sufficient co-solvent evaporated and non-solvent vapor mixed with the polymer solution in order to complete perforation. For further studies, T_{vapor} was fixed at 30°C.

b. LIPS: Water bath coagulation time

Using vapor bath conditions of $T_{\text{vapor}}=30^{\circ}\text{C}$ and $t_{\text{vapor}}=3$ min, microsieves were immersed in the water bath (at room temperature) for different times (0, 60 and 90 s). When a cast film on the mold was left long enough in the vapor bath and no immersion in the water bath took place, perforation was already complete. The microsieve was then released from the mold and immersed in the water bath to allow further solvent/non-solvent exchange.

No significant differences could be seen among the perforation degree of microsieves immersed in the water bath during different times. However, the microsieves produced after 60 and 90s immersion have very different mechanical properties compared to the membrane that was not placed in the water bath before release. Since the concentration of NMP in the polymer solution is still high, the microsieve can easily be deformed during the release process. Therefore, the water bath is required for further water-NMP exchange. As standard procedure, immersion time before release was selected as 3 min. In all cases, to ensure complete removal of NMP a total immersion time ≥ 5 min was needed.

From the previous results we can summarize that phase separation for microsieve fabrication consisted of two stages: VIPS and LIPS. VIPS takes place in the vapor bath, where also perforation occurs (induced by shrinkage caused by acetone evaporation). t_{vapor} has a significant effect on perforation, and should be kept higher than 2 min. T_{vapor} does not seem to influence perforation in a great extent. Complete coagulation and NMP removal occurs in the water bath (LIPS), where an immersion time of 5 minutes is required.

c. Influence of co-solvent or volatile additive

The microsieve structure obtained with MEK as co-solvent is depicted in Figure 9. When using a less volatile co-solvent than acetone, perforation was not complete for the same casting conditions ($T_{\text{vapor}}= 30^{\circ}\text{C}$, $t_{\text{vapor}}=3$ min and immersion time in water bath= 3 min).

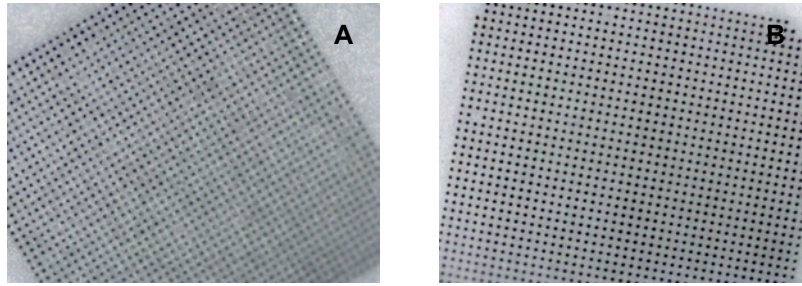


Figure 9. PES microsieve casted with MEK as co-solvent (A) and fully perforated PES microsieve with acetone as co-solvent (B).

MEK requires longer t_{vapor} than acetone to obtain full perforation. If the co-solvent exchange is too slow, the polymer film can already solidify before there is enough thickness shrinkage. In such case, less perforation occurs, as observed in the previous figure.

d. Mold design: influence of the support structure

The dimensions of the mold support structure are critical with respect to defects like tearing at the edge/corner of a microsieve field. Figure 10 shows the structure at the corner of a field of microsieves fabricated with molds 1 and 2.

Vogelaar reported that the width of the replicated structures is directly proportional to the distance between the mold features [4]. During phase separation the film contracts towards the areas where more material is present, resulting in stretching. This effect is very well observed for microsieves cast from mold 1 (see Figure 10a for the microsieve and 6a for the mold), where the field corners are further apart from each other. In that zone polymer shrinkage is more acute, resulting in defects like tearing and stretched or bigger pore dimensions.

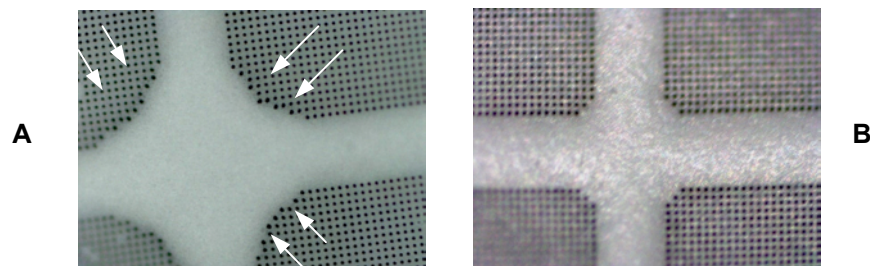


Figure 10. Optical microscope images (20x) of PES microsieves fabricated with mold 1 (A) and 2 (B), respectively. The arrows indicate the regions with deformed pores.

In mold 2 the corner features are closer to each other, therefore less lateral shrinkage and more homogeneous pores at the field corners of microsieves cast with such mold are observed (see Figure 10b for the cast microsieve and 6b for the mold).

e. Optimized PES microsieves

The best structures were obtained using freshly prepared standard PES solutions (9.8 wt% PES, 49 wt% NMP, 39.2 wt% acetone and 2 wt% SPAN). The optimum settings for PES microsieve fabrication were the following: $t_{\text{vapor}}=3$ min, $T_{\text{vapor}}=30\pm 1^\circ\text{C}$ and water bath coagulation time = 3 min.

SEM images of PES microsieves produced with the previous settings are displayed in Figure 11. The microsieves produced have a uniform intrinsic porosity and are slightly more porous at the top ('air' side) and denser on the back or 'mold' side. The average pore diameter is 5 μm , membrane thickness 10 μm , and support thickness is about 30 μm . The periodicity is around 9.5 μm .

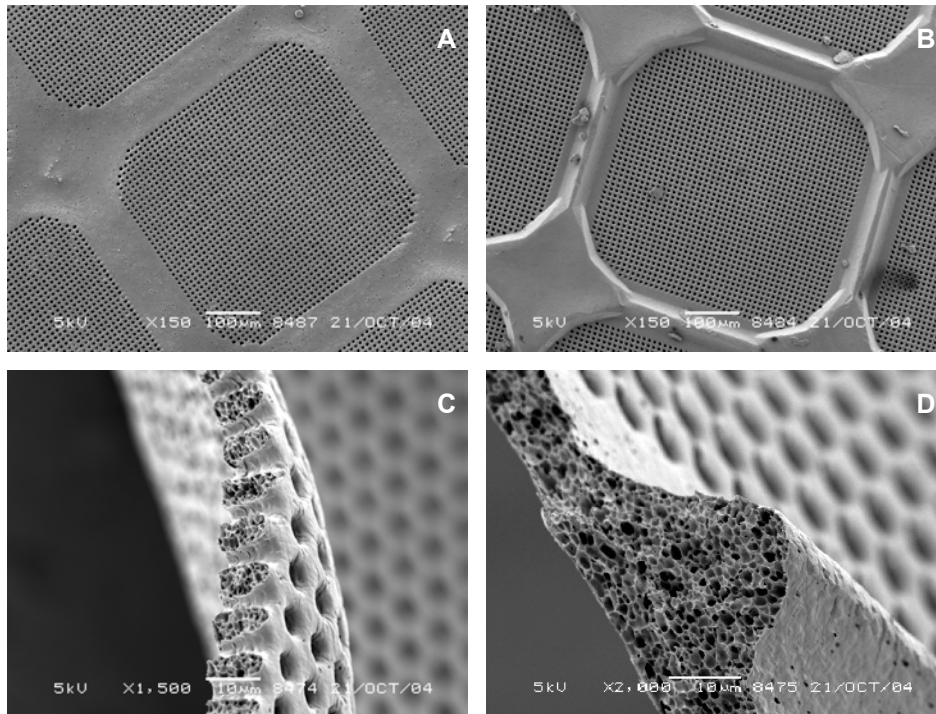


Figure 11. PES microsieves fabricated by PS μ M: top view of a field (A), view of the backstructure (B), cross-section of selective layer (C) and cross-section of the support (D).

7.4.2 Fabrication of PES/PVP and PES-PEO microsieves

a. PES/PVP

The addition of a mixture of PVP K90 and K30 to a reference PES solution resulted initially in a very high viscosity. When very viscous solutions were employed, inhomogeneous perforation was observed: while the edges of a field were open the central zone was completely closed.

First, the ratio between the two polymers (PES/PVP) was considered. Two solutions (12.7 wt% polymer, 43.6 wt% NMP and 35.54 wt% acetone) with the same overall polymer concentration (PES+PVP) but different PES/PVP ratios, equal to 4:3 and 3:4, were selected. In both cases tearing is evident at the edge of the field (Figure 12), being most severe for the membrane with the highest PVP content (Figure 12b). For this microsieve (PES/PVP = 3/4), the tearing was so acute that it almost ruptured and detached whole fields from the support structure. Little or no perforation was detected, in contrast to the membrane with PES/PVP = 4/3 (Figure 12a).

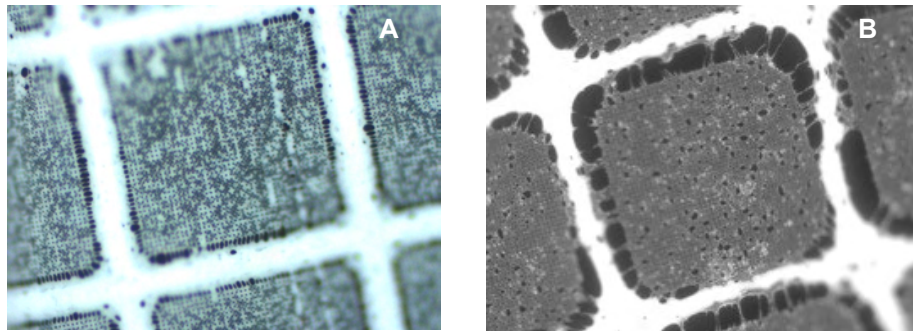


Figure 12. Microsieves casted from a solution with 12.7% polymer concentration with PES/PVP = 4/3 (A) and PES/PVP = 3/4 (B).

Tearing occurred at the zones with highest shrinkage during phase inversion (edge fields). From these results it was obvious that a higher PES content was needed. Besides, shrinkage could also be controlled by the ratio of the two PVP polymers used. It was expected that the polymer with highest molecular weight would be responsible for the highest shrinkage. Consequently, reducing its percentage in the casting solution would result in less defects at the high-stress zones.

Several solutions with different PVP K90 and K30 ratios, constant polymer concentrations (17 wt%) and PES/PVP ratio (10/7) were prepared. The composition of such solutions, together with the codes of the optical images corresponding to each produced microsieve (Figure 13), are given in Table 1.

Table 1. Polymer compositions of the solutions used to fabricate the microsieves displayed in Figure 13.

<i>Image</i>	<i>PES (wt %)</i>	<i>PVP K90 (wt %)</i>	<i>PVP K30 (wt %)</i>
A	10	7	0
B	10	6	1
C	10	3.5	3.5
D	10	1	6
E	10	0	7

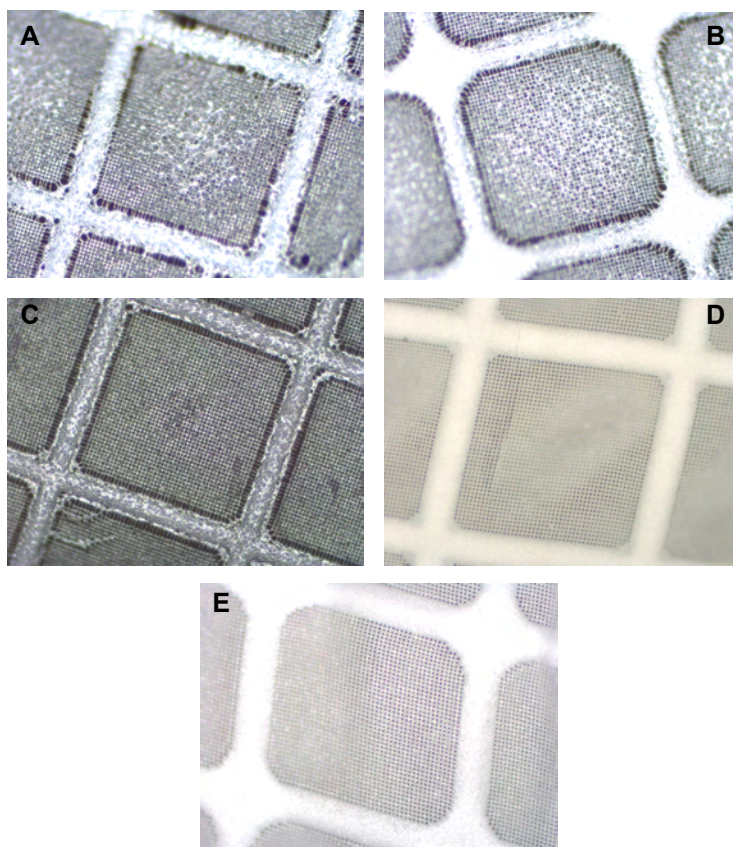


Figure 13. PES/PVP microsieves (17% Polymer, PES/PVP= 10/7) with different PVP K90/PVP K30 ratios.

Microsieves with the highest PVP K90 content (A, B) resulted in tearing at the edge of the field, as expected. At the center of the field a thicker layer of polymer was observed, which resulted in no perforation. Such phenomenon was already found on the microsieves prepared from very viscous solutions. Shrinkage induced defects and tearing were also found on microsieves with PVP K90/K30= 1 (C). However, complete and defect-free perforation was obtained throughout the field.

No defects or tearing at the field edges were seen on the microsieves with little or no PVP K90 (D, E). Full perforation was confirmed for both cases. However, the higher K30 content resulted in reduced mechanical stability, and deformation occurred upon release.

The K90/K30 ratio does not only determine the membrane morphology but also its hydrophilicity. This is displayed in Figure 14, where the water contact angles on PES/PVP films are shown.

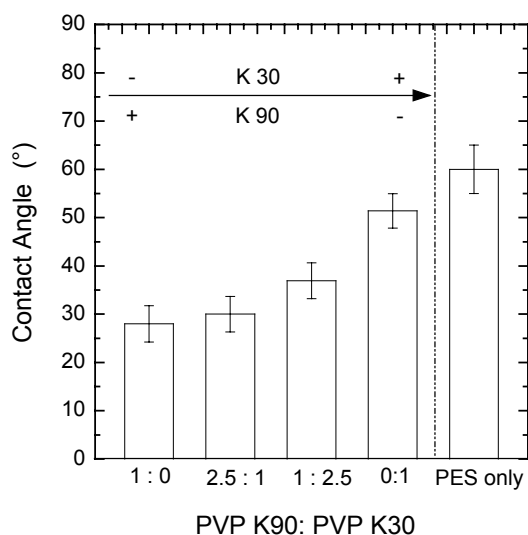


Figure 14. Contact angle on PES/PVP films (17% Polymer, PES/PVP = 10/7) with different PVP K90/PVP K30 ratios (1:0, 2.5:1, 1:1, 1:2.5, and 0:1).

As the content of PVP K90 increases, the water contact angle decreases, leading to more hydrophilic materials. The highest contact angle was measured on the film without PVP K90, while the lowest contact angle was measured on the film without PVP K30. The lowest molecular weight PVP (K30) was probably rinsed out more easily in the water bath, therefore higher contact angles were measured. Static contact angles were measured only a couple of

seconds after the water drop was in contact with the surface. However, this method may not give a full insight into the real hydrophilicity of the films. Even though contact angles around 30° were measured for the most hydrophilic films (highest PVP K90 content), complete spreading of the water droplet was subsequently observed, indicating the high hydrophilicity of such surfaces.

From the previous findings we can conclude that a combination of PVP with different molecular weights is needed for producing defect-free and mechanically stable microsieves. The total concentration of PVP should be kept low to avoid tearing.

After a variety of trials with different formulations (not all presented here), the most optimal composition of the PES/PVP blends was found to be very similar to the PES reference solution, except for the fact that no SPAN was added. The solution used contained 12% polymer, PVP K90/K30=1 and PES/PVP=5 (9.8 wt% PES, 1.96% PVP, 49 wt% NMP, 39.2 wt% acetone). Figure 15 shows the surface morphology of such PES/PVP microsieves, which were more hydrophilic than PES.

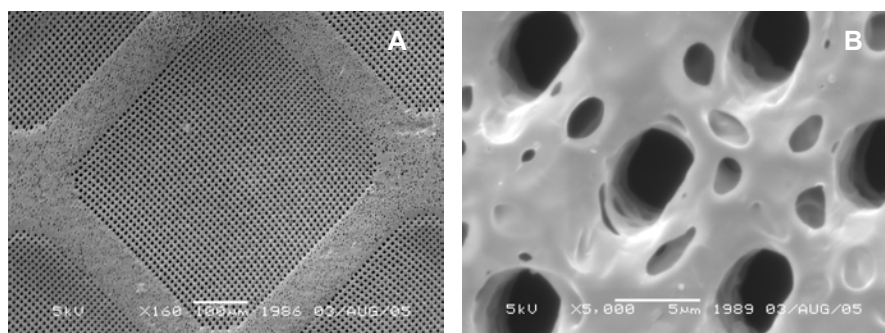


Figure 15. SEM images of a defect-free PES/PVP microsieve, with 12 wt% total polymer concentration, PVPK90/K30=1 and PES/PVP=5. Image (A) depicts a top view of a field and (B) is a close-up of the pores.

b. PES-PEO

Microsieve replicas were obtained with the PES-PEO copolymer, using a similar casting solution composition as PES. No defects at the field edge or in the pores were detected (see Figure 16).

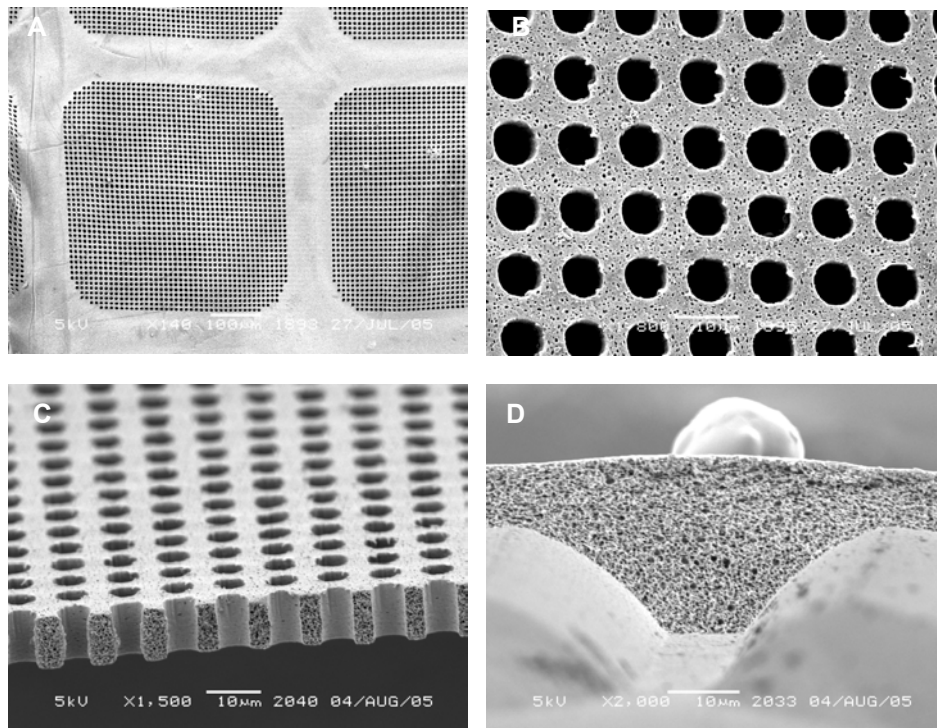


Figure 16. SEM images of PES-PEO microsieves: top view of a field (A), close-up of the pores (B), cross-section of selective layer (C) and cross-section of the support (D).

The fabrication conditions for PES-PEO microsieves were the following: $t_{\text{vapor}} = 3 \text{ min}$, $T_{\text{vapor}} = 30 \pm 1^\circ\text{C}$ and water bath coagulation time = 3 min. The obtained membranes presented an average pore diameter of $6.20 \pm 0.15 \mu\text{m}$, membrane thickness of $9 \mu\text{m}$, and support thickness of approx. $25 \mu\text{m}$. The periodicity of these membranes was $9.6 \mu\text{m}$. A water contact angle of $55 \pm 5^\circ$ was measured on a PES-PEO polymer film, although complete wetting also took place within seconds, probably by water penetration into the porous polymer.

c. Comparison of the materials and microsieves produced by PS μ M

Microsieves produced with PES, PES-PEO and PES/PVP presented the characteristics displayed in Table 2. They possessed similar thickness (PES-PEO membranes were slightly thinner) and pore sizes. PES-PEO microsieves, though, have slightly larger pore diameters (approx. $6 \mu\text{m}$), due to different shrinkage of the polymer with respect to the other materials. Pore periodicities determined by laser diffraction are in good agreement with the results

obtained by SEM. These results indicate that optical diffraction can be used as a non-destructive method to measure this specific characteristic.

Table 2. Polymer composition, thickness (δ), pore diameter (ϕ) determined by SEM, periodicity determined by SEM (d_{SEM}) or diffraction ($d_{diffraction}$) of PES, PES-PEO and PES/PVP microsieves. The water contact angles were measured on unperforated films with the same composition as microsieves

Material	Polymer (wt%)	δ (μm)	ϕ_{SEM} (μm)	d_{SEM} (μm)	$d_{diffraction}$ (μm)	θ ($^{\circ}$)
PES	9.8	10	4.5	9.42 ± 0.18	9.48 ± 0.14	60 ± 4.7
PES-PEO	9.8	8.9	6	9.7 ± 0.2	9.6 ± 0.2	55 ± 5
PES/PVP	12	10	4.5-5	9.7 ± 0.15	9.83 ± 0.2	≤ 45

Even though the static contact angles of the various materials did not differ extremely among each other, it was clearly observed that PES had different wettability than PES/PVP and PES-PEO. For the latter, water spread very fast on the films after some seconds. As mentioned previously, static contact angles may not be reliable enough to quantify the hydrophilicity of these films.

For all microsieves, differences in surface intrinsic porosity were observed between the top and backside of the membrane. Inner and surface porosity was higher in the case of PES-PEO in comparison to PES and the blends with PVP (see Figure 17). Differences in inner and surface porosity stem from the phase inversion recipe and casting conditions.

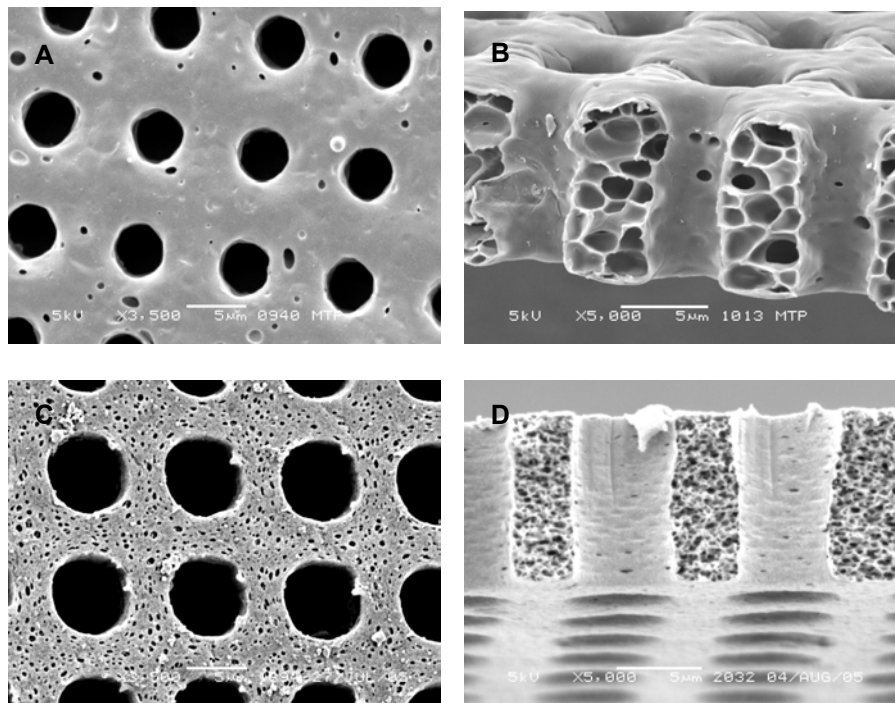


Figure 17. SEM images of PES (A, B) and PES-PEO (C, D) microsieves. Close-up of the pores on the ‘air’ side are displayed in (A, C) and cross-sections of the selective layer are shown in (B, D).

7.4.3 Microsieve pore downscaling: pillar design and thermal reduction of PES and PES-PEO microsieves

a. Tuning of perforation diameter as a function of pillar dimensions

The dimensions of the structures obtained by Phase Separation Micromolding directly depend on the mold features and the shrinkage of the polymer during phase inversion. Up to now, microsieves with perforations around 5 μm could be obtained. In this section, PES microsieves with perforations or pore diameters ranging from 3 to 1 μm were fabricated (see Figure 18), using the molds displayed in Figure 7. The top or ‘air’ surfaces are depicted in Figures A, C and E, whereas the back or ‘mold’ surfaces are displayed in figures B, D and F.

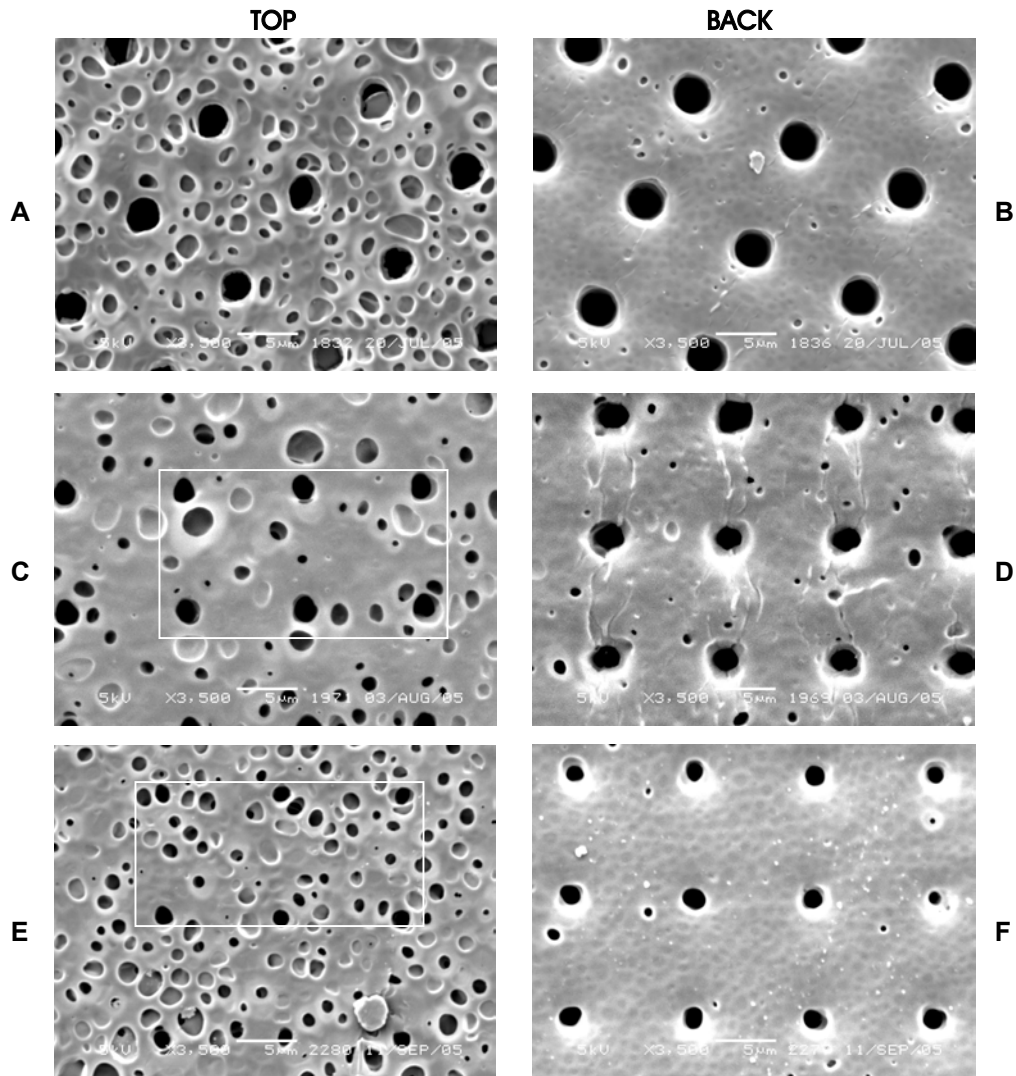


Figure 18. SEM images of the top and back surfaces of microsieves fabricated with molds M3 (A, B), M2 (C, D) and M0.8 (E, F). In Figures C and D six of the perforations are indicated to ease their identification.

In Table 3 the pore dimensions of the produced PES microsieves are shown, together with the dimensions of the mold pillars.

Table 3. Dimensions of the pillars from M3, M2 and M0.8 at the base and middle of their length, and pore diameters from PES microsieves cast from such moulds (top and back of the membrane).

<i>Mold</i>	$\phi_{pillar} (\mu m)$		$\phi_{pore} (\mu m)$	
	<i>middle/base</i>		<i>Top</i>	<i>back</i>
M 3	2.3	2.9	2.5 \pm 0.1	3.1 \pm 0.1
M 2	1.5	2	1.7 \pm 0.2	2.4 \pm 0.1
M 0.8	0.5	0.8	1.2 \pm 0.1	1.6 \pm 0.2

The conical shape of the pillars resulted in pores that are slightly larger at the ‘mold’ side. At the ‘air’ side pore sizes from 2.5 to 1.2 μm were produced. The perforation sizes were, in any case, around 0.3-0.4 μm larger than pillar sizes, due to lateral shrinkage. As mentioned before, the distance between the pillars affects shrinkage, which simultaneously limits the minimum pore size that can be obtained for a given periodicity.

Mold stability can limit the minimum perforation size. Positive taping is necessary to improve the mechanical strength of the pillars and facilitate the release. When the aspect ratios increase, they become more fragile at the zones that experience higher stress upon release, thus at the base. Figure 19 clearly demonstrates that straight pillars with diameters close to 2 μm did not withstand release of the polymer film and were pulled off the mold.

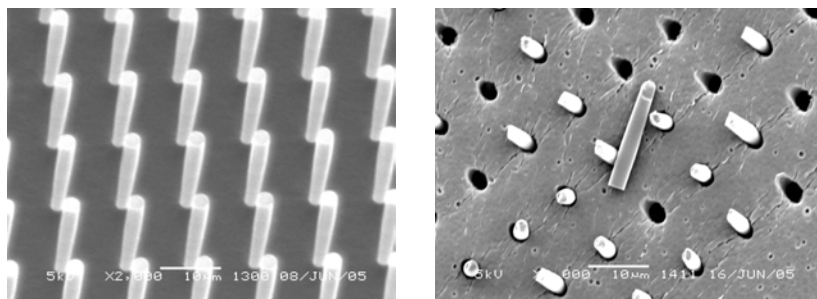


Figure 19. SEM images of a mold with straight pillars and a PES microsieve released from the mold, with broken pillars in its structure.

b. Tuning of perforation diameter by thermal treatment

Significantly smaller microsieve pores or perforations can also be obtained by densification or shrinkage of the membrane. The internal microsieve porosity allows the collapse of the intrinsic inner pores when the polymer is heated close to its T_g .

PES microsieves with 5 μm perforations were heated varying the heating time (15, 30, 60 min) and temperature (240, 245, 250 and 255°C). Figure 20a displays the obtained perforation diameters as a function of temperature for 3 different treatment times. The perforation diameter ($\phi_{\text{perforation}}$) decreases with increasing temperature and time. As the temperature increases, the treatment time becomes less significant and smaller differences are seen between the $\phi_{\text{perforation}}$. At the highest temperature maximum shrinkage occurred, reducing the perforation diameter to approx. 1.5 μm .

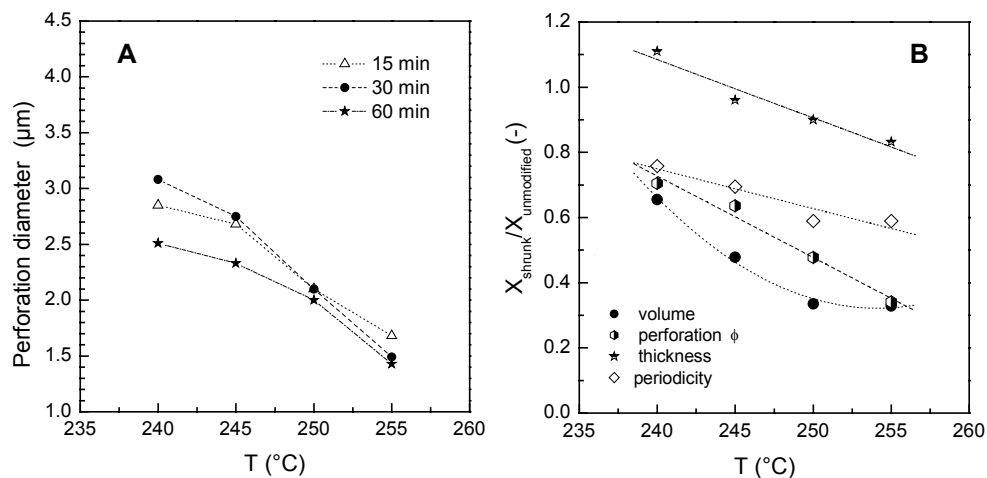


Figure 20. (A): Perforation diameter of PES microsieves heated at different times and temperatures. (B): Normalized values of microsieve characteristics (X) such as volume, perforation diameter, thickness and periodicity after heat treatments at 240, 245, 250 and 255°C during 30 min.

Figure 20b displays the relative reduction in volume, perforation diameter, thickness and periodicity for a treatment at 250°C for 30 min. The volume of the matrix is the volume taken by porous polymer around a perforation, which decreases in time as inner pores collapse. The shrinkage in thickness is smaller than the reduction in pore diameter. While the thickness was only reduced by 16% at the highest temperature, the periodicity and the perforation dimensions decreased in 40 and 70% respectively.

Figure 21 illustrates the morphology of the microsieves treated with the protocols described above, resulting in ϕ perforation of 3.1 (A), 2.8 (B), 2.1 (C) and to 1.5 μ m (D) for treatment T equal to 240, 245, 250 and 255 $^{\circ}$ C.

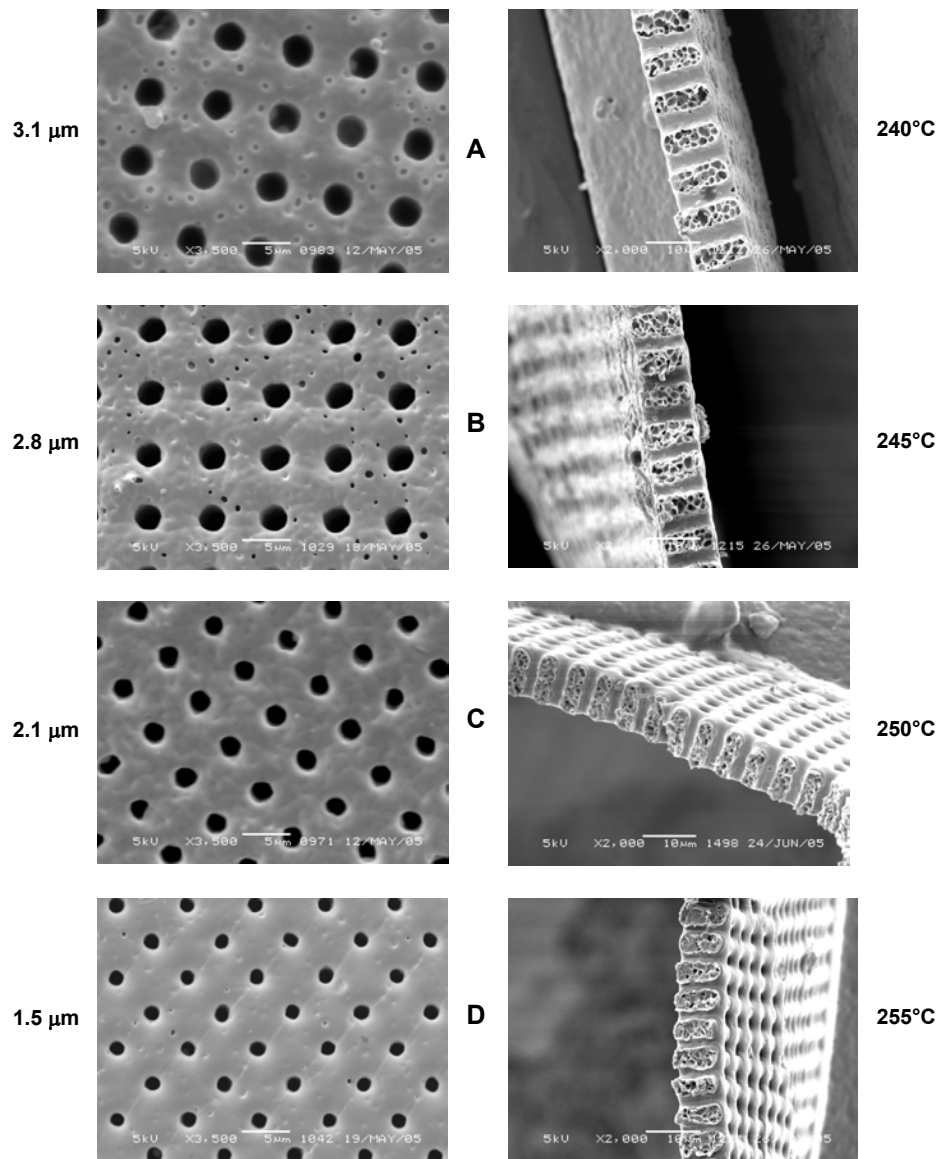


Figure 21. Surfaces and cross-sections of PES microsieves submitted to a heat treatment at different temperatures for 30 min.

Eventually, collapse of the intrinsic inner porosity with temperature resulted in a densified structure, which experienced more reduction in the lateral direction compared to the thickness. The asymmetric shrinkage may be a consequence of the curvature of the perforation [24]. This curvature will cause enhanced perforation shrinkage compared to the periodicity shrinkage.

With the highest temperature, pore features of approx. $1.5 \mu\text{m}$ were obtained by thermal treatment of PES microsieves. The limit temperature was found to be 260°C , since non-homogeneous shrinkage and complete densification started to occur.

This approach also reduced the pore/perforation size of **PES-PEO** microsieves, with initial perforations close to $6 \mu\text{m}$ and periodicity of $9.6 \mu\text{m}$. T_g of the block copolymer is around 180°C . Temperatures between 180°C and 210°C were chosen, with a treatment time of 30 min. Figure 22 shows the reduction in periodicity and perforation dimensions after the heating treatments.

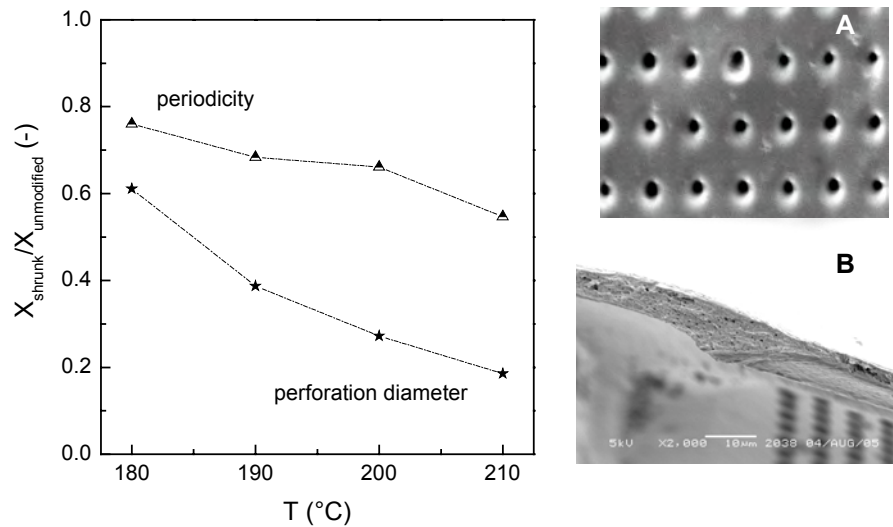


Figure 22. Relative perforation diameter and periodicity as a function of heating temperature for PES-PEO microsieves. SEM images of the membrane surface after heating at 210°C during 30 min (A) and the support structure after heating at 180°C (B) are also displayed.

The highest shrinkage corresponded to the perforation diameter, due to its curvature. Periodicity and the $\phi_{\text{perforation}}$ decreased 45% and 82% respectively. PES-PEO microsieves have a larger inner porosity compared to PES. Therefore, shrinkage occurred in a greater

extent along all directions. Contrary to PES structures, the relative decrease in pore dimensions and film thickness was similar. Maximum shrinkage occurred at 210°C, resulting in pore sizes of approx. **1.2 μm** (80% smaller than the unmodified membranes).

PES microsieves with initial perforations of 2.5 microns (cast from mold M3) were treated with controlled heating. The selected temperature was 250°C and the treatment time varied from 15 to 60 min. Results for the relative perforation diameter for both top and back surfaces and the periodicity are shown in Figure 23. A SEM image of the microsieve with the highest homogeneous shrinkage (250°C, 60 min), which resulted in a **0.5 μm** diameter at the top surface and **1.1 μm** at the back, is also displayed.

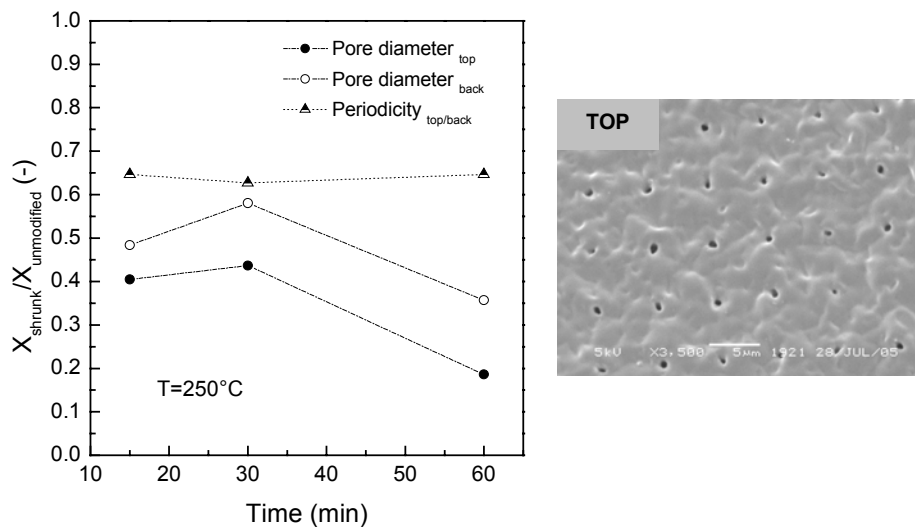


Figure 23. Normalized values of perforation or pore diameter and periodicity (X) at the top and back surfaces of PES microsieves treated at 250°C during 15, 30 and 60 min. Initially, their perforations had diameters of 2.5 (top) and 3.1 μm (back). The surface morphology of the membrane that resulted in more shrinkage is displayed as well.

Although little differences in shrinkage took place for the treatments at 15 and 30 min (as already observed previously for 5 μm PES), a larger reduction in pore diameter was observed for the longest procedure. Periodicity remained constant independently of the treatment or pore dimensions obtained.

The correlation of the periodicity and perforation dimensions of several thermally treated PES microsieves with initial $\phi_{\text{perforation}} = 5 \mu\text{m}$ is illustrated in Figure 24. As perforations become smaller, the perforation/periodicity ratio deviates more from the isotropic case. This can be a consequence of the perforation curvature.

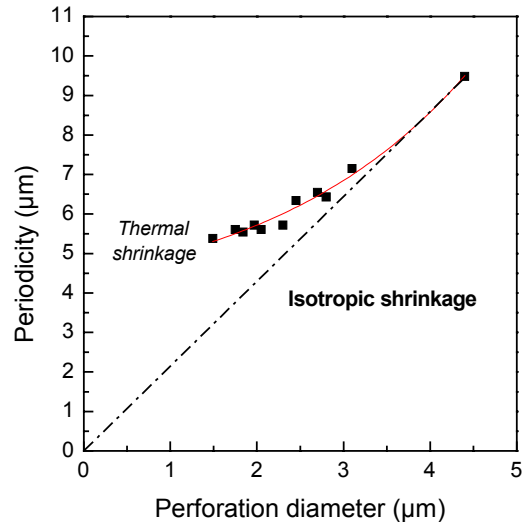


Figure 24. Periodicity as a function of perforation dimensions of thermally treated PES microsieves (initially with $\phi_{\text{perforation}} = 5 \mu\text{m}$). The dotted line indicates the periodicity obtained if isotropic shrinkage takes place.

7.5 Conclusions

Polymeric microsieves fabricated by Phase Separation Micromolding were obtained using PES, PES-PEO copolymers and blends of PES/PVP.

Phase separation takes place in two-stages, first in the vapor bath (VIPS) and then in the water bath (LIPS) for NMP removal. Perforation occurs in the vapor bath, induced by acetone evaporation and vapor induced demixing. The most determining parameter for perforation is the vapor bath residence time (whenever the casting thickness is optimized).

When PES/PVP blends are used as fabrication material different outcomes are observed. High total PVP content in respect to PES leads to increased viscosity and low perforation at the middle of a field. Higher PVP K90 content, in respect to lower molecular weight K30, results in severe tearing at the edges of a field. Higher K30 percentages provide membranes with deformations upon release due to limited mechanical stability. The most optimal

formulation (9.8% PES, 2% PVP, K90/K30=1) results in increased hydrophilicity compared to PES. With the PES-PEO copolymer very porous and thinner polymer replicas than PES are obtained.

Two approaches were investigated to decrease the size of the microsieve perforations:

- 1) microsieves with perforations between 5 and 1.2 μm were obtained with molds containing different pillar dimensions.
- 2) Smaller perforations were also achieved by thermally treating the polymer above its T_g .

Perforation diameters and periodicity decreased with increasing temperature. Starting with microsieves with pore sizes around 5 μm , perforations were reduced to 1.5 and 1.2 μm for PES and PES-PEO membranes, respectively. Even lower perforation dimensions (0.5 μm) were achieved by shrinking microsieves with initially pore diameters around 2.5 μm .

Phase Separation Micromolding seems to be a very suitable process for fabrication of polymeric microsieves with tunable pore dimensions in the micrometer range. In the next chapter, the filtration performance of such membranes will be described.

7.6 Acknowledgements

The author would like to thank Imam Akbarsyah for his input on the microsieve fabrication, Dr. Henri Jansen, from the Transducers Science and Technology Group (University of Twente) for the fabrication of the molds with conical pillars. Besides, Lydia Bolhuis-Versteeg is acknowledged for the technical assistance, Laura Vogelaar for the collaboration on the shrinking tests and Bernd Krause from Gambro (Germany) for kindly providing the PES-PEO copolymer.

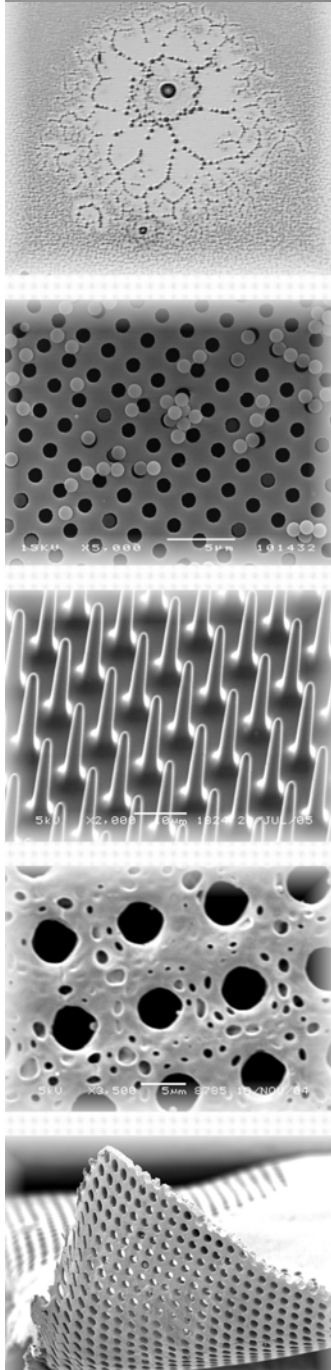
7.7 References

- [1] M. Gironès, Chapters 5 and 6 of this thesis.
- [2] S. Kuiper, Development and applications of microsieves. PhD Thesis, University of Twente, The Netherlands, 2000.
- [3] C.J.M. van Rijn, W. Nijdam, S. Kuiper, G.J. Veldhuis, H.A.G.M. van Wolferen, M.C. Elwenspoek, Microsieves made with laser interference lithography for micro-filtration applications. *J. Micromech. Microeng.* 9 (1999) 170.

- [4] L. Vogelaar, Phase separation micromolding, Ph.D. Thesis, University of Twente, The Netherlands, 2005.
- [5] L. Vogelaar, J.N. Barsema, C.J.M. van Rijn, M. Wessling, Phase Separation Micromolding, *Adv. Mater.* 15 (2003) 1385.
- [6] L. Vogelaar, R.G.H. Lammertink, J.N. Barsema, W. Nijdam, L.A.M. Bolhuis-Versteeg, C.J.M. van Rijn, M. Wessling, Phase Separation Micro Molding: a new generic approach towards microstructuring a wide range of materials, *Small* 1 (2005) 645.
- [7] H. Xu and W.A. Goedel, Polymer-silica hybrid monolayers as precursors for ultrathin free-standing porous membranes, *Langmuir* 18 (2002) 2363.
- [8] H. Xu and W.A. Goedel, From particle-assisted wetting to thin free-standing porous membranes *Angew. Chem. Int. Ed.* 42 (2003) 4694.
- [9] H. Xu and W.A. Goedel, Particle-assisted wetting, *Langmuir* 19 (2003) 4950.
- [10] Y. Xu, B. Zhu, Y. Xu, A study on formation of regular honeycomb pattern in polysulfone film, *Polymer* 46 (2005) 713.
- [11] B. de Boer, U. Stalmach, H. Nijland, G. Hadziioannou, Microporous honeycomb-structures films of semiconducting block-copolymers and their use as patterned templates, *Adv. Mater.* 12 (2000) 1581.
- [12] E. Krämer, S. Förster, C. Göltner, M. Antonietti, Synthesis of nanoporous silica with new pore morphologies by templating the assemblies of ionic block copolymers, *Langmuir* 14 (1998) 2027.
- [13] A. Imhof, D.J. Pine, Uniform macroporous ceramics and plastics by emulsion templating, *Adv. Mater.* 10 (1998) 697.
- [14] J.H. Moon, S. Kim, G. Yi, Y. Lee, S. Yang, Fabrication of ordered macroporous cylinders by colloidal templating in microcapillaries, *Langmuir* 20 (2004) 2033.
- [15] B.K. Chaturvedi, A.K. Ghosh, V. Ramachandran, M.K. Trivedi, M.S. Hanra, B.M. Misra, Preparation, characterization and performance of polyethersulfone ultrafiltration membranes, *Desalination* 133 (2001) 31.
- [16] Z.L. Xu, F.A. Qusay, Polyethersulfone (PES) hollow fiber ultrafiltration membranes prepared by PES/non-solvent/NMP solution, *J. Membr. Sci.* 233 (2004) 101.
- [17] M.H.V. Mulder, *Basic Principles of Membrane Technology*, Kluwer Academic Publishers, Dordrecht, 1996.
- [18] L.Y. Lafreniere, F. Talbot, T. Matsuura, S. Sourirajan, Effect of polyvinyl-pyrrolidone additive on the performance of polyethersulfone membranes, *Ind. Eng. Chem. Res.* 26 (1987) 2385.
- [19] E. Roesink, *Microfiltration: Membrane development and module design*, Ph.D. thesis, University of Twente, The Netherlands, 1989.
- [20] J. Barzin, S.S. Madaeni, H. Mirzadeh, M. Mehrabzadeh, Effect of polyvinylpyrrolidone on morphology and performance of hemodialysis membranes prepared from polyether sulfone, *J. Appl. Polym. Sci.* 92 (2004) 3804.
- [21] B. Torrestiana-Sánchez, R.I. Ortiz-Basurto, E. Brito-De La Fuente, Effect of nonsolvents on properties of spinning solutions and polyethersulfone hollow fiber ultrafiltration membranes, *J. Membr. Sci.* 152 (1999) 19.
- [22] J. Marchese, M. Ponce, N.A. Ochoa, P. Prádanos, L. Palacio, A. Hernández, Fouling behaviour of polyethersulfone UF membranes made with different PVP, *J. Membr. Sci.* 211 (2003) 1.
- [23] Adixen Micro Machining Systems (www.adixen.com), Alcatel Vacuum Technology, Annecy Cedex, France.
- [24] L. Vogelaar, M. Gironès, J.N. Barsema, C.J.M. van Rijn, R.G.H. Lammertink, M. Wessling, Freestanding polymeric etch and deposition masks: fabrication, application and further size reduction, submitted to *Chemistry of Materials*.

Chapter 8

Microfiltration with polymeric microsieves



8.1 Introduction

Nowadays, both ceramic and polymeric membranes are widely used for the filtration of dairy foods and beer, replacing conventional Kieselguhr filtration or pasteurization. Crossflow microfiltration is currently used to remove bacteria from raw milk, separate casein from whey and recover serum proteins from cheese whey, for instance [1-4]. In the brewing industry, current industrial crossflow microfiltration applications concern the clarification of rough beer to eliminate yeast and colloids responsible for haze, and sterile filtration of clarified beer.

Milk is a very complex fluid, mainly constituted by water (87.4%) and solids (12.6%). The components in whole milk are shown in Table 1.

Table 1. Average sizes and molecular weights of milk components [2, 4].

Component	Size or molecular weight
Fat globules	0.1-15 μm
Casein micelles	0.02-0.03 μm
α -Lactalbumin	14 kDa
β -lactoglobulin	18 kDa
BSA	69 kDa
Immunoglobulins	150-1000 kDa
Lactose	0.35 kDa
minerals	few \AA

For the recovery of the milk protein fraction, skimmed milk is normally used as feed. Skimmed milk contains < 0.5 wt/v % fat, 3.3 wt/v % proteins, 4.6-5.0 wt/v % lactose and minerals like calcium, sodium and potassium [4]. Fouling in skimmed milk filtration is normally associated to the protein fraction, formed by casein micelles and whey proteins like β -lactoglobulins, α -lactalbumins, immunoglobulins, BSA and others. Precipitation of calcium phosphates can also result in flux reduction. Currently used strategies to reduce fouling in milk involve mainly the use of backpulsing, acoustic or ultrasonic waves, turbulence promoters, vibrating modules (VSEP), rotating disk modules and air sparging. A recent review of Brans *et al.* [3] has covered the state-of-the-art of these techniques and their possible disadvantages in milk fractionation. The differences between such strategies are their principle of operation, efficiency and costs. Turbulence promoters, vibration and rotating disk modules increase the shear rate close to the membrane, while backpulsing removes the cake layer by reversing the

flow through the membrane. Air sparging reduces concentration polarization by mixing. Industrial implementation of these methods is very dependant on their efficiency (this at the same time depends on the feed and process parameters) and feasibility in terms of costs, upscaling and energy consumption.

Beer is a multi component feed, containing polysaccharides, higher dextrans and glucans, proteins and alcohols. The key membrane foulants in beer are protein, carbohydrates (β -glucan, pentosan, etc) and starch molecules or particles.

Crossflow microfiltration intends to replace conventional dead-end filtration with diatomaceous earth, for example. The main components of beer to be removed during clarification are yeast cells and haze (polyphenols, proteins, carbohydrates and metal ions), the dimensions and concentrations of which are shown in Table 2.

Table 2. Compounds to be removed from beer during clarification (chill haze= protein-polyphenol complexes) [5].

<i>Compound</i>	<i>Size (μm)</i>	<i>Concentration (g dry matter/l)</i>
Yeast cells	3.5-8.5	0.01-0.5
Particles/colloidal haze	0.1-10	0.2-0.8
Chill haze	0.001-0.5	0.05-0.3

To maximize the removal of chill haze, beer is normally filtered at 0°C. This causes a flux limitation due to the increased solution viscosity. A number of mechanisms can be used to improve beer flux, including backpulsing or backflushing [6, 7], flow pulsation and oscillatory flow on the feed [8]. Oscillatory flow consists of sinusoidal oscillations with flow reversal and no net forward flow, while pulsatile flow is based on steady feed flow with sinusoidal superimposed oscillations. Both techniques are based on disturbing concentration polarization and the cake layer.

Today, commercially relevant fluxes in beer filtration are between 10-100 kg h⁻¹m⁻² [6]. Microsieve membranes could very well supply the requirements needed for this application, because of their high fluxes and selectivity/permeability features. Currently, silicon nitride microsieves are being introduced in dairy and brewing industry as a breakthrough technology. In spite of their advantages, there is a trade-off associated with the high fluxes that such membranes can deliver: fouling.

A new approach is being developed as an alternative to silicon nitride microsieves: polymeric microsieves. Microfiltration with novel polymeric microsieves represents a revolutionary and challenging technology with great potential. These membranes exhibit similar selectivity/separation characteristics to inorganic microsieves, but at much lower production costs. Due to the versatility of the fabrication process (PS μ M) different pore sizes and shapes can be obtained. Microsieves with pore diameters ranging from 5 μ m (or higher) to approximately 0.5 μ m are currently available [9]. Polymeric microsieves can deliver large product volumes operating at very low pressures, together with selective separations due to their pore size and shape.

Fouling can be limited by choosing a suitable membrane material, depending on the specifications of the feed. Strategies such as backpulsing, forward pulsing or vibrational shear can be applied to reduce fouling, since these membranes are strong enough to resist the forces and pressures applied. Backpulsing, for instance, might be an efficient way to enhance permeation, because of the freestanding selective layer (without backstructure) and its little resistance to the flow.

Since polymeric microsieves are currently an emerging technology and no information about their performance in real filtrations is available yet, the outcome of the investigations in this chapter will serve as a guidance for future applications. The main goal of this work is the evaluation of the filtration performance and fouling behavior of PES microsieves, using model protein solutions (BSA) and real complex beverages like skimmed milk and beer. Microsieves with pore diameters of 2 μ m (obtained from thermally treated microsieves with $\phi_{\text{perforation}}=5$ μ m) have been selected as membranes for the fouling tests. Strategies extensively studied in the previous chapters, like air sparging or backpulsing, have also been applied in order to enhance permeation. The backpulsing performance of polymeric microsieves in aqueous solutions will be compared to other systems, like track-etched membranes and depth-filters.

8.2 Materials and methods

8.2.1 Materials

Microsieve PES membranes (pore size 5 and 2 μ m) were used for the crossflow BSA filtration experiments. For skimmed milk and beer filtration, 2 μ m PES microsieves were exclusively used. The fabrication of such microsieves is discussed in detail in Chapter 7. To compare the effect of backpulsing, commercial track-etched membranes like Nuclepore (polyethylene, 2

μm) and Millipore RAWP (cellulose esters, 1.2 μm) were also used. Nuclepore membranes (low porosity) had a thickness of approximately 10 μm . Millipore RAWP had a porosity of 82% and an average thickness of 150 μm .

Ultrapure water (18.2 M Ωcm) for flux measurements was obtained with a Millipore purification unit (MilliQ plus). Bovine Serum Albumin (BSA) (Fraction V, Fluka) was used as model protein. The feed solutions consisted of 1 g/l BSA dissolved in filtered phosphate buffer 50 mM at $\text{pH}=6.8 \pm 0.1$. Solutions were freshly prepared and stored at 8°C for maximum 2 hours before use. Commercially available sterilized skimmed milk (Euroshopper, $\text{pH}=6.9-7$) and white Belgian beer (Hoegaarden, $\text{pH}= 4.4$) were used directly without any pre-treatment.

8.2.2 Crossflow microfiltration of BSA, skimmed milk and beer

The microsieves and commercial membranes were glued onto a spacer acting as support (0.1 mm pore size) to enhance their mechanical strength, and then to a polysulfone sample holder. All membranes were wetted with water or a mixture of water and isopropanol prior to use.

The clean water permeability was measured in the pressure range of 10-30 mbar at $20 \pm 2^\circ\text{C}$ before any protein filtration. Prior to the water flux measurements the membranes were inspected under an optical microscope to check their integrity. For the microsieves with pore diameter equal to 5 μm wettability tests were performed in order to establish an appropriate wetting method. The clean water flux of a microsieve was successively measured during 40 minutes. For microsieves with pore diameter equal to 2 μm , wetting was performed in water for 30 min or in a 1:1 mixture of water/isopropanol for 15 min.

The permeation experiments were performed in a cross-flow module with a channel height of 700 μm and an effective membrane area of approx. $0.5 \times 10^{-4} \text{ m}^2$. The BSA permeability was measured at a transmembrane pressure of approx 18 mbar at $10 \pm 2^\circ\text{C}$, with an average crossflow velocity of 0.165 m/s. The filtrations of milk and beer were performed at approx. $10 \pm 2^\circ\text{C}$ and an average operating pressure of 20 mbar. In all filtrations, the feed was stirred and pumped to the membrane module using a microannular pump with recirculation.

Variable frequencies and backpulsing power were applied in the backpulsing experiments with BSA solutions. Frequencies were varied from 2 to 6.7 Hz, power was varied from 30 to 50% and the pulse length was kept constant at 20 ms. In all experiments the tail was suppressed so that a symmetrical backpulsing profile was applied. Only in the case of the preliminary tests with the 2 μm microsieves a tail was applied (100 ms). For milk and beer filtrations, the backpulse frequency was varied from 2.5 to 6.7 Hz at a constant pulse power and length of 45% and 20 ms, respectively.

8.2.3 Scanning Electron (SEM) and Optical Microscopy

The morphology of the microsieve membranes was visualized by Scanning Electron Microscopy (SEM, Microscope JEOL JSM-5600LV, at 5 kV). Quick microsieve inspection before and after the flux measurements was performed with an optical microscope (Zeiss Axiovert 40).

8.2.4 Analysis

The concentration of BSA and milk proteins in the feed and permeate was analyzed with a Cary 300 Scan UV-VIS spectrophotometer at $\lambda = 280$ nm. Single wavelength measurements were also performed to the beer feed and permeate fractions in the visible region, at $\lambda = 450, 500, 600$ and 800 nm. The solid content of the fractions was determined by weight difference of evaporated samples with the same initial weight or volume. Samples were evaporated in a desiccator for 48 h and in a vacuum oven at 30°C for 5 days.

8.3 Results and discussion

8.3.1 Fouling studies with a model protein (BSA)

a. PES unmodified microsieves ($5\ \mu\text{m}$)

As a standard characterization procedure, the clean water flux of PES microsieves with $5\ \mu\text{m}$ average pore diameter was measured. Different wetting procedures were applied: no wetting, wetting with water for 30 min, wetting with Ethanol for 5 minutes, wetting with a 1:1 mixture of Isopropanol/water for 5 min and wetting with 100% Isopropanol for 5 min. No significant differences in the clean water permeability were observed for the different wetting procedures, indicating that PES microsieves were wettable in any of the mentioned conditions. The average clean water permeability values of microsieves with $5\ \mu\text{m}$ pore diameter varied between 2 and $4 \times 10^6\ \text{l/m}^2\text{hbar}$. The scattering in these results originates from the differences in the intrinsic porosity, thickness difference among membranes and error in membrane area determination. From the SEM pictures shown in Chapter 7 we can observe that, even though the microsieves present low perforation porosity, additional intrinsic porosity created by the phase inversion method is present. Micropores in the unperforated zones may also contribute to such large fluxes.

Preliminary experiments were made with PES-PEO microsieves, which resulted in clean water permeabilities slightly higher than the ones of PES microsieves, due to lower

thicknesses. SEM inspection of the PES-PEO surfaces indicated an increased surface intrinsic porosity and lower membrane thickness compared to PES.

After characterization of PES microsieves in terms of water permeability, the fouling behavior was studied with BSA as model protein. Microsieves with such large pore sizes and large fluxes were hard to measure, since large flux fluctuations occurred when either air bubbles or changes in pressure took place. However, when relatively stable BSA filtrations were analyzed we observed that flux decline took place in a great extent. This effect is displayed in Figure 1, where the relative BSA permeability of a 5 μm microsieve at pH=6.7 is shown in time. The filtration was performed at an operating pressure of 21.5 ± 1.5 mbar.

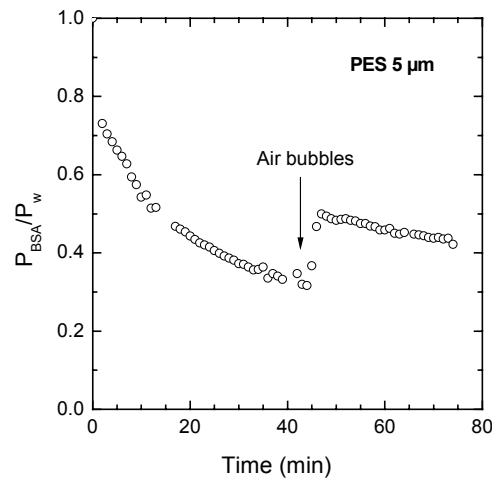


Figure 1. Flux decline versus time of 1 g/l BSA pH=6.7 with a 5 μm PES microsieve at constant pressure.

Permeability declined very rapidly in the first minutes of filtration, due to fast aggregate deposition. BSA aggregation during filtration was already confirmed in Chapter 4 for 1.2 μm microsieves. When air bubbles were present in the system ($t=45$ min) permeability was slightly recovered because of partial aggregate removal. The same effect was already demonstrated previously with silicon nitride microsieves.

PES membranes have been extensively used by many authors to study the flux decline of BSA solutions. Zeta-potential measurements on PES surfaces, reported by Pontié and coworkers [10] indicated that PES is negatively charged at neutral pH. Therefore, little electrostatic interactions with the negatively charged BSA can occur. This reasoning and the findings of other authors [11-14], together with our results in Chapter 4 point thus to

aggregate deposition as responsible mechanism for flux permeability loss for PES microsieves in BSA filtration.

From these observations it was clear that fouling is a critical aspect to be considered, even if microsieves with large pore sizes were used. Microsieves with 5 μm pores presented extremely large fluxes, which made it difficult to discriminate between flux anomalies caused by air, pressure changes or just protein fouling. That is why we opted for a more controllable system; PES microsieves with an average pore size of 2 μm .

b. Thermally-treated PES microsieves (2 μm)

Thermally-treated PES microsieves (250°C, 60 min) with 2 μm average pore diameter (see Figure 2) display an average clean water permeability of 3.4×10^5 l/m²hbar, which is a closer value to the water permeability of Si_xN_y microsieves.

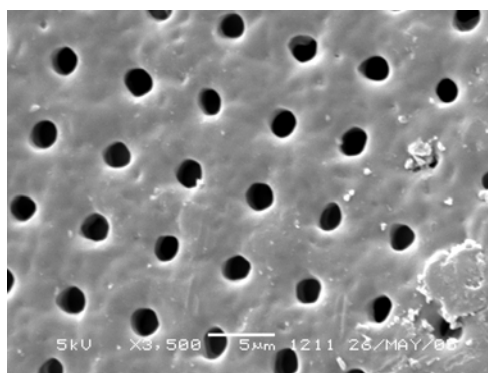


Figure 2. Surface morphology of a PES microsieve with 2 μm pore diameter, fabricated by thermal treatment (250°C, 60 min).

A good agreement is found between these values and the permeability calculated with van Rijn's equation described in Chapter 3 (page 42). For a microsieve of approx. 2 μm pore diameter and 8.5 μm pore length and porosity of 6%, a permeability of about 3×10^5 l/m²hbar is calculated, which agrees quite nicely with the measured values.

These microsieves were used to investigate the flux decline of a 1g/l BSA solution at pH= 6.8 at 31 ± 1 mbar. Figure 3 shows how the membrane permeability decreased to 50% in the first 5 minutes of filtration. After one hour the microsieve was completely blocked and no permeation was observed.

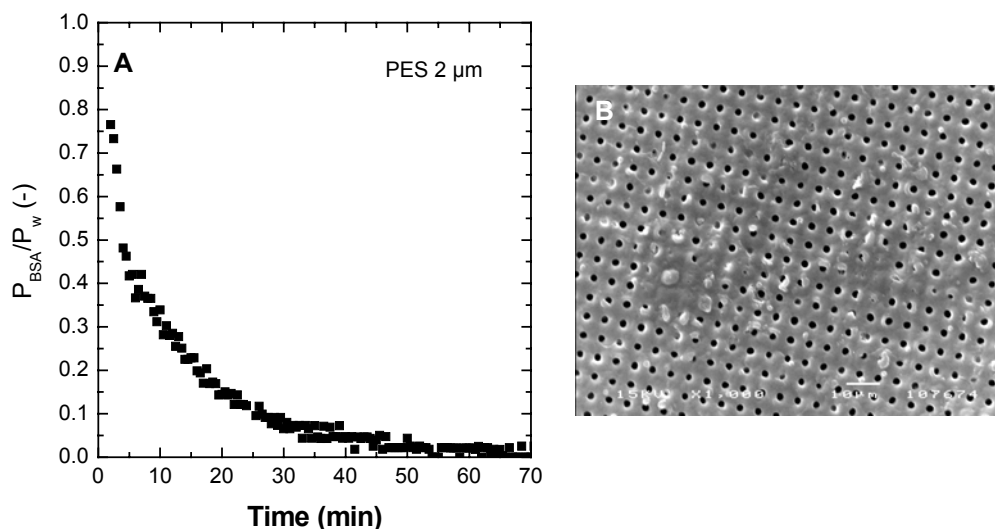


Figure 3. Flux decline versus time of 1g/l BSA pH=6.8 with a 2 μm PES microsieve (A), together with its surface morphology depicted with a SEM image after BSA filtration (B).

The BSA retention of a shrunk PES microsieve after 20 minutes of filtration was approx. 4.5%. After approx. 40 min, retention increased to 6%. Image B (Figure 3) displays blocked areas on a microsieve after use, after flushing with water. It is clearly seen how some pores are completely covered by a thick protein aggregate layer. The previous results suggest that pore blocking is also the mechanism responsible for the severe BSA flux decline with membranes with large pore sizes such as 2 or 5 μm . For a microsieve with 2 μm perforations the best fit for the experimental data results gives a beta value of 2.35 ± 0.11 , using the model of Bowen *et al.* [15]. This clearly confirms the behavior predicted by the classical pore blockage model, even if the pore sizes used are large (2 μm).

c. Fouling reduction strategies

From the experience gained with inorganic microsieves, fouling prevention was studied with techniques such as backpulsing and air sparging. With polymeric microsieves, backpulsing settings had to be optimized and adapted to the system in preliminary experiments. The protein filtration performance was evaluated for a shrunk microsieve (2 μm pore diameter) to investigate backpulsing and forward flushing-backflushing effectiveness. The results are shown in Figure 4, together with the corresponding backpulsing settings.

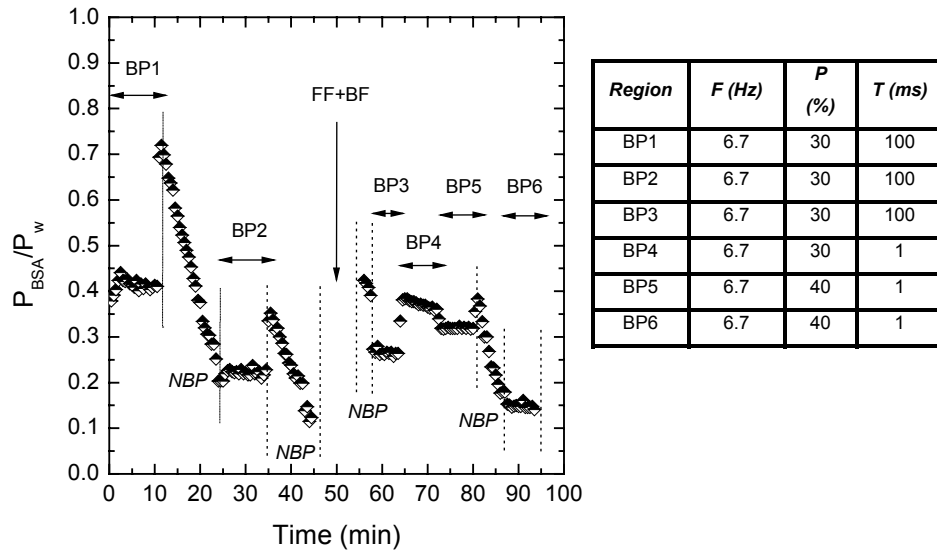


Figure 4. Relative permeability versus time of 1mg/ml BSA pH=6.8 filtered through a 2 μm at 20°C. The BP sections are the intervals where backpulsing was applied, during the NBP sections no backpulsing was applied. FF+BF stands for forward flushing and backflushing. The frequency (F) and the pulse length were kept constant at 6.7 Hz and 20 ms respectively, while the power (P) and the tail settings (T) were varied.

When backpulsing was applied (region BP1 and BP2) permeability remained constant, even though a 60% loss in total permeability was observed initially. For the first time constant permeabilities with BSA solutions were measured, in combination with backpulsing.

When backpulsing was stopped, a sudden increase of permeability was observed (due to reduced resistance offered by the backpulsing), declining rapidly afterwards (NBP regions). After 50 min of filtration, when only 10% of the permeability remained, water forward and backflushing were applied offline. After reinitiating the filtration without backpulsing, permeability could be successfully but temporarily recovered up to 40% of its maximum value. At BP3 reinitiation of backpulsing led again to constant permeability (25%, like in BP2). If the backpulsing tail was suppressed (BP4), an increase in permeability was observed, indicating that the pulse was more effective. But, since a slight flux decline occurred in this region (10%), backpulsing power was increased. This resulted in constant permeability (BP5). When backpulsing was stopped and then restarted with the same settings as in BP5, the same trend occurred as in the other intervals: first permeability declined and then it stabilized as backpulsing was activated (BP6).

The decrease in permeability when pulses were applied is a consequence of the pressure considered in our calculations. When pulses are applied the average flux is lower because the average pressure at the permeate side is elevated. For the permeability calculation the pressure drop across the membrane and the backpulsing is normally considered. This pressure is lower than the operating pressure (average pressure at the feed side). For our permeability calculations only the operating pressure is considered, which is normally constant and independent of backpulsing. Once backpulsing stopped, a sudden flux increase could be obtained, until protein deposition occurred and caused permeability decline.

From the filtration of a BSA solution with the combination of backpulsing and polymeric microsieves several observations should be made:

- 1) backpulsing at 6.7 Hz resulted in constant BSA permeability (which had not yet been observed, even for silicon nitride microsieves)
- 2) suppression of the pulse tail led to increased permeability values.

The fact that backpulsing was more effective with polymeric compared to silicon nitride microsieves might be based on the fact that the polymeric structures can experience motion during pulses. Moreover, contrary to the inorganic microsieves, they do not damp the pressure pulse. In this way permeation enhancement by backpulsing is more likely to occur by membrane motion rather than by permeate flow reversal (flow reversal takes place but permeation in that direction is low). Vibration of the microsieve can be visually observed during a filtration. Figure 5 demonstrates that the PES microsieves act as a pulse transmitter. Figure 6 shows the effect of the power and the pulse frequency on the pulse profile.

In the first place, when no membrane is present in the system (see Figure 5a), we can observe that the feed pressure equals the permeate pressure, so the pulses are 100% transmitted. From Figures 5b and c it can be appreciated that the pulse is completely registered in the feed pressure (set at 20 mbar, without pulses) when applied through a PES microsieve. During a pulse the feed pressure has almost the same value as the permeate pressure, resulting in almost no negative TMP.

In between pulses, feed pressure gradually increases until its set value (20 mbar). Another observation is the peak value of the permeate pressure at its maximum, which increases with the applied power and results in more negative TMP values.

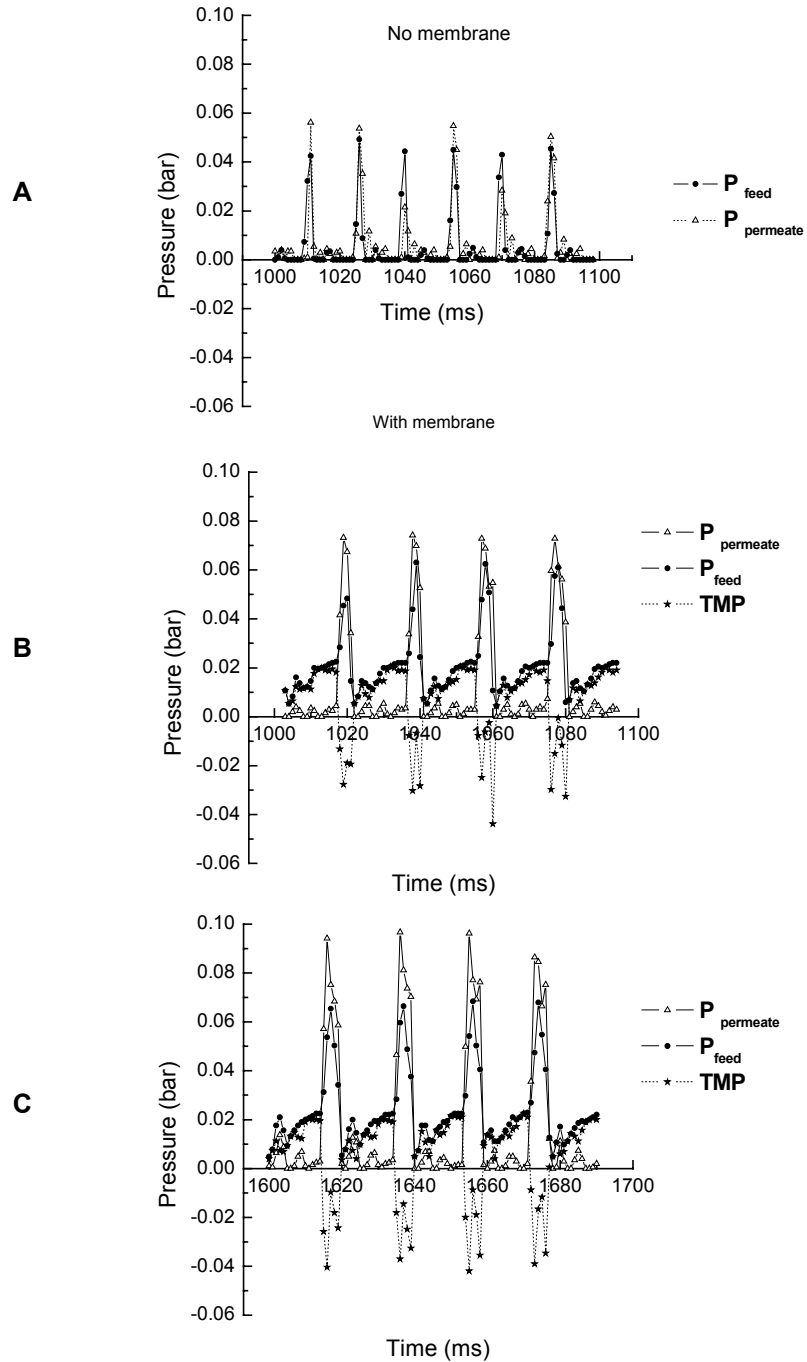


Figure 5. Pressure as a function of time when backpulsing water (3.3 Hz, 20 ms) without membrane (A) and 45% power (A) and with a PES microsieve at 45% (B) and 64 % (B) power.

In Figure 6 the pulse profiles as a function of time for different frequencies are displayed, for a pulse power and length of 45% and 20 ms, respectively.

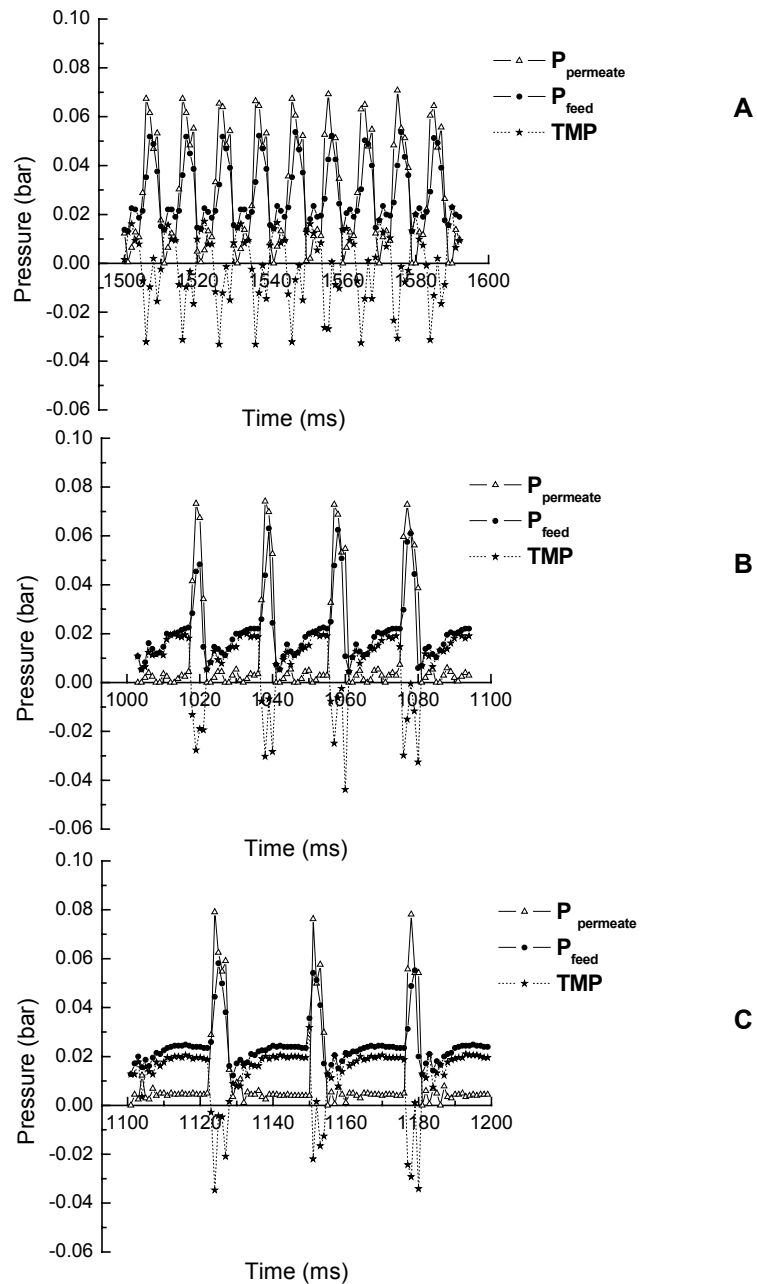


Figure 6. Pulse profiles when backpulsing water at 45% power, 20 ms pulse and 6.7 Hz (a), 3.3 Hz (b) or 2.5 Hz (c), with a PES microsieve.

In all cases the pulse is clearly transmitted to the feed side, because p_{feed} is almost equal to p_{permeate} . In such case very little negative transmembrane pressures are reached, indicating that also little backtransport occurs. An increase in pulse frequency results in less flux. Furthermore, at lower frequencies there is more time for the pressure to be stabilized before a pulse.

The previous results confirm that the fact that stable protein fluxes are obtained with BSA solutions is more likely to be caused by significant membrane motion rather than by a large backflow through the membrane. Mechanical motion was visually observed in our experiments during pulses and, furthermore, differences between feed and permeate pressure were low and only measured during a couple of ms for each pulse. Membrane motion can change fluid hydrodynamics on the membrane surface and decrease concentration polarization. Rodgers and co-workers [16] already reported this effect and postulated that membrane motion allowed an alteration of the solute concentration profile within the boundary layer so that the system concentration remains constant during the pulsing period.

Higher membrane productivity can be reached by tuning either the frequency or the power of the backpulses. Lower frequencies may lead to higher permeabilities. Polymeric microsieves would still be able to experience motion at lower frequencies and keep protein aggregates lifted off the surface.

Two approaches were applied to optimize backpulsing and increase membrane productivity. For the first one, the process started without pulsing for a couple of minutes and then backpulsing was applied at high frequency (6.7 Hz), and regularly switched off for some seconds. Throughout the course of the experiment the frequency was varied as well. The outcome of this experimentation is presented in Figure 7.

As already noted in Figure 4, stopping the pulses for some seconds increased permeability temporary. Lowering the frequency from 6.7 to 2.86 or 4 Hz resulted in an increase in permeability (approx. 10%) and constant permeation rate. Slightly rinsing the membrane with water did not lead to an increase in permeability, probably because of little deposition on the surface. Relatively stable permeabilities (around 50%) were measured at intermediate pulse frequencies (2-4 Hz). After a non-pulsing period, backpulsing reinitiation at 2.86 Hz resulted in

a constant permeability, indicating that the deposited aggregates were successfully removed from the surface.

Fairly constant permeability and enhancement were found when systematically stopping pulses and lowering the frequency.

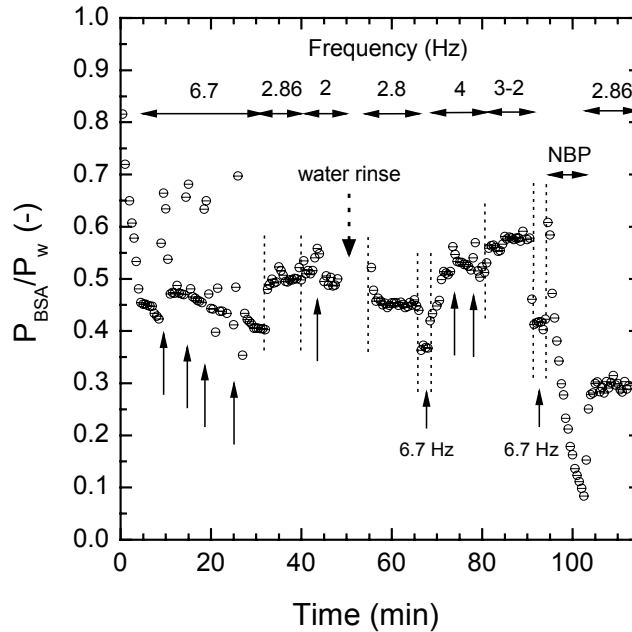


Figure 7. Relative permeability versus time of a BSA solution at pH=7 through a 2 μm PES microsieve. The arrows indicate the exact points where backpulsing was stopped and above the plot the different intervals with variable frequency are shown.

Our second approach assumed that, if backpulsing would be initially started at lower frequencies, much higher permeability values might be obtained. A confirmation of this hypothesis and a glimpse on the effect of air sparging is provided in Figure 8.

Backpulsing was initiated at 2.86 Hz and a relatively constant and high permeability was observed for the first time. A successive decrease of frequency increased the permeability even further.

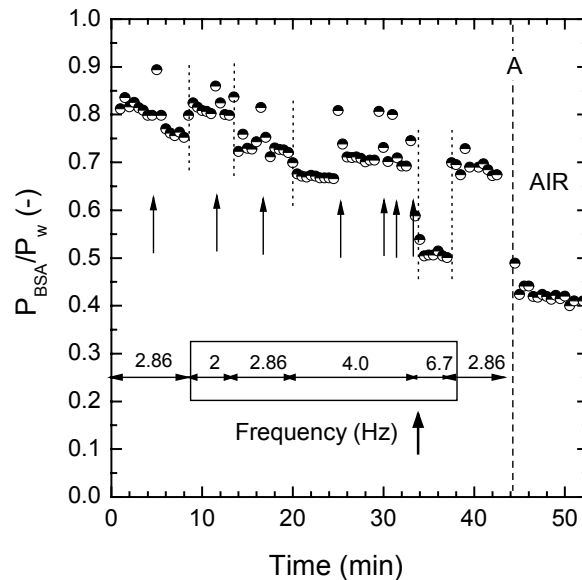


Figure 8. Relative permeability versus time of a BSA solution at pH=7 through a 2 μm PES microsieve. The arrows indicate the exact points where backpulsing was stopped. At (A) backpulsing was stopped and air was dosed to the system at 10 ml/min.

Then frequency was increased stepwise, from 2 to 2.86, 4 and 6.7 Hz. Once the frequency was increased, a decrease in permeability occurred, as expected. Fortunately, permeability could be increased in each regime by shortly stopping the pulses. In this way, little overall permeability loss took place (only 18% decrease in one hour). The largest loss in BSA permeability was at 6.7 Hz (from 70 to 50%), but it could easily be restored to the average value (70%) if frequency was lowered to 2.86 Hz. The influence of air sparging on the total permeability was also studied here. Like with silicon nitride microsieves, the dose of air resulted in a constant permeability. However, with air sparging a permeability loss of 40% took place with respect to the backpulsing situation, due to a reduction of the liquid volume in the feed ($V_{\text{air}}/V_{\text{liquid}}=6\%$) and the dynamic equilibrium between deposited and removed protein. Since air cannot remove all deposited protein, a steady state is reached. For this particular microsieve the average flux was calculated to be 9800 l/m²h during backpulsing.

8.3.2 Comparison of polymeric microsieves and commercial membranes

From the previous section the main observation is that backpulsing BSA solutions at low frequencies is a very effective method to achieve stable fluxes with polymeric microsieves. In this situation, the determining factor in stabilizing permeability might be the mechanical motion of the microsieve during pulses. Such findings are a great breakthrough for microfiltration and potential applications of polymeric microsieves. But in principle, this phenomenon might also be applicable to polymeric commercial screen filters, like track-etched membranes.

For comparison with current commercial systems, BSA was also filtered through Nuclepore track-etched membranes, with 2 μm pore diameter and average clean water permeability of $2 \times 10^5 \text{ l/m}^2\text{hbar}$. In Figure 9 the outcome of a filtration experiment with BSA at $\text{pH}=7.1$ and backpulsing at different frequencies (20 ms pulse length, 45% power) is presented.

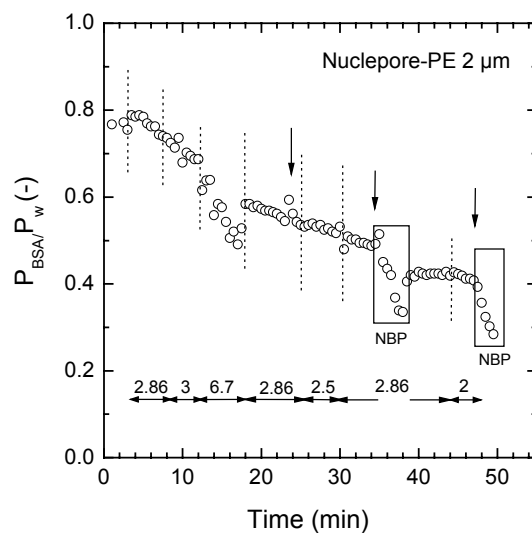


Figure 9. Relative permeability versus time of a BSA solution at $\text{pH}=7.1$ through a 2 μm PE track-etched Nuclepore membrane. The arrows indicate the exact points where backpulsing was stopped.

BSA permeability experienced decline even though backpulsing was applied. The most unfavorable conditions were obtained at high pulse frequencies, leading to flux instabilities and rapid decline. No backpulsing led to fast flux decline due to aggregate deposition.

Initially, permeability did not remain constant for frequencies of 2.86-3 Hz, and declined even more at 6.7 Hz. After approx 20 min the frequency was varied around 2.86-2.5 Hz and a gradual permeability decline of 10% was observed. When backpulsing was stopped for

several minutes and restarted at 2.86 Hz, permeability stabilized at 40% of the maximum value.

In this experiment, even though the backpulsing settings were varied, permeability declined and not even successive pulse stops could recover it. These results indicate that backpulsing a BSA solution was less effective for track-etched membranes than for microsieves, with these particular settings and solution properties. Direct comparison among these membranes in terms of BSA fouling should be done with caution, because even though their structures are rather similar in terms of thickness and pore design, the material properties, porosities and permeabilities are significantly different. More importantly, different surface-protein interactions may also occur depending on the membrane material. Therefore, it is difficult to establish if either adsorption, backpulsing inefficiency or reduced membrane motions are the causes for flux decline.

The pulse profiles with Nuclepore membranes, compared to PES microsieves are depicted in Figure 10. For additional comparison, pulse profiles through a depth-filter Millipore RAWP and silicon nitride microsieves (both with pore diameter 1.2 μm) are also provided. The tests were performed with water, at a feed pressure of 20 mbar, constant frequency of 3.3 Hz, 45% power and a pulse length of 20 ms.

The main differences between the pulses through these membranes are the feed pressure profiles and corresponding TMP values. For the track-etched and the depth-filter membranes the profiles are very similar: the pulse is registered at the feed side, reaching a value of approx. 35 mbar. The differences between backpulsing with such membranes and polymeric microsieves are striking. In the first place, considerably high feed pressures are measured with polymeric microsieves during a pulse, almost as high as the permeate pressure. This points out that the pulse is almost completely transmitted through the membrane and that maybe only little permeate backflow exists. Nonetheless, backpulsing is very efficient because it can cause membrane motion and result in constant permeability.

Between pulses, the feed pressure also varied considerably (from 10 to 20 mbar). A pressure pulse is followed by a pressure dip, which is shown in the profile. The differences between silicon nitride and polymeric microsieves are even more obvious. The rigid membrane backstructure of Si_3N_4 microsieves damps the pulse and very little pressure variations can be seen at the feed side. However, in this case there is indeed backtransport of permeate through the microsieve, because highly negative TMPs are recorded [17].

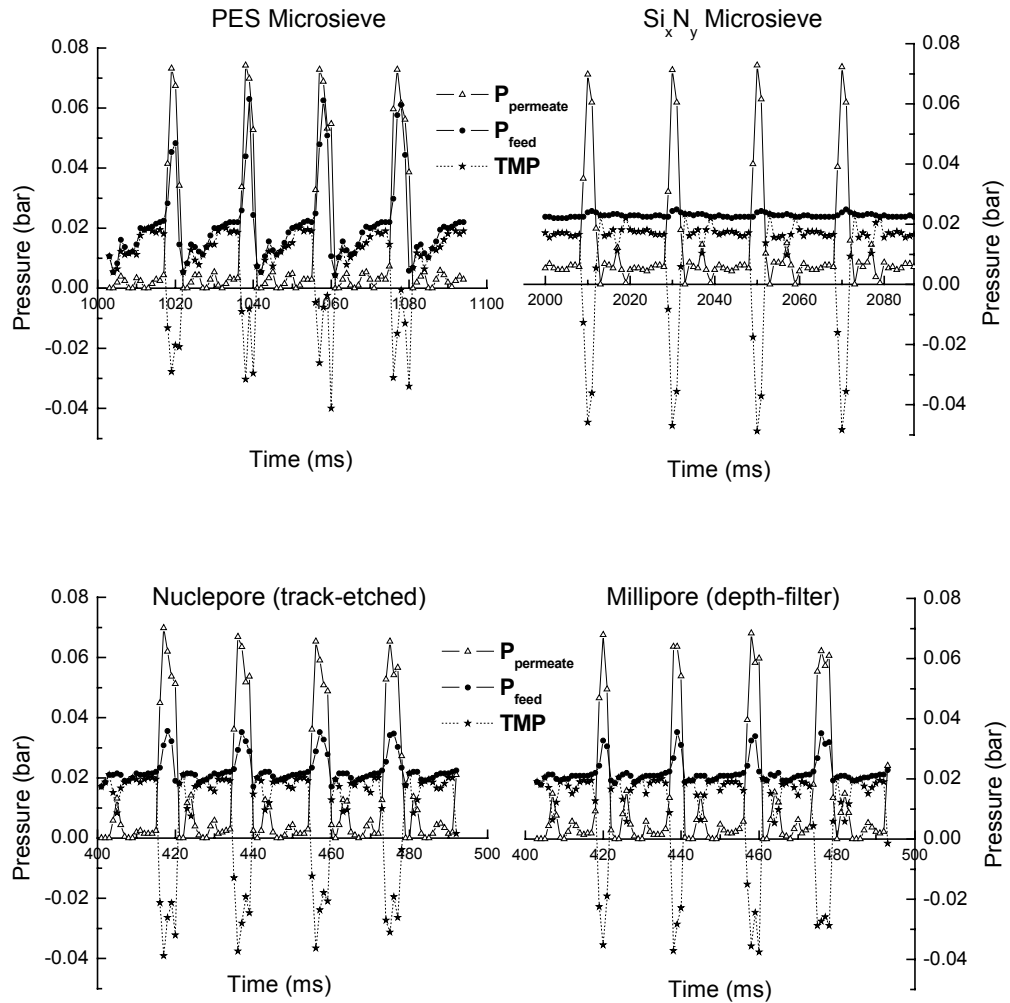


Figure 10. Pulse profiles when backpulsing water (3.3 Hz, 45% power, 20 ms pulse) with a 2 μm PES microsieve, 2 μm Nuclepore track-etched, 1.2 μm silicon nitride microsieve and 1.2 μm Millipore depth-filter membrane.

8.3.3 Skimmed milk filtration

Skimmed milk was successfully filtered with a constant permeability around 20% of the maximum value when backpulsing at constant operating pressure (20 ± 2 mbar) and variable frequency (see Figure 11). Permeability reached a constant value independent of the pulse frequency. An exception can be observed at 6.7 Hz, where lower permeation was obtained.

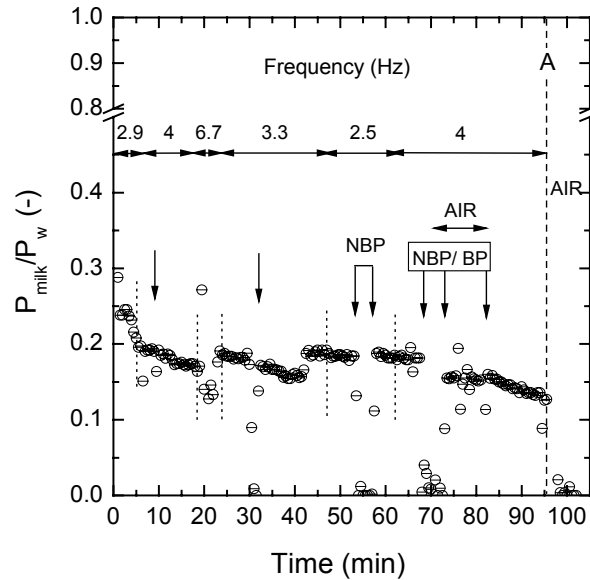


Figure 11. Relative permeability of skimmed milk versus time (pH=7, 9°C), through a 2 μm PES microsieve. The arrows indicate pulse stops for approx. 30 seconds; NBP indicates the regions where no pulses were applied for periods longer than 30 s.

When the pulses were stopped for a short period (minimum 30 s, indicated by the arrows), permeability did not increase (contrary to the results with BSA). Milk permeability decreased immediately and, if the pulses were suppressed for longer time, no permeate was obtained at all. Restarting the pulses with the same conditions successfully led to a permeability recovery to the last measured value. Such findings point to the fact that backpulsing is very effective in keeping the foulants fluidized above the membrane so that no deposition and further cake formation can occur.

As soon as pulsation was stopped, a cake layer from milk components such as casein micelles or whey proteins could settle down, thereby completely blocking the membrane surface. The deposited layer might be very compact, because flux descended to zero within a minute. In such case air sparging was not able to restore the flux (see Figure 11, $t=70$ min),

even though air flow rates were varied from 12 to 20 ml/min. Permeability could only be recovered if backpulsing was reinitiated. When air sparging was dosed at 47 ml/min (A), permeability dropped from 13% to zero, indicating that air dosage was not suitable to be applied with milk feeds.

Mercier-Bonin and co-authors already reported low efficiency of two-phase flows in the enhancement of skimmed milk flux, during the separation of casein micelles from whey proteins [18, 19], compared to the non-gas sparging situation. Moreover, this method is unlikely to be used in dairy food application, mainly because of foaming risks and protein damage.

To confirm the reproducibility of the method, a longer experiment was performed for more than 2 hours. The influence of the feed pressure on the milk flux was investigated, because we believed that the most optimal conditions to achieve higher permeabilities would be at lower pressures. At higher pressures more flux is permeated and more foulant deposition is likely to occur. At that point the backpulsing settings would have to be adapted to overcome the deposition rate of the milk components. The outcome of variable operating pressure on the milk permeability is shown in Figure 12.

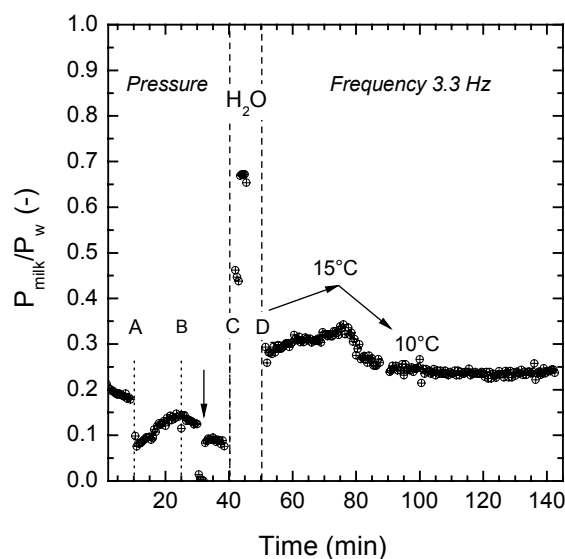


Figure 12. Relative permeability of skimmed milk versus time (pH=7, 7°C), through a 2 μm PES microsieve. From the initiation of the filtration until (C) pressure was successively varied. Until (A) pressure was 22 mbar, at (A) it was increased to 32 mbar for a minute, then decreased stepwise to 13.5 mbar until (B), where pressure was 16.4 mbar. During (B-C) pressure increased to 19 mbar after the pulse stop. At (C) forward and backflushing were applied, followed by feed exchange to water (C-D); from D to the end of the experiment milk was reintroduced as feed and the pressure and pulse frequency were kept constant (12 mbar, 3.3 Hz).

The filtration was initiated with backpulsing at 3 Hz and 22 mbar. At (A) the pressure was increased to 32 mbar and permeability suddenly dropped. After one minute, pressure was gradually lowered from 21 to 13.5 mbar (B), resulting in 50% permeability increase. From (B) until the pulses were stopped (indicated by the arrow) pressure was kept constant at 16.4 mbar, resulting in a stable flux, except when the pulses were suppressed. After backpulsing reinitiation, pressure was slightly increased until 19 mbar and permeability was constant for several minutes. At (C) water forward and backflushing were applied to rinse milk deposits, and the clean water flux was measured for 5 min. The rinsing step was proved to be very efficient, since the clean water permeability reached 70% of its maximum value. Such results also mean that little adhesion of the milk components on the microsieve surface occurs. After the forward and backflushing step, the pulsation of milk at 3.3 Hz and 12 ± 1 mbar resulted in stable permeability for more than 90 minutes, with a flux of $1600 \text{ l/m}^2 \text{ h}$. The slight increase in milk permeability until $t=80$ min was probably caused by an increase in feed temperature until 15°C . When the feed was rapidly cooled down to 10°C permeability decreased until 27%, where it remained constant until the end of the test. A decrease of solution viscosity may have been the cause for the slight permeability increase ($\eta_{\text{milk } 11^\circ\text{C}}=2.1 \text{ mPas.s}$, $\eta_{\text{milk } 15^\circ\text{C}}=1.84 \text{ mPas.s}$).

Constant milk permeability was obtained in other tests when pressure was kept under 20 mbar and backpulsing frequency around 2.5 Hz.

Sterilized skimmed milk mainly contains lactose, casein, whey proteins and minerals like calcium. Fat is present as well, with a concentration $<0.5\%$. Filtration of skimmed milk through $2 \mu\text{m}$ PES microsieves could remove some of the remaining fat and some protein aggregates or casein micelles, which have normally mean diameters of 100 nm and are believed to form deposits on and inside the membrane pores [4]. During the course of the experiment, the absorbance of permeate samples was analyzed together with the feed at $\lambda=280 \text{ nm}$, in order to detect differences in the total protein content. The same absorbance results were obtained at this wavelength, indicating that no protein was retained. Our findings indicate that the feed and permeate fractions collected during backpulsing had a very similar absorbance due to low concentration of the 'retainable' components (also at higher wavelengths than 280 nm).

With Dynamic Light Scattering measurements no conclusive results could be obtained for the particle size of both feed and permeate fractions.

From the outcome of the milk filtration experiments, several recommendations can be made to optimize permeation and productivity. Backpulsing is necessary to avoid flux decline. Moreover, operating at relatively low frequencies and lower pressures permeation is

enhanced. The use of air sparging with milk would not be recommended because it does not improve the permeation or flux recovery. In summary, more insight into retention and backpulsing influence might be gained by using semi-skimmed milk, which has a higher concentration of retainable components like fat globules.

8.3.4 Microfiltration of white Belgian beer

The white beer used as feed had certain turbidity characteristics, due to its yeast content. Our goal was to separate the largest suspended solid fraction and maybe part of the yeast, which normally has sizes between 1 and 10 μm [5]. The filtration of white beer at constant backpulsing frequency is shown in Figure 13. The same procedure and similar backpulsing settings were applied as with milk. When the feed was not degassed, large fluctuations in pressure occurred at the initial moments of filtration due to CO_2 . However, once the system was free of gas a stable situation was achieved.

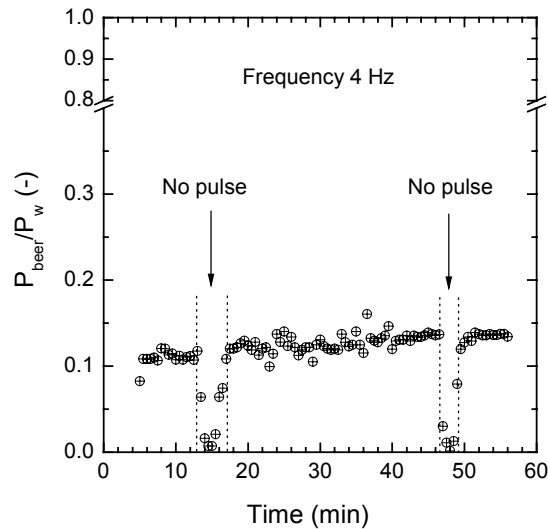


Figure 13. Relative beer permeability versus time (13°C), through a 2 μm PES microsieve. During the filtration backpulsing was applied at constant frequency, power and pulse length (4.4 Hz, 45%, 20ms). The operating pressure was 18 ± 1 mbar. Backpulsing was stopped twice, indicated by the arrows.

After stabilization, backpulsing was initiated at 4 Hz. The pressure remained constant at an average value of 18 ± 1 mbar for almost one hour. Throughout such period permeability was successfully stabilized and it remained constant just over 10 %. Pulses were suppressed twice (indicated by the arrows) resulting in immediate permeability loss. Restarting the pulses led to the same permeabilities than before the backpulsing stop, indicating that the deposited layer

was removed. The average flux in the section between (C) and (D) was calculated to be 1900 l/m²h.

After SEM inspection of the membrane surface, it was observed that some deposits were present in different zones. However, the deposition was not extensive and most of the pores remained open for permeation, as shown in Figure 14.

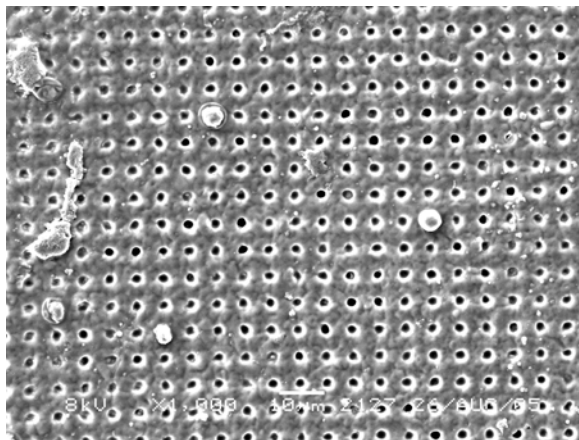


Figure 14. SEM image of the microsieve surface after a beer filtration.

After filtration, clear differences in turbidity were observed between the feed, retentate and permeate. The feed and permeate were analyzed with a UV-VIS spectrophotometer at different wavelengths, between 450 and 800 nm (Figure 15).

The differences in absorbance of the two fractions suggest retention of beer components in the visible range.

The temperature throughout the experiment was about 13°C. Temperature has a very strong influence in beer filtration, because below 4°C flocs of chill haze and other particles can sedimentate. This is important when these components are to be retained. According to Gan and coworkers [6], temperature also has an influence on the flux. Their experiments at 10°C versus 2°C, presented a higher beer flux but the permeate quality was reduced with respect to increased chill haze level. This effect was also observed in our different permeate fractions, which varied slightly in absorbance throughout the filtration. Those differences, though, were not significant compared to the feed, which presented much higher turbidity.

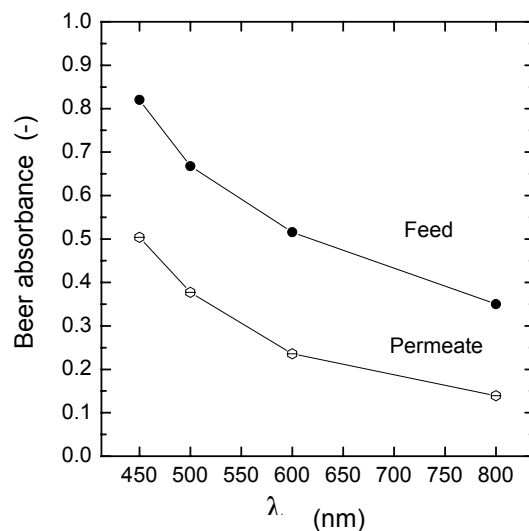


Figure 15. Absorbance of the beer feed and permeate versus wavelength, directly after filtration.

The retained solid fraction by the PES microsieves was determined by weight differences of evaporated samples. The solid fraction for the feed was determined to be 1.18 wt% and for the permeate 0.56 wt%.

8.4 Conclusions

In this chapter we have investigated the performance and fouling of 2 μm PES microsieves, with model proteins like BSA, skimmed milk and beer. For all cases, when no strategies as backpulsing were applied, severe and rapid flux decline took place, more acute for milk and beer than for BSA.

In the case of BSA, pore blocking by aggregate deposition was likely to be the determining mechanism behind flux decline, confirmed by the classical pore blocking theory. Since larger components were present in the other feeds, we also believe that the same mechanism may cause permeability loss in milk and beer filtrations.

From all fouling reduction strategies investigated in this work, backpulsing at low frequencies was the most successful method to enhance permeation, since it worked very well independently of the feed. Air sparging at low air flows was only applicable to BSA feed solutions in order to stabilize permeation rate. Air sparging in combination with milk was completely inefficient. On top of this, little potential for this technique is available in dairy food processing, because of risk of foaming and protein damage. The highest permeabilities were achieved when backpulsing at low operating pressures, with beer or milk.

The mechanism behind fouling reduction with polymeric microsieves and backpulsing is more likely to be mechanical motion of the membrane during pulsing rather than backflow. Feed pressure during pulsations is almost as high as permeate pressure. This points out that the pulse is completely transmitted through the membrane and that very little permeate flow reversal exists. Enhanced permeation by microsieve motion represents an exceptional improvement, uncommonly seen for commercial systems.

Remarkably, the best performance with BSA as feed, in terms of backpulsing effectiveness and membrane productivity was achieved by using polymeric microsieves, when compared to commercial track-etched membranes and silicon nitride microsieves presented in previous chapters.

The average productivity of the PES microsieves presented in this chapter was found to be ≥ 6000 l/m²h BSA, 1600 l/m²h milk and 1900 l/m²h of beer. These results are outstanding in comparison to conventional systems. For instance, a productivity of 100 l/m²h beer is required for a membrane system to be implemented in industry. So, if microsieves with smaller pore sizes are fabricated, it is very likely that the process productivity will still be above average.

Due to their excellent filtration performance and the large fluxes obtained, microsieves can greatly change the membrane market for applications in dairy and brewing industry, but also other areas related to microfiltration.

8.5 Acknowledgements

Lydia Bolhuis-Versteeg is acknowledged for the technical support and Maik Geerken for the assistance with the backpulsing profile measurements.

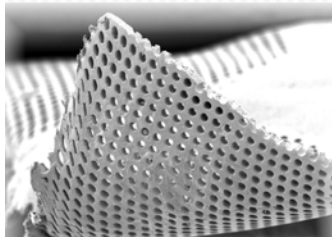
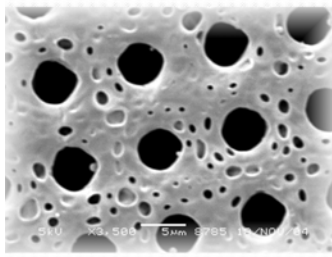
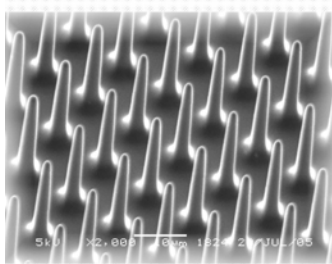
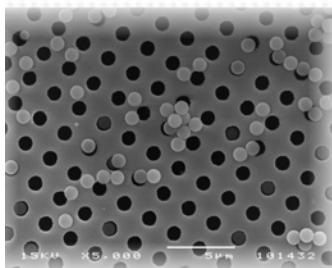
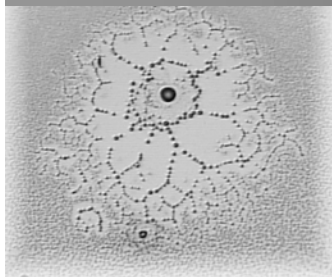
8.6 References

- [1] M. Roshenberg, Current and future applications for membrane processes in the dairy industry, *Trends in Food Sci. and Technology*, 6 (1995) 12.
- [2] A.L. Zydney, Protein separations using membrane filtration: new opportunities for whey fractionation, *Int. Dairy Journal*, 8 (1998) 243.
- [3] G. Brans, C.G.P.H. Schroën, R.G.M. van der Smaan, R.M. Boom, Membrane fractionation of milk: state of the art and challenges, *J. Membr. Sci.* 243 (2004) 263.
- [4] A.D. Marshall, G. Daufin, Physico-chemical aspects of membrane fouling by dairy fluids, in *Fouling and Cleaning in pressure driven membrane processes*, International Dairy Federation, Belgium, 1995.
- [5] L. Fillaudeau, H. Carrère, Yeast cells, beer composition and mean pore diameter impacts on fouling and retention during cross-flow filtration of beer with ceramic membranes, *J. Membr. Sci.* 196 (2002) 39.
- [6] Q. Gan, J. A. Howell, R. W. Field, R. England, M. R. Bird, C. L. O'Shaughnessy, M. T. MeKechinie, Beer clarification by microfiltration - product quality control and fractionation of particles and macromolecules, *J. Membr. Sci.* 194 (2001) 185.
- [7] Q. Gan, Beer clarification by cross-flow microfiltration - effect of surface hydrodynamics and reversed membrane morphology, *Chemical Engineering and Processing* 40 (2001) 413.
- [8] P. Blanpain-Avet, N. Doubrovine, C. Lafforgue, M. Lalonde, The effect of oscillatory flow on crossflow microfiltration of beer in a tubular mineral membrane system - Membrane fouling resistance decrease and energetic considerations, *J. Membr. Sci.* 152 (1999) 151.
- [9] M. Gironès, Chapter 7 of this thesis.
- [10] M. Pontié, X. Chasseray, D.Lemordant, J.M. Lainé, The streaming potential method for characterization of ultrafiltration organic membranes and the control of cleaning treatments, *J. Membr. Sci.* 129 (1997) 125
- [11] G. Belfort, R.H. Davis and A.L. Zydney, The behavior of suspensions and macromolecular solutions in crossflow microfiltration, *J. Membr. Sci.* 95 (1994) 1.
- [12] S. T. Kelly, A. L. Zydney, Mechanisms for BSA fouling during microfiltration, *J. Membr. Sci.* 107 (1995) 115.
- [13] S. T. Kelly, W. Senyo Opong, A. L. Zydney, The influence of protein aggregates on the fouling of microfiltration membranes during stirred cell filtration, *J. Membr. Sci.* 80 (1993) 175.
- [14] S. T. Kelly, A. L. Zydney, Protein Fouling during microfiltration: comparative behavior of different model proteins, *Biotechnol. Bioeng.* 55 (1997) 91.
- [15] W.R. Bowen, J.I. Calvo, A. Hernández, Steps of membrane blocking in flux decline during protein microfiltration, *J. Membr. Sci.* 101 (1995) 153.
- [16] V.G.J. Rodgers, R.E. Sparks, Effect of transmembrane pressure pulsing on concentration polarization, *J. Membr. Sci.* 68 (1992) 149.
- [17] M. Gironès, Chapter 5 of this thesis
- [18] M. Mercier-Bonin, C. Fonade, G. Gésan-Guiziou, Application of gas-liquid two-phase flows during crossflow microfiltration of skimmed milk under constant flux conditions, *Chem. Eng. Sci.*, 59 (2004) 2333
- [19] M. Mercier-Bonin, G. Gésan-Guiziou, C. Fonade, Application of gas-liquid two-phase flows during crossflow microfiltration of skimmed milk under constant transmembrane pressure conditions, *J. Membr. Sci.* 218 (2003) 93.



Chapter 9

Conclusions and Outlook



9.1 Introduction

In this thesis, strategies to reduce protein fouling of silicon nitride and polymeric microsieves were studied, together with aspects involved in the fabrication of polymeric microsieves. The main conclusions and an outlook on the most remarkable issues for future applications will be discussed in the following section.

9.2 Conclusions

- The selective layer of inorganic microsieves is made of silicon nitride. Silicon nitride surfaces usually present a native oxide layer (**Chapter 2**). A variety of surface modification strategies were tested to homogenize, hydrophilize or hydrophobize silicon nitride for further use of microsieves. When a hydrophilic surface is desired, oxygen plasma is a very effective treatment to create a more homogeneous and less contaminated oxide layer than the native oxide. Although this modification method can provide hydrophilicity, its life-time is limited because of contaminant adsorption. Silanization with perfluorinated chlorosilanes (FOTS) can provide hydrophobic thin coatings, stable in aqueous solutions and with contact angles around 100°. Physical adsorption of polymers is not a very suitable option when thin and stable coating layers are desired.

- The performance of silicon nitride microsieves in aqueous solutions strongly depends on their surface properties, as well as the feed characteristics (**Chapter 3**). Wetting is a key parameter to achieve maximum water flux with microsieves of 1.2 µm pore diameter ($P_w=3 \times 10^5$ l/m²hbar). Unmodified microsieves are best wettable with isopropanol or isopropanol/water mixtures, hydrophilic (oxygen plasma treated) membranes are wettable with water and hydrophobized microsieves are wettable in 100% isopropanol.

- Maximum and stable water fluxes can be achieved for microsieves with water contact angles close to 90°, if an adequate wetting protocol is applied and the system is free of air (**Chapter 3**). When air is present in the system, the flux of hydrophilized microsieves is hardly affected, however, dewetting of hydrophobic surfaces with contact angles close to 90° can occur, leading to permeability losses. Hydrophobized microsieves with contact angles close to 110° are dewetted to a great extent, resulting in unstable fluxes.

- A severe and rapid flux decline is observed in crossflow filtration of BSA solutions through microsieves with 1.2 µm pore diameter (**Chapter 4**), even though protein retention is low. Such decline depends strongly on the solution properties like concentration, pH, ionic

strength, etc. but also on the membrane surface and the equipment used. With our system, the main cause for decline is aggregate formation and protein deposition, resulting in pore blocking. The most severe decline is observed near the isoelectric point of the protein (aggregation due to reduced electrostatic repulsions), when using a pump that can generate high shear rates. In-line pre-filtration of the protein solutions results in a constant permeability, due to aggregate removal.

- In **Chapter 4** the performance of silicon nitride microsieves with other model solutions, such as lysozyme or latex particles, is presented. With a globular protein like lysozyme, more severe flux loss is observed than with BSA at neutral pH, due to electrostatic interactions between the positively charged protein and the negatively charged microsieve surface. Dead-end filtrations with latex particles provide information about the blocking mechanism of straight-through pores in a very illustrative way. Particles with diameter equal or $\frac{1}{2}$ of the membrane pores result in complete pore blocking.

- A variety of strategies can be used to enhance BSA permeability with inorganic silicon nitride microsieves. Air sparging at low flow rates seems to be the most successful technique to reduce/suppress flux decline and deliver constant BSA permeation (**Chapter 5**). Air generates a transverse recirculating flow away from the surface, capable to remove deposited aggregates. Moreover, it is also applicable to other proteins like lysozyme. Backpulsing at frequencies up to 6.7 Hz can enhance permeation and reduce fouling rate, although a decrease in permeability is observed in time. Flow reversal takes place when backpulsing, due to an inversed transmembrane pressure. Furthermore, backflushing is only partly successful in terms of flux recovery.

- The combination of surface modification with PEG-based polymers (poly (TMSMA-r-PEGMA) and backpulsing leads to increased permeation compared to the unmodified surfaces (**Chapter 6**). Adhesion is reduced with a PEG-containing polymer coating, which provides large exclusion volume and steric repulsion to the protein molecules. Static adsorption experiments on the coating confirm the excellent antifouling properties of such: after almost a week no detectable amounts of protein are present on coated surfaces. Air sparging at low flow rates also results in a constant permeability. After protein filtration and water rinsing, the coated microsieves do not present visible deposits on the surface, in contrast to the uncoated membranes.

- **Chapter 6** presents results obtained with skimmed milk filtration using coated and uncoated microsieves. In both cases flux decreases to zero within a couple of minutes when no backpulsing is applied. However, the combination of PEG-coated microsieves and backpulsing results in a phenomenon not seen before, even in single protein filtration. Stable and higher milk fluxes are obtained with coated microsieves, independently of the applied pressure and backpulsing frequency. Uncoated microsieves present temporary stable fluxes, when operating at low pressures and intermediate pulse frequencies. When pressure is increased backpulsing loses its efficiency and permeability is low. In none of these situations air sparging results in flux increase or stabilization.

- Phase Separation Micromolding is very suitable to prepare microstructures like polymeric microsieves, which can be made from a variety of materials including PES, PES-PEO and PES/PVP (**Chapter 7**). This method allows the production of more economical microsieves with tunable features (pore size, shape or porosity). The phase separation process consists of two stages: vapor-induced phase separation (VIPS), where perforation occurs, followed by liquid-induced phase separation (LIPS). Lateral shrinkage occurs in some extent and allows easy release of the replica.

- The dimensions of the perforations can be tuned in two directions: either by using molds with different pillar diameters or by thermally treating the microsieve above the T_g of the polymer, as described in **Chapter 7**. Microsieves with pore sizes down to 1.2 μm can be obtained with the molds used in our research. By thermal treatment, pore diameters of 5 μm can be easily reduced to 1.5 μm , while initial pore diameters of 2.5 μm are successfully reduced to submicron sizes (0.5 μm).

- In **Chapter 8** several findings related to microfiltration with PES microsieves (pore diameter=2 μm) are presented. For the first time constant fluxes are obtained while filtering BSA solutions at neutral pH in combination with backpulsing. The flexibility of the polymeric microsieves allows a complete pulse transmission. Due to this, almost no transmembrane pressure reversal is present, and backflow is limited. Membrane motion varies the fluid hydrodynamics on the membrane and disturbs the polarization layer. Polymeric microsieves also deliver outstanding results with skimmed milk and white beer filtration. While no detectable retention is measured for the first, white beer can be successfully clarified, and 50% of the solid content is retained. The results obtained in this chapter can represent a breakthrough for polymeric microsieves in microfiltration, due to their high permeabilities, low fouling characteristics and beneficial sieving properties. To conclude, a comparison between

the outcome in BSA and skimmed milk filtrations for inorganic and polymeric microsieves is shown in Table 1.

Table 1. Summary of the performance of silicon nitride and polymeric PES microsieves, with feeds like BSA and skimmed milk. The productivity in terms of permeability is given for each case.

Feed characteristics	Sieve used	Observation	Productivity
BSA solution 1 g/l, pH≈7 (recirculated retentate with microannular pump)	Si_xN_y , 1.2 μm , circular	<ul style="list-style-type: none"> ▪ Flux decline without backpulsing ▪ Retarded flux decline with backpulsing ▪ Settings: 6.7 Hz, Power 64% ▪ Water backflushing recovers flux up to 30% ▪ With air sparging: constant flux 	100 to 20x10 ³ l/m ² h bar (BP, in 20 min) 70x10 ³ l/m ² h bar (Air)
	Si_xN_y , 1.2 μm , circular + PEGMA- <i>r</i> -TMSMA	<ul style="list-style-type: none"> ▪ Flux decline without backpulsing ▪ Flux decline is retarded/slowed down ▪ Settings: 6.7 Hz, Power 64% ▪ Permeated volume is higher ▪ After washing with water, surface is clean upon visual inspection 	120 to 25x10 ³ l/m ² h bar (BP, in 25 min) 70x10 ³ l/m ² h bar (Air)
	Polymer microsieves PES 2 μm (shrunk from 5 μm)	<ul style="list-style-type: none"> ▪ Backpulsing results in constant flux ▪ Optimization possible by backpulsing settings (intermediate frequencies ≈ 3 Hz, Power 45%) ▪ Pulse is transmitted to feed side ▪ Membrane motion is visible ▪ Air sparging is not as effective as backpulsing, permeability is constant but lower 	750x10 ³ l/m ² h bar
Skimmed milk pH=7 (sterilized, recirculated with microannular pump)	Si_xN_y , 1.2 μm , circular	<ul style="list-style-type: none"> ▪ No backpulsing leads to zero permeability ▪ Backpulsing at lower frequency (3 Hz) gives constant flux temporarily ▪ Pressure increase leads to permeability loss ▪ Even if backpulsing is optimized permeability is low ▪ Air sparging is not effective 	40 to 10x10 ³ l/m ² h bar (BP, in 60 min)
	Si_xN_y , 1.2 μm , circular + PEGMA- <i>r</i> -TMSMA	<ul style="list-style-type: none"> ▪ No backpulsing leads to zero permeability ▪ Complete recovery if backpulsing is restarted ▪ Constant flux with backpulsing ($P_{milk} = 20\% P_w$) ▪ Air sparging is not effective ▪ Stable operation over a wide range of processing settings (P, f) 	36x10 ³ l/m ² h bar
	Polymer microsieves PES 2 μm (shrunk from 5 μm)	<ul style="list-style-type: none"> ▪ No backpulsing leads to zero permeability ▪ Complete recovery if backpulsing is restarted ▪ Constant and high flux with backpulsing ($P_{milk} = 25\% P_w$) ▪ Membrane motion is visible ▪ Stable operation over a wide range of processing settings (P, f) ▪ Air sparging is not effective 	125-160 x10 ³ l/m ² h bar

9.3 Relevant aspects for future applications

9.3.1 Si_xN_y microsieves

Silicon nitride microsieves may be desired for certain applications, e.g. where harsh cleaning conditions or high temperatures are involved. In order to be able to be implemented in real separations their performance/cost relationship should be feasible. Nowadays, one of the main bottlenecks of commercial silicon nitride microsieves lies in their backstructure design. As discussed in this thesis and by Brans and coworkers [1], the channels underneath the thin membrane layer may hamper the backpulse and backflush efficiency. Currently, the improvement of the backstructure design is thoroughly taken into consideration and microsieves free of channels can be manufactured, like the ones shown in Figure 1.

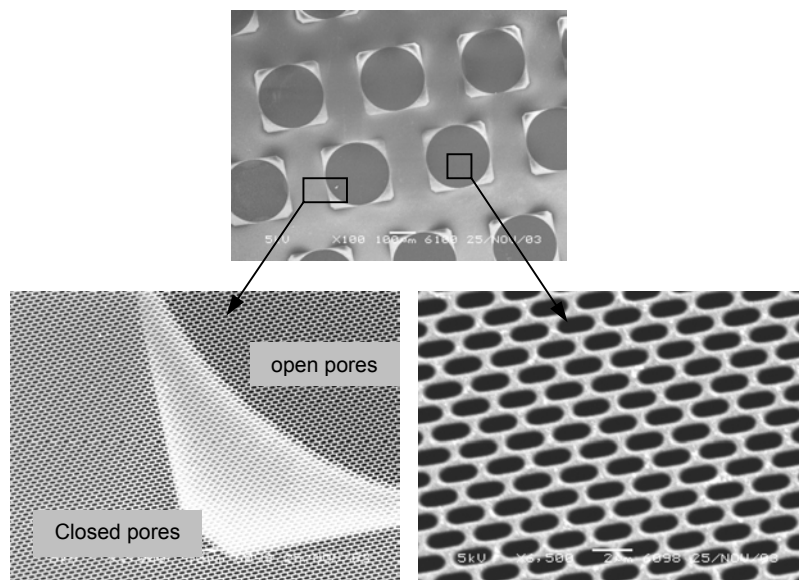


Figure 1. SEM images of a microsieve with freestanding slit-shaped pores zones (only the circular zones belong to open pores, the rest of the surface contains the pore pattern but pores are not open).

Contrary to our experimental findings with hydrophobized backstructured microsieves discussed in Chapter 3, these membranes could be fully rewetted with isopropanol (IPA) after air dewetting (Figure 2).

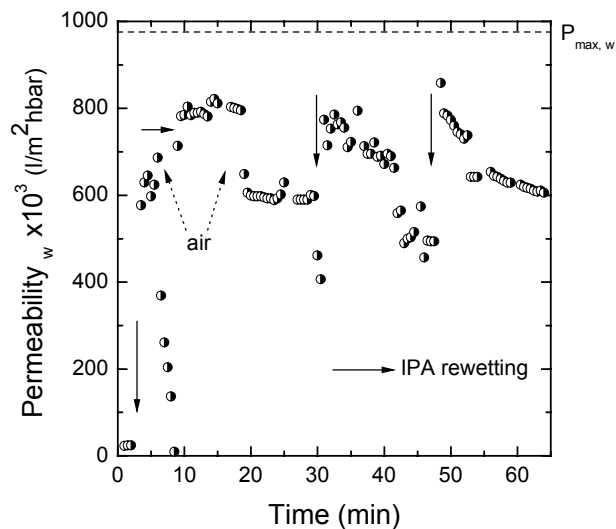


Figure 2. Clean water permeability of a microsieve with slit-shaped pores. The dotted arrows indicate when air bubbles traveled along the module, while the black arrows indicate when IPA rewetting was applied.

The surface features can also be optimized, in terms of pore size and shape, in order to reduce fouling. The use of slit-shaped pores can be an aid to avoid pore blocking by spherical particles, for instance.

Some of the most optimal conditions to reduce protein fouling are high crossflow velocities and low operating pressures [2]. However, it is crucial that pumping equipment does not involve high shear rates and causes protein denaturation/aggregation (rotary systems could supply an alternative to reach these purposes).

Even though air sparging was the most successful method to achieve constant protein permeability, it cannot be applied in most protein-containing feeds and industrial applications. Therefore, other alternatives must be considered. One of the approaches frequently used to enhance protein fluxes is pulsed feed flow. When the liquid feed is periodically dosed in pulses, hydrodynamic conditions change periodically as well.

Recently, Friesland Brands B.V. has developed a high frequency backpulsing system with a shut-off valve (with an incorporated rotating camshaft that controls the backpulse frequency) connected to the permeate side [3]. When the valve is closed, the pressure at the permeate side is increased and backflow occurs. Moreover, the system is designed so that a crossflow is maintained on both permeate and retentate sides, without compromising the capacity of the

apparatus by the backpulsing. Such system is currently being used in combination with inorganic microsieves for milk fractionation, although it can be suitable for other applications using silicon nitride microsieves in microfiltration.

In dairy food processing, if the membrane surface requires modification for reduced adhesion, food compatible polymers must be used. From literature and results shown in this thesis, PEG is a highly recommended polymer. In this sense, polyelectrolyte layers containing positively charged aminoacids covalently grafted with PEG could provide temporary but non-harmful coatings, able to be attached to negatively charged oxide surfaces. PEG-poly (L-lysine) complexes [4, 5] could be suitable as microsieve coatings in dairy, because they would provide food compatible thin layers capable to repel proteins. Also, they can be easily regenerated, for instance by immersion or rinsing in-line with the polyelectrolyte solution.

9.3.2 Polymeric microsieves

Polymeric microsieves could, in the near future, be launched as alternatives to commercial membranes for microfiltration applications. Nevertheless, upscaling and continuous production must be designed so that commercialization is feasible. A continuous casting process is currently being developed by other researchers and industrial partners.

The flexibility of the membrane structure enables membrane motion, which is extremely beneficial to reduce fouling and increase productivity. Such motion is not a very common property among commercial membranes, by methods like backpulses, feed pulses and vibratory shear, for instance.

Due to their selectivity and the fact that they can virtually be made of any polymer, polymeric microsieves could be implemented in the biological and biomedical fields. Fast screening, or separation of blood cells by polymeric microsieving could be one of the target applications.

For this target, hydrophilicity, low adhesion and also hemo/biocompatibility should be maintained. A variety of materials are currently used to fabricate blood compatible devices, which should avoid blood clotting and inflammation. Some examples of these materials are polyurethanes, silicone based polymers, block copolymers of (ethylene oxide-propylene oxide) and polysiloxane-polycaprolactone, among others. Recently, tri-block copolymers having a central PDMS block flanked by two caprolactone blocks have been reported to possess low thrombogenicity and low inflammatory and protein adsorption properties [6, 7]. Such materials could be used for blood-contacting microsieves fabrication.

When molds with narrow pillars are used, sometimes the material or intrinsic surface porosity of the produced microsieves is so high that pores originated from the phase inversion process are larger than the perforations. Intrinsic porosity can enhance permeability without

compromising selectivity, whenever $\phi_{\text{pore}} < \phi_{\text{perforation}}$. In Phase Separation Micromolding, the phase inversion process is so versatile that different surface structures can be obtained. For instance, delayed demixing can be achieved to obtain denser surfaces but open inner structures. To achieve that, either phase separation conditions (temperature, evaporation time, composition coagulation bath, etc.) or polymer solution properties (polymer type, solution composition, etc.) can be tuned [8]. For the first approach, the kinetics of solvent/non-solvent exchange can be slowed down by using a non-solvent that has low miscibility with the solvent, introducing a flow of inert gas to the vapor bath or adding solvent to the non-solvent bath. From literature it is also known that increasing the polymer concentration, adding non-solvent or other polymeric additives in the solution can facilitate the transition to delayed demixing [8, 9].

An example of two microsieves with different surface porosities is shown in Figure 3. By tuning the casting polymer solution (increased polymer content) a denser microsieve surface is obtained, with smaller pore dimensions than the perforation diameter.

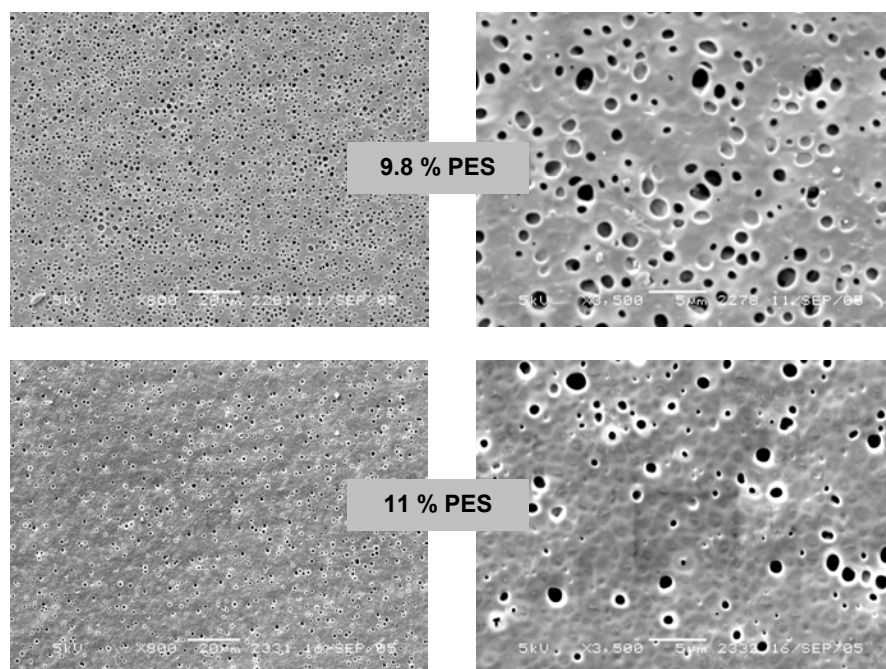


Figure 3. SEM images of microsieves fabricated with different polymer concentration, with mold M0.8. Denser surfaces with smaller intrinsic pores are obtained with a higher PES content.

Polymeric microsieves can be also used as templates or supports for freestanding membranes fabricated by particle-assisted wetting [10-12]. With this technique homogeneous pore sizes around 50-100 nm can be obtained, as shown in Figure 4.

In this case the microsieve serves as a support for the thin patterned layer, with nanopores directly on the original perforation being fully freestanding. This approach is very innovative in membrane technology, and it can open a new window for a whole range of separations, not only in MF but also in UF.

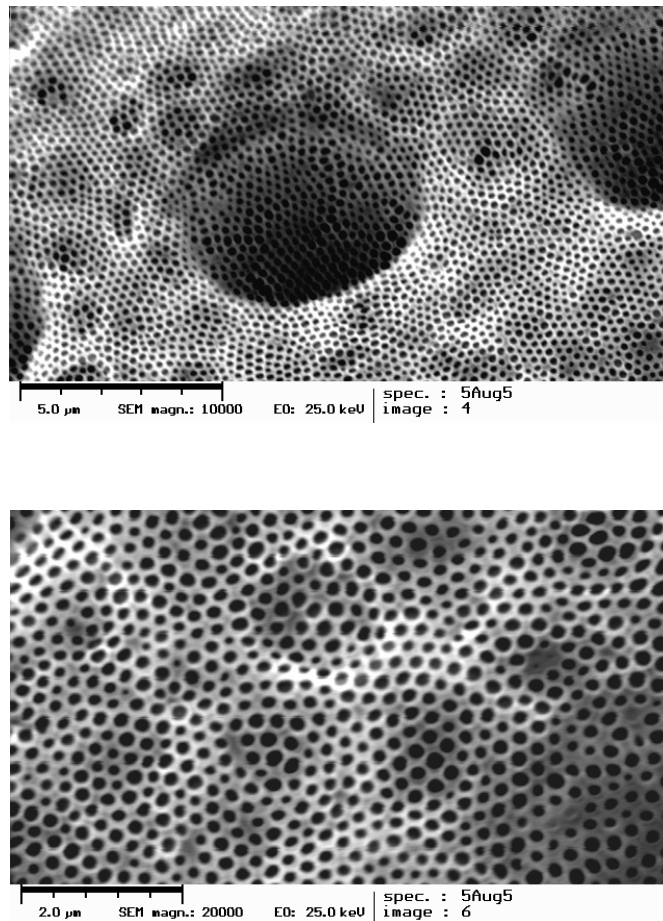


Figure 4. SEM images of a freestanding layer with nanopores, supported on a PES microsieve (images provided by Ailin Ding, Technical University Chemnitz)

In summary, polymeric microsieves have great potential in terms of structure (perforation shape and dimensions, thickness, materials used, porosities, etc.). This can be useful in fractionations, using a stack of membranes with different pore sizes. Their structural properties and outstanding filtration performance make them unique, and will definitely offer new possibilities in the upcoming years.

9.4 Acknowledgements

The author wishes to acknowledge Dr. Rolf Bos, from Friesland Foods (Deventer) for providing the unsupported silicon nitride microsieves, and Prof. W. Goedel and Ailin Ding, from the Technical University Chemnitz (Germany) for kindly preparing the nanopores on PES microsieves.

9.5 References

- [1] G. Brans, J. Kromkamp, N. Pek, J. Gielen, J. Hek, C. J. M. van Rijn, R. G. M. v. d. Sman, C. G. P. H. Schroën, R. M. Boom, Relation between flux behavior and microsieve design for latex particle filtration, in preparation.
- [2] A.D. Marshall, P.A. Munro, G. Trägårdh, The effect of protein fouling in microfiltration and ultrafiltration on permeate flux, protein retention and selectivity: a literature review, *Desalination* 91 (1993) 65.
- [3] J. Kromkamp, A. van der Padt, C.P. J. M. Van der Vorst, WO Patent 2005/082499 A1 (2005).
- [4] G.L. Kenausis et al., Poly (L-lysine)-g-Poly (ethylene glycol) layers on metal oxide surfaces: attachment mechanism and effects of polymer architecture on resistance to protein adsorption, *J. Phys. Chem. B* 104 (2000) 3298.
- [5] N. P. Huang et al., Poly (L-lysine)-g-Poly (ethylene glycol) layers on metal oxide surfaces: surface-analytical characterization and resistance to serum and fibrinogen adsorption, *Langmuir* 17 (2001) 489.
- [6] L. Tang, M. Sheu, T. Chu, Y. H. Huang, Anti-inflammatory properties of triblock siloxane copolymer-blended materials, *Biomaterials* 20 (1999) 1365.
- [7] M.A. Childs, D.D. Matlock, J.R. Dorgan, Surface Morphology of poly (caprolactone)-b-poly(dimethylsiloxane)-b- poly (caprolactone) copolymers: effects on protein adsorption, *Biomacromolecules* 2 (2001) 256.
- [8] M. H. V. Mulder, *Basic Principles of Membrane Technology*, Kluwer Academic Publishers, Dordrecht, 1996.
- [9] W.F.C. Kools, *Membrane Formation by phase inversion in multicomponent polymer systems*, Ph.D. thesis, University of Twente, The Netherlands, 1998.
- [10] H. Xu and W.A. Goedel, Polymer-silica hybrid monolayers as precursors for ultrathin free-standing porous membranes, *Langmuir* 18 (2002) 2363.
- [11] H. Xu and W.A. Goedel, From particle-assisted wetting to thin free-standing porous membranes *Angew. Chem. Int. Ed.* 42 (2003) 4694.
- [12] H. Xu and W.A. Goedel, Particle-assisted wetting, *Langmuir* 19 (2003) 4950.

Summary

The research presented in this thesis describes several aspects concerning the use of high-flux screen filters like microsieves in microfiltration. The main focus of this work is based on fouling of both inorganic and polymeric microsieves with model solutions, so that fundamental knowledge and insight is gained and applied to a possible application like milk filtration.

Chapter 2 describes the properties and some modification strategies for the fabrication material of inorganic microsieves: silicon nitride (Si_xN_y). To homogenize and modify Si_xN_y several routes can be followed: oxygen plasma is effective for hydrophilization because it creates a very hydrophilic but unstable oxide layer; silanization with perfluorinated chlorosilanes results in hydrophobic thin coatings, stable in aqueous solutions at different temperatures and pHs. Physical adsorption of polymers is not very suitable when thin and stable coating layers are desired.

The performance of Si_xN_y microsieves in terms of clean water fluxes is presented in Chapter 3. A proper wetting procedure and the feed properties are crucial to achieve a maximum filtration performance. When hydrophobized surfaces are used, parameters like air can cause anomalies in the flux values, dewetting, and very low performances. Generally, the maximum water permeability can be achieved with a fully wetted, clean and air-free system.

Subsequently, once this step is overcome, the microsieve performance with more complex feeds can be investigated. Fouling with different model solutions like BSA, lysozyme or latex is investigated in Chapter 4. In a crossflow filtration of a BSA solution at neutral pH with inorganic microsieves (pore diameter 1.2 μm) a severe and rapid flux decline is observed, even though the membrane pore size is much larger than the protein size and only little retention is measured. The permeability loss depends strongly on the solution properties (concentration, pH, ionic strength, etc.) but also on the membrane surface and the equipment used. In our system, the main cause for flux decline is aggregate formation and protein deposition. The most severe decline is observed near the isoelectric point of the protein for BSA (aggregation due to reduced electrostatic repulsions) and at neutral pH for lysozyme, due to electrostatic interactions between the positively charged protein and the negatively charged microsieve surface. In most of the cases, the fouling mechanism is pore blocking regardless of the feed, and can be determined by using the classical pore blockage theory.

Chapters 5 and 6 describe some strategies to retard/suppress flux decline and enhance permeation of BSA solutions. In Chapter 5 strategies like forward and backflushing, together with backpulsing and air sparging are presented. Air sparging at low flow rates is the most

successful technique to achieve constant BSA permeation because of its ability to generate a transverse recirculating flow that can remove deposited aggregates. Backpulsing (flow reversal) up to 6.7 Hz can enhance permeation and retard fouling, but it cannot deliver constant fluxes. In Chapter 6 the synthesis and application of an antifouling polymer coating: poly(TMSMA-r-PEGMA) on silicon-based materials and microsieves is presented. Backpulsing with PEG-coated microsieves is more successful compared to unmodified membranes because it results in higher permeation and cleaner surfaces, due to the ability of the PEG-coating to repel the protein molecules by steric repulsion (reduced adhesion). For PEG-coated microsieves air sparging at low flow rates also results in a constant permeability. As a final application, skimmed milk filtration is considered at the end of this chapter. Regardless of the microsieve used (unmodified and PEG-coated), a very rapid permeability loss occurs when no backpulsing is applied. However, contrary to unmodified microsieves, stable and higher milk fluxes are obtained with coated membranes with backpulsing, independently of the settings. Air sparging is not applicable to milk filtration because of foaming and because it is unable to either recover/stabilize fluxes.

The fabrication procedure and properties of more economical and more feasible microsieves made from polymers are described in Chapter 7. PES, PES-PEO and PES/PVP microsieves are manufactured by Phase Separation Micromolding, a versatile method capable of using a great variety of polymers to replicate microstructures on a silicon mold. In order to obtain a perfect microsieve replica a suitable mold and casting solution must be used. Perforation of the polymer film is a critical step, which occurs during VIPS (Vapor induced-phase separation), and it can be influenced by the polymer film thickness, the vapor concentration and the residence time in the vapor bath where VIPS occurs. The dimensions of the perforations can be tuned either by using molds with different pillar diameters or by thermally treating the polymeric microsieve, reaching pore diameters of about 1.5 μm and also in the submicron range.

Fouling studies with BSA, milk and beer are performed in Chapter 8. Constant protein, skimmed milk and beer permeabilities are obtained by using polymeric PES microsieves in combination with backpulsing. Enhanced permeation by microsieve motion represents an exceptional improvement, uncommonly seen for commercial systems. The capacity of polymeric microsieves to vibrate and avoid foulant deposition, while maintaining a very selective separation can offer an economically attractive process and a revolutionary challenge for implementing such novel membranes in industrial applications.

Samenvatting (voor niet membraan-technologen)

Het onderzoek in dit proefschrift behandelt diverse aspecten met betrekking tot het gebruik van hoge-flux filters zoals microzeven in microfiltratie. Het grootste deel van dit werk bestaat uit het bestuderen van vervuiling van anorganische en polymere microzeven met modeloplossingen zodat fundamentele kennis en inzicht kan worden toegepast bij de applicatie van melkfiltratie.

Hoofdstuk 2 beschrijft de eigenschappen van silicium nitride (Si_xN_y), het fabricagemateriaal voor anorganische microzeven. De neiging van Si_xN_y om vervuiling te absorberen uit zijn omgeving vereist oppervlaktemodificatie. Afhankelijk van de toepassing kan Si_xN_y hydrofiel of hydrofoob gemaakt worden.

De prestaties van Si_xN_y microzeven met betrekking tot de schoon water fluxen is een zeer belangrijk aspect en wordt behandeld in hoofdstuk 3. Water permeabiliteit (oftewel het volume van water per membraanoppervlak, druk en tijd) is een hele belangrijke parameter. Permeabiliteit is karakteristiek voor elk membraan en bepaalt de maximale productiviteit van een filter. Uit het onderzoek blijkt dat een geschikte bevochtigingsprocedure en de eigenschappen van het voedingswater cruciaal zijn om maximale prestaties te halen. In het algemeen geldt dat maximale waterpermeabiliteiten kunnen worden bereikt met een volledig bevochtigd, schoon en luchtarm systeem (lucht kan zorgen voor afwijkingen in fluxen en ontvochtiging, meestal met hydrofobe membranen).

Vervolgens, wanneer deze stappen zijn ondervangen, kunnen complexere voedingen voor verschillende toepassingen worden onderzocht. Om dit doel te bereiken zijn modelsystemen zeer nuttig, omdat het proces dan op een simpele manier bestudeerd kan worden. Eiwitten bevinden zich in vele voedingsmiddelen en deze zijn meestal verantwoordelijk voor membraanvervuiling; daarom worden ze heel vaak als model oplossingen gebruikt. In hoofdstuk 4 wordt de crossflow-filtratie van eiwitten, zoals BSA en lysozyme, besproken. Daar wordt geconstateerd dat een snelle fluxafname plaats vindt, ook al is de poriegrootte van het membraan veel groter dan de afmeting van het eiwit. Het verlies in permeabiliteit wordt veroorzaakt door de vloeistofeigenschappen (concentratie, pH, etc.) maar ook door het gebruikte membraanoppervlak en de filtratie-apparatuur.

Hoofdstukken 5 en 6 behandelen de strategieën om de fluxafname te vertragen/beperken en vervuiling te voorkomen. Backpulsing (het permeaat terug door het membraan pulseren) tot 6.7 Hz kan de permeatie verbeteren en vervuiling vertragen, maar zorgt niet voor constante fluxes. Air sparging (lucht langs het membraan stromen) is de meest succesvolle techniek om constante BSA permeatie te verkrijgen. Air sparging is niet toepasbaar voor voedingsmiddelen vanwege het ontstaan van schuim. Andere technieken, zoals het

aanbrengen van antivervuilende polymere coatings gemaakt van polyethyleenglycol (PEG), moeten worden onderzocht. Backpulsing met PEG gecoate microzeven is succesvoller dan met de niet gemodificeerde membranen want dit resulteert in hogere fluxen en schonere zeven (eiwitten plakken minder aan het oppervlak). Dit fenomeen is ook geconstateerd in een toepassing zoals magere melk filtratie. Met de gecoate membranen en backpulsing kunnen stabiele melkfluxen worden gemeten en een hogere hoeveelheid product kan worden verkregen.

Hoewel de resultaten die met de coating bereikt zijn heel positief zijn, moet de coating toepasbaar zijn in de voedingsmiddelenindustrie. De coatings moeten de schoonmaak procedures, waarbij vaak zure en basische componenten worden toegepast, kunnen doorstaan.

Als alternatief voor de relatief dure anorganische microzeven zijn goedkopere polymere zeven gemaakt en deze worden besproken in hoofdstuk 7. Hun fabricagemethode is zeer veelzijdig. Microstructuren kunnen gemaakt worden door gebruik te maken van een gestructureerde mal en een geschikt polymeer recept. De poriegrootte van microzeven kan worden aangepast door gebruik te maken van verschillende malstructuren en/of een temperatuurbehandeling van de gemaakte polymere zeef.

In het één-na-laatste hoofdstuk worden de vervuilingresultaten van polymere zeven met BSA, magere melk en bier gepresenteerd. Constante eiwit-, melk- en bierfluxen zijn mogelijk met behulp van backpulsing. Dit is bereikt door de unieke eigenschap van de polymere zeven om te vibreren waardoor de vervuilingsslaag boven het oppervlak wordt gehouden. Dit fenomeen is een buitengewoon belangrijke vooruitgang die de weg vrij maakt om deze nieuwe membranen te implementeren in industriële applicaties.

Resum (per a no-membranòlegs)

La recerca descrita en aquesta tesi descriu varis aspectes relacionats amb l'ús de membranes de microfiltració amb permeabilitats superiors a les convencionals: microsieves. Els microsieves (o 'microsedassos') inorgànics són filtres fabricats amb mètodes usats per produir microxips, i es caracteritzen per tenir una estructura completament homogènia i precisa. Actualment, també es poden fabricar amb mètodes més senzills i materials més econòmics com polímers, i així reduir el seu cost. El nostre treball descriu ambdós tipus de microsieves, inorgànics i polimèrics. El primer tipus és relativament un producte jove, ja que fou desenvolupat a la Universitat de Twente per primera vegada fa uns deu anys. Els microsieves polimèrics han estat desenvolupats íntegrament dins el Membrane Technology Group durant els últims tres anys.

El gol de la nostra recerca esta basat en l'aplicació dels microsieves i, en concret, en l'estudi del seu comportament durant la filtració per tal de poder assolir màxima productivitat. A més, és important que el fenomen anomenat 'fouling' (inutilització de la superfície o interior de la membrana degut a la deposició de material filtrat, és a dir, l'embrutiment o embossament del filtre) sigui reduït al màxim. Idealment, si el 'fouling' pot ser controlat i el process és econòmicament atractiu, els microsieves poden ser implementats comercialment al sector alimentari holandès en un futur pròxim, per exemple en la filtració de llet o cervesa entre d'altres. En el cas de filtració de llet, l'objectiu és fraccionar la llet en els seus components (greix, proteïnes, lactosa, sucres, etc.) per tal de poder enriquir altres productes (complements alimentaris, menjar per nadons,...) i també poder produir un producte (per exemple, baix en greix) amb propietats molt millors que la llet pasteuritzada o esterilitzada.

En primer lloc, donat que el nostre estudi és un dels pioners pel que fa a l'ús d'aquest tipus de filtres, és necessari caracteritzar el material que compona els microsieves inorgànics. Degut a que la superfície de la membrana té tendència a contaminar-se, sol ser necessari aplicar un recobriment amb materials que evitin l'embrutiment. Els materials usats poden ser tan bé hidrofílics (és a dir, que adsorbeixin aigua) o hidrofòbics (per aconseguir membranes que repeleixin l'aigua), depenent de l'ús de la membrana. Després de modificar la superfície en funció de l'aplicació, és molt important mesurar i optimitzar la permeabilitat d'aigua (o volum d'aigua per superfície, pressió i temps) que el microsieve pot permear, ja que aquest valor és un paràmetre característic de cada membrana que determina la seva màxima productivitat. Un cop assolit això, dissolucions més complexes poden ser investigades per diferents usos. En determinades ocasions cal però usar models senzills que permetin simular el comportament d'un microsieve en una aplicació real, i simplificar i optimitzar el procés. Les

proteïnes són presents en molts dels productes alimentaris i són normalment responsables per l'embrutiment o 'fouling' de les membranes. Així, utilitzant proteïnes com BSA (present a la llet o a la sang de bovins), informació sobre 'fouling' pot ser obtinguda. Aquest estudi també ens ha permès investigar mètodes per tal d'incrementar el volum de producte filtrat i reduir l'embrutiment de la membrana, ja que, degut a l'elevada quantitat de flux que pot ser filtrat pels microsieves, aquests esdevenen completament bloquejats i inutilitzats ràpidament. Tant l'ús de pulsacions del filtrat (és a dir, retornar el líquid permeat a través de la membrana) com de turbulències amb aire serveixen per aconseguir que el flux de filtrat no disminueixi tan severament (ja que remouen la proteïna depositada a la superfície).

Malgrat tot, com que l'aire no és aplicable a molts productes alimentaris ja que origina escuma, i les pulsacions no són suficients per mantenir la membrana neta, ha calgut fer ús de recobriments o polímers (com el polietilè glicol) que repeleixen proteïnes. D'aquesta manera, la combinació d'un recobriment i pulsacions és molt més efectiva ja que resulta en més permeabilitat de producte i en microsieves més lliures de producte depositat. Aquest fenomen ha estat corroborat positivament en filtracions preliminars de llet desnatada, i ha donat encara millors resultats que amb la proteïna. Amb el recobriment es pot filtrar llet durant un temps molt més llarg sense que el microsieva esdevingui bloquejat.

Malgrat que els resultats aconseguits amb membranes inorgàniques recobertes amb polímers capaços de repel·lir proteïna o llet han estat positius, el recobriment ha de ser apte per ser usat en productes de consum alimentari. Com a alternativa als relativament costosos microsieves inorgànics, hem desenvolupat una sèrie de microsieves més econòmics i fàcils de fabricar fent ús de polímers. Degut a la versatilitat del mètode de fabricació, una gran varietat de materials que poden ser aplicats tant en el sector alimentari o biomèdic, per exemple, poden ser processats. Afegidament, diferents estructures i mides de porus poden ser creades, arribant a obtenir dimensions al voltant de 1.5 micròmetres (1 micròmetre equival a 0.000001 metres) o inferiors. Una de les troballes més interessants d'aquest projecte ha estat el fet que els microsieves polimèrics tenen la capacitat única de vibrar quan pulsos són aplicats, de manera que la solució filtrada no es pot depositar a la superfície de la membrana i aquesta es manté neta i efectiva durant un llarg període de temps. Amb aquest principi hem demostrat que al filtrar tant proteïna, llet com cervesa, el flux de fluid permeat no disminueix i un volum major de producte pot ser obtingut. Tenint en compte aquests excepcional resultats i el baix cost dels microsieves polimèrics, un nou repte per implementar d'aquestes membranes en sectors dominats per filtres menys efectius i mètodes molt més complexos pot ser acomplert en un futur proper.

Acknowledgements

These four years have been an unforgettable journey, a self-discovery experience with ups and downs. At the end, I keep what I've learned, the personal satisfaction and perseverance that has led to where I am today. During this period I have come across many people, many of whom have accompanied me in my journey and have actively contributed to this thesis. I would like to dedicate some words to those who have meant so much for me, but first, to the rest of you ...THANKS !!!

First of all, I would not be writing these words today if it weren't for Clàudia Fontàs. She believed in me six years ago when I was just a Chemistry student in Girona and made it possible for me to come to Enschede and work with Bernd Krause in the MTO. Those three months meant the beginning of the journey...thanks to both of you, I'm so glad you both can attend the defence!!

I would also like to thank my promotor Matthias Wessling for believing in me and opening a door to my new life. Coming back to the group, first as a research assistant and then as a PhD student, meant much more to me than just a professional challenge. Thank you for trusting the microsieve legacy to me and for your endless suggestions, some of which have made us both a little bit happier.

I'd like to thank Zandrie Borneman, who supervised my work during the first two years and made the struggle of a beginner PhD a little more bearable.

There are not enough words of gratitude for my assistant promotor and supervisor, Rob Lammertink, who joined the project two years ago and supplied tones of creativity, knowledge, patience, motivation and great ideas. Rob, thank you very much for your input in the thesis, but mostly for your patience and being so professional (especially during my writing period !).

I am also very grateful to the members of the promotion committee for being part of this special day. It is an honour for me that Prof. Feijen, Prof. Van der Meer, Dr. Rolf Bos, Prof. Boom and specially Prof. Belfort (who will make such a long journey) can attend the promotion ceremony. I'm also proud that two special people, Laura Vargas and Jörg Balster, can be my paranims and can accompany me in such important moment: muchas gracias and vielen dank!

The D-Force team deserves a special mention for contributing to the project from the very beginning: Rolf Bos, Albert van der Padt, Janneke Kromkamp and Frank Hollander (Friesland Foods), Remko Boom, Ruud van der Smaan, Karin Schroën and Gerben Brans (WUR) and Cees van Rijn and Wietze Nijdam (Aquamarijn). Such an assembly of different people with different backgrounds always resulted in very interesting and fruitful meetings.

Some of my lab work was eased by several people. Jorg Nijkamp (student assistant), Dirk-Jan Wilbrink and Imam Akbarsyah (master students): thanks to all of you for your effort, specially Imam, whose persistence resulted in more than 400 membranes and a chapter of this thesis. A special word of appreciation goes to Lydia, who helped me with all kinds of topics during four years. You have become one of the 'microsieve specialists' of the group. Bedankt voor alles!!

And talking about help in the lab... the list of people I am grateful to for that is endless!! Jörg and Wilbert took care of keeping me out of trouble (mainly of causing a blackout in Langezijds) with electrical wiring. Jörg, thanks for helping me build my super controlled set-up (probably I would still be measuring fluxes by hand ☺). Marcel, Wilbert and Hylke, thanks also for contributing to that. Thanks also to: Joao and Magda, for your aid with the UV-VIS; Laura, for the shrinking tests; Bernke for your skills in SEM during the last weeks of writing and your company in Houston; Rob for spending so many hours in the cleanroom making wafers; Maik for your input on the pulse measurements; Wika for the DLS measurements and all the technicians and John for their help when I needed it. Being in three different offices in four years is quite a record. It has been a pleasure to share them with Jörg (it was fun being your roommate, especially in the mythical 'chicken-box'), Maik and Joao (the latter was not strictly a roommate but as if, the walls in the chicken-box were so thin...), Kitty (bedankt voor de vele bemoedigende praatjes), Magda (thanks for the delicious cakes), Ana, Saiful and Srivatsa.

During the most stressful period of my thesis I've also had the helping hand of several colleagues who have made sure that the final result is more than fine. Dimitris, thank you for your always useful advice and, together with Jorrit, your suggestions and being so critical with a couple of my chapters, they are definitely much better now! Jörg, Hylke, Joao, Marcel and Greet: thanks for checking the spelling and my Dutch mistakes (Greet, ook bedankt voor alle hulp met het 'saaie' werk). And Rob, millions of thanks for reading, correcting and mostly improving the thesis.

Throughout the years I've also learned my way outside the group and worked with people who have enriched this work with their contributions. I'd like to thank to Dr. Wormeester (Applied Optics, UT) for performing all ellipsometric measurements; Clemens Padberg for all the assistance with the goniometer, FTIR, MW, etc.; Lourdes, Alessio and Francesca for their help and discussions about fluorescence, polymer synthesis and NMR; Rob Velthuis for his input and realization of the casting machine, as well as repairing the old one a million times; Prof. Goedel and Ailin Ding (Chemnitz University) for the 'nano-microsieves'; Ronald Jansen from Fluxxion for making the completion of the Si_xN_y chapters real; and Laura Vargas and

specially Dr. Henri Jansen from TST (UT) for the great input on the needle-like molds that made Chapter 7 possible (we still have so much to do!!).

Someone once told me that home is where your shoes are. I want to thank some people that have helped me to feel more at home in Enschede. Ten eerste, wil ik mijn Nederlandse familie bedanken: Wim en Heiltje, Bert en Jolanda en Elly, vanaf het eerste moment ben ik als een dochter en zus voor jullie geweest, jullie hebben me altijd gesteund en zijn altijd zo zorgzaam geweest...bedankt! Cas en Laura, bedankt voor jullie vriendschap, gastvrijheid en dansavonden (Laura, gracias de corazón por tu amistad y por estar siempre ahí); Henri, ook bedankt voor de lachmomenten tijdens de Ierse danslessen en je hulp; Cindy en Yorick, bedankt voor jullie vriendschap en de fijne etentjes en uitjes (ook wanneer ik alleen over werk praat). Iedereen van de dansles, Iers, orkest en Geus-POTM avonden, bedankt!

A part of my heart is not in Enschede but in Girona, where some of my loved ones are. I want to dedicate a few words in Catalan to my family, who are the ones who keep me grounded and have supported me from the beginning.

Pares, sense vosaltres no hauria arribat on sóc ara, vosaltres m'heu motivat sempre per treure el millor de mi, i m'heu recolzat quan ho necessitava. Sempre us estaré en deute. Marta, a part de germana ets la meva millor amiga, i encara que estem tan lluny sé que sempre em faràs costat. Sort d'internet i del telèfon perquè sinó et trobaria a faltar tant... Xevi, gràcies per cuidar de la Marta, és un plaer ser la teva cunyada. A tots quatre: em fa molta il·lusió que pogueu fer-me costat a la defensa. Avis, espero que estigueu orgullosos de mi. Jo ho estic de vosaltres, i només espero que tots junts poguem estar junts molts anys més. A tots, us tinc lluny però us porto al cor. Us estimo!!

Anna and Eva, you are my dearest friends, always ready for me when I come to Girona. Anna, I hope we can share many things together at least 16 years more. Eva, I appreciate so much that you can attend the promotion, gràcies de tot cor!

The other part of my heart is in Enschede, with the person that has always been my support and my companion. Marcel, you are not only my husband, but also my friend, my colleague and my soulmate. I do not have enough words to express how grateful I am to you and what you mean to me. Without you and your endless help this thesis would not have been possible.... thank you for believing in me, being there and for the years to come !!

Miriam



Curriculum Vitae

Miriam Gironès was born on 4th January 1977 in Girona (Catalonia), Spain. In 1995 she received her Secondary Education Diploma with honors at the Ext. Batxillerat Dalmau Carles, and in early 2001 she obtained her Master of Science in Chemistry at the University of Girona. During her studies she pursued a practical training under the supervision of Bernd Krause at the Membrane Technology Group (MTG) of the University of Twente (The Netherlands). From November 2000 to September 2001 she joined the MTG as a research assistant in the framework of the PhD research of Magda Avramescu, working in the development of mixed matrix membranes. From September 2001 until September 2005 she was employed at the same group as a PhD student, focusing on the research topic presented in this dissertation: fouling of inorganic and polymeric microsieves. From January 2006 she will remain at the Membrane Technology Group as a Postdoc in Tissue Engineering.

Publications

M. Gironès, L. Bolhuis-Versteeg, R.G.H. Lammertink, M. Wessling, Flux stabilization of silicon nitride microsieves, in preparation.

M. Gironès, I. J. Akbarsyah, H.V. Jansen, R.G.H. Lammertink, M. Wessling, Tailoring polymeric microsieves produced by Phase Separation Micromolding, in preparation.

M. Gironès, R.G.H. Lammertink, M. Wessling, Vibrating polymeric microsieves: antifouling strategies for microfiltration, in preparation.

M. Gironès, R.G.H. Lammertink, M. Wessling, Protein aggregate deposition and fouling reduction strategies with high-flux silicon nitride microsieves, *J. Membr. Sci.* (2005) in press.

M. Gironès, R.G.H. Lammertink, M. Wessling, Vibrating microsieve, EP 05077172, 2005.

M. Gironès, Z. Borneman, R.G.H. Lammertink, M. Wessling, The role of wetting on the water flux performance of silicon nitride microsieves, *J. Membr. Sci.* 259 (2005) 55.

D.F. Stamatialis, H.H.F. Rolevink, M. Gironès, D.C. Nijmeijer, G.H. Koops, In vitro evaluation of a hydroxypropyl cellulose gel for transdermal delivery of timolol, *Current Drug Delivery* (2004) 1

M.E. Avramescu, M. Gironès, Z. Borneman, M. Wessling, Preparation of mixed matrix adsorber membranes for protein recovery, *J. Membr. Sci.* 218 (2003) 219.

